Flame Structure and Emissions of Strongly-Pulsed Turbulent Diffusion Flames with Swirl

Ying-Hao Liao

A dissertation

submitted in partial fulfillment of the

requirements for the degree of

Doctor of Philosophy

University of Washington

2012

Reading Committee:

James C. Hermanson, Chair

Robert Breidenthal

Dana Dabiri

Program Authorized to Offer Degree:
Aeronautics & Astronautics

University of Washington

Abstract

Flame Structure and Emissions of Strongly-Pulsed Turbulent Diffusion Flames with Swirl

Ying-Hao Liao

Chair of the Supervisory Committee:
Professor James C. Hermanson
Aeronautics & Astronautics

This work studies the turbulent flame structure, the reaction-zone structure and the exhaust emissions of strongly-pulsed, non-premixed flames with co-flow swirl.

The fuel injection is controlled by strongly-pulsing the fuel flow by a fast-response solenoid valve such that the fuel flow is completely shut off between pulses. This control strategy allows the fuel injection to be controlled over a wide range of operating conditions, allowing the flame structure to range from isolated fully-modulated puffs to interacting puffs to steady flames. The swirl level is controlled by varying the ratio of the volumetric flow rate of the tangential air to that of the axial air.

For strongly-pulsed flames, both with and without swirl, the flame geometry is strongly impacted by the injection time. Flames appear to exhibit compact, puff-like structures for short injection times, while elongated flames, similar in behaviors to steady flames, occur for long injection times. The flames with swirl are found to be shorter for the same fuel injection conditions. The separation/interaction level between flame puffs in these flames is essentially governed by the jet-off time. The separation between flame puffs decreases as swirl is imposed,

consistent with the decrease in flame puff celerity due to swirl. The decreased flame length and flame puff celerity are consistent with an increased rate of air entrainment due to swirl.

The highest levels of CO emissions are generally found for compact, isolated flame puffs, consistent with the rapid quenching due to rapid dilution with excess air. The imposition of swirl generally results in a decrease in CO levels, suggesting more rapid and complete fuel/air mixing by imposing swirl in the co-flow stream. The levels of NO emissions for most cases are generally below the steady-flame value. The NO levels become comparable to the steady-flame value for sufficiently short jet-off time. The swirled co-flow air can, in some cases, increase the NO emissions. The elevated NO emissions are due to a longer combustion residence time due to the flow recirculation within the swirl-induced recirculation zone.

The reaction zone structure, based on OH planar laser-induced fluorescence (PLIF) is broadly consistent with the observation of luminous flame structure for these types of flames. In many cases, the reaction zone exhibits discontinuities at the instantaneous flame tip in the early period of fuel injection. These discontinuities in the reaction zone likely result from the non-ignition of injected fuel, due to a relatively slower reaction rate in comparison with the mixing rate. The discontinuity in the OH zone is generally seen to diminish with increased swirl level. Statistics generated from the OH PLIF signals show that the reaction zone area generally increases with increased swirl level, consistent with a broader and more convoluted OH-zone structure for flames with swirl. The reaction zone area for swirled flames generally exhibits a higher degree of fluctuation, suggesting a relatively stronger impact of flow turbulence on the flame structure for flames with swirl.

TABLE OF CONTENTS

LIST OF FIGURES

LIST OF TABLES

ACKNOWLEDGEMENTS

I would like to attribute this dissertation to my beloved family, including my aunt, who have been encouraging and supporting me emotionally and financially through all the years. In particular, my parents and my auntie have devoted themselves tirelessly to our family and children's education. Their unselfish dedication has always been the motivation that keeps driving me working diligently. In all of my success, every credit would be ascribed to them.

My girlfriend, Fanny Yang, is another person whom I would like to thank. She has been keeping me company and comforting me during those rough days. I am very grateful to have her around.

Over my years at the UW I have received considerable help from many people in the Department of Aeronautics and Astronautics. Ms. Wanda Frederick has provided professional assistance regarding academic affairs. Mr. Robert Gordon was very generous in providing equipment and helping to set up experiment. I also appreciated the professional advice and help from Mr. Dzung Tran, Mr. Dennis Peterson, and Mr. Art Blair. I was very honored to be the instructor of AA210 and was grateful to Dr. Carl Knowlen and Prof. Adam Bruckner for that opportunity and their confidence in me.

I especially thank Prof. Seong-Young Lee at the Michigan Technological University who provided valuable suggestions and advice on OH PLIF experiment.

Finally, I would like, from the bottom of my heart, to thank my advisor, Prof. Jim Hermanson. Jim has been a great adviser, not just research but also as a personal mentor. I cherish all the discussions we had and very much enjoyed working with Jim. I wish the best of luck to Jim in every aspect of his career.

CHAPTER 1

INTRODUCTION

1.1 Motivation

According to Department of Energy, the annual consumption of fossil fuels in the US has tripled since 1949 and exceeded 80 quadrillion BTU's in 2010 [1]. Even very small increases in combustion efficiency can result in a substantial decrease of fuel consumption and a significant reduction in harmful exhaust emissions. With the increasing attention on the shortage of fossil fuels and increasing concern on the protection of the environment, new challenges are presented for developing innovative combustion strategies. The development of such combustion strategies is largely driven by ever-increasing requirements for low emissions, especially CO and NO_x, while at the same time satisfactory combustion stability and high thermal efficiency must be maintained. In addition, from the economic point of view, it is important to avoid complex configuration designs and focus on reliable and simple combustion configuration.

Control of turbulent combustion by intentionally exciting the large-scale turbulent structures has been seen to have significant advantages in terms of combustion efficiency and emissions [2]. This manipulation of the large-scale turbulent structures to modify their interaction can also ultimately improve the rate of oxidizer entrainment and the fuel/air mixing. Such excitation can be achieved by different techniques, including acoustic forcing [3, 4], pulsed combustors [5, 6], and strongly-pulsing by fast-response valves [7, 8]. Practical benefits associated with these approaches include the generation of compact flames and combustors [7], high combustion and thermal efficiencies [4, 5], and low combustion emissions [6].

A strongly-pulsed fuel injection technique (e.g. the fuel injection is completely shut off between each injection pulse) is used in the current study. This control strategy allows the fuel injection to be controlled over a wide range of operating conditions and can give rise to drastic modification of the combustion and flow characteristics of flames, leading to enhanced fuel/air mixing mechanisms not operative for the case of acoustically excited or partially-modulated jets [7]. In addition, this technique, due to its simplicity, can be readily combined with other combustion enhancements, such as swirl employed in the present research, to further improve the combustion efficiency and emissions.

Swirl has been widely used in non-premixed turbulent flames to broaden the flammability limit [9, 10], shorten the flame length [11], and reduce the NO_x emissions [12, 13]. In non-reacting flow, a recirculation zone has been seen to be produced with sufficiently strong swirl [9]. The reverse flow is due to the presence of an adverse pressure gradient in the flow direction, due to the tangential motion in the flow, which induces a radial pressure gradient (with a lower pressure at the center of the flow). As swirl decays with downstream distance, the pressure at the center rises, thus causing an adverse pressure gradient along the axis of the flow, resulting in flow recirculation [9, 14]. This recirculation zone can improve the stability of flames by transporting hot combustion products back to the injection plane, thus providing a stable source of heat and reactive species for flame ignition [14]. Due to its toroidal vortex structure, a high turbulence level is typically present on the boundaries of the recirculation zone [14], suggesting that a potentially higher rate of oxidizer entrainment and enhanced mixing can be achieved, potentially leading to a decrease in flame length, thus resulting in low NO_x emissions [15]. In addition, due to the many similarities between the recirculation zone and a well-stirred reactor, the temperature and gas composition within the reverse flow can be essentially uniform [9]. With a sufficiently high combustion temperature, but below that at which significant thermal NO is produced, and given sufficient oxidizer for CO oxidation [16], the CO level in swirled flames can possibly be decreased, or prevented from increasing, while the NO emissions are also reduced.

Despite the large number of studies on the control of non-swirling, turbulent flames, there is a relative lack of information on the active control of flames with swirl [17, 18]. Investigations of unsteady swirling flames have typically involved acoustic excitation, either as self-excited flame oscillations [19] or by acoustic energy input directly into the flame [17, 20]. The more drastic modification of these structures in swirl combustion by the strong-pulsing technique could reasonably be expected to play a significant role in the control of the combustion process. In any case, effective control of these swirling flames depends critically on understanding in detail the nature of the large-scale turbulent flame structures under swirled conditions. It is proposed in this research to use a simple swirl burner without confinements to study the behaviors of strongly-pulsed, turbulent jet diffusion flames in the presence of a swirling co-flow.

1.2 Entrainment

The rate of oxidizer entrainment is of central importance in any non-premixed combustion system given that chemical reactions require the molecular mixing of fuel and air, which in turn depends directly on said entrainment. The combustion process is also directly related to the rate and efficiency of the fuel/air mixing (again, limited by the rate of entrainment), given that the chemical kinetic time scales in turbulent flames are usually shorter than the turbulent time scales [21].

The large-scale coherent structures in turbulent flow have been known to play an important role in oxidizer entrainment and thus fuel/air mixing, and to have an impact on combustion and heat release processes in non-premixed flames [22, 23]. Excitation of large-scale structures has been extensively employed to achieve enhanced mixing in both non-reacting jets and combustion systems. An early study on a non-reacting pulsed jet (by exciting the organ-pipe resonance of the fuel delivery tube) showed that the entrainment brought about by pulsing at the resonant frequency could be up to four times over that in the unpulsed jet [24]. Lakshminarasimhan *et al*. [25] studied the mixing characteristics in a strongly-forced (by acoustic forcing) non-premixed methane jet flame. In that study, the mean mixture fraction along the jet centerline in the pulsed jet decayed below 0.08 in as little as three fuel-nozzle-diameters downstream of the nozzle exit; while the mean mixture fraction for the unpulsed jet remained close to unity over the same distance. Lakshminarasimhan *et al*. suggested that the enhanced entrainment and mixing due to strong forcing could be the predominant mechanism that caused the reduction in flame length and luminosity. A subsequent study done by the same group [26] reported a significant reduction of 70% in mean flame length for a first-resonance pulsed flame as compared to the unpulsed flame at a Reynolds number of about 2,500.

A recent study of the velocity field of isolated turbulent puffs using the Particle Image Velocimetry was performed by Johari's research group [27]. The jet pulsing in that case was achieved by a fast-response solenoid valve, similar to the pulsing technique employed in the current study but with different injection conditions. Specifically, that study was conducted at a sufficiently low pulsing frequency (~ 1 Hz) such that each puff cleared the test section before a subsequent puff was generated. The results from phase-locked measurements indicated that as the injection volume decreases, the fluctuating velocities, associated with the turbulence level, increase. The maximum turbulent shear stress within the puff could be as much as 2.5 times the steady jet value. The entrainment rate (the ratio of the volumetric flow rate within puff to that of the injected jet) for the smallest injection volume was reported to be up to a factor of 2.4 greater than that of the steady jet. This is attributed to the fact that a puff may entrain ambient air over a relatively larger surface area as compared to a steady jet.

In addition to intentional flow excitation, enhancement of entrainment is often achieved by the imposition of swirl. Feikema *et al*. [28] employed planar Rayleigh scattering to image the structure of the mixture fraction field and the scalar dissipation layers near the base of a non-reacting turbulent jet, both with and without swirl. The results showed that when swirl was added to the coaxial air stream, the mean mixture fraction on the jet centerline at a downstream location of 14 fuel-nozzle diameters decreased to a value of 0.26, which was half of the value in the jet without swirl. The value of the mean dissipation rate, an indicator of the local mixing rate [29], also doubled over the same region as swirl was added. The authors attributed the increased dissipation rate to the increased number of flow interfaces per unit volume, which resulted from the entrainment of large numbers of "islands" of ambient air. Feikema *et al*. also suggested that the swirl employed in their study was not sufficient to cause recirculation, but that the swirl essentially broadened the jet and produced centrifugal forces that helped to entrain ambient air.

Furthermore, Masri *et al*. [30] used Raman-Rayleigh-LIF (laser-induced fluorescence) to study the compositional structure of a highly swirling, turbulent non-premixed flame. The range of swirl level in that study was sufficient enough to produce a distinct recirculation zone. Similar to Feikema *et al*.'s study [28], the results from Masri *et al*. showed that the centerline decay of the mean mixture fraction was faster for highly swirling flames with a swirl number of S = 1.59 than for flames with a swirl number of S = 0.66. The faster decay of the mean mixture fraction was a result of more intense mixing due to the increased swirl. In the same study, the RMS (root-mean-square) fluctuations of mixture fraction also exhibited a higher value for swirling flames than for non-swirling flames. Masri *et al*. suggested that these excess fluctuations may be genuine since higher turbulence levels were also measured in a turbulent jet flame with swirl [31].

As mentioned previously, the pressure gradients resulting from strong swirl can cause vortex breakdown, resulting in recirculating-flow near the burner exit [32]. This recirculation has been known to produce high turbulence and thus result in enhanced entrainment and intense mixing [9, 11]. Tangirala *et al*. [33] used Laser Doppler Velocimetry (LDV) to measure the velocity field of a swirl-stabilized flame and found that the turbulence level appeared to peak at the boundary of the recirculation zone, consistent with Syred & Beér's study on a non-reacting, swirling jet [34]. The volumetric flow rate of the recirculating flow was up to a factor of 3 for flames with a strong swirl (S = 2.0) compared to flames with a relatively weak swirl (S = 1.0), suggesting the enhancement of entrainment due to the swirl-induced recirculation zone.

1.3 Emissions

A major challenge in developing a modern combustor is to meet the increasingly rigorous regulations on exhaust emissions. An efficient combustor can lead to not only fuel savings, but also a corresponding reduction in CO and NO_x emissions. It is well known that pulsed combustion can have advantages in terms of high combustion and thermal efficiencies and low emissions [2]. In addition to pulsed combustion, swirl serves as an alternative in lean combustion applications to reduce emissions of CO and NO_x [17].

Zinn [2] suggested that the advantages of a pulse combustor are strongly related to the presence of pulsations, in the following sense. First, the pulsations enhance mixing rates between various species, which in turn accelerates the combustion process and reduces the required amount of air for complete combustion. Furthermore, the more complete combustion due to the enhanced mixing reduces the amount of unburned hydrocarbon and thus CO emissions. Keller *et al*. [6] showed that a pulse combustor can be operated in a lean premixed mode with the concentration of CO being as low as 5.0 ppm without the use of any post-combustion cleanup technologies. Chao *et al*. [35] found that reduction of both NO_x and CO emissions was possible in an acoustically-forced propane jet flame.

Paschereit *et al*. [17] employed a closed-loop active control system to suppress the thermoacoustic pressure oscillations and to reduce NO_x emissions in a swirl-stabilized, acoustically-forced combustor. Their results showed simultaneous reduction of emissions of both NO_x and CO. The authors argued that fluctuations in heat release and consequently in temperature in unstable lean combustion may lead to a simultaneous increase in NO_x and CO, due to the exponential dependence of both emissions on temperature, and by stabilizing the combustion process it was possible to simultaneously decrease both emissions levels. Paschereit & Gutmark [36] also found a reduction in both NO_x and CO emissions in an elliptic swirl-stabilized burner: NO_x by up to four times and CO by a factor of 2-3. In Masri *et al*.'s study [30], the higher swirl level reduced the formation of CO, but led to increasing levels of NO, which, the authors suggested, may be possibly due to the longer residence time induced by the stronger flow recirculation in a highly swirling flow.

Cheng *et al*. [37] measured concentrations of NO_x and CO in a swirling methane jet flame and found a decrease in NO levels, accompanied by increased CO levels, with increasing swirl. Newbold *et al*. [38] obtained a similar result in their swirling propane turbulent diffusion flames, in which high values of CO levels and NO_2/NO_x was observed in a highly swirling flame, while NO emissions were reduced compared to the flame with a relatively weak swirl. Both studies observed a significant decrease in flame length and flame temperature and suggested that the reduced NO_x levels were the result of a lower flame temperature and a shorter global residence time, due to the decreased flame length; while the high CO emissions were associated with the cold air quenching by rapid entrainment of excess cold air due to swirl.

Regarding the formation of CO, Puri & Santoro [39], in their study of laminar diffusion flames, found evidence supporting their hypothesis that the observed strong correlation between soot and CO was a result of competition between soot and CO for the oxidizing species OH. Turns & Bandaru [16] found that the CO emissions in a jet flame correlated strongly with the global residence time and suggested that more complete mixing and combustion would lead to more complete CO burn-out and lower levels of CO.

In general, control of NO_x emissions in combustion involves more complicated mechanisms than that of CO emissions [40, 41] and thus has extensively received more attention in combustion emissions research [42, 43]. For hydrocarbon fuels, three primary mechanisms are responsible for NO production [42]: (1) the thermal, or Zeldovich, mechanism; (2) the Fenimore mechanism; and (3) the N_2O mechanism. In non-premixed hydrocarbon combustion, the majority of NO is produced via the first two mechanisms [42, 44]. The N_2O mechanism involves a three-body recombination reaction and generally becomes more important as the fuel-air ratio decreases, or as pressure increases [43].

The thermal mechanism consists of three chain reactions [40]:

$N_2 + O \leftrightarrow NO + N$ (R_1);

$O_2 + N \leftrightarrow NO + O$ (R_2);

$OH + N \leftrightarrow NO + H$ (R_3).

By assuming that N atoms are in steady state and the NO concentration is small compared to its equilibrium value, the reverse reactions can be neglected, leading to the rate of NO formation [40]:

$$d[NO]/dt = 2k_1[O][N_2] \qquad \text{Eq. 1-1,}$$

where k_1 is the rate coefficient of reaction (R_1) and $k_1 = 1.84 \times 10^{14} \exp(-38{,}370/T)$ cm^3/gmol-s [40]; and T is the temperature in Kelvin. As shown in Eq. 1-1, the production rate of NO has a very strong temperature dependence; the concentration of NO grows exponentially with temperature and linearly with residence time. Due to the relatively large activation energy [42], the NO production through the thermal mechanism is slow and the thermal mechanism is relatively less important at temperatures below 1,800 K [40]. However, due to the strong coupling between O atoms and the combustion chemistry [40, 43], the equilibrium assumption may not be valid in active oxidation zones within flames and superequilibrium concentrations of O atoms can exist, leading to acceleration of thermal NO production even below 1,800 K.

Following Bowman [43], prompt NO is defined here as the rapid NO production, which occurs long before there would be time to form NO by the thermal mechanism. Therefore, the NO production by the Fenimore and N_2O mechanisms are all considered to be prompt NO. The Fenimore mechanism generally involves reactions of hydrocarbon radicals with molecular nitrogen and has relatively more importance in fuel-rich hydrocarbon combustion [43]. The NO production by the N_2O mechanism increases under conditions where the total NO formation rate is relatively low and combustion is in fuel-lean operation mode [43].

Keller & Hongo [45] found that the mechanism responsible for suppressing NO formation in their pulse combustor was the short residence time at high temperature. The short residence time at high temperature was caused by rapid mixing of hot products with relatively cooler residual gases that were lower in temperature due to the increased rate of heat transfer in a pulsating flow. Chao *et al*. [35] found a significant reduction of NO_x for some low-frequency excitation cases in their hydrogen-air jet flames. They suggested that the reduced levels of NO_x were results of a short residence time, primarily due to the decreased flame length by acoustic excitation. Similarly, Kim *et al*. [46] measured a 15% reduction in flame length of a turbulent hydrogen-air jet flame by acoustic excitation using forced coaxial air. Consequently, a 25% reduction in levels of NO_x was achieved, compared to conditions without acoustic excitation.

Syred & Beér [34] reported that a swirling flame had better flame stability as a result of the formation of the toroidal recirculation zone, and had the shorter flame length as a result of the high rates of oxidizer entrainment for combustion. The shorter flame length is beneficial for reducing NO formation, due to the decreased global residence time, which scales linearly with the cube of the flame length [47]. Chen [15] reported that when the height of the recirculation zone was comparable to the flame length, NO_x was formed in the recirculation zone and was strongly impacted by the characteristic time of the recirculation zone, similarly reported in Masri *et al*.'s study [30].

1.4 Non-Swirled, Strongly-Pulsed, Turbulent Diffusion Flames

Previous research on strongly-pulsed flames without swirl has shown that the flame geometry is strongly impacted by the injection time [48]. For short jet injection times, depending on the jet-off time, such flames appear to exhibit compact, puff-like structures. Elongated flames, similar in behaviors to steady flames, occur for long injection times. The separation/interaction level between the turbulent flame puffs in these flames is essentially governed by the jet-off time. These flame puffs tend to have a higher celerity (i.e. the bulk velocity of the puff) for short jet-off times than those for long jet-off times, where isolated flame puffs occur. For a given injection time or fuel volume, this higher celerity is consistent with a decreased rate of momentum exchange with the co-flow that would accompany a decreased rate of oxidizer entrainment. This decreased rate of entrainment, also consistent with the observed longer flame length, has been suggested to occur since each flame structure has to compete with its neighbors for the same oxidizer, thus decreasing the rate of oxidizer entrainment into each structure [48].

The highest levels of CO emissions are found for compact, isolated flame puffs, consistent with the rapid quenching due to rapid dilution with excess air [48, 49, 50]. The amount of CO for the case of compact flame puffs decreases substantially as the jet-on fraction and the residence time associated with the increased flame length increase. At the same time, for most injection conditions the measured exhaust-point NO/NO_x concentrations in these flames are below those of the steady flame. The NO_x levels become comparable to the steady-flame value for sufficiently short jet-off time, while the flame length is shorter than that of the steady flame. There appear to be combinations of injection time and jet-off time that produce a turbulent jet flame that is more compact than a steady flame and with lower NO_x emissions, while achieving CO levels comparable to those of steady flames [48].

1.5 Swirled, Turbulent Diffusion Flames

An example that illustrates how a flame interacts with a vortex is a swirl-stabilized flame. Syred & Beér [34] pointed out that for sufficiently strong swirl a toroidal recirculation zone can form and increase the flame stability by recirculating hot products and acting as a heat reservoir.

In Chen & Driscoll's study [11], the overall fuel-air mixing rate within a swirl-stabilized flame was found to be a factor of five greater than that of a simple jet flame, as evidenced by a fivefold shortening of the flame length. The enhancement of mixing was the result of the formation of the recirculation zone, which acted like a large eddy with a characteristic velocity and length scale that were much larger than those associated with eddies in a simple jet [11]. In another study of Chen & Driscoll [51], the measured levels of NO_x in a non-premixed jet flame was reduced as swirl was added to the coaxial air stream. The reduced levels of NO_x, accompanied with higher levels of NO_2, was attributed to the increased rate of fuel-air mixing and the decreased flame length due to swirl [51].

1.6 Flame Zone Structure

The interaction between flow phenomena and chemical kinetics plays an important role in turbulent combustion processes. Although much insight into these processes has been gained from statistical, time-averaged data [52], temporally- and spatially-resolved measurements in combustion processes are needed for a better understanding of the evolution of the turbulent flame structures. In order to resolve temporal and spatial flame structures, planar laser-induced fluorescence (PLIF) diagnostics is often employed. This technique is species-selective and enables the detection of reactive intermediates in combustion at low levels (ppm level). The hydroxyl radical (OH) has been commonly imaged using PLIF to study the reaction zone structure of flames, mainly due to its peak concentration being typically near the peak combustion temperature [53]. A more detailed introduction of PLIF imaging and the study review of OH PLIF on the flame zone structure of turbulent non-premixed flames can be referred to Appendix A.

It is well-known that the large-scale structure of turbulent flows plays a crucial role in the combustion performance and resulting pollutant emissions [23, 46]. For strongly-pulsed flames, the reaction zone structure of these flames, not surprisingly, can be significantly impacted by the unsteady, large-scale turbulent structure induced by the fuel pulsing and the co-flow air swirl. The OH PLIF technique thus helps to understand the impact of swirl and pulsing on the behaviors of swirled, strongly-pulsed flames, and enables the exploration of the reaction zone structure of these flames and possible ignition/extinction issues.

1.7 Research Objectives

The overall objective of this research is to better understand the fundamental processes that govern the combustion characteristics of strongly-pulsed, turbulent jet diffusion flames with the presence of swirl. Specific objectives include:

- Study the large-scale turbulent flame structures at different injection conditions with the presence of swirl. The large-scale flame structural features of interest include the flame length, the degree of flame puff interaction, and the flame puff celerity.
- Examine the implications of the large scale turbulent structure dynamics on the time-varying rate of oxidizer entrainment.
- Study the effect of the volumetric co-flow flow rate and the presence of a quarl on the behaviors of strongly-pulsed flames in the presence of a swirling co-flow.

- Determine the exhaust concentrations of CO and NO in swirled, strongly-pulsed flames over a wide range of injection parameters and swirl levels to determine the combustion efficiency and emissions levels.
- Study the reaction zone structures and look for possible extinction/ignition issues in swirled, strongly-pulsed diffusion flames by performing hydroxyl (OH) planar laser-induced fluorescence (PLIF).
- Explore the existence of optimal strongly-pulsed injection conditions for producing compact, swirled flames with low emissions.

CHAPTER 2

EXPERIMENTAL SETUP

All of the experiments reported here were performed in the Combustion Laboratory in the Department of Aeronautics and Astronautics at the University of Washington. The experimental facility consisted of a combustor, exhaust hood, fuel/air supplies, and optical and gas-sampling diagnostics. For the purpose of this study, the combustor was designed and constructed to produce a strongly-pulsed turbulent jet diffusion flame with a swirled, air co-flow. Characterization of the combustor and determination of the swirl level were performed with by hot-wire anemometry. Three major diagnostics techniques were employed in the study: High-speed video imaging, standard emissions analyzers, and planar laser-induced fluorescence (PLIF). The high-speed video imaging of the flame luminosity allowed for the determination of the flame length and the flame puff celerity as well as the detailed study of the flame puff interactions. Emissions measurement was performed using standard emissions analyzers combined with an aspirated sampling probe. Finally, planar laser-induced fluorescence of the hydroxyl radical (OH) was employed to study the structure of reaction zones within the flame.

2.1 Experimental Apparatus

The combustor in the current study had a fuel nozzle with inner diameter d = 2 mm centered in a coaxial, swirled air stream, as shown schematically in Fig. 2.1. The fuel nozzle tip was located 6 mm downstream of the throat of the co-flow duct, at which point the combustor diameter was D = 35 mm. An optional diverging nozzle (quarl) downstream the fuel nozzle was employed in most cases to help stabilize the swirling co-flow. The diverging portion of the quarl began 9.2 mm downstream of the fuel nozzle exit. The quarl had a divergence half angle of 28° and the length of the conical portion was 47.4 mm. The design of the quarl was based on that of Beer & Chigier [14] to produce the optimum stabilizing effect on the swirling flow. The contracted section of the co-flow duct was designed to avoid any unwanted flow turbulence (such as flow separation) and to produce an effectively top-hat velocity profile when swirl was not added to the co-flow stream.

The fuel was 99.5% pure ethylene (C_2H_4). Ethylene was selected as the fuel due to its easy ignitability and high sooting tendency, which facilitated direct visualization of the flame. The flow rate of the injected fuel under steady injection conditions was monitored by a digital flow meter, *Omega* Model FMA1826, to ensure a fuel injection velocity that corresponded to the desired Reynolds number. The fuel nozzle tube had a length of approximately 40*d* to allow for a fully-developed turbulent velocity profile at the nozzle exit once a steady injection velocity was achieved [48]. The fuel flow was controlled by a fast-response (≈ 160 μs) solenoid valve, *Parker Hannifin* model Series 9, actuated in an on-off (rectangular wave) fashion for a range of injection times and jet-off times. A similar fuel injection technique was employed in previous research on non-swirled, strongly-pulsed flames [54]. The injected volume associated with the overshoot and oscillations was measured to be less than 3% of the total. A continuously energized igniter wire (≈ 76 μm in diameter), situated 2 mm downstream of the fuel nozzle tip, ensured ignition of all injected fuel. The igniter wire was made of *Kanthal* material for its high temperature resistance without creeping or rapid oxidization. Igniter wires near the fuel nozzle tip in non-swirled, strongly-pulsed turbulent jet flames have been shown to have negligible impact on the configuration on these flames [7].

The co-flow oxidizer was standard room air, consisting of 21% O_2 and 78% N_2 by volume. The air was supplied by a building laboratory compressed-air supply, with a flow rate measured using a pressure gauge and two rotameters. This delivery system ensured a steady supply of co-flow oxidizer during the experiment (the airflow was not modulated in this research). The amount of supplied air varied by less than ± 2%. The co-flow swirl was achieved by a combination of axially- and tangentially-injected air and the amount of axial and tangential air was controlled by the two rotameters, respectively. The axial air was delivered to the combustor through four inlets (0.72 cm I. D.) at the base of the combustor and conditioned by a perforated plate and a honeycomb section (1/8” cell size, 1” thick), as shown in Fig. 2.1. Four tangential air inlets with inner diameter of 0.79 cm were located 11.8 cm upstream of the combustor diverging exit. The exhaust gases from the combustor and any excess air were discharged into an exhaust fume hood. All reactants were unheated ($T \approx 300$ K) and all experiments were conducted at atmospheric pressure.

To minimize complications in the swirling flow, such as jet precession, possible acoustic instabilities, and an outer recirculation zone due to the presence of confinement [55], an unconfined combustion environment was used in the current study. In order to reduce effects of possible room disturbances on the flame, the combustor was surrounded on all sides by a fine mesh wire screen cube (60 cells per square inch) with each side 1 m × 1 m.

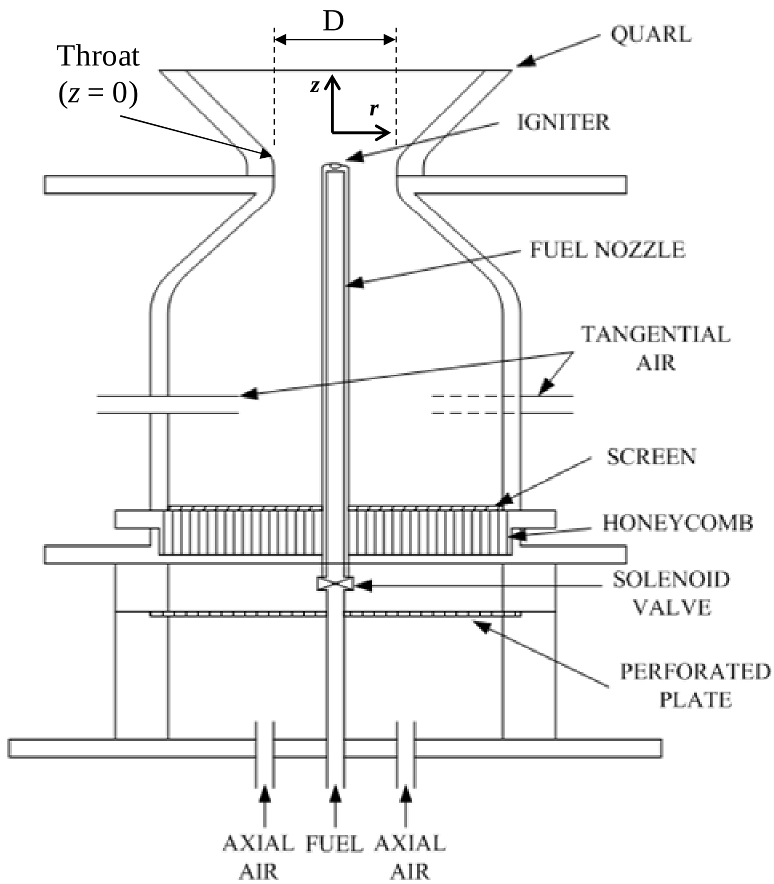

Figure 2.1 – Schematic of the swirl, pulse combustor.

2.2 Flow Conditions

The Reynolds number of the flame was based on jet-on conditions at the fuel nozzle exit. A Reynolds number of Re_{jet} = 5,000, corresponding to a nominal, steady jet velocity of U_{jet} = 22.2 m/s at the exit of the fuel nozzle, was used for all experiments. This Reynolds number ensured that the fuel jet was fully turbulent [48]. Although Hermanson *et al*. [54] reported that the fuel injection technique employed in the current study resulted in a certain amount of velocity overshoot and oscillations, the amount of those was small (less than 3% of the total) and thus the jet-on velocity was essentially constant during each injection interval.

The injection time, t_{on}, in this work ranged from 11.3 ms to 155.7 ms. It has been shown that the injection time governs the nature of isolated turbulent flame structures and the dimensionless injection time parameter, $P = (U_{jet}t_{on}/d)^{1/3}$, effectively characterizes the structure of the puffs in strongly-pulsed flames [48]. The parameter P is similar to the "formation number" employed by Gharib *et al*. [101] and Krueger *et al*. [102] to characterize the dependence of vortex-ring formation on the stroke length of the piston generating the ring. In addition, this parameter has been shown previously to characterize the visual length of strongly-pulsed flames consisting of isolated puffs [48]. For ethylene/air flames without swirl, P = 8 is the approximate upper limit for compact, individual puff-like flame structures, while the higher values of P lead to elongated turbulent flame structures, not puff-like but rather resemble segments of a steady flame [7]. The lowest P value to be investigated in this work was P = 5, corresponding to t_{on} = 11.3 ms; the highest was P = 12, corresponding to t_{on} = 155.7 ms.

The jet-off time, t_{off}, is directly connected to the degree of the flame puff interaction [48]. The initial separation distance between flame puffs in the vicinity of the fuel nozzle exit scales with the product of jet-off time and the jet exit velocity. This relation along with the fuel nozzle diameter can be used to define a dimensionless jet-off time parameter, $\tau_{off} = U_{jet}t_{off}/d$. A dimensionless jet-off time of $\tau_{off} = 444$ has been observed, for strongly-pulsed flames without swirl, as a threshold value between isolated ($\tau_{off} > 444$) and interacting ($\tau_{off} \leq 444$) flames puffs [48]. Those flames without swirl are considered here as a baseline case. The jet-off time in this work ranged from $t_{off} = 10$ ms ($\tau_{off} = 111$) to $t_{off} = 100$ ms ($\tau_{off} = 1110$). The injection times and jet-off times as well as the corresponding values of their dimensionless parameters are summarized in Table 2.1.

The corresponding injection frequency, depending on the injection time and the jet-off time, varied from 3.9 Hz to 47 Hz. These injection frequencies led to the value of the Strouhal number at injection, $St = fd/U_{jet}$, ranging from 3.5×10^{-4} to 4.2×10^{-3}. These Strouhal numbers were far below the criterion ($St \approx 0.25$) associated with the natural instability in the near-field region of the jet, so the phenomena described here were essentially decoupled from the natural instability of the momentum-driven jet [56, 57].

One consideration in the case of strongly-pulsed diffusion flame is whether the flame is driven primarily by buoyancy or by momentum. Becker & Yamazaki [58] investigated the effect of buoyancy forces on the characteristics and structure of turbulent nonpremixed jet flame. The effect of buoyancy can be characterized using the parameter $\xi_L = (\rho_a dg/\rho_{jet}U_{jet}^2)^{1/3}(L/d)$, where ρ_a and ρ_{jet} are the density of the co-flow and the fuel jet, respectively, g is the gravitational acceleration, and L is the flame length. For $\xi_L < 2$, the flame is considered to be momentum-driven and for $\xi_L > 10$, it is considered to be buoyancy-driven. For the steady flames in the present study, $\xi_L = 6.9$, thus indicating that the steady flames were likely primarily buoyancy driven. This argument would not necessarily be expected to hold for strongly-pulsed flames. In these flames, if anything, the transition to buoyancy-dominated flow occurs for values less than

ξ_L =10 because of the loss of jet momentum due to the rapid entrainment and mixing of ambient air that occur for widely spaced puffs. Alternatively, the buoyancy effect in strongly-pulsed flames can be determined by a local, bulk Richardson number, $Ri \equiv (\rho_a - \rho(z))g\delta(z)/\rho(z)c(z)^2$, where $\rho(z)$ is the gas density in the flame structure, $\delta(z)$ is the maximum width of the puff structure, and $c(z)$ is the convection speed of the center of the structure [7]. In this work, except the region near the nozzle, most of the resulting values of Richardson number were much higher than 0.05, a threshold value where buoyancy effect became more dominant [59]. Therefore, the majority of the flames considered here were expected to be buoyancy driven.

Two co-flow volumetric flow rates, 2.5 SCFM (≈ 1.18 L/s) and 3.5 SCFM (≈ 1.65 L/s), were employed in the study, and provided an overall air/fuel volume ratio of 16.92 and 23.69, respectively, based on steady fuel injection conditions. The stoichiometric air/fuel ratio, Ψ, on a volume basis, for an air/ethylene flame is 14.34, indicating that all flames studied here were fuel-lean, with more than sufficient air from the injected co-flow to fully ventilate the flame. The coaxial swirl was produced by a combination of axially- and tangentially-injected air. The swirl level, quantitatively represented by a swirl number, S, was controlled by varying the ratio of the volumetric flow rate of the tangential air to that of the axial air [33]. The swirl number and the associated volumetric flow rates of the axial and the tangential air are given in Table 2.2. The swirl number is commonly defined as the ratio of the flux of angular momentum (G_θ) to that of axial momentum (G_x) at the throat of the combustor, divided by the throat radius, R [9, 14]:

$$S = \frac{G_\theta}{G_x R} \qquad \text{Eq. 2-1}$$

$$G_\theta = \int_0^R \rho U_z U_\theta r 2\pi r \, dr \qquad \text{Eq. 2-2}$$

$$G_x = \int_0^R \rho U_z^2 \, 2\pi r \, dr \qquad \text{Eq. 2-3}$$

where U_z, U_θ are the axial and azimuthal components of the mean velocities respectively.

In this work, hot-wire anemometry was used to measure the velocity components of the swirling flow at the throat, which subsequently can be applied to determine the swirl number. A single hot-wire sensor probe, 50.8 μm in diameter, was placed in the throat of the combustor without the fuel nozzle installed to characterize the swirl levels. By rotating the probe 90 degrees along the combustor axis, both the mean axial and azimuthal velocities can be measured. The radial component of the mean velocity at the throat was relatively small compared to the other two components [60, 61], and was taken here to be negligible. The signals from the probe were analyzed by the *Dantec* Model 54T30 miniature constant-temperature anemometer. Time-averaged velocity surveys at the combustor throat are shown in Fig. 2.2. Each point plotted represented the ensemble average of 6,000 velocity samples. The presence of swirl is seen to modify the axial velocity profile. The radial shift of the location of the maximum axial velocity indicates the spreading of the flow due to swirl. The mean azimuthal velocity profile shows an increasing trend with the increasing swirl level, as expected. The nearly-linear growth of the azimuthal velocity with radius is suggestive of a forced vortex, consistent with Gupta *et al*.'s study [9]. The mean axial and azimuthal velocity profiles were then numerically integrated along the radius of the throat to produce the swirl number, as defined in Eq. 2-1.

Another characterizing feature of the swirling flow is the decay of the mean axial velocity along the combustor centerline, as shown in Fig. 2.3. The dashed line indicates the location of the quarl exit. The rate of centerline velocity decay increases as the swirl level is increased, implying an increased rate of entrainment and spreading of the flow by the introduction of swirl. Although the accuracy of a single-sensor probe in measuring the centerline velocity in the downstream regions of a swirling flow is difficult to ascertain, due to the complex and three-dimensional velocity field, the centerline velocity decay measured here is consistent with other studies of swirled flow that employed LDV (Laser Doppler Velocimetry) for determining the velocities [62, 63]. The stabilizing effect of the quarl on the swirling flow was also characterized, as shown in Fig. 2.3. The more rapid decay of the centerline velocity, when the quarl is present, is consistent with the effectiveness of the quarl on the stabilization of the swirling flow. For this reason, all experiments in the current study were performed with the presence of the quarl unless specified otherwise. A similar characterization was also carried out for swirling flows with different volumetric flow rates; those results are shown in Fig. 2.4. For swirling flows with a comparable swirl number, the normalized centerline velocity exhibits a quite similar decay with downstream distance for the two different air flow rates, while the rate of velocity decay is slightly higher for flows with the higher volumetric flow rate. An increased rate of the centerline velocity decay may suggest an even more increased rate of entrainment. Accordingly, flames with varied both co-flow flow rates will be conducted in this work to study the effect of co-flow strength on behaviors of swirled, strongly-pulsed flames.

Injection Time, t_{on} (ms)	Dimensionless Injection Time, P		Jet-Off Time, t_{off} (ms)	Dimensionless Jet-Off Time, τ_{off}
11.3	5		10	111
19.46	6		20	222
46.13	8		40	444
90.1	10		100	1110
155.68	12			

Table 2.1 – Fuel jet injection conditions. The nominal fuel jet velocity is 22.2 m/s during injection; Reynolds number ≈ 5,000.

	Total Co-Flow Air Flow Rate: Q_{air} = 2.5 SCFM				Total Co-Flow Air Flow Rate: Q_{air} = 3.5 SCFM	
Swirl number (S)	Axial Air Flow Rate (Unit: SCFM)	Tangential Air Flow Rate (Unit: SCFM)		Swirl number (S)	Axial Air Flow Rate (Unit: SCFM)	Tangential Air Flow Rate (Unit: SCFM)
0	2.5	0		0	3.5	0
0.15	2.0	0.5		0.15	2.8	0.7
0.41	1.8	0.7		0.44	2.5	1.0
0.87	1.3	1.2		0.87	1.8	1.7
1.61	0.7	1.8		1.64	1.0	2.5

Table 2.2 – Swirl number and its associated volumetric flow rates of axially- and tangentially-injected co-flow air.

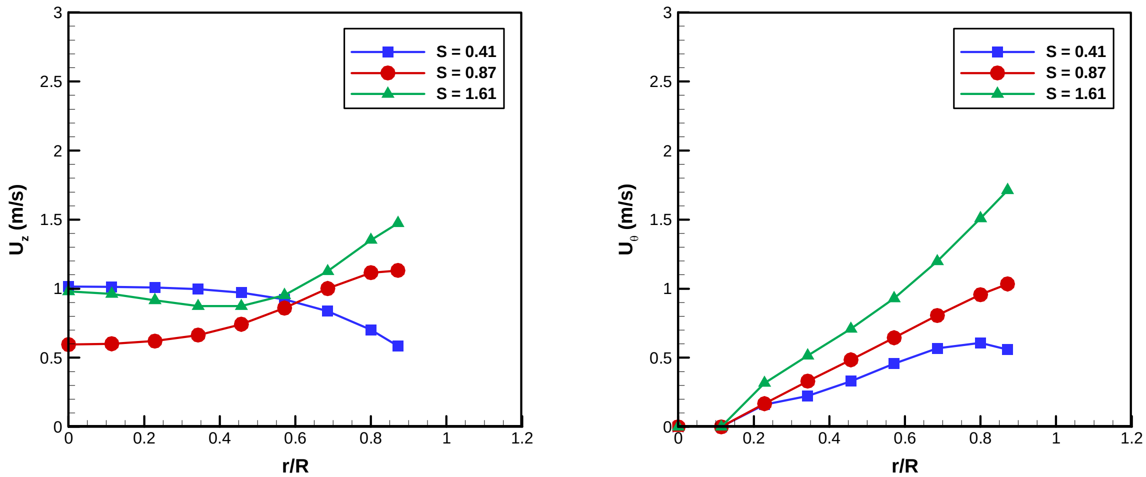

(a) Axial velocity **(b) Azimuthal velocity**

Figure 2.2 – Radial profiles of the mean velocity distribution for different swirl strengths. (a) Axial velocity (U_z); (b) Azimuthal velocity (U_θ).

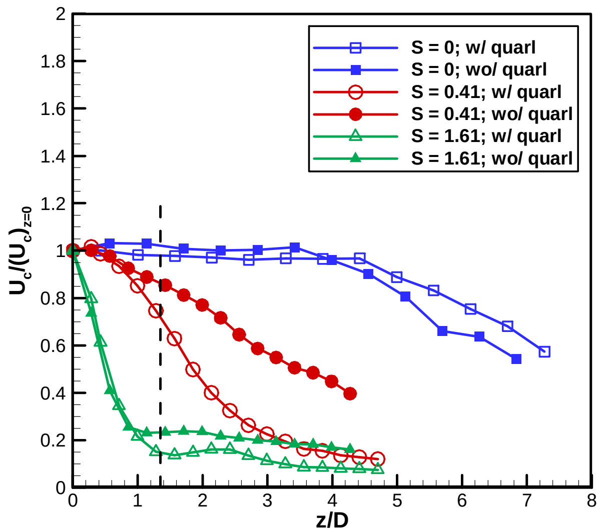

Figure 2.3 – Normalized centerline velocity along downstream distance for flows for various swirl strengths, both with and without the quarl. The volumetric flow rate is 2.5 SCFM.

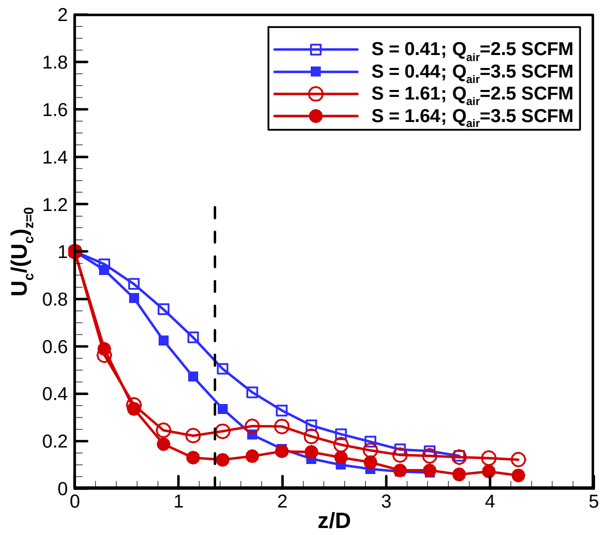

Figure 2.4 – Normalized centerline velocity profiles with downstream distance for different swirl strengths and volumetric air flow rates. The quarl is present for all conditions.

2.3 Diagnostics

2.3.1 High-Speed Video Imaging

Images of the flames were acquired using an 8-bit black and white CCD array with a spatial resolution of ≈ 1.8 mm/pixel at a framing rate of up to 400 frames/second. The camera was a *Kodak Megaplus* camera Model ES 310 Turbo with a *Computar* lens Model T2Z1816CS. The camera's maximum image size was 648 × 484 pixels at 85 fps; this was reduced to 320 × 101 pixels at a framing rate of up to 400 fps. The primary luminosity in these flames is due to radiating soot, which is roughly associated with the local reaction surfaces [64]. The 400 fps framing rate was sufficiently high to allow for both the accurate determination of the flame length, even for the shortest injection time in the current study, and also allow for the detailed study of the interactions between flame puffs.

The flame length for each flame puff was determined by *Spotlight*, an imaging tracking program developed by NASA, which effectively tracked the most downstream elements of the luminous flames as they approached burn-out. A luminosity level of 128 (a half of the pixel depth of an 8-bit grayscale image), where the luminosity had the sharpest spatial gradient [48], was chosen as the threshold for the flame edge determination. The ensemble average of these measurements was referred to here as the mean flame length. The measured mean flame length had an estimated error of 5-7%, depending on the test condition, based on the standard deviation in the measurement.

The motion of the luminous flame structures was investigated by the visual tracking of the time-resolved image sequences. Each 2-D flame image, taken at 400 fps, was effectively rendered through time, in a similar approach as 3-D volume rendering, but using time as the third dimension [65]. The volume rendering was performed by the volumetric data visualization software, *Slicer-Dicer* by *PIXOTEC LLC*. A 2-D image was then taken through the time axis from the created 3-D volume at the flame centerline (i.e. the centerline of the fuel nozzle). Thus, this 2-D image showed the evolution of puffs with time at the centerline of the fuel nozzle. The celerity of the turbulent flame puffs (i.e. the bulk velocity of puffs) was measured from the slope of the flame edges at various locations in the image. An example of the 2-D image from *Slicer-Dicer* is shown as Fig. 2.5. The error of the measured flame puff celerity was approximately 9-18% based on the standard deviations of the measured values.

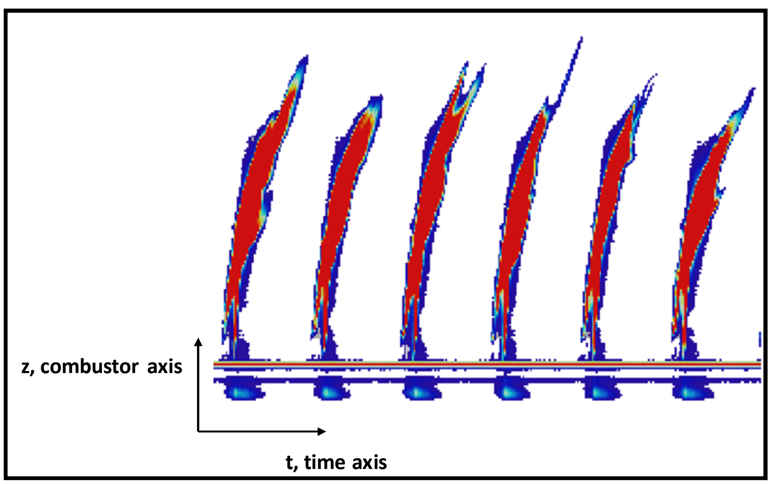

Figure 2.5 – Two-dimensional slice in (*z*, *t*) of a flame luminosity. The injection conditions were P = 6 and τ_{off} = 111.

2.3.2 Emissions Measurement

Measurements of emissions were performed using standard emissions analyzers combined with an aspirated sampling probe located downstream of the visible flame tip. A schematic diagram of the emission system layout is shown in Fig. 2.6. A chiller was to remove water from the sample gas stream and particle filters (μm scale) were used to eliminate soot. The concentrations of NO and the total NO_x were measured using a *ThermoElectron* Model 42C chemiluminescent analyzer. The levels of CO were determined by a *California Analytical Instruments* Model 602P non-dispersive infrared analyzer. The analyzer was also equipped with a paramagnetic oxygen detector for the measurement of oxygen concentration. Emissions analyzers were calibrated with a zero gas and various span gases with a specific concentration respectively. The zero gas was 99.99% nitrogen (N_2).

The emissions measurements were taken on the centerline of the combustor at a location downstream of the visible flame tip, at $z \approx 1.8\ L$; where z was the downstream distance and L was the averaged flame length. A survey of emissions versus downstream distance was performed to ensure that by that downstream location all chemical reactions were complete. Recording of emissions data commenced 3 minutes after the start-up of every test condition and lasted for another 3 minutes. During recording, the emissions data were taken every 30 seconds to allow for the relatively long response time of the emissions instruments (10-30 seconds). These data were then averaged as the mean concentration of sample gas from which the Emission Indices were calculated.

The uncooled sampling probe [66] was made of stainless steel. The probe had a tapered tip with a 3 mm inlet orifice, as shown in Fig. 2.7. In order to counteract a possible drift in the calibration of each analyzer and improve the accuracy of emissions measurement, the instruments were re-calibrated approximately every 1-2 hours.

The Emission Index (EI) was used to characterize the emission levels in this investigation. By directly comparing the amount of each emissions species to that of the injected fuel, the EI effectively takes into account all effects of variable air entrainment and dilution due to pulsing [49]. Neglecting any soot downstream of the flame tip and assuming that all the fuel carbon appears as either CO_2 or CO, the emission index can then be defined as [40]:

$$EI_i = \left(\frac{\chi_i}{\chi_{CO} + \chi_{CO_2}} \right) \left(\frac{xMW_i}{MW_f} \right) \qquad \text{Eq. 2-4}$$

where χ is the mole fraction of species *i*, CO, and CO_2, respectively. *x* is the number of moles of carbon in a mole of fuel C_xH_y, and MW_i and MW_f are the molecular weight of species *i* and the fuel, respectively. The uncertainty in the emission indices was ± 6%, based on the standard deviation from the measurements.

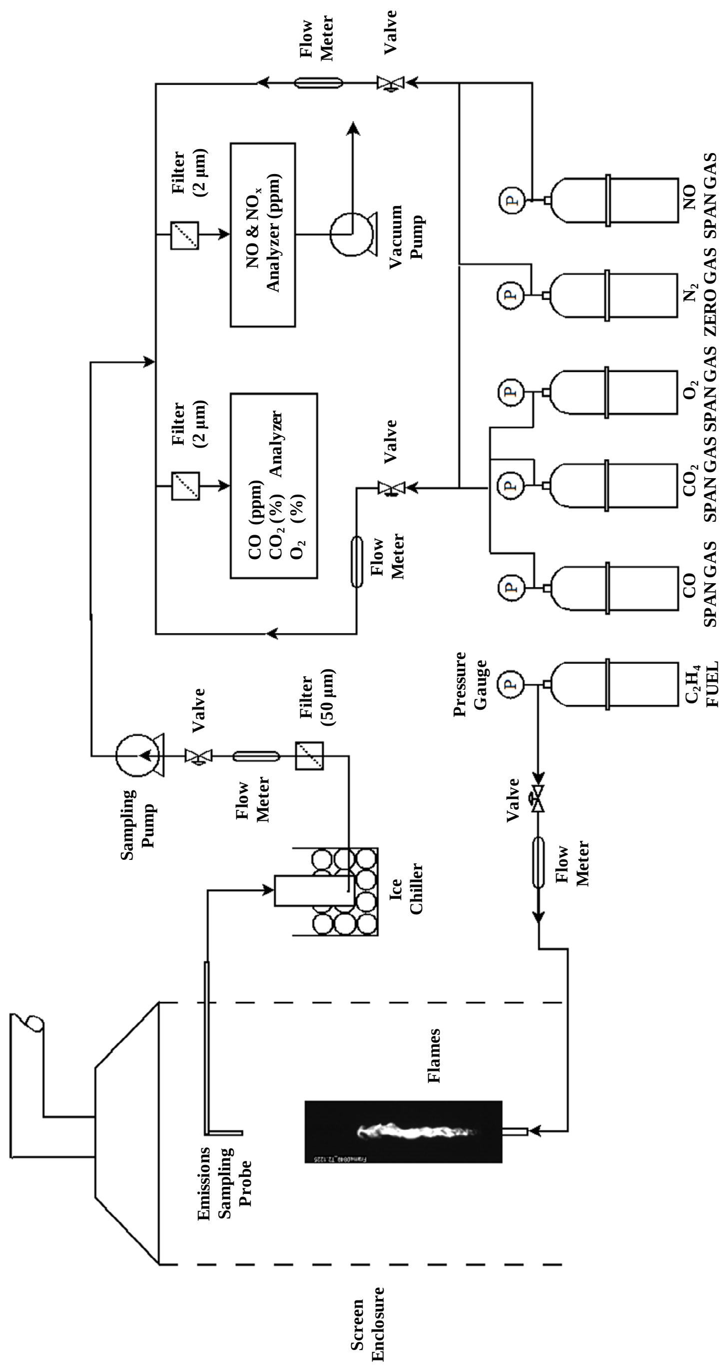

Figure 2.6 – Schematic of emissions measurement system.

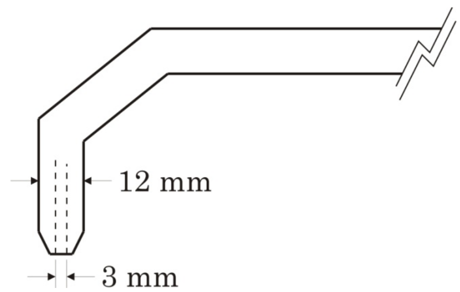

Figure 2.7 – Schematic of emissions sampling probe [48].

2.3.3 OH Planar Laser-Induced Fluorescence (PLIF) Imaging

The arrangement of OH PLIF imaging system is shown in Fig. 2.8. The PLIF system consisted of an Nd:YAG laser, a dye laser with a frequency extension unit, laser sheet forming optics, an intensified CCD camera, and appropriate optical filters. The Nd:YAG laser was a *Spectra-Physics* Model GCR-130 operated at a wavelength of λ = 532 nm with a repetition rate of 10 Hz and a pulse duration of 6-8 ns. The output beam at 532 nm had an energy of approximately 200 mJ per pulse. The dye laser, pumped by the Nd:YAG laser, was *Continuum* Model ND6000 with a wavelength tuning range of 420-590 nm, depending on the selection of laser dye. For the current research, the laser dye was Rhodamine 6G (also known as Rhodamine 590) dissolved in methanol. The output of the frequency-doubled dye laser was at a wavelength of around 283 nm, with an energy of approximately 10 mJ/pulse. The selection of the $Q_1(6)$ excitation line (283 nm) at the transition band of $A^2\Sigma^+$ (v' = 1) – $X^2\Pi$ (v'' = 0) was to provide reasonably strong OH PLIF signals while minimizing the Boltzmann population sensitivity to temperature in a range of 1,400-2,200 K [67]. A brief introduction of PLIF imaging and a discussion of the challenges of performing PLIF in hydrocarbon-fueled flames is found in Appendix A.

To allow for spatial PLIF imaging, the laser beam was expanded into a laser sheet, with approximately 15 cm in height and estimated 300 μm thickness at the center of the imaging plane (i.e. the fuel nozzle centerline). The sheet forming optics consisted of two fused-silica cylindrical lenses with focal lengths of 40 and 1000 mm respectively. The laser sheet inhomogeneity was taken into account in processing the PLIF images by using a test image consisting of the laser-induced fluorescence of a volume of uniform acetone vapor [67]. However, no attempt was made to correct for the variation of the sheet intensity along the beam propagation direction, thus some laser sheet attenuation across the flame may be present.

The OH fluorescence from the $A^2\Sigma$ ($v' = 0$) – $X^2\Pi$ ($v'' = 0$) and the $A^2\Sigma$ ($v' = 1$) – $X^2\Pi$ ($v'' = 1$) transition bands (λ = 306-320 nm) was collected by an intensified CCD camera (*Princeton Instruments* Model PI-MAX2, 512 × 512 pixels) equipped with an UV 105 mm, *f*/4.0 lens (*UKA Optics*). The camera, placed orthogonally to the laser sheet, was fitted with a WG-305 and UG-1 glass filters to reject the flame luminosity and scattering from the incident laser sheet. Any unwanted signal can be further diminished by setting the exposure time to be as short as 20 ns. The field-of-view was set to be about 79.4 × 79.4 mm, which was spatially sufficient to image the full width of the flame at the location of its maximum width. This allowed imaging of a region of flames extending over 75 jet nozzle diameters, implying that a maximum of approximately five image planes will suffice to image the entire regions of all the flames in this study. To improve the signal-to-noise ratio (S/N ratio), each 4 × 4 pixel region was spatially averaged (data binning) [68], resulting in a spatial resolution of 620 μm/pixel. The camera was synchronized with the laser pulse, with the laser being the master clock. Although the available Nd:YAG pump laser was limited to a pulsing rate of 10 Hz, the OH PLIF imaging on strongly-pulsed flames can be carried out by phase-locking the laser to the jet injection (i.e. the initiation of the jet injection was triggered by the laser pulse).

In this work, the OH radical was primarily used as an approximate marker of the reaction zone and the OH PLIF imaging was to study the reaction zone structure. The imaging regions of OH PLIF are shown in Fig. 2.9. For steady flames, the OH PLIF imaging was employed to cover the entire flame, while, for strongly-pulsed flames, the imaging of OH PLIF was only performed at two downstream regions of LOC I and LOC II, due to the lack of OH signal downstream of the relatively short flame length of strongly-pulsed flames. The laser energy was monitored before and after the image acquisition for each test condition and the variation in laser energy was found to be less than 2%.

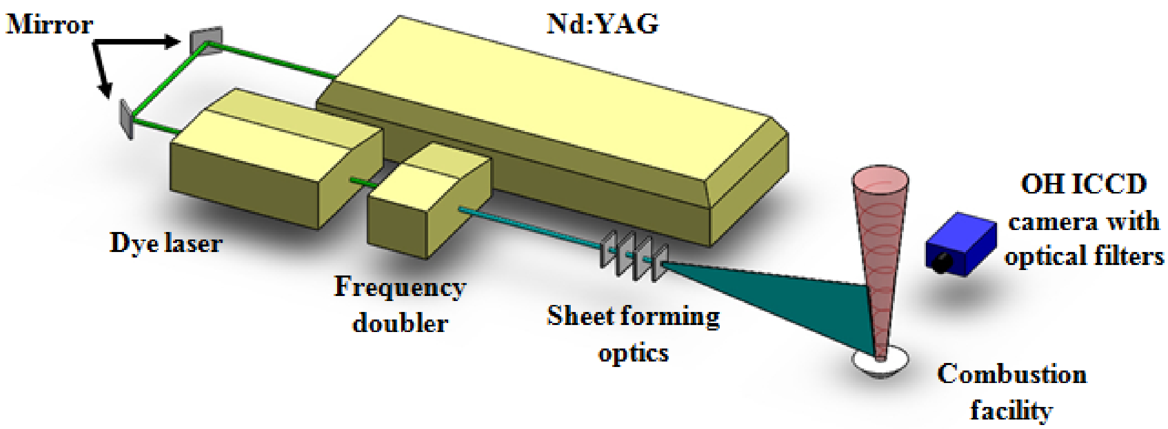

Figure 2.8 – Schematic of the OH PLIF imaging system.

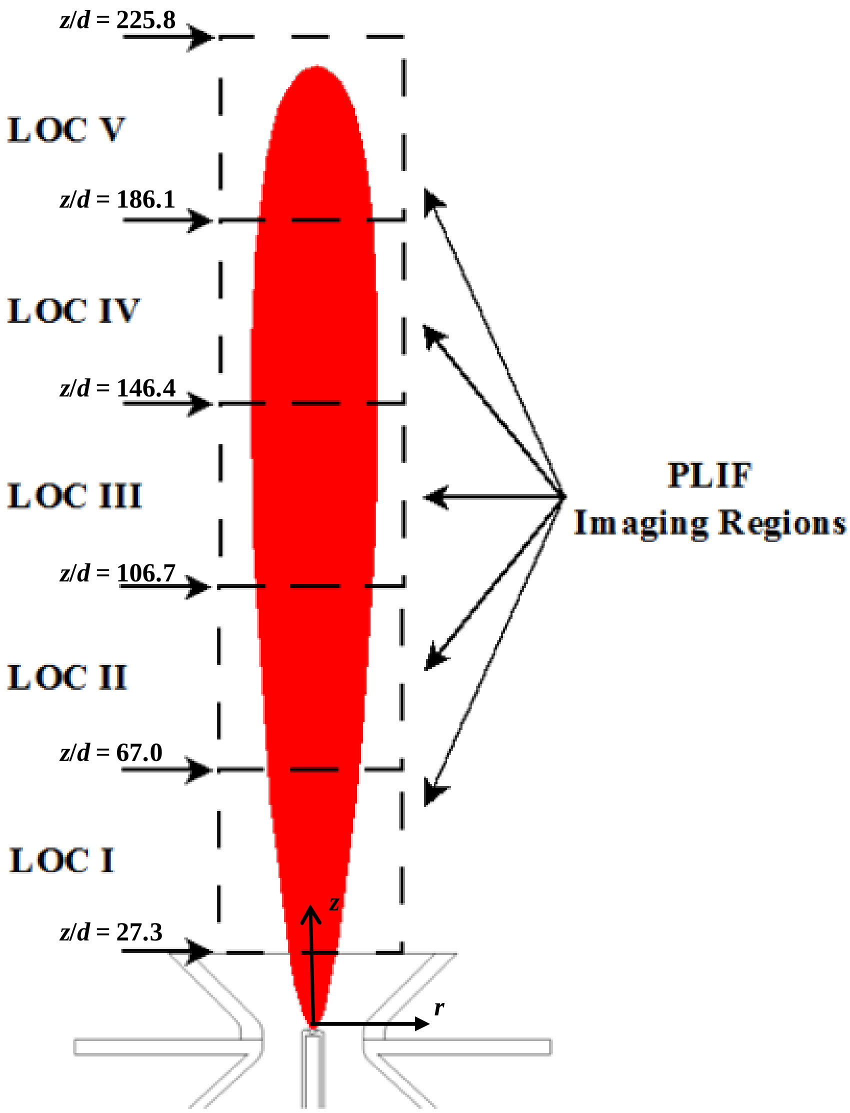

Figure 2.9 – Sketch of OH PLIF imaging regions.

CHAPTER 3

TURBULENT FLAME STRUCTURE

One goal of the current research is to study the large-scale turbulent structure of strongly-pulsed flames with the presence of a swirling co-flow. The effect of swirl on the structure dynamics of turbulent jet flames, including steady and strongly-pulsed flames, is presented and discussed in this chapter. Steady flames, both with and without swirl, are discussed first, followed by strongly-pulsed flames with and without swirl. For strongly-pulsed flames, several important factors, such as the fuel injection conditions, the co-flow strength, and the addition of a quarl are discussed. Three scaling relations are presented to account the impact of the volumetric fuel-to-air flow rate ratio and swirl on the visible flame length. All of the results presented here are with the presence of the quarl, unless otherwise stated.

3.1 Structure of Steady Flames with/without Swirl

The flame length of a diffusion flame, in general, is considered to be the distance required to entrain sufficient oxidizer to dilute the fuel to the stoichiometric ratio, the dilution being primarily governed by the rate of oxidizer entrainment [69]. That suggests that altering the mechanism by which the oxidizer is entrained and mixed with the fuel can significantly modify the flame length.

Representative images of turbulent steady flames, both with and without the quarl, with different swirl levels and with two volumetric co-flow flow rates are shown in Fig. 3.1. A typical long and slender turbulent jet flame structure is observed for non-swirled flames. A gradual decrease in the visual flame length with the increased swirl level is apparent for both co-flow

flow rates employed here. In addition, the flames with swirl are seen to become somewhat wider with increasing swirl, specifically with the high co-flow flow rate and with the addition of the quarl, as can be seen in Fig. 3.1. The swirled flames also appear to exhibit a somewhat more convoluted flame surface than non-swirled flames. The effect of swirl on the normalized length of steady flames is quantified in Fig. 3.2. The maximum reduction in the visible flame length is up to 35% for a swirl number of S = 1.6 with the quarl present. The shorter flame length with increasing swirl suggests an increased rate of entrainment due to swirl, and implies that the rate of entrainment in swirled flames can be varied by controlling the amount of swirl. A comparable result was also found in Chen & Driscoll's study [11] for a similar mass flow rate ratio of fuel to air, but for a different fuel and Reynolds number.

For non-swirled steady flames, the variation in the strength of co-flow employed in the current study is not seen to have a significant impact on the flame length. Chen & Driscoll [51], by contrast, reported that an increased coaxial flow can cause a significant reduction in flame length. One difference between that work and the current study is the choice of fuel. Ethylene was used as the fuel in the current study with an air-to-fuel velocity ratio of 0.05 and 0.08 for a co-flow of 2.5 SCFM and 3.5 SCFM, respectively. By contrast, Chen & Driscoll used hydrogen and methane fuels, observing reductions in flame length of 18% and 3%, respectively, for a similar range of air-to-fuel velocity ratio employed here. One possibility accounting for the difference could be the ventilation condition of flames. All flames in the current study were over-ventilated, e.g. the volumetric fuel-to-air flow ratio was below the stoichiometric fuel-air ratio; however, most flames in Chen & Driscoll's study [51] had a fuel-to-air flow ratio that exceeded the stoichiometric ratio. In addition, with the similar fuel nozzle diameter employed in their study and the current work, the relatively low density of hydrogen and methane implies that a given Reynolds number (≈ 5,000 in both studies) led to a higher jet velocity; hence a larger increase in the amount of co-flow air within an identical range of air-to-fuel velocity ratio, than for the case of ethylene fuel. This large increase in the amount of co-flow air, implying more air dilution, can be expected to result in a shorter downstream distance needed in order to dilute the fuel to stoichiometric proportions [74], thus leading to a more obvious variation in flame length. In any case, results reported in the current study and observations from Chen & Driscoll's study are both in agreement with the analytical formulations of Dahm & Mayman's analysis [70] on the effect of coaxial air on the length of a turbulent non-premixed flame.

The addition of the quarl has a negligible impact on the flame length for the non-swirled flames studied here. It should be pointed out that since the amount of the co-flow in all cases reported here is sufficient to significantly over-ventilate the flame, air from the surroundings has little impact on the flame in the vicinity of the combustor exit plane when the quarl is not present.

For swirled, steady flames, the co-flow strength is seen to have an impact on the flame length, an effect not observed for the non-swirled cases mentioned previously. For most cases studied here, swirled flames with the higher co-flow flow rate (3.5 SCFM) are shorter than those with the lower co-flow flow rate (2.5 SCFM), regardless of the presence of the quarl. In general, a greater reduction of 8-10% in flame length is observed for swirled flames with a co-flow of 3.5 SCFM than for those with 2.5 SCFM.

The volumetric flow ratio of fuel to air has been shown to have an impact on the flame structure of swirled diffusion flames [11,37]. In Chen & Driscoll's study [11], lowering the volumetric fuel-to-air flow ratio by decreasing the flow rate of the fuel, while keeping the air flow rate fixed resulted in a shortening of the flame by approximately 20% for a given swirl level. Although a detailed explanation of that observation was not provided, the study supports the argument that the mixing for swirled flames depends not only on the fuel flow conditions, but also on the air co-flow conditions [9]. In the current study, decreasing the fuel-to-air flow ratio was achieved by increasing the volume of the co-flow air. For a fixed swirl number, an increased air flow leads to a higher angular momentum flux and a higher angular velocity, which could, in turn, increase the turbulence level [14], leading to an increased entrainment and mixing and resulting in a shorter flame.

In addition to the impact of co-flow strength on the flame length of swirled flames, a greater reduction of flame length, up to 10%, is seen for swirled flames with the presence of the quarl than those without the quarl (see Fig. 3.2). The effect of the nozzle geometry on the flow pattern of a swirling jet was reported by, for example, Beér & Chigier [14]. Their study suggests that the use of a divergent nozzle has a combined effect of stabilizing the swirling flow and increasing the recirculating mass flow rate. Based on this finding, the addition of the quarl in the current study is believed to improve the stability of the swirl flow and favor the formation of a recirculation zone for a sufficiently strong swirl [9, 14]. Chen & Driscoll [11] have shown that the air engulfment mechanism within the recirculation zone is similar to that in an eddy in a shear layer proposed by Broadwell & Breidenthal [100] while the characteristic velocity and length scale of the recirculation zone could be larger, compared to those of an eddy. Swirl and the accompanying recirculation zone tend to increase the turbulence in the flow field [9] and are expected to improve, in turn, the rate of oxidizer entrainment and mixing, resulting in a shortened flame length.

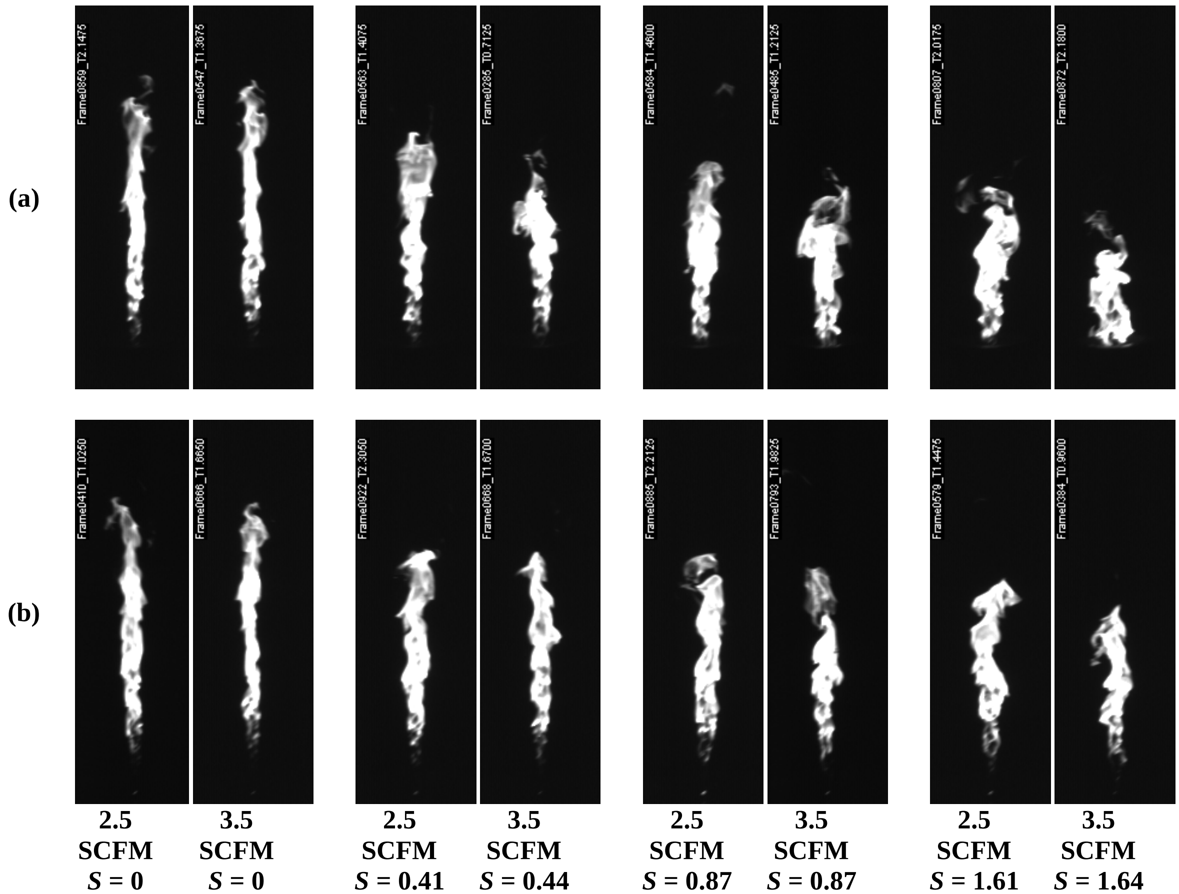

Figure 3.1 – Instantaneous visual flame images of steady flames with different swirl levels for co-flow strengths of 2.5 and 3.5 SCFM. (a) With quarl; (b) without quarl. The image height is 57.9 cm.

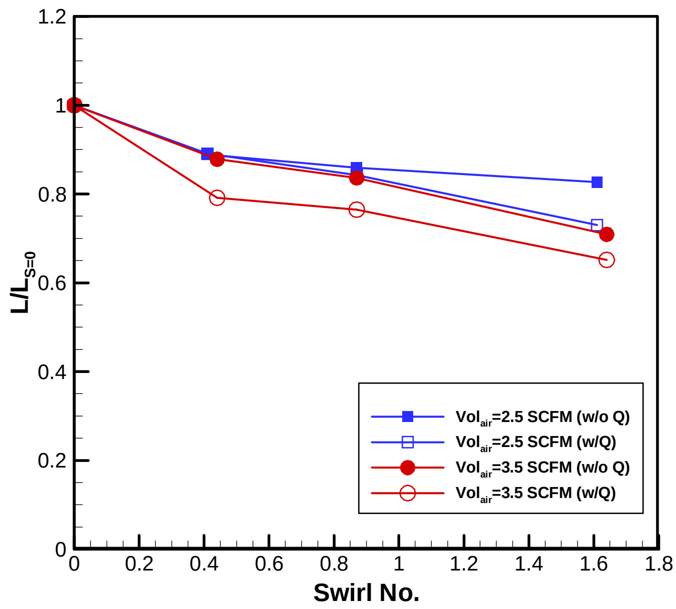

Figure 3.2 – Impact of swirl on the normalized visual flame length of steady flames, with and without the quarl, for co-flow strengths of 2.5 and 3.5 SCFM.

3.2 Structure of Strongly-Pulsed Flames with/without Swirl

Distinctive types of flames are shown in Fig. 3.3 for various injection times with co-flow strengths of 2.5 and 3.5 SCFM and different swirl levels, and in Fig. 3.4 for various jet-off times, respectively. The non-swirled strongly-pulsed flames exhibit an elongated structure for high injection times ($P > 8$), similar in behavior to that of steady flames; while, for short injection times ($P \leq 8$), flames appear to be more compact and have puff-like structures, depending on the jet-off time. Flames with interacting structures ($\tau_{off} \leq 444$) have a relatively longer flame length than those with isolated puff structures ($\tau_{off} > 444$), presumably due to the more competition between the flame puff and its neighboring structures for the available oxidizer, resulting in a decreased rate of entrainment [71], leading to a long flame length. For a fixed jet-off time, a shorter injection time implies a smaller injected fuel volume, thus resulting in a shorter flame length. Flames with a relatively shorter flame length also occur with relatively longer jet-off times for a fixed injection time, due to the decreased competition between flame puff structures, resulting in an increased rate of entrainment and a shorter flame length. All of the results on the flame structure of strongly-pulsed flames without swirl are applicable to both of the co-flow strengths applied here and are fully consistent with the previous research on these types of flames [48], for a different co-flow strength and combustor geometry. According to Hermanson *et al*. [7], a dimensionless injection time of $P = 8$ is a threshold value between elongated ($P > 8$) and compact, puff-like ($P \leq 8$) flame structures; while the dimensionless jet-off time of $\tau_{off} \approx 400$ is the threshold value for interacting ($\tau_{off} \leq 400$) and isolated ($\tau_{off} > 400$) flame puff structures, very similar to the results reported here.

As seen in steady flames, a decrease in the visible flame length of strongly-pulsed flames, due to swirl, is evident in Fig. 3.3 and Fig. 3.4 for all injection conditions. Although swirl is seen to decrease the flame length of strongly-pulsed flames, the impact of swirl on the length of strongly-pulsed flames can depend on the injection conditions and the co-flow strength, as discussed later in this chapter. Similar to steady flames, strongly-pulsed flames with swirl appear qualitatively to exhibit a somewhat more convoluted flame surface compared to the cases without swirl, in particular for flames with a strong swirl (S = 1.6) and the higher co-flow strength. At a given swirl level, flames with long injection times (i.e. flames with elongated structures; $P > 8$) exhibit a similar structure to that of steady flames. In addition, the length of flames with elongated structures seems to be impacted more by swirl than that of flames with puff-like structures ($P \leq 8$). For flames with $P \leq 8$, increasing the swirl level from S = 0.4 to S = 1.6 seems to have comparatively little impact on the length of these flames, regardless of the jet-off time. Explanations accounting for these observations will be provided in Section 3.2.2 along with the quantitative measurement of the visible flame length.

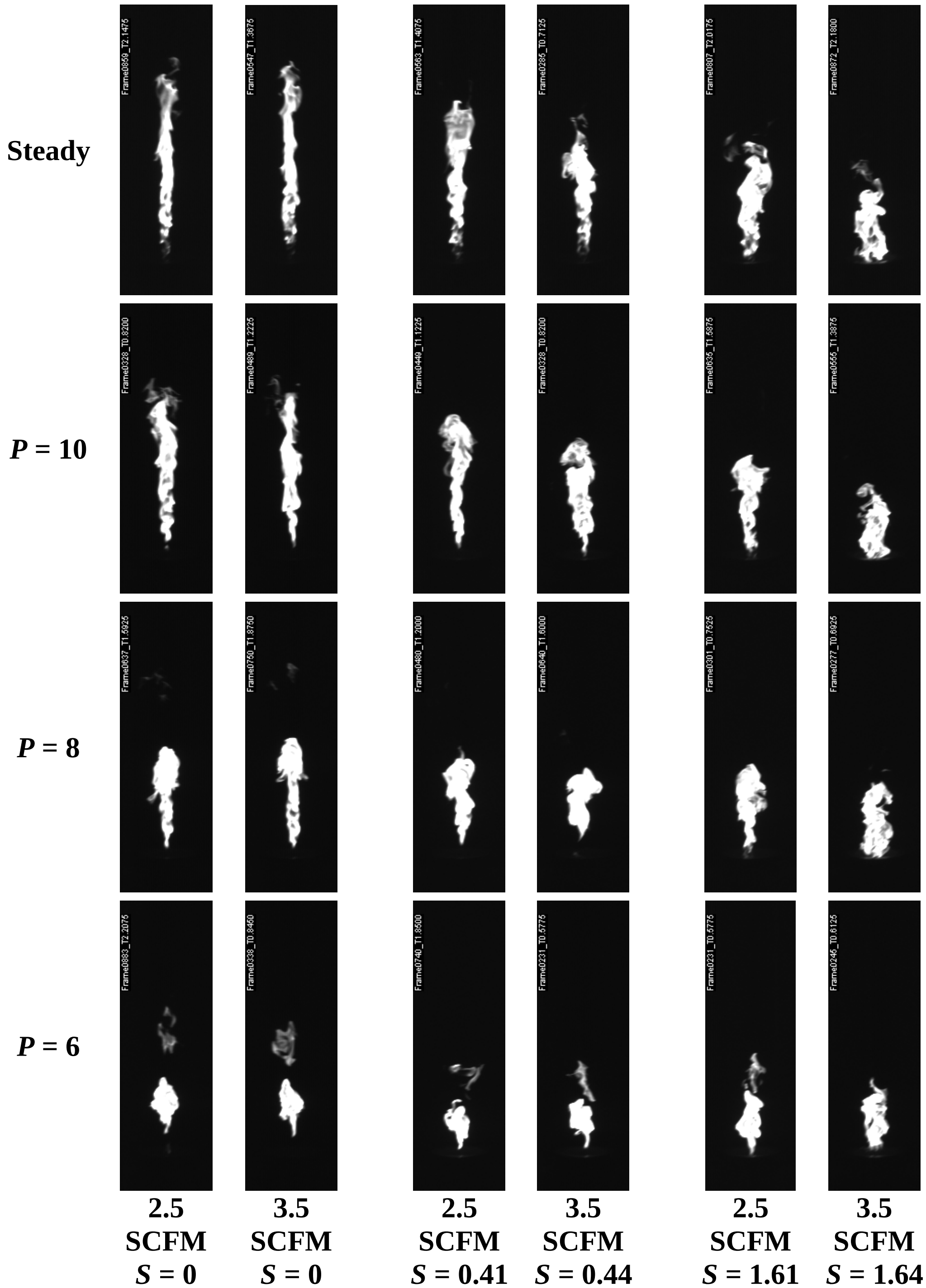

Figure 3.3 – Representative instantaneous flame images with different injection times, different swirl levels, and two co-flow flow rates of 2.5 and 3.5 SCFM. The dimensionless jet-off time for all the cases of strongly-pulsed flames is τ_{off} = 111 (t_{off} = 10 ms). The image height is 57.9 cm.

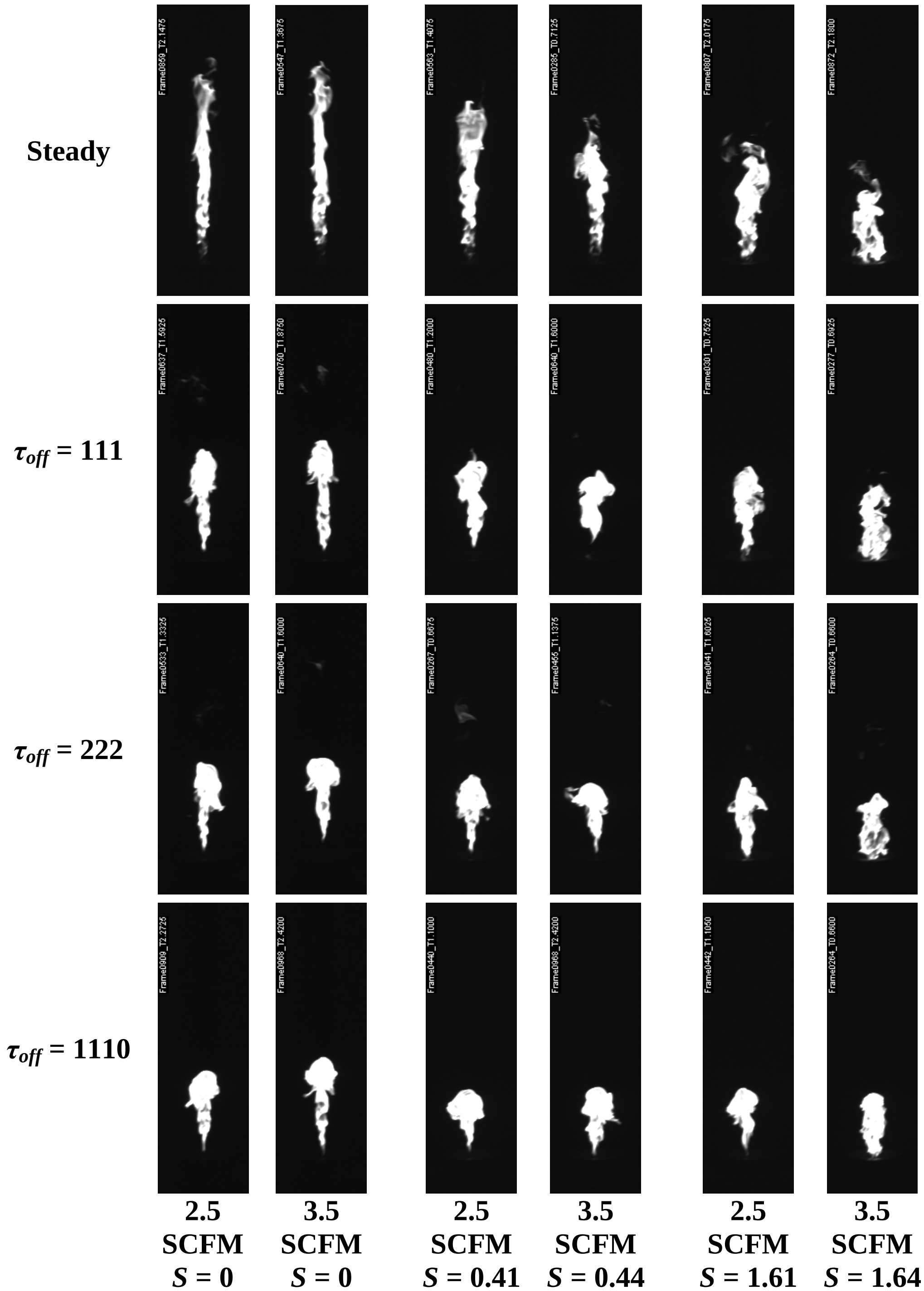

Figure 3.4 – Representative instantaneous flame images with different jet-off times, different swirl levels, and two co-flow flow rates of 2.5 and 3.5 SCFM. The dimensionless injection time for all the cases of strongly-pulsed flames is P = 8 (t_{on} = 46.17 ms). The image height is 57.9 cm.

3.2.1 Impact of Swirl on Flame Puff Separation

For strongly-pulsed flames, the separation between a given flame puff and its neighboring structures is mainly governed by the jet-off time. This separation has been considered as an indication of the degree of competition between structures for the entrainment of the available oxidizer, as mentioned previously. In addition to the jet-off time, swirl is also seen to have an impact on the flame puff separation. Examination of the videos showed that the separation distance between adjacent puffs at a given point in the cycle was generally decreased by swirl and further decreased with increased co-flow strength for a given swirl level. Time-resolved image sequences of the flame luminosity for a typical interacting flame structure are shown in Fig. 3.5 for different levels of swirl. The high-speed visual imaging (such as that shown in Fig. 3.5) indicates both a decrease in flame puff separation and a decrease in flame puff celerity with increasing swirl. The decreased celerity of puffs is consistent with a more rapid momentum exchange between the fuel jet and the surrounding co-flow air, suggesting an increased rate of air entrainment due to swirl. However, the effect of swirl on the entrainment could be limited by the nature of strongly-pulsed flames. Specifically, for strongly-pulsed flames, a decreased separation would be expected to result in a stronger competition between flame puffs, leading to a decreased rate of oxidizer entrainment and mixing [54]. Thus, the amount of such an increase in the rate of entrainment due to swirl could be limited by the decreased flame-puff separation. With sufficiently strong swirl, the flame puff separation becomes almost indistinguishable in strongly-interacting flames ($\tau_{off} < 222$) and these flames appear to resemble steady flames, as shown in Fig. 3.5. In addition, the co-flow strength is also seen to have an impact on the flame puff separation for strongly-pulsed flames, both with and without swirl. The effects of co-flow strength on the flame structure of strongly-pulsed flames, both with and without swirl, are discussed further in Section 3.2.3. The celerity of the flame puffs is discussed further in Section 3.4.

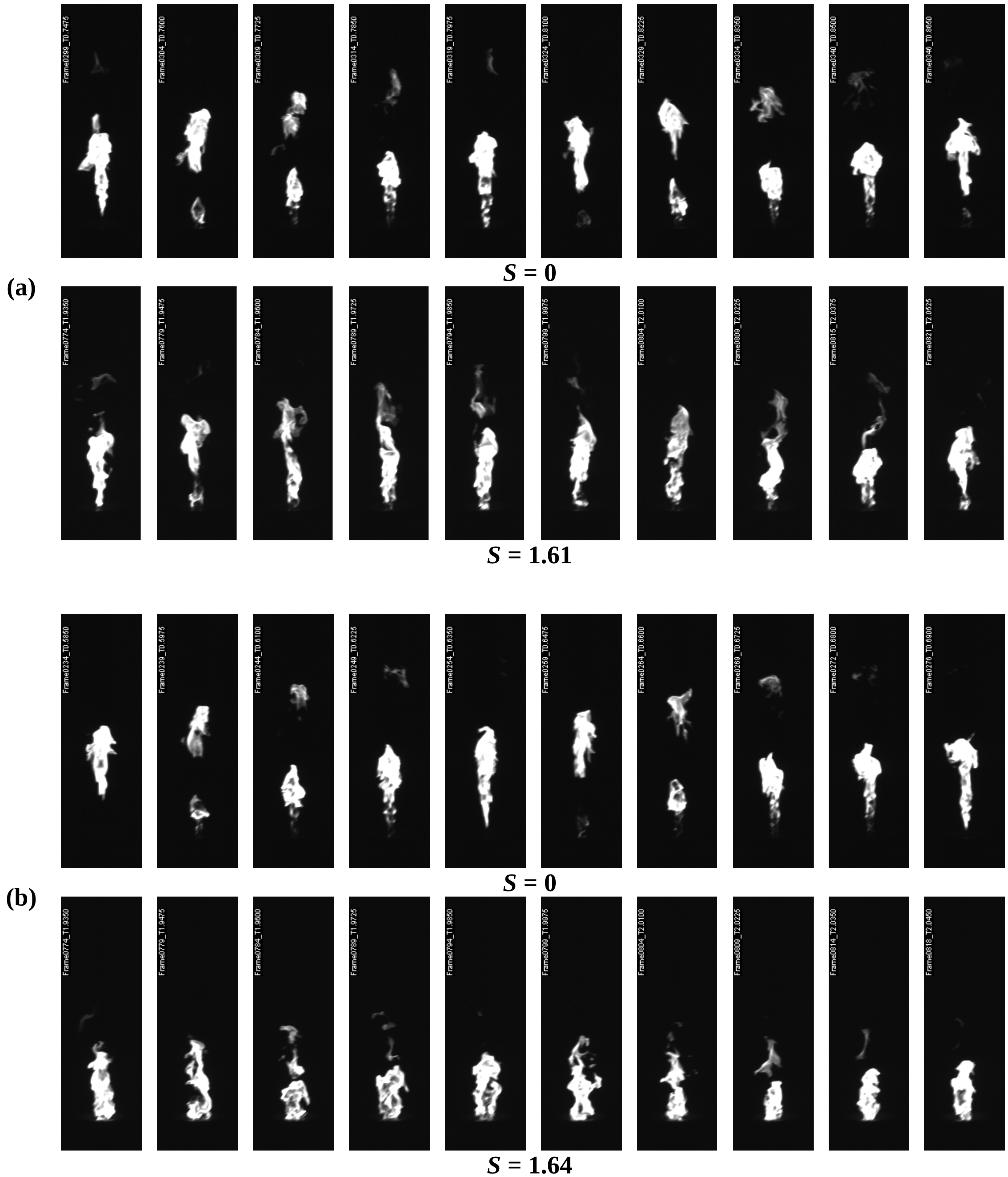

Figure 3.5 – Sequence of flame luminosity through a typical injection cycle of strongly-pulsed flames, both with and without swirl, with interacting flame structures. (a) Co-flow 2.5 SCFM. (b) Co-flow 3.5 SCFM. The injection conditions are P = 8 and τ_{off} = 111. The time interval between each image is 12.5 ms and the image height is 57.9 cm. All results are with the quarl present.

3.2.2 Impact of Swirl on Visible Flame Length

For non-premixed flames, the flame length serves as a good indication of the overall rate of entrainment, with a shorter flame length suggesting a more rapid rate of entrainment and mixing [69]. The normalized flame length for strongly-pulsed flames, both with and without swirl, with various injection conditions is quantified in Fig. 3.6 with a co-flow of (a) 2.5 SCFM and (b) 3.5 SCFM. In the current study, the flames with swirl are found to be 4-34% shorter than non-swirled flames for the same injection conditions, depending on the co-flow strength. The imposition of swirl is found to have a relatively stronger effect on the flame length of steady flames than that of strongly-pulsed flames, as shown in Fig. 3.6. In addition, the length of strongly-pulsed flames seems to be impacted more by swirl for higher injection times than for shorter injection times, as seen in Fig. 3.6. For example, steady flames with a co-flow flow rate of 2.5 SCFM have a reduction of 15% in flame length at S = 0.41; a further increase in swirl level from S = 0.41 to S = 1.61 appears to lead a reduction in flame length up to 24%. However, such increased swirl level only leads to 7% more reduction in flame length for flames with P = 10 and no apparent decrease in flame length is evident for flames with $P \leq 8$ when the swirl level is increased from S = 0.41 to S = 1.61. Similar observations are also made for flames with a co-flow flow rate of 3.5 SCFM. These effects are explained below.

The relatively weaker effect of swirl on the length of strongly-pulsed flames compared to the steady flames could be due to a combination of 1) the relatively shorter residence time and 2) the lesser amount of heat release (due to the smaller volume of the injected fuel) of strongly-pulsed flames than that of steady flames. Regarding the first point, flames with relatively longer injection times (P > 8) exhibit a relatively longer flame length, suggesting a longer residence time for fuel to interact with the swirling co-flow air, leading to a greater decrease in flame length than those with relatively shorter injection times ($P \leq 8$). On the second point, for strongly-pulsed flames, the injected fuel volume, directly governed by the injection time, affects not only the residence time of interaction between the fuel and the co-flow air, but also the amount of heat release, which could in turn affect the flow recirculation and thus mixing and flame length [33]. Specifically, Tangirala *et al*. [33] found that increasing the amount of heat release resulted in a number of benefits, including an increase in the recirculation, the turbulence levels, and the flame stability. They suggested that heat release helps to drive the recirculation due to the gas expansion due to combustion.

Although swirl was seen to result in a decrease in the flame puff separation, the impact of swirl on the flame length, in most cases, was similar for each value of the jet-off time, as seen in Fig. 3.6. The similar impact of jet-off time on the flame length of strongly-pulsed flames, both with and without swirl, suggests that the degree of competition between flame structures has a similar, significant impact on the flame length of strongly-pulsed flames, regardless of the co-flow swirl.

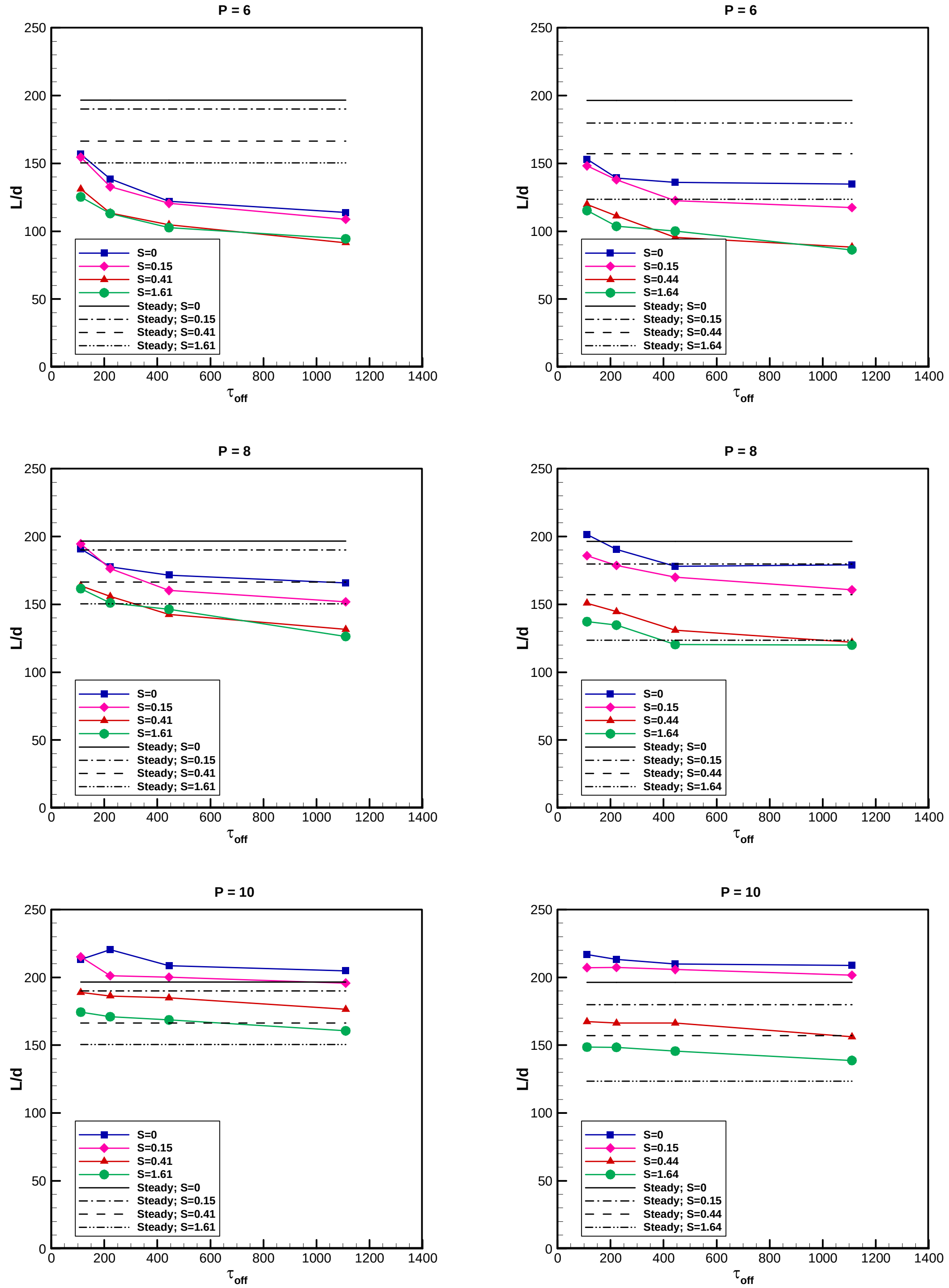

(a) Q_{air} = 2.5 SCFM **(b) Q_{air} = 3.5 SCFM**

Figure 3.6 – Normalized flame length of strongly-pulsed flames, both with and without swirl, for various injection conditions, with a co-flow of (a) 2.5 SCFM. (b) 3.5 SCFM. All results are with the quarl present.

3.2.3 Impact of Co-Flow Strength on Large-Scale Flame Structure

The co-flow strength is found to have an impact on the flame puff separation and the visible flame length of strongly-pulsed flames, both with and without swirl, as shown in Figs. 3.5 and 3.6.

- **Impact of co-flow strength on non-swirled, strongly-pulsed flames**

For non-swirled, strongly-pulsed flames, the separation between flame puffs for interacting flames ($\tau_{off} \leq 444$) is seen to increase slightly with increased co-flow strength, as seen in Fig. 3.5. The increased separation is possibly due to the decreased shear between the fuel jet and the surrounding co-flow air, in that the decreased shear would be expected to decrease the rate of entrainment, leading to less momentum exchange between the fuel jet and the surrounding co-flow air. Thus, the flame puff would travel downstream while retaining relatively more of its initial injected momentum, resulting in a higher celerity leading to the observed modest increase in separation between flame puffs.

In addition, it is found that the higher co-flow strength resulted in a relatively greater increase in flame length for isolated puff-like flames ($P \leq 8$) than for elongated flames ($P > 8$), as seen in Fig. 3.6. As the P value increases (beyond $P = 8$) and more elongated flames result, the sensitivity of the mean flame length to the co-flow strength decreases markedly, regardless of the jet-off time. The effect of non-swirling co-flow on the length of non-swirled, strongly-pulsed flames was also studied by Hermanson *et al*. [72], who reported little impact of co-flow strength on elongated flames. It is also found in the current study that for flames with $P \leq 8$, the co-flow strength has different degrees of impact on the length of these flames with interacting and isolated flame puff structures, depending on the jet-off time. The flame length is found to be somewhat less sensitive to the co-flow strength for flames with highly-interacting puff structures (τ_{off} ≤ 111) than those with more-spaced puff structures (τ_{off} ≥ 222) for P ≤ 8. All of the dimensionless jet-off times (τ_{off}) in Hermanson *et al.*'s study [72] were around 3,000, considerably larger than the maximum value of τ_{off} = 1110 in the current study.

- **Impact of co-flow strength on swirled, strongly-pulsed flames**

As seen in Fig. 3.5 and in Appendices B and C, increasing the co-flow strength generally decreases the separation between flame puffs for swirled, strongly-pulsed flames for a fixed swirl level. A similar cause described in Section 3.1 could account for this decreased flame puff separation. That is, for a fixed swirl level, the higher co-flow strength would result in higher angular momentum than the lower co-flow strength, which could, in turn, increase the turbulence in the flow, leading to an increased rate of entrainment, resulting in a more rapid momentum exchange between the fuel jet and the swirling co-flow. Thus, a decreased separation between flame puffs, due to the increased strength of co-flow, could be expected.

A decrease in flame length up to 14% is observed for the higher co-flow strength, depending on the fuel injection conditions and the swirl level. In contrast to non-swirled flames, the flame length of swirled, strongly-pulsed flames, for P > 8, is found to be more sensitive to changes in the co-flow strength than that for P ≤ 8, regardless of the jet-off time. For P ≤ 8, the strength of co-flow has a proportionally greater impact on the flames with interacting structures (τ_{off} ≤ 444) than the flames with isolated flame puffs (τ_{off} > 444). The impact of co-flow strength on the mean flame length of swirled, strongly-pulsed flames gradually decreases as the value of P decreases, as seen in Fig. 3.6.

The different sensitivities to co-flow strength for interacting flames and isolated flames, both with and without swirl, could be attributed to the combination of the degree of competition between flame puffs due to their separation, and the residence time available for fuel to interact with the co-flow air. For strongly-pulsed flames without swirl, the degree of competition is presumably highest for flames with closely-spaced, interacting structures ($\tau_{off} \leq 111$). Due to the high competition, there would be expected to be limited momentum exchange between the fuel jet and the co-flow air, in which case the flame puffs would be expected to persist downstream while retaining relatively more of their initial injection momentum. This effect would not be expected to be significantly impacted by changes in the co-flow strength. On the other hand, flames characterized by relatively more-spaced flame structures that occur for $\tau_{off} \geq 222$ would be expected to have a more rapid momentum exchange with the surroundings, due to the relative lack of competition between structures for the surrounding co-flow air [48]. Thus, any change of the co-flow momentum would affect the momentum exchange between the fuel and the co-flow relatively more strongly for these flames, and would thus result in the observed changes in flame length. The available residence time for fuel to interact with the swirling co-flow will be directly related to the distance the flame puffs travel before burn-out. The further downstream the flames travel before burn-out, the more impact the swirling co-flow would be expected to have on the flames due to the longer residence time. This would be the case for flames with interacting flame puffs, which exhibit a longer flame length than those with isolated flame puffs for a given injection time. Similarly, flames with a long injection time ($P > 8$) have a relatively longer flame length, suggesting the longer residence for fuel to interact with the swirling co-flow air. Therefore, the high strength of the swirling co-flow would be expected to result in a greater decrease in the length of interacting flames and flames with long injection times, while having comparatively less impact on the length of isolated flames and flames with short injection times, as seen for flames with $\tau_{off} > 444$, and $P = 6$ and $P = 8$ in Fig. 3.6.

3.2.4 Effect of the Quarl on Flame Structure

The addition of the quarl stabilizes the swirling flow and helps the formation of the recirculation zone [14]. The normalized flame length of strongly-pulsed flames, both with and without swirl, without the presence of the quarl is shown in Fig. 3.7 (the corresponding results with the quarl present were shown in Fig. 3.6). For non-swirled, strongly-pulsed flames, the addition of the quarl apparently results in no significant impact on the flame length, as was seen to be the case in steady flames. It should be pointed out that any given co-flow volume flow rate sufficient to fully ventilate steady flames will be even more abundant in providing oxidizer to strongly-pulsed flames. Therefore, any possible additional air drawn into the flame from the surroundings when the quarl is absent is not expected to significantly affect the flame length of non-swirled, strongly-pulsed flames.

However, the addition of the quarl does impact the flame length of strongly-pulsed flames with swirl, in a fashion similar to steady flames, as shown in Fig. 3.2. The addition of a quarl has been suggested to favor the formation of a recirculation zone where rapid entrainment and intense mixing occur [14], as mentioned in Section 3.1. In general, the maximum reduction in flame length for flames without the quarl is about 23% with strong swirl, compared to 34% for the cases with the quarl.

In addition to the impact on the flame length, the presence of the quarl is also found to have an impact on the separation between flame structures for swirled, strongly-pulsed flames. Image sequences of typical strongly-pulsed flames with interacting flame structures without the quarl are shown in Fig. 3.8. As compared to the images in Fig. 3.5 where the quarl was present, the separation between flame structures for swirled flames without the quarl is more apparent than those with the quarl and only slightly decreases as swirl is imposed. The more decrease in flame length and flame puff separation for the cases with the quarl is consistent with the increased rate of entrainment and mixing due to the addition of the quarl, as discussed in Section 3.1.

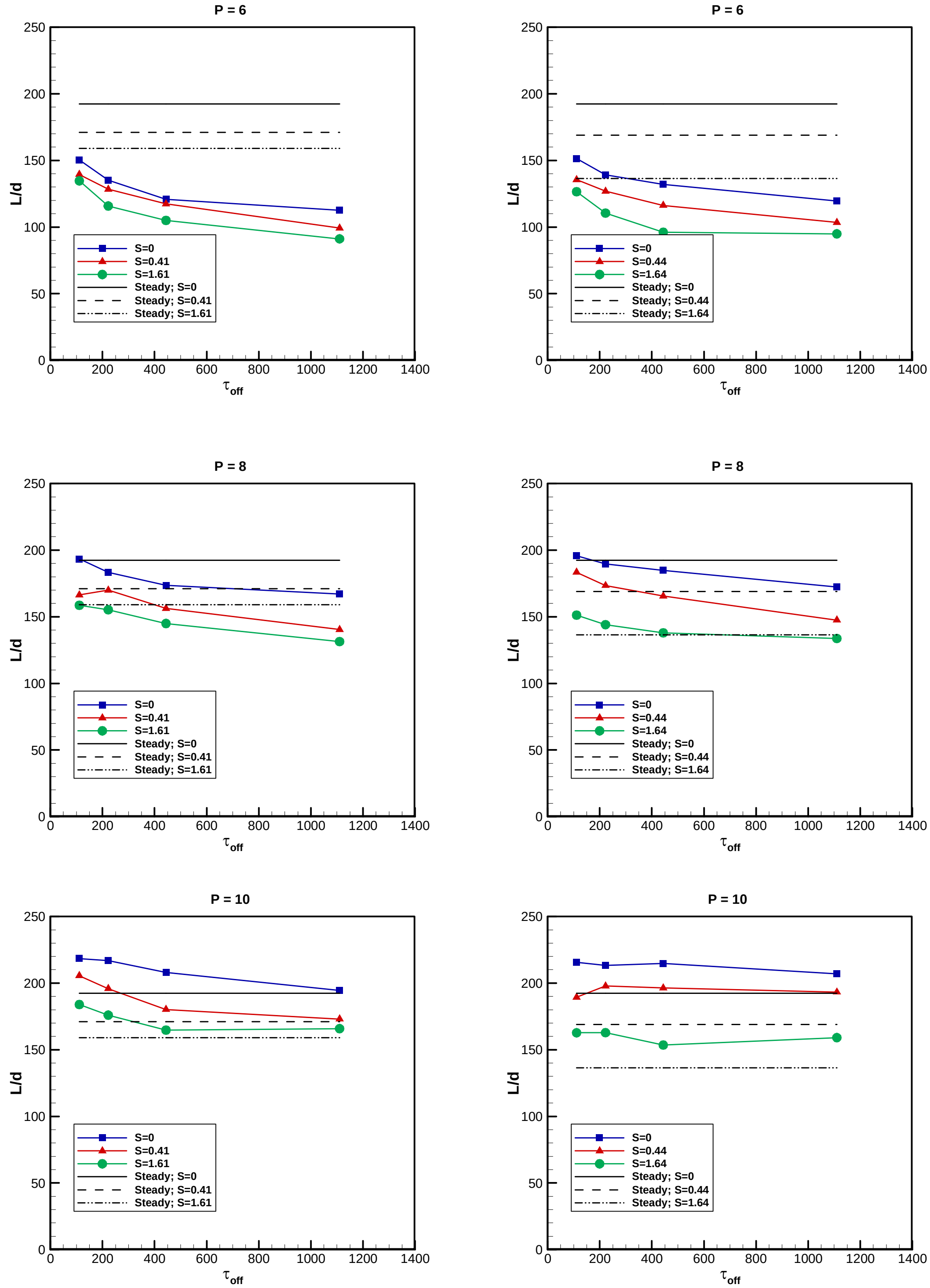

(a) Q_{air} = 2.5 SCFM (b) Q_{air} = 3.5 SCFM

Figure 3.7 – Normalized flame length of strongly-pulsed flames, both with and without swirl, for various injection conditions, with a co-flow of (a) 2.5 SCFM and (b) 3.5 SCFM. All results are without the quarl present.

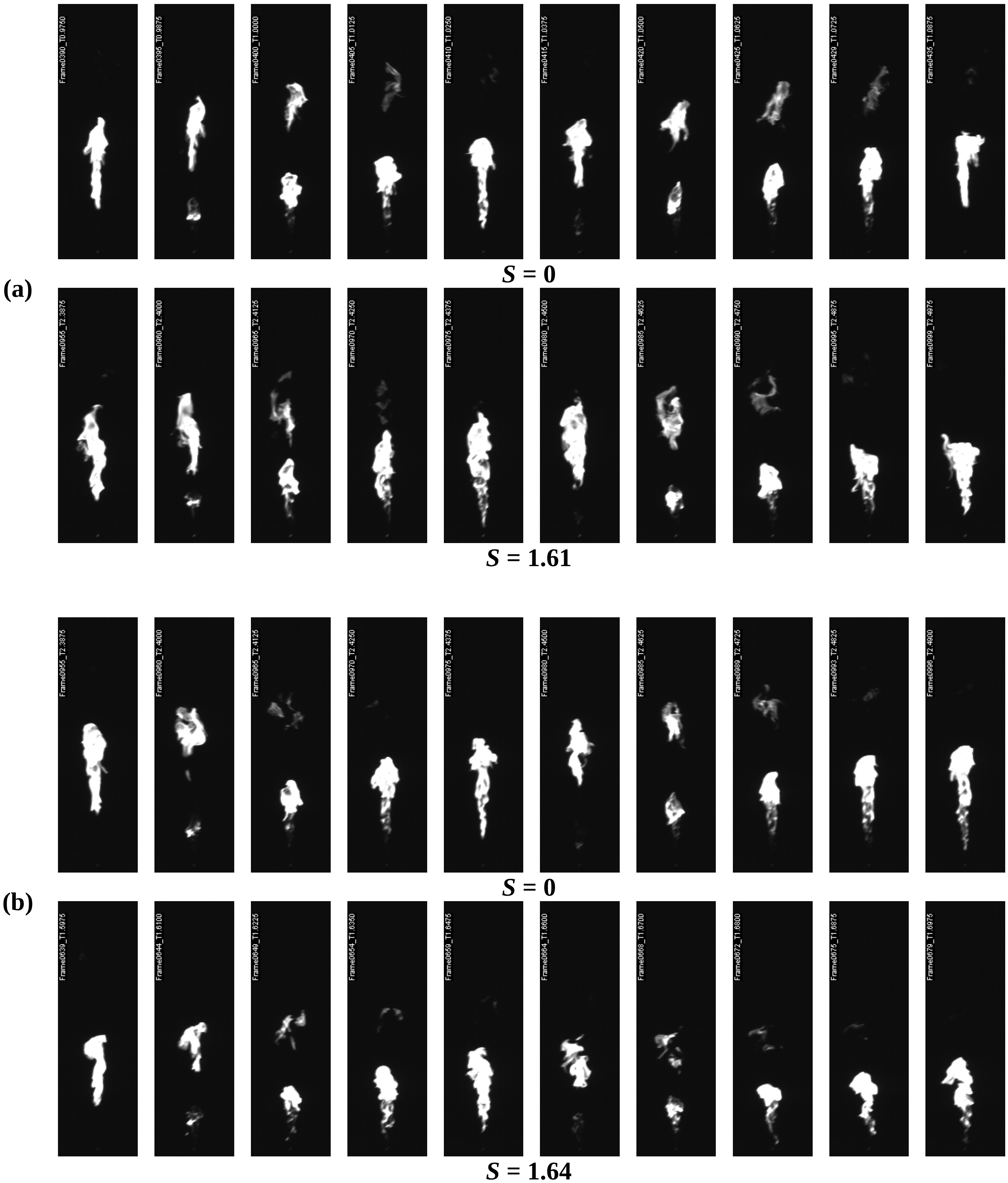

Figure 3.8 – Sequence of flame luminosity through a typical injection cycle of strongly-pulsed flames, both with and without swirl, with interacting flame structures. (a) Co-flow of 2.5 SCFM. (b) Co-flow of 3.5 SCFM. The injection conditions are P = 8 and τ_{off} = 111. The time interval between each image is 12.5 ms and the image height is 57.9 cm. All results are without the quarl present.

3.3 Flame Length Scaling

The flame length of both swirled and non-swirled, strongly-pulsed flames has been seen to be strongly dependent on the injection time. Thus, it is expected that the injected volume of fuel could have a significant impact on the flame length of these flames. The classical concept presented by Hawthorne *et al*. [69] for the length of a turbulent jet flame burning in ambient air without a co-flow is useful here to relate the injected volume of fuel to the average visible flame length of strongly-pulsed flames, both with and without swirl. According to Hawthorne *et al*., the flame length can be considered to be the distance needed to entrain sufficient air to dilute the fuel to the stoichiometric ratio. For all strongly-pulsed flames, both with and without swirl, the volume of the injected fuel is directly proportional to the cube of the dimensionless injection time, P, by definition. Assuming that, for a given jet-off time, the combustion is essentially complete (i.e. the fuel is completely consumed during the combustion process) during every jet-injection cycle, the volume of air entrained into the flame would be proportional to the cube of the average flame length. This suggests that the normalized flame length in strongly-pulsed flames, both with and without swirl, can be written as:

$$L/d \sim \Psi^{1/3} P \ ,$$

where Ψ is the stoichiometric air-fuel ratio on a volume basis with the value of Ψ = 14.34 for ethylene/air flames. Figure 3.9 shows the result of employing this flame length scaling relation versus the jet-off time. This scaling is seen to be of some utility in characterizing the observed flame length for all injection times (i.e. values of P) considered here. A very similar scaling approach was used in Johari's study [73] for isothermal buoyant puffs in aqueous media, in which the volume of buoyant puffs consisted of the entrained fluid and the injected fluid, resulting in a different scaling constant than that for jet flames.

The results presented in Figs. 3.6 and 3.7 showed that the effect of swirl on the length of strongly-pulsed flames is evidently more dependent on the jet injection time (*P*) than the jet-off time (τ_{off}). This variation in flame length with *P* is taken into account in the scaling employed in Fig. 3.9. The effect of co-flow strength on strongly-pulsed flames, both with and without swirl, is also shown in Fig. 3.9. With the higher co-flow strength, the flame length showed somewhat less dependence on jet-off time at any imposed swirl level than for the case of the lower co-flow strength. The scaling employed in Fig. 3.9 also reflects a somewhat stronger effect of co-flow on non-swirled, isolated flame puffs and swirled, interacting flames, as discussed previously.

A further scaling to account for variations in flame length can be developed to take into account the volume flow rate ratio of the injected fuel to the co-flow air over the injection cycle. It has been shown that the normalized flame length for strongly-pulsed flames without swirl appears to scale linearly with the dimensionless injection time, *P*, which is based on the cube root of the injected fuel volume for different jet-on fractions [7, 48]. In the previous scaling relation based on the Hawthorne concept, the normalized flame length, taking into account the variation in injection times, is a clear function of the jet-off time. All of these scaling relations reflect the fact that the nature of the interaction between the injected fuel and its surrounding co-flow has a significant impact on the flame length. The modified scaling is shown in Fig. 3.10, for a co-flow of (a) 2.5 SCFM and (b) 3.5 SCFM, with the volume flow rate ratio of the injected fuel to the supplied co-flow air in an injection cycle, $(Q_{fuel}/Q_{air})_{cycle}$, on the abscissa. This scaling parameter takes into account the variation in the jet-off time and the co-flow flow rate. Figure 3.10 shows that when taking into account the variations in injection times, the normalized flame length appears to scale linearly with the volume flow rate ratio of the injected fuel and the supplied co-flow air during the corresponding injection cycle. This scaling relation does not explicitly reveal the interaction level between flame puffs on the co-flow air, but indicates the overall impact of co-flow air dilution on the flame length.

The effect of co-flow air dilution on the reduction in flame length for turbulent jet diffusion flames was reported by Driscoll *et al*. [10, 51], as discussed previously in Section 3.1. It was shown there that the increased co-flow air in that case reduced the downstream distance needed in order to dilute the fuel to stoichiometric proportions [74], thus reducing the flame length. For flames studied here with a given injection time, a long jet-off time means more air provided for a given injected fuel volume in an injection cycle, resulting in a relatively shorter flame length for flames with such jet-off time than that for flames with a short jet-off time. Similarly, for a given jet-off time, longer injection times lead to a higher overall fuel-to-air volume flow rate ratio during each injection cycle, resulting in a longer flame length for flames with long injection times than that for flames with relatively shorter injection times.

The scaling relation shown in Fig. 3.10 shows similar trends for all strongly-pulsed flames, both with and without swirl, but with a slightly different slope and level, depending on the swirl level and the co-flow strength. This similarity in normalized flame length with the fuel/air volume ratio over each cycle could reasonably be expected for both swirled and non-swirled flames, while a shorter flame is achieved with swirl imposed. An apparent decrease in the scaled flame length due to swirl is apparent, as shown in Fig. 3.10. In addition, the effect of co-flow strength (as mentioned in Section 3.2.3) on the flame length of strongly-pulsed flames, both with and without swirl, can also be seen in Fig. 3.10.

For non-swirled, strongly-pulsed flames, it has been shown that for any given injection time the flame length normalized by the fuel nozzle diameter appears to be directly proportional to the jet-on fraction, α, where $\alpha = t_{on}/(t_{on} + t_{off})$ [48]. However, the proportionality constant varies with the value of the injection time, decreasing as the injection time increases [48]. The normalized flame length was also reported to scale linearly with the dimensionless injection time, P [48]. Furthermore, when taking into account the dimensionless injection time, the normalized flame length scales linearly with the volumetric fuel-to-air flow rate ratio, $(Q_{fuel}/Q_{air})_{cycle}$, as shown in Fig. 3.10. As mentioned previously, the volume of the injected fuel over each injection cycle is proportional to the cube of the dimensionless injection time. This suggests a scaling relation for the jet-on fraction in the strongly-pulsed flames, both with and without swirl and the developed scaling argument is shown in Fig. 3.11. The parameter on the ordinate is analogous to $(Q_{fuel}/Q_{air})_{cycle}$ but with Q_{fuel} being replaced by the volume occupied by the visible flame length. This corresponds to the assumption mentioned previously that the injected fuel is completely consumed by the combustion process during each injection cycle. This scaling relation shows that for strongly-pulsed flames, both with and without swirl, at a specific injection time, the length of flames would increase as the jet-on fraction increases (i.e. the jet-off time decreases) and reach a plateau where the jet-off time is short, suggesting the degree of the flame puff interaction being high, and the flames have a comparable length, regardless of the injection time. The values of the two plateaus for non-swirled flames with different co-flow strength are very comparable, but generally lower for swirled flames with the high co-flow strength, consistent with more decrease in flame length due to swirl for flames with the higher co-flow strength.

The three scaling relations presented here simply account for three distinctive characteristics for strongly-pulsed flames, both with and without swirl. First, the Hawthorne concept characterizes the impact of the injection time on the length of strongly-pulsed flames. Second, the volumetric flow rate ratio of $(Q_{fuel}/Q_{air})_{cycle}$ shows the significance of co-flow air dilution in each injection cycle on the these flames, which is mainly governed by the jet-off time.

The last scaling relation sums up the significance of the first two and reveals that when the amount of co-flow air in an injection cycle is taken into account, there would be a strong correlation between the jet-on fraction and the flame length of strongly-pulsed flames, both with and without swirl.

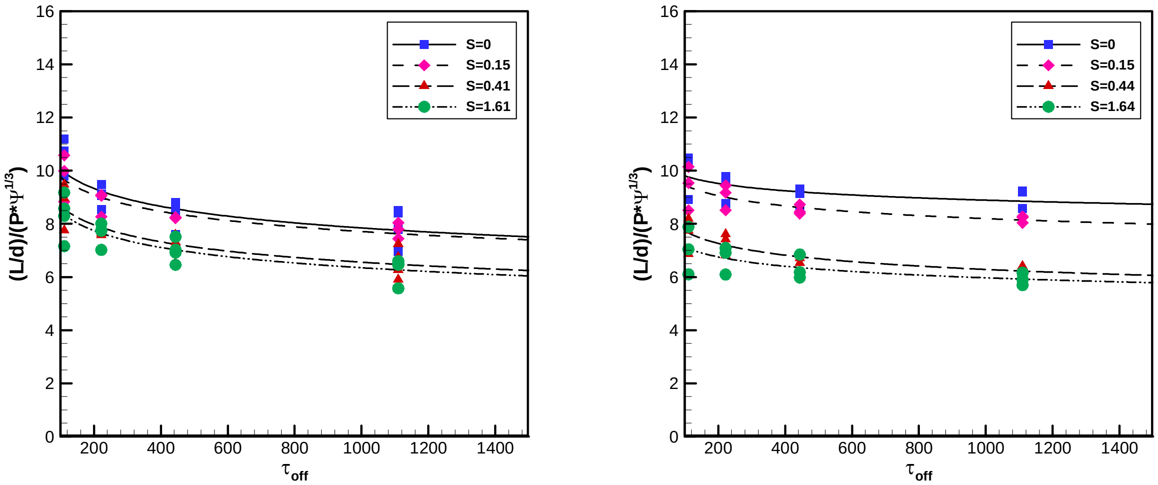

(a) Q_{air} = 2.5 SCFM **(b) Q_{air} = 3.5 SCFM**

Figure 3.9 – Scaling relation I: scaling of the mean flame length to take into account variations in injection times. Co-flow flow rate is (a) 2.5 SCFM and (b) 3.5 SCFM. All values of *P* for a given swirl level are plotted.

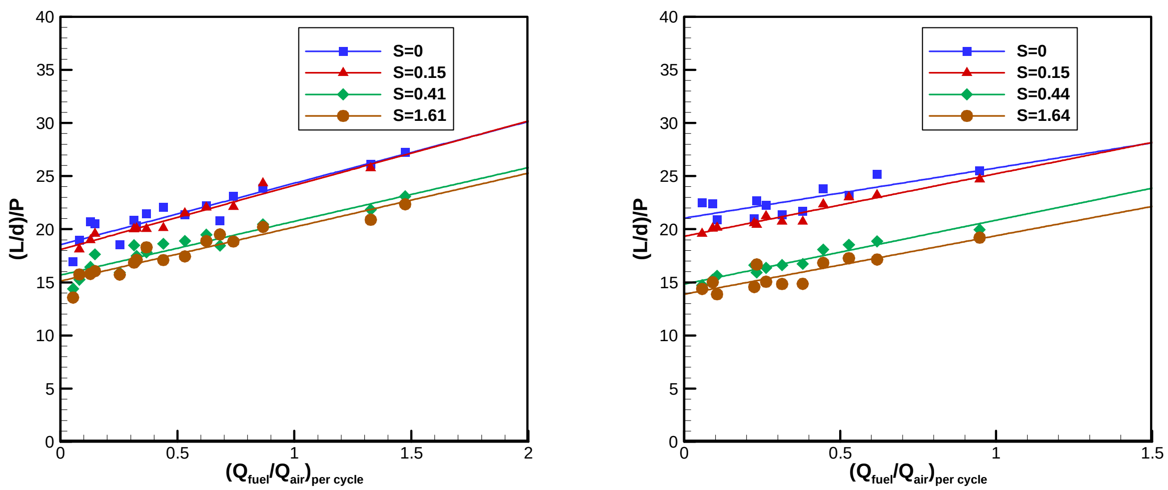

(a) Q_{air} = 2.5 SCFM **(b) Q_{air} = 3.5 SCFM**

Figure 3.10 – Scaling relation II: scaling of the normalized flame length, taking into account variations in injection times, and injected fuel and air volume flow rates in each injection cycle. Co-flow flow rate is (a) 2.5 SCFM and (b) 3.5 SCFM.

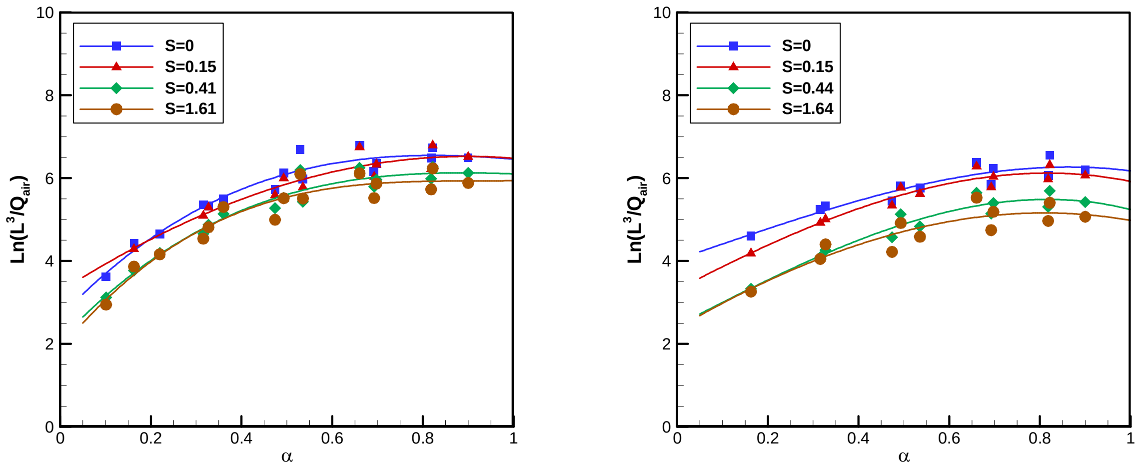

(a) Q_{air} = 2.5 SCFM **(b) Q_{air} = 3.5 SCFM**

Figure 3.11 – Scaling relation III: scaling of the flame length and the jet-on fraction, taking into account the volumetric flow rate of co-flow air in an injection cycle. Co-flow flow rate is (a) 2.5 SCFM and (b) 3.5 SCFM.

3.4 Flame Puff Celerity

The impact of swirl on the celerity of the large-scale flame structures, determined by using the visual tracking method discussed previously is presented in Fig. 3.12 for various downstream distances normalized by the flame length. The flame-puff celerity in strongly-pulsed flames, both with and without swirl, is strongly impacted by the jet-off time, increasing markedly for most injection times and downstream locations as the time between pulses is decreased, presumably due to the increased competition of air entrainment between a puff and its neighbors, as mentioned previously. This competition would serve to decrease the momentum exchange with air and would result in an increase in flame puff celerity, i.e. the celerity stays higher for a given downstream distance. A similar trend in celerity was reported by Fregeau [48] in non-swirled, strongly-pulsed flames for most injection conditions, as stated in the introduction. However, this trend in celerity is not seen to occur for one case, that of the shortest injection time with long jet-off time (P = 6, τ_{off} > 444), relatively near the nozzle exit at z/L = 0.5. For this injection condition, the flames appear to be relatively shorter and more compact than those with higher injection times and shorter jet-off times. The high flame puff celerity may have been due to the high fuel jet momentum at this location under this injection condition, leading to an increased celerity as τ_{off} increases.

The strongly-pulsed flames with swirl, for most injection times ($P \geq 6$) and downstream locations ($z/L \geq 0.7$), are generally seen to exhibit a lower celerity than those without swirl. The decrease in celerity due to swirl is up to 39%, depending on downstream locations and injection conditions. The decreased celerity occurs for all jet-off times at any downstream locations, even at z/L = 0.85, which is close to the visible flame tip, consistent with a greater momentum exchange between the fuel jet and air brought about by the presence of swirl. This is consistent with changes in flame length for strongly-pulsed flames with swirl.

Similar to non-swirled flames, for low dimensionless injection time, P = 6, swirled, strongly-pulsed flames also show an increased celerity with increased jet-off time. This increased celerity at close-to-nozzle downstream locations is presumably due to the high jet momentum, as stated previously, along with relatively closer distance from the nozzle, resulting in an even higher value in celerity. In addition, the swirled, strongly-pulsed flames at low injection times exhibit a rapid and drastic decrease of celerity in a very short downstream distance, particularly for high jet-off times. This drop in celerity is up to 80%, 33% more than that for non-swirled, strongly-pulsed flames. This is consistent with a more rapid and greater air entrainment for strongly-pulsed flames as swirl is imposed.

(a)

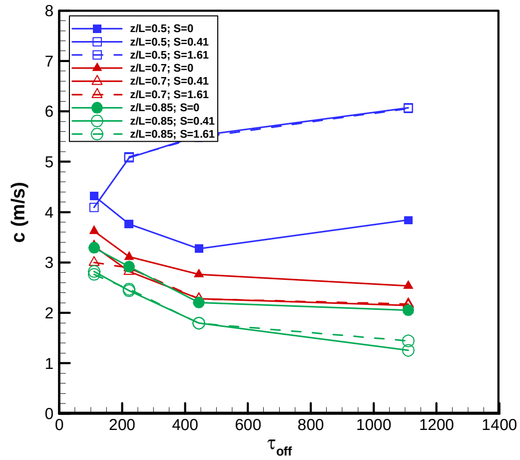

(b)

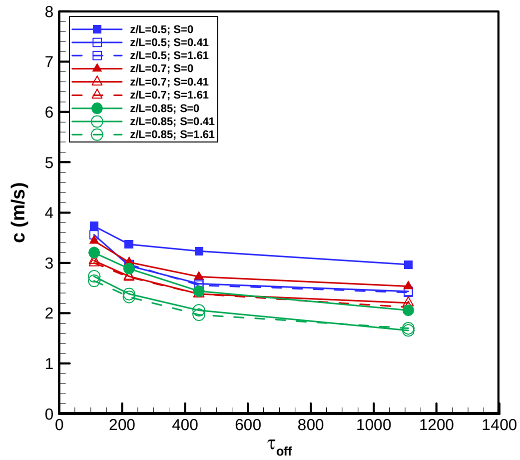

(c)

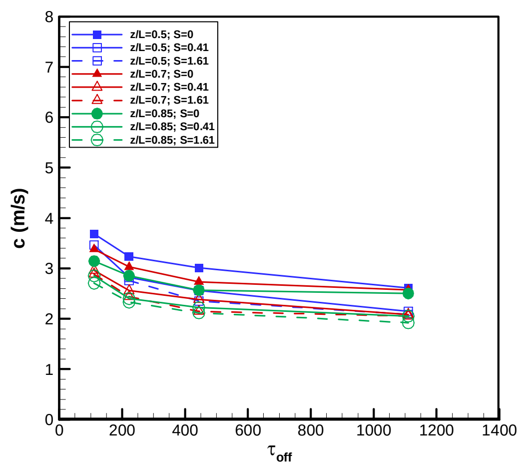

Figure 3.12 – Flame structure celerity in function of jet-off time at different downstream locations for various injection time of (a) *P* = 6, (b) *P* = 8, and (c) *P* = 10.

CHAPTER 4

EMISSIONS

The CO and NO_x emissions of steady and strongly-pulsed flames, both with and without swirl, are presented and discussed in this chapter. In particular, the impact of swirl on the emissions of the strongly-pulsed flames as well as the effect of the co-flow strength and the presence of a quarl on the emissions are discussed. The profile of emissions versus downstream distance is presented first; this survey ensured that the sampling probe location had no significant impact on the measured emissions of the flames. Similar to the flame structure scaling argument presented in the previous chapter, the volumetric fuel-to-air flow rate ratio can also be applied to account for the impact of air dilution on the emissions of strongly-pulsed flames, both with and without swirl.

The effect of the sampling probe position on the measured emission levels was investigated by situating the probe at different downstream locations relative to the visible flame tip, as shown in Fig. 4.1. A marked decrease in the CO levels, as indicated by the emission index, is observed as the probe location moves beyond the visible flame tip and the CO levels remain at a constant value for probe positions beyond that point. A more modest decrease in the level of NO is seen with downstream distance, with the NO emission index reaching a stable value at $z = 1.6L$ for most cases. In any case, the emission indices of CO and NO achieve stable values for $z \geq 1.8L$. This normalized location is comparable to that employed in the study of Drake *et al*. [66] where measurements were performed at the location $z = 2.0L$. In that work, probe conversion reactions (such as NO to NO_2) and the catalytic reduction of NO_x were found to be negligible for all probes employed. A similar situation is expected here owing to the relatively low average temperature (700-900 *K*) of the fuel-lean environment at downstream of the visible flame tip [7, 75]. All the emission measurements presented here were performed at z = 1.8L and with the quarl attached at the combustor exit, unless specified otherwise.

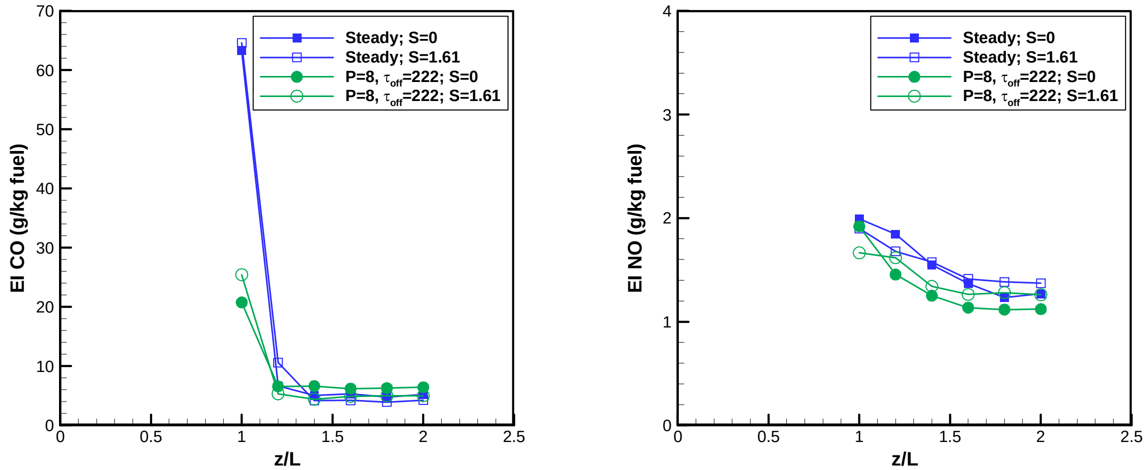

(a) EICO **(b) EINO**

Figure 4.1 – Impact of downstream location on measured (a) CO and (b) NO emission indices.

4.1 CO Emissions

The variation in the emission index of CO for strongly-pulsed flames, both with and without swirl, is shown in Fig. 4.2 for different injection conditions and for a co-flow of 2.5 SCFM. The overall CO emissions trends for the case of the higher co-flow flow rate are similar to those seen in Fig. 4.2. For non-swirled, strongly-pulsed flames, the highest EICO occurs with the shortest injection time, possibly due to quenching within the flame puffs owing to very rapid air entrainment and dilution [49]. For flames with $P \geq 10$, the EICO becomes comparable to the steady flame value for all values of jet-off time. The observed, relatively low emission index of CO with short jet-off time is consistent with the increased interaction between flame puffs, which generally results in a longer flame length due to a decreased rate of air entrainment per amount of fuel injected [48, 54]. The longer flame length implies a longer combustion residence time, allowing for more complete combustion and thus a lower amount of CO. These flames show broadly similar trends to those reported by Fregeau [48] for strongly-pulsed flames without swirl; the specific impacts of swirl are discussed next.

4.1.1 Impact of Swirl on CO Emissions

The imposition of co-flow swirl is generally seen to decrease the CO emissions of strongly-pulsed flames for some injection conditions, as seen in Fig. 4.2. This effect is strongest for flames with short injection times. Specifically, for a dimensionless injection time of $P \leq 8$, the EICO for flames with moderately interacting structures ($222 \leq \tau_{off} \leq 444$) with strong swirl ($S = 1.6$) decreases up to a factor of 2.5 compared to non-swirled flames, becoming comparable to that of steady flames. Swirl has comparatively less impact on the emission index of CO for flames with strongly interacting structures ($\tau_{off} \approx 111$) and flames with completely isolated puffs

($\tau_{off} \approx 1110$). For flames with sufficiently long injection times ($P \geq 10$), the imposition of co-flow swirl has relatively little impact on the CO emissions of these flames, regardless of the jet-off time. At these injection conditions, flames exhibit a comparable flame structure to that of a steady flame. Thus, the effect of swirl on the CO emissions of these flames appeared to be, not surprisingly, similar to that of the steady flames.

The decreased CO emissions, consistent with more complete combustion and increased combustion efficiency [2], suggest more rapid and complete mixing between the fuel and the air resulting from the imposition of swirl in the co-flow stream. The highest EICO of swirled, strongly-pulsed flames, comparable to that of non-swirled flames, is found at the longest jet-off time for each value of the injection time, as seen in Fig. 4.2. These conditions (completely isolated flame puffs) also result in the largest decrease in celerity, due to a large momentum loss of the fuel jet to the surrounding co-flow air, as mentioned in the previous chapter. This large momentum exchange between the fuel jet and the air suggests that the very rapid air entrainment resulting from the lack of competition between flame puffs could induce rapid quenching within the flame, leading to the observed high values of EICO. In general, the CO emissions of swirled, strongly-pulsed flames are seen to decrease with decreased jet-off time for most injection conditions, similar to that of non-swirled flames, possibly due to the relatively longer flame length leading to more time for CO oxidation.

It can be noted that swirl appears to have a stronger impact on the CO emissions for flames with short injection times ($P \leq 8$) than those with long injection times ($P \geq 10$). This is apparently in contrast with the observed stronger impact of swirl on the flame length for long injection times ($P \geq 10$). For flames with a co-flow flow rate of 2.5 SCFM and a dimensionless jet-off time of $\tau_{off} \approx 222$, the value of EICO for flames with $P = 6$ decreases up to 49% with a swirl of S = 1.6, compared to the flames without swirl. However, little apparent decrease of EICO is seen for flames with P = 10 when the swirl level is increased from S = 0 to S = 1.61. One might expect that flames with a decreased flame length caused by swirl would exhibit a different level of CO emissions than those flames that do not undergo changes in flame length. However, this is not the case for some of the flames studied here. For example, for flames with a long injection time, such as P = 10, the flame length is decreased about 9% for all jet-off times when the swirl level is increased from S = 0.41 to S = 1.61, but the values of EICO for these flames are relatively independent of the swirl level. However, for flames with a short injection time of P = 6, the flame length is found to be comparable at S = 0.41 and S = 1.61 for any given jet-off time, but a reduction of EICO, up to about 41% for $\tau_{off} \approx 222$, is observed when the swirl level is further increased from S = 0.41 to S = 1.61. All of these observations could imply that the rapidity of fuel-air mixing and CO oxidation in the upstream regions of flames (in the vicinity of the quarl) may play an important role on the global CO emissions, especially when the flame is comparatively short, such as the flames with short injection times in the current study.

The rapid mixing and CO oxidation in the vicinity of the quarl could reasonably be associated with the swirl-induced recirculation zone where the rapid entrainment and mixing between products and reactants and between the fuel and the air occur [14]. Although the flow field of the swirling flow was not surveyed in the current study, an estimate recirculation zone height of h/D = 3-5 is expected for S = 1.6, based on the study of Tangirala *et al*. [33]. For S = 0.4, it can be expected that there will be little or no recirculation according to that study, given that the combustor geometry, the quarl diverging angle, and the swirl number were all similar to those employed here. This being the case, most of the flames for short injection times ($P \leq 8$) lie within the recirculation zone. The short flame length of these flames ($P \leq 8$) would imply a lack of time for CO oxidation, so that any changes on the oxidizer entrainment brought by swirl could significantly affect the CO emissions of these flames. On the other hand, the long flame length of elongated flames ($P \geq 10$) provides sufficiently long residence time for CO oxidation. The presence of the recirculation zone, thus, may have relatively less impact on the CO levels of these flames ($P \geq 10$). The impact of the recirculation zone, induced by the strong swirl, on the CO oxidation may decrease as the jet-off time decreases, due to the resulting longer flame length. Likewise, the rapid entrainment brought by the strong swirl could induce rapid quenching within the flame puffs as the jet-off time increases, due to the lack of competition between flame puffs, as seen in Fig. 4.2.

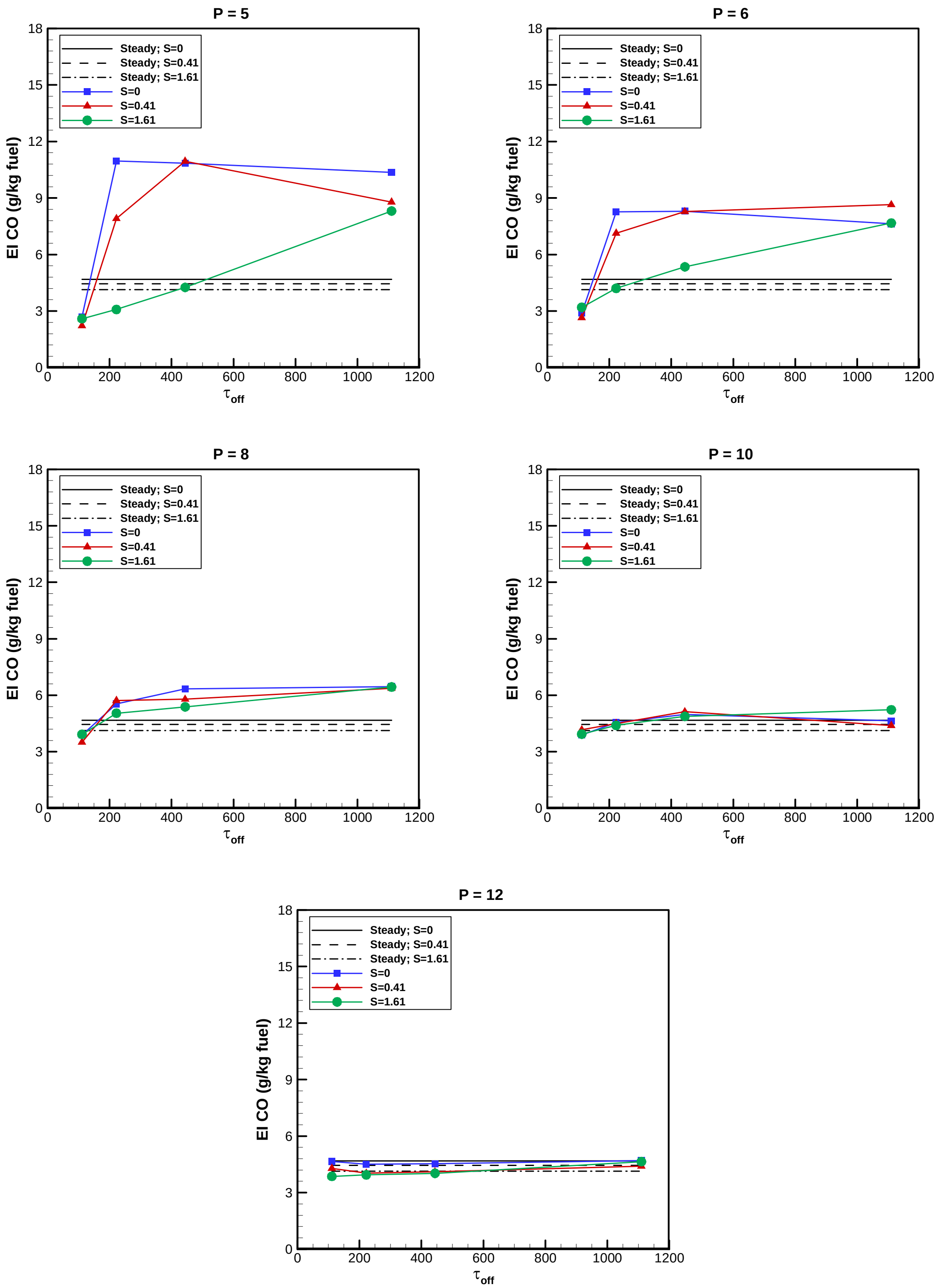

Figure 4.2 – Emission indices of CO for strongly-pulsed flames, both with and without swirl, on the combustor centerline at *z*/*L* = 1.8 for various injection conditions. Co-flow 2.5 SCFM.

4.1.2 Impact of Co-Flow Strength on CO Emissions

The co-flow strength is found to have some impact on the CO emissions of strongly-pulsed flames, both with and without swirl, as shown in Fig. 4.3. The overall CO emissions trends for both co-flow flow rates, 2.5 and 3.5 SCFM, employed in the current study are similar, but the increase of the co-flow strength is generally seen to modestly increase the values of EICO for most injection conditions at any given swirl level.

- **Non-swirled, strongly-pulsed flames**

For non-swirled, strongly-pulsed flames, a higher co-flow flow rate is seen to increase the flame length of flames with compact, isolated flame puff structures ($\tau_{off} > 444$) for $P \leq 8$, as seen in Fig. 3.6. Although a longer flame length implies a longer combustion residence time, a slower rate of air entrainment due to the decreased shear between the fuel jet and the co-flow air could be expected to cause a slower rate of mixing between the fuel and air, possibly accounting for the observed increased values of EICO for these flames. This decreased rate of air entrainment could also impact the CO emissions for flames with interacting flame structures ($\tau_{off} \leq 444$), where the relatively high competition between flame puffs could result in an even slower rate of air entrainment and mixing. This could, in turn, further increase the values of EICO even though the increased co-flow strength shows little impact on the length of these flames. The co-flow strength gradually shows less impact on the CO emissions for non-swirled, strongly-pulsed flames as the injection time is increased, consistent with the observation that the strength of co-flow has a negligible impact on the flame length of these flames with a dimensionless injection time of $P \geq 10$. This could imply that for steady and strongly-pulsed flames with sufficiently long injection times ($P \geq 10$), the long flame length of these flames may already provide sufficient residence time at high temperature for a high level of CO oxidation even though an increased co-flow strength may serve to retard somewhat the rate of entrainment and mixing between the fuel and the air.

- **Swirled, strongly-pulsed flames**

The co-flow strength is also seen to have an impact on the CO levels for strongly-pulsed flames with swirl, as shown in Fig. 4.3. Similar to non-swirled flames, the co-flow strength has a relatively stronger impact on the CO emissions for swirled flames for $P \leq 8$. It was seen in the previous chapter that the co-flow strength had a lesser impact on the flame length for swirled flames with $P \leq 8$, suggesting that the flames with shorter injection times would have more comparable combustion residence time, leading to more comparable EICO, but this is not seen to be the case for swirled flames with $P \leq 8$. Instead, flames with these injection conditions ($P \leq 8$) are generally seen to have higher values of EICO with an increased co-flow strength at a given swirl level. This is consistent with the observation in Section 4.1.1 that the CO emissions of these flames were more subject to the change of entrainment caused by the swirling co-flow than is the flame length. The somewhat higher values of EICO for flames with the higher co-flow strength is presumably due to more rapid dilution and mixing with the cold oxidizer brought by the higher swirling co-flow air strength [38]. Although relatively higher values of EICO are seen with a higher co-flow strength, the reduction in the EICO in this case (3.5 SCFM) is as much as 54% from S = 0 to S = 1.6, compared to 48% with a co-flow of 2.5 SCFM. The co-flow strength is found to have a negligible impact on the values of EICO for flames with sufficiently long injection times ($P \geq 10$), while the length of these flames is seen to decrease with an increased co-flow flow rate. This is consistent with the previous presumption that the long length of these flames may already provide sufficient combustion temperature and residence time for CO oxidation, resulting in little variation in the values of EICO with the variation in co-flow strength.

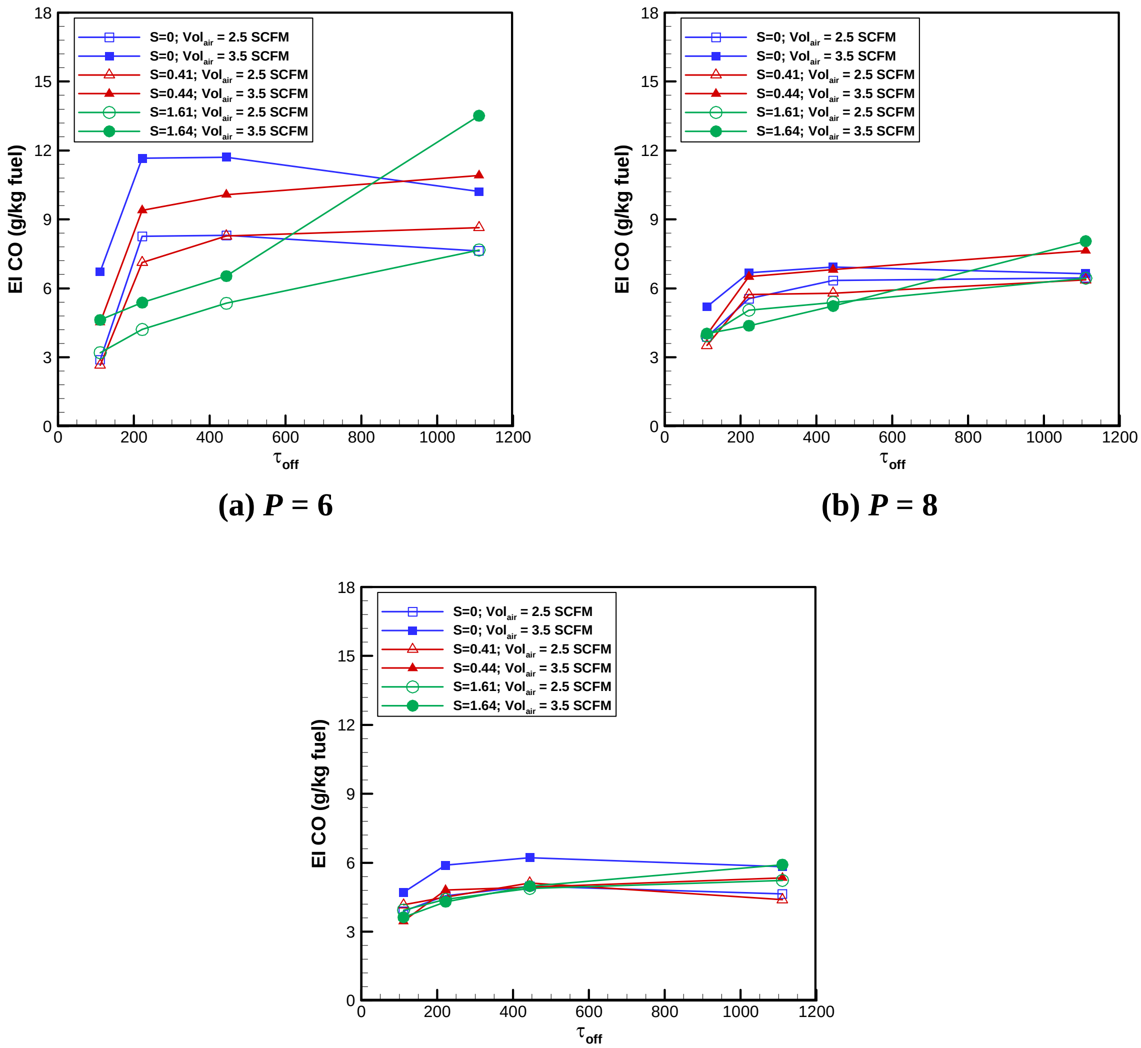

(a) *P* = 6 **(b) *P* = 8**

(c) *P* = 10

Figure 4.3 – Comparisons of the emission indices of CO for strongly-pulsed flames, both with and without swirl, on the combustor centerline at z/L = 1.8 for the varied co-flow air of 2.5 and 3.5 SCFM. The injection time is (a) *P* = 6, (b) *P* = 8, and (c) *P* = 10.

4.1.3 Effect of the Quarl on CO Emissions

The configuration of the combustor exit nozzle has been shown to affect the structure and visible flame length of swirled flames, as described in Chapter 3. The effect of a diverging quarl attached to the combustor exit on the CO emissions of strongly-pulsed flames, both with and without swirl, is shown in Fig. 4.4. The presence of the quarl is found to have a negligible impact on the CO emissions for non-swirled, strongly-pulsed flames. The impact of the quarl on the values of EICO becomes apparent when swirl is imposed. In the absence of the quarl, the values of EICO, regardless of the co-flow strength, increase for most cases as the swirl level is increased, even though the flame length of these flames is generally and slightly longer than that with the presence of the quarl, as seen in Figs. 3.7 and 3.8. The addition of the quarl leads, by contrast, to a decrease in the values of EICO amounting to as much as 55% for the swirl level of S = 1.6. This decrease is apparent for essentially most values of jet-off time. The addition of the quarl has been shown to favor the presence of an enlarged recirculation zone [9], in which intense turbulence and large flow recirculation are present [6, 33]. This large recirculation could allow the fuel to more effectively interact with more co-flow air, resulting in the lower values of EICO for the swirled flames with the presence of the quarl. This outcome is consistent with the presumption that the recirculation zone formed in the upstream regions of the flames could have a significant impact on the global CO oxidation, as mentioned previously.

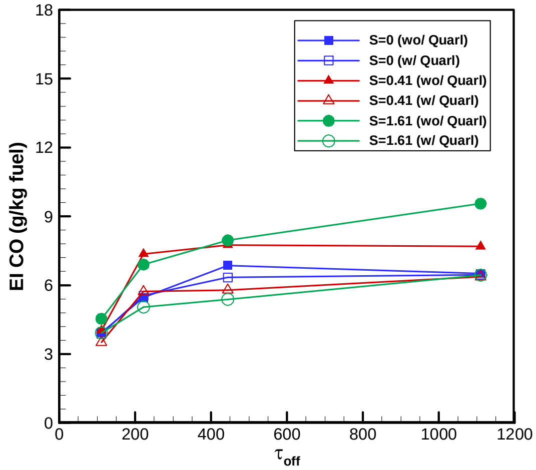

(a) Q_{air} = 2.5 SCFM

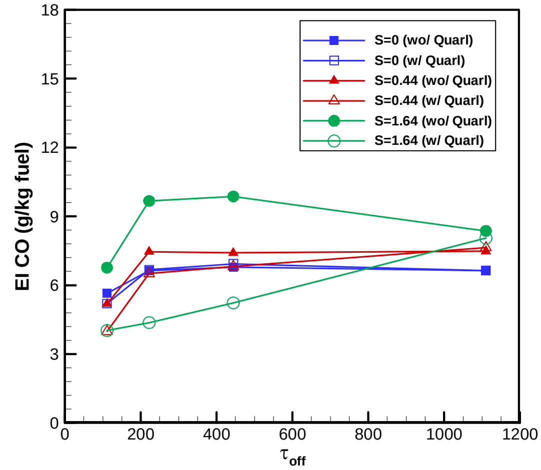

(b) Q_{air} = 3.5 SCFM

Figure 4.4 – Emissions indices of CO taken at z/L = 1.8, both with and without the quarl, with P = 8 and a co-flow of (a) 2.5 SCFM and (b) 3.5 SCFM.

4.2 CO Emissions Scaling

The volumetric flow rate ratio of the injected fuel to the co-flow air over each injection cycle, Q_{fuel}/Q_{air}, has been shown to be an appropriate parameter for scaling the flame length of strongly-pulsed flames, both with and without swirl [76]. The flame length is broadly indicative of the residence time within the flame, which previous research on strongly-pulsed flames without swirl suggests as a reasonable correlating factor for the CO emissions of turbulent jet flames with a fixed injection velocity [48]. Fundamentally, the global residence time characterizes the time required for a stoichiometric mixture of hot products to pass through a volume equal to that occupied by the visible flame. These scaling methods suggest a potential relation between the CO emissions and the volumetric fuel-to-air flow rate ratio for strongly-pulsed flames, both with and without swirl. The utility of such a scaling relation for flames studied here collapsing the CO emissions data is shown in Fig. 4.5. The inclusion of the dimensionless injection time parameter, P, in the ordinate addresses the expectation that the amount of CO would scale inversely with the global residence time [16], due to the lack of reaction time for complete combustion. The scaling parameter employed on the abscissa reflects the cube of the normalized flame length normalized by the volumetric flow ratio of fuel-to-air, taking into account the impact of air dilution over an injection cycle on the variations of the global residence time. The cube of the normalized flame length combined with the volumetric flow rate ratio of fuel-to-air is due to the proportional correlation between each other, as shown in Fig. 3.10. With the amount of the co-flow air provided over each injection cycle being increased relative to the volume of fuel supplied for long jet-off times (i.e. more air dilution), the flame length would decrease (see Fig. 3.10), due to a more rapid rate of entrainment due to the lack of competition between flame puffs, resulting in a short combustion residence time. Thus, the CO emissions quickly rise with jet-off time and reach an asymptote, where the amount of the co-flow air shows no further impact on the CO emissions, as seen in Fig. 4.5. The long jet-off times associated with isolated flame puffs lead to an increase in the co-flow air volume and the resulting asymptotic state. Given that swirl impacts the flame length and emissions levels, this scaling also implicitly accounts for the effect of swirl on the CO emissions. The values of the two asymptotes in Fig. 4.5 for two different co-flow flow rates are similar, consistent with the fact that any additional co-flow air dilution at these conditions has no significant impact on the CO emissions.

Although the proposed scaling between the CO emissions and the global residence time appears to be reasonably successful for the flames studied here, additional investigations on the impact of swirl on the CO emissions of pulsed flames are indicated. In particular, when the recirculation zone has a comparable length to that of the flames, the impact of the recirculation zone on the CO emissions would need to be considered since sufficient amount of entrainment and intense mixing are found to be associated with or within the recirculation zone for these flames [22, 33].

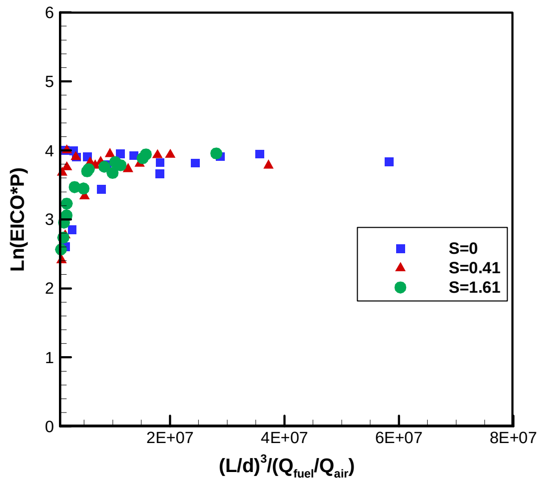

(a) Q_{air} = 2.5 SCFM

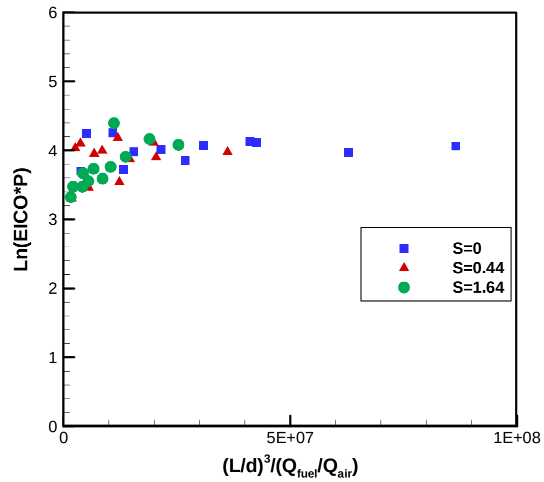

(b) Q_{air} = 3.5 SCFM

Figure 4.5 – Scaling of the emission indices of CO, taking into account the variation in injection times, the combustion residence time, and the volumetric fuel-to-air flow rate in an injection cycle. Co-flow flow rate is (a) 2.5 SCFM, and (b) 3.5 SCFM.

4.3 NO_x Emissions

The emission indices of total NO_x (in general, NO_x consists of NO and NO_2) for strongly-pulsed flames, both with and without swirl, with various injection conditions are shown in Fig. 4.6 for a co-flow of (a) 2.5 SCFM and (b) 3.5 SCFM. For most cases, the concentration of NO_x is not seen to be significantly impacted by the co-flow swirl level and the co-flow strength. For short injection times ($P \leq 8$), the values of $EINO_x$ for strongly-pulsed flames, both with and without swirl, appear to be somewhat impacted by the degree of competition between flame puffs (i.e. by the jet-off time). As the jet-off time decreases, flames exhibit a longer flame length than those with relatively longer jet-off times, presumably due to an increased competition between flame puff structures for the available oxidizer. The increased flame length, implying a relatively longer combustion residence time, is more likely to favor the production of thermal NO [77], thus increasing the overall level of NO_x. For flames with $P > 8$, the competition between flame structures evidently results in little impact on the values of $EINO_x$, due a more comparable flame length for any given jet-off time.

4.3.1 NO Emissions

The emission indices of NO for strongly-pulsed flames, both with and without swirl, are shown in Figs. 4.7 and 4.8 for co-flow strengths of 2.5 and 3.5 SCFM, respectively. For most injection conditions, the measured NO concentrations, as being one of the major pollutants by combustion [40, 41], of these flames are below those of steady flames. The reduction in the NO emissions, compared to steady flames, is found to be as much as 41% and 49% for non-swirled and swirled, strongly-pulsed flames, respectively. For non-swirled, strongly-pulsed flames, the lowest values of EINO occur for the longest jet-off times for a given injection time, consistent with the fact that flames at these injection conditions are relatively short and more subject to rapid dilution, due to the lack of competition between flame puffs for the entrainment of the available air, as discussed previously. The highest values of EINO are generally seen for flames with long injection times ($P \geq 10$), being in that case comparable to those of steady flames. This is in agreement with previous investigations in steady, non-swirled turbulent diffusion flames showing that the EINO is generally proportional to the combustion residence time (according to the thermal-NO theory [77]). In addition, the accompanying slower rate of excess air dilution for a given amount of injected fuel in turn results in generally higher temperatures [78, 79]. A similar trend in NO emissions for strongly-pulsed flames without swirl was reported by Fregeau [48].

In contrast to the observed decrease in EICO caused by swirl, the imposition of swirl in the co-flow stream is seen to result in a modest increase in the values of EINO for some injection conditions, as seen in Figs. 4.7 and 4.8. In general, the CO and NO emissions results, for most cases, are consistent with the typical overall trend that low CO emissions are generally accompanied by high NO emissions, and vice versa [40]. For some specific cases, a simultaneous decrease in both CO and NO levels, due to swirl, is however observed and this observation will be discussed later. The increase in EINO with increased swirl is most apparent for flames with interacting flame structures ($\tau_{off} \leq 444$) and short injection times ($P \leq 8$). This is consistent with the large decrease in EICO observed for flames at these injection conditions. The decreased EICO, comparable to that of steady flames, suggests more efficient and complete combustion, possibly due to the rapid entrainment and mixing brought by swirl-induced recirculation zone. The flow recirculation may lead to a longer combustion residence time [12], resulting in the observed elevated NO emissions, although in most cases the NO levels remain below those of steady flames. These outcomes, low NO with no substantial CO penalty, combined with the much shorter flames resulting from the combination of swirl and strong pulsing, as seen in Chapter 3, suggest the potential utility of swirled, strongly-pulsed flames in the development of efficient, compact, and low emissions combustors. For flames with sufficiently long injection times ($P \geq 10$), the impact of swirl on the NO emissions of these flames is found to be similar to that of steady flames and smaller than that of the shorter flames ($P \leq 8$). The values of EINO for those flames are lower in most cases than those of steady flames at any given swirl level. This is possibly due to a somewhat lower combustion temperature due to pulsing [48, 54] while the lengths of these flames are comparable to that of steady flames. The overall effect of jet-off time on EINO for swirled, strongly-pulsed flames is consistent with that on EICO, showing the expected generally-opposite trend with jet-off time to that of EICO. That is, the high values of EINO generally occur with short jet-off times and the values of EINO decrease as the jet-off time increases, consistent with the fact that the lack of competition between flame puffs could induce rapid quenching within flames, resulting in low values of EINO for flames with long jet-off times, as seen previously for non-swirled, strongly-pulsed flames.

The co-flow strength is also seen to have an impact on EINO, but not to the extent observed for EICO discussed previously. This may be due to the more complicated and generally slower formation mechanisms of NO than those of CO [40, 41]. The values of EINO of swirled flames are generally seen to slightly decrease with the increased co-flow strength, as seen in Figs. 4.7 and 4.8; a concomitant and relatively greater increase in the EICO was noted previously, as seen in Fig. 4.3.

These results suggest that there are combinations of injection conditions and swirl that can lead to a simultaneous reduction on both CO and NO levels for strongly-pulsed flames. Specifically, flames with highly interacting flame structures ($\tau_{off} \approx 111$) with a co-flow of 3.5 SCFM and S = 1.6 appear to have both EINO and EICO lower than those of strongly-pulsed flames without swirl. The decrease amounts to as much as 25% and 31% for EINO and EICO, respectively. The simultaneous reduction in NO and CO emissions has been reportedly achievable in swirl-stabilized combustion [36, 80, 81]. That research showed that if the oxidizer could be rapidly entrained and thus cause some partially premixing with the fuel, but not rapid enough to induce quenching of CO oxidation, the NO emissions could be somewhat reduced along with decreased CO emissions. This may be the case for the specific condition cited here.

Similar to the impact of swirl on EICO, swirl appears to have a relatively stronger impact on the NO emissions for flames with short injection times ($P \leq 8$) than those with long injection time ($P \geq 10$), especially for the cases with the strongest swirl level employed here. The stronger impact of swirl on the NO emissions for $P \leq 8$ could be associated with the swirl-induced recirculation zone, as mentioned previously. The impact of the recirculation zone on the NO_x emissions of swirled, steady hydrogen-air flames was studied by Chen [15]. Chen showed that the characteristics of the recirculation zone can have a significant impact on the NO_x formation when the flames have a comparable length to that of the recirculation zone, due to the fact that combustion takes place largely in that reverse flow region. Thus, the characteristic time in the recirculation zone (defined as the ratio of the width of recirculation zone to the bulk velocity of the recirculation flow) [15] may be more relevant to the NO emissions of these flames than the overall flame residence time.

Other than the thermal NO production, it is important to point out other factors and mechanisms that could also affect the NO formation in the non-premixed turbulent diffusion flames. Those factors or mechanisms that have been experimentally or numerically studied include a) the aerodynamic strain [82, 83], b) the flame radiation loss [47], c) the O atom superequilibrium [66, 84], and d) the prompt-NO chemistry [85, 86]. In most hydrocarbon flames, these factors exist simultaneously and most of them are highly temperature-related, which make it even more difficult to correlate the NO concentration with any single parameter, such as the mean flame length or global residence time. In addition, the ethylene fuel used in the current study has a very strong sooting tendency, implying that the flame temperature could significantly deviate from the equilibrium temperature due to soot radiation. The temperature change could, in turn, cause the radical concentration to deviate from the equilibrium level, thus affecting the NO formation [42]. A high strain rate has been shown to reduce the amount of NO, due to the decreased residence time for reaction to occur [83]. The global strain rate downstream of fuel nozzle would be expected to vary for flames studied here due to the fuel pulsing and the co-flow swirl. Variations in the global strain rate are suggested by variations in the flame puff celerity and the flame width at a given downstream location. The flame puff celerity, shown in Fig. 3.12, increases as the injection time is decreased for any given jet-off time. The flame width is observed to increase with increased injection time at a given jet-off time. For example, for a jet-off time of τ_{off} = 222, the visible flame width of non-swirled flames at a downstream location of z/L = 0.85 is approximately 19.3 mm for P = 6, and increases to 24.6 mm for P = 10. Thus, the flames with a short injection time likely have the higher global strain rate than those with a relatively longer injection time. Once swirl is imposed, the flame puff celerity generally decreases and the flame width is seen to increase, resulting in a decreased global strain rate. By further increasing the swirl level or, alternatively, increasing the co-flow strength at a given swirl level, the strain rate would be expected to change further. This variation of strain in the flow may thus have an impact on the NO concentration of swirled, strongly-pulsed flames, as seen in Figs. 4.7 and 4.8.

In many studies on turbulent hydrocarbon diffusion flames, the predicted NO concentration based on the thermal theory generally deviates from that measured in experiments [51, 82, 84, 87]. Part of this deviation is considered to be due to the prompt-NO mechanism (sometimes called Fenimore mechanism) [51, 87]. The prompt-NO chemistry is quite complicated and usually involves intermediate radicals that occur in the early stage of the combustion process, such as CH and HCN [85]. The prompt pathway of NO formation is usually found to dominate in the low temperature and fuel-rich hydrocarbon combustion, while the thermal mechanism dominates near the stoichiometric regions of the reaction zones with high temperature [42]. Some prompt-NO formation is expected in these hydrocarbon-fueled flames. It is not yet clear what the relative contributions of the thermal and prompt mechanisms are to the NO production for the flames studied here. To resolve this issue will require uncoupling of the factors mentioned earlier, and knowledge of the detailed temperature distribution and species concentration, and the flow-flame interactions, such as the aerodynamic strain, are known. However, for cases of flames with long jet-off times and short injection times, the prompt mechanism may play an important role on the NO formation of these flames, due to the lack of residence time and low temperature [48, 54] for thermal-NO formation to occur.

The NO emissions levels of swirled, strongly-pulsed flames were also measured both with and without the quarl, as shown in Fig. 4.9. It is found that the presence of a quarl has little impact on the values of EINO for strongly-pulsed flames, both with and without swirl. It should be mentioned that such comparison was only performed for flames with a dimensionless injection time of P = 8, where most of the flames relatively compact and with a shorter flame length than steady flames. As mentioned previously, the addition of the quarl tends to favor the formation of an enlarged recirculation zone. It is not yet clear in this study whether the role of the recirculation zone is favorable or unfavorable for NO production even though the addition of the quarl results in a negligible impact on the indices of NO. This result may suggest that most of the NO, at least for flames with P = 8, could possibly be formed in the downstream regions of the flame (i.e. downstream of the location corresponding to the quarl exit). This is somewhat consistent with the fact that much of the thermal-NO production for diffusion jet flames occurs in the reaction zones relatively near the flame tip [44]. This could be the case for some flames with P = 8 since these flames have a long flame length comparable to that of steady flames.

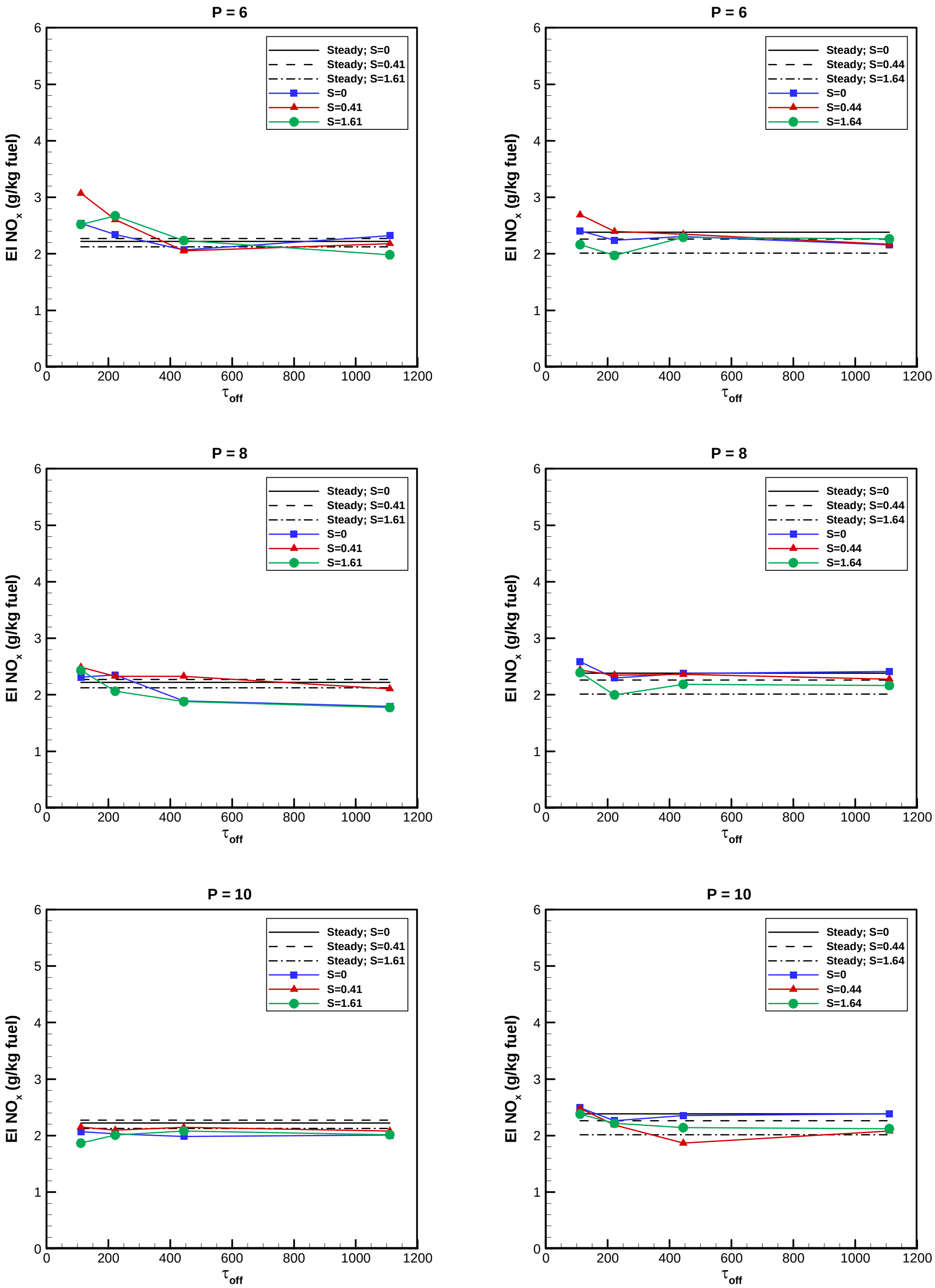

(a) Q_{air} = 2.5 SCFM **(b) Q_{air} = 3.5 SCFM**

Figure 4.6 – Emission Indices of NO_x for strongly-pulsed flames, both with and without swirl, on the combustor centerline at z/L = 1.8 for various injection conditions. (a) Co-flow 2.5 SCFM. (b) Co-flow 3.5 SCFM.

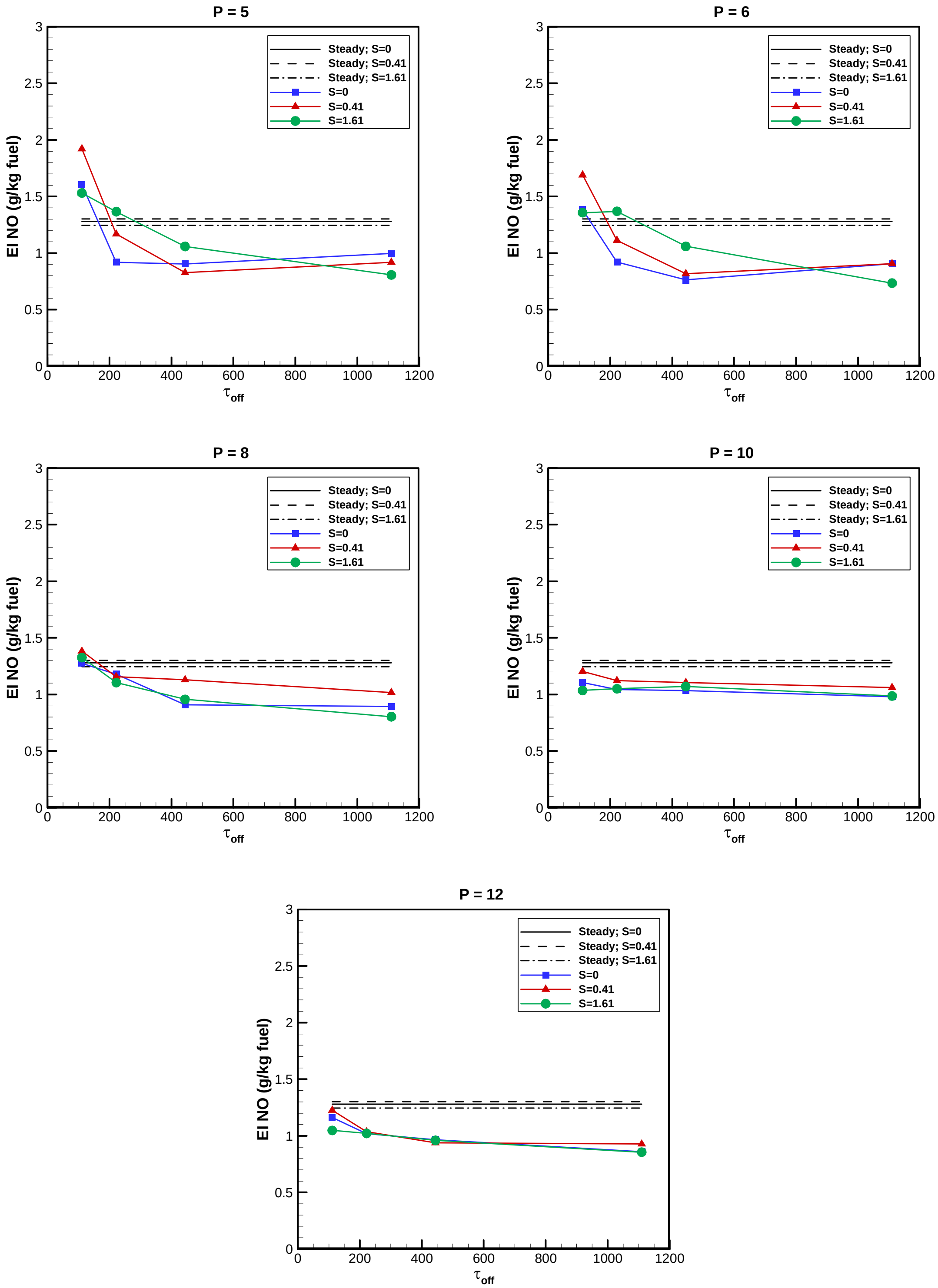

Figure 4.7 – Emission indices of NO for strongly-pulsed flames, both with and without swirl, on the combustor centerline at z/L = 1.8 for various injection conditions. The co-flow is 2.5 SCFM.

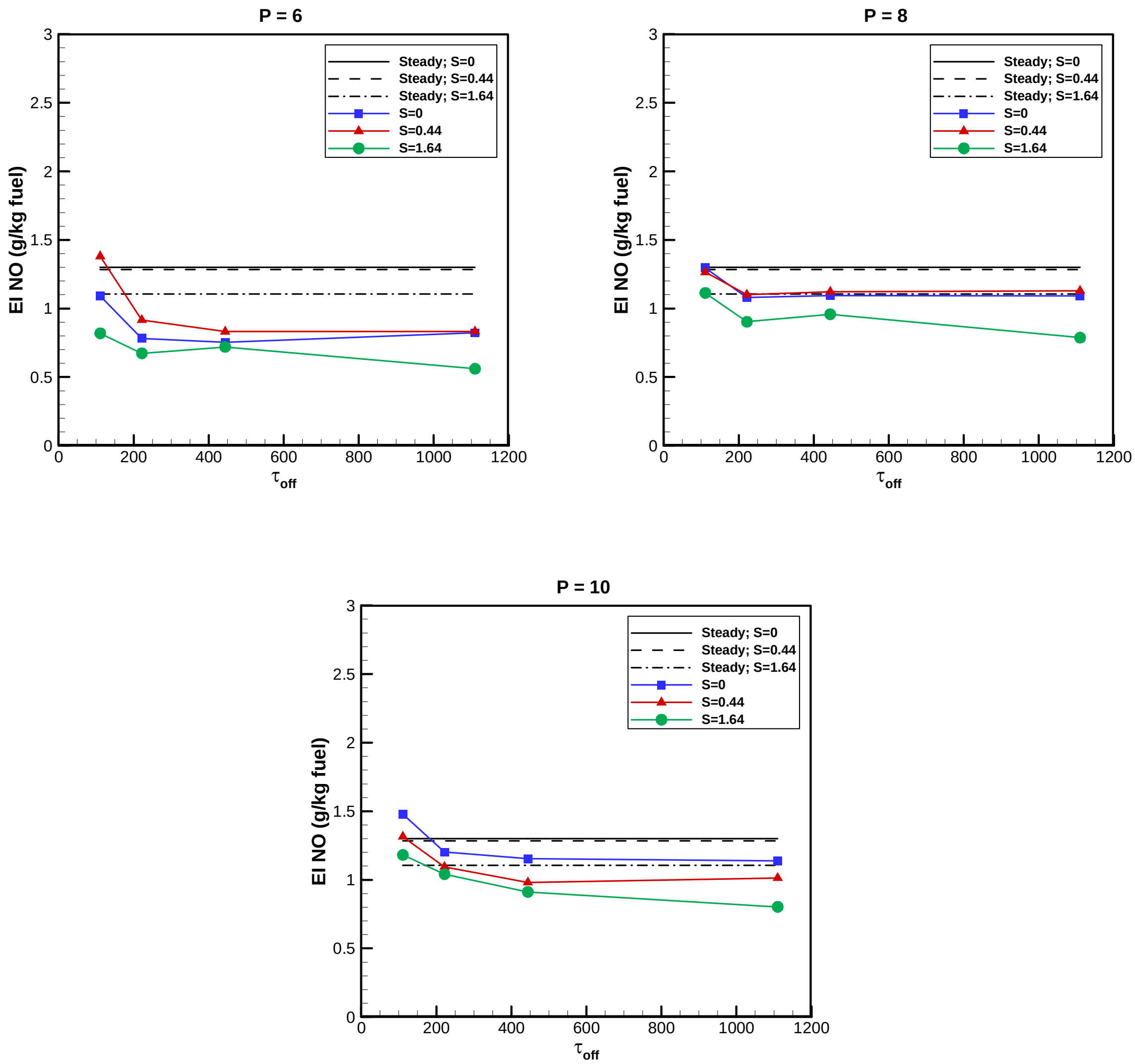

Figure 4.8 – Emission indices of NO for strongly-pulsed flames, both with and without swirl, on the combustor centerline at *z*/*L* = 1.8 for various injection conditions. The co-flow is 3.5 SCFM.

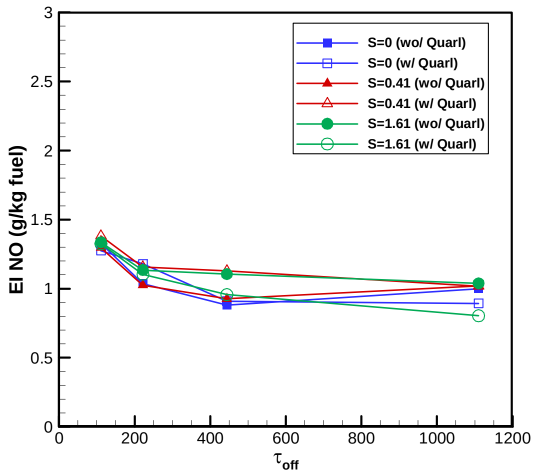

(a) Q_{air} = 2.5 SCFM

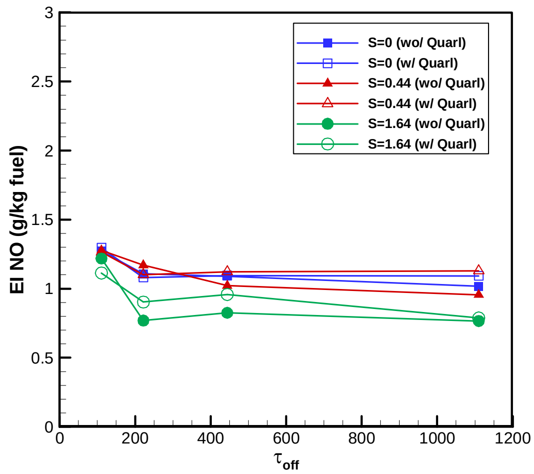

(b) Q_{air} = 3.5 SCFM

Figure 4.9 – Emissions indices of NO taken at z/L = 1.8, both with and without the quarl, with a co-flow of (a) 2.5 SCFM and (b) 3.5 SCFM. The dimensionless injection time is P = 8.

4.3.2 NO Emissions Scaling

A similar scaling approach, as seen in the CO emissions, is applied to the NO emissions to study the impact of the global residence time and the air dilution over the injection cycle on the variations of EINO. The scaling relation is shown in Fig. 4.10. The EINO normalized by the dimensionless injection time takes into account the impact of the injection time and the flame length, therefore residence time, as we discussed previously, on the NO emissions. As compared to the scaling for EICO in Fig. 4.5, the normalized EINO for most flames quickly decreases as the amount of air over the injection cycle is increased which is accompanied with decreased flame length; while the associated EICO quickly increases to an asymptote, as seen in Fig. 4.5. The decrease in EINO is presumably due to the decreased flame length, leading to the shorter combustion residence time, consistent with decreased levels of thermal NO and thus the low values of EINO. The decrease of EINO with the decreased flame length suggests that the bulk of the NO is generated by the thermal-NO mechanism. Although the normalized EINO for a co-flow strength of 2.5 SCFM, regardless of the swirl level, appears to reach an asymptote where the amount of the co-flow air over each injection cycle shows little impact on the NO emissions, this is not as apparent for flames with a co-flow of 3.5 SCFM. In addition, the normalized EINO for the flames with a co-flow of 3.5 SCFM is generally seen to be slightly lower than that for the flames with a co-flow of 2.5 SCFM, particularly for the cases of the strong swirl (S = 1.6). The normalized EINO for a co-flow of 3.5 SCFM also seems to converge to different values for the different swirl levels. The fact that the normalized EINO does evidently not collapse to a single curve with the combustion residence time, as was seen for the case of the EICO, is probably not unexpected due to the complex NO formation chemistry. A similar treatment for the NO emissions on steady flames with hydrocarbon fuel has been proposed in other studies [51, 82], but with generally unsuccessful results. Thus, this scaling relation, simply based on the thermal-NO suggestion, may not be sufficient to account all the factors for the NO production in hydrocarbon flames and suggest other NO production mechanisms likely need to be taken into account when developing the NO emissions scaling for such flames.

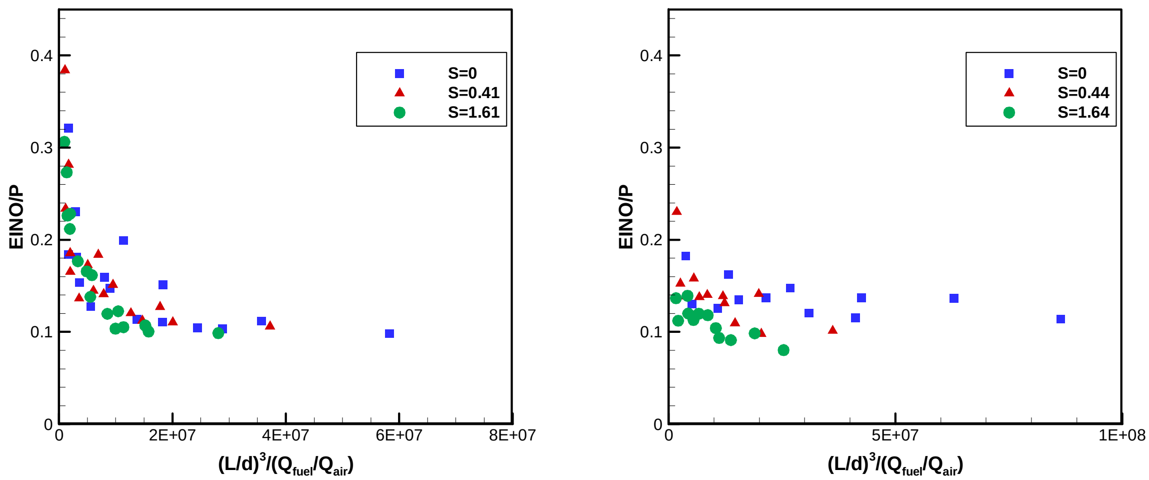

(a) Q_{air} **= 2.5 SCFM** **(b)** Q_{air} **= 3.5 SCFM**

Figure 4.10 – Scaling of the emission indices of NO, taking into account the variation in injection times, the combustion residence time, and the volumetric fuel-to-air flow rate in an injection cycle. Co-flow flow rate is (a) 2.5 SCFM, and (b) 3.5 SCFM.

4.3.3 NO_2 Emissions

The normalized emission indices of NO_2 for strongly-pulsed flames, both with and without swirl, are shown in Figs. 4.11 and 4.12 for co-flow strengths of 2.5 and 3.5 SCFM, respectively. The primary formation route of NO_2 has been proposed as the oxidation of NO with the HO_2 radical, where the latter is generally found to have a high concentration during the rapid cooling process [40, 88]. The HO_2 is not normally found in large amounts near the reaction zone, where high temperature prevails and a high concentration of NO is found [44, 88]. In general, the NO_2 emissions profiles versus jet-off time resemble those of the CO emissions, as seen in Figs. 4.2 and 4.3, presumably due to the fact that both the CO and NO_2 emissions for the flames studied here are presumably strongly sensitive to rapid quenching. On the other hand, since the values of $EINO_x$ (NO_x consists of NO and NO_2 mentioned previously) are very comparable for most of the flames studied here, a decrease in EINO is generally accompanied by an increase in $EINO_2$. Although the profiles of the $EINO_2$ and the EICO are very similar, the production mechanisms for NO_2 and CO are quite different. The main production of NO_2 is due to the quenching reaction of NO with HO_2, but the high concentration of CO in flames is a result of the competition between the soot and the CO on the oxidizing species, such as OH [16].

For non-swirled, strongly-pulsed flames, the high value of $EINO_2$ is generally seen with long jet-off times. The high $EINO_2$, consistent with the high EICO and the low EINO, is possibly due to the rapid quenching within the flame puff owing to the rapid entrainment, due to the lack of competition between flame puffs for the available air [49]. The $EINO_2$ of these flames is generally seen to decrease as the injection time increases, where the flames have the relatively longer flame length than those with short injection times. The longer flame length implies the longer combustion residence time, which suppresses the NO-NO_2 conversion due to the relative lack of HO_2 radical [88], resulting in the low values of $EINO_2$, consistent with the low EICO and the high EINO for flames with long injection times. The normalized $EINO_2$ gradually approaches to that of steady flames as the injection time is increased, consistent with the observation on the flame structure and the CO/NO emissions.

A similar trend to the EICO is also observed for the values of $EINO_2$ for flames with swirl. In general, the profiles of the $EINO_2$ along with the observations for EICO and EINO suggest more rapid air entrainment when swirl is added to the co-flow stream. By comparing Fig. 4.11 to Fig. 4.12, the normalized $EINO_2$ for flames with $S = 1.6$ (strong swirl) is generally higher with a co-flow of 3.5 SCFM than that with a co-flow of 2.5 SCFM at any given injection time. This is consistent with the CO emissions, as seen in Fig. 4.3, and in agreement with previous studies of steady swirled flames [51, 88]. It was suggested by Hori [88] that a substantial amount of NO_2 would be formed due to the rapid cooling of NO by the surrounding co-flow and the $EINO_2/EINO_x$ ratio thus increases with the resulting increased mixing rate. In the current study, the increased $EINO_2/EINO_x$ ratio may suggest that there is an increased rate of air entrainment, possibly due to the enlarged recirculation zone, caused by the increased co-flow strength.

The information on the flame structure and CO/NO emissions for swirled, strongly-pulsed flames suggest the potential of this technique for developing an innovative combustor with a compact flame and low emissions, while at the same time satisfactory combustion stability and high thermal efficiency are still maintained. It has been shown that the imposition of co-flow swirl can decrease the length and simultaneously lower the CO emissions of strongly-pulsed flames to a level comparable to that of steady flames for most injection conditions. At the same time, the NO emissions of these flames can, in many cases, be comparable to those of non-swirled, strongly-pulsed flames, and lower than those of steady flames. For example, for non-swirled, strongly-pulsed flames with P = 6 and τ_{off} = 444, the length of these flames are 38% shorter with 77% higher of EICO than those of non-swirled steady flames, while the NO emissions are 40% lower than the steady flame level. As a strong swirl level is imposed in the co-flow stream, a decrease of 32% in flame length, an increase of just 30% in EICO, and a reduction of 15% in the NO emissions are observed, compared to steady flames with the identical swirl level. However, these swirled, strongly-pulsed flames are 16% shorter, accompanying with a lower CO emission of 36% than strongly-pulsed flames without swirl.

More importantly, it was shown earlier that there are combinations of injection conditions and swirl that can lead to slightly lower both CO and NO emissions for swirled flames than those for non-swirled, strongly-pulsed flames. For example, for a co-flow strength of 3.5 SCFM, for flames with P = 6 and τ_{off} = 111, an increase in the swirl level from S = 0 to S = 1.64 leads to the simultaneous decrease of 31% and 25% for EICO and EINO, respectively. At the same time, the increased swirl level results in a reduction of 25% in the flame length.

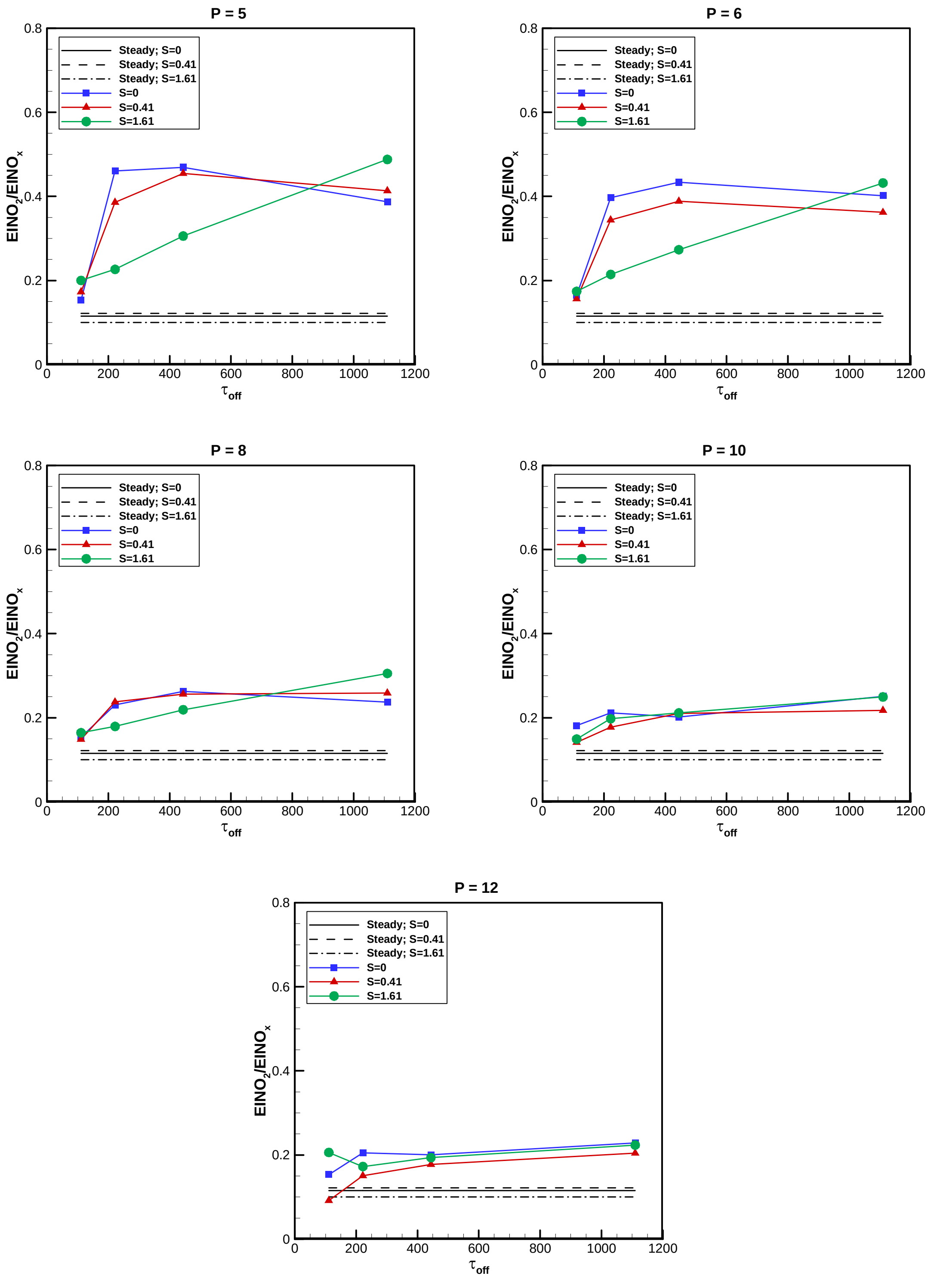

Figure 4.11 – Normalized emission indices of NO_2 for strongly-pulsed flames, both with and without swirl, on the combustor centerline at *z*/*L* = 1.8 for various injection conditions. The co-flow is 2.5 SCFM.

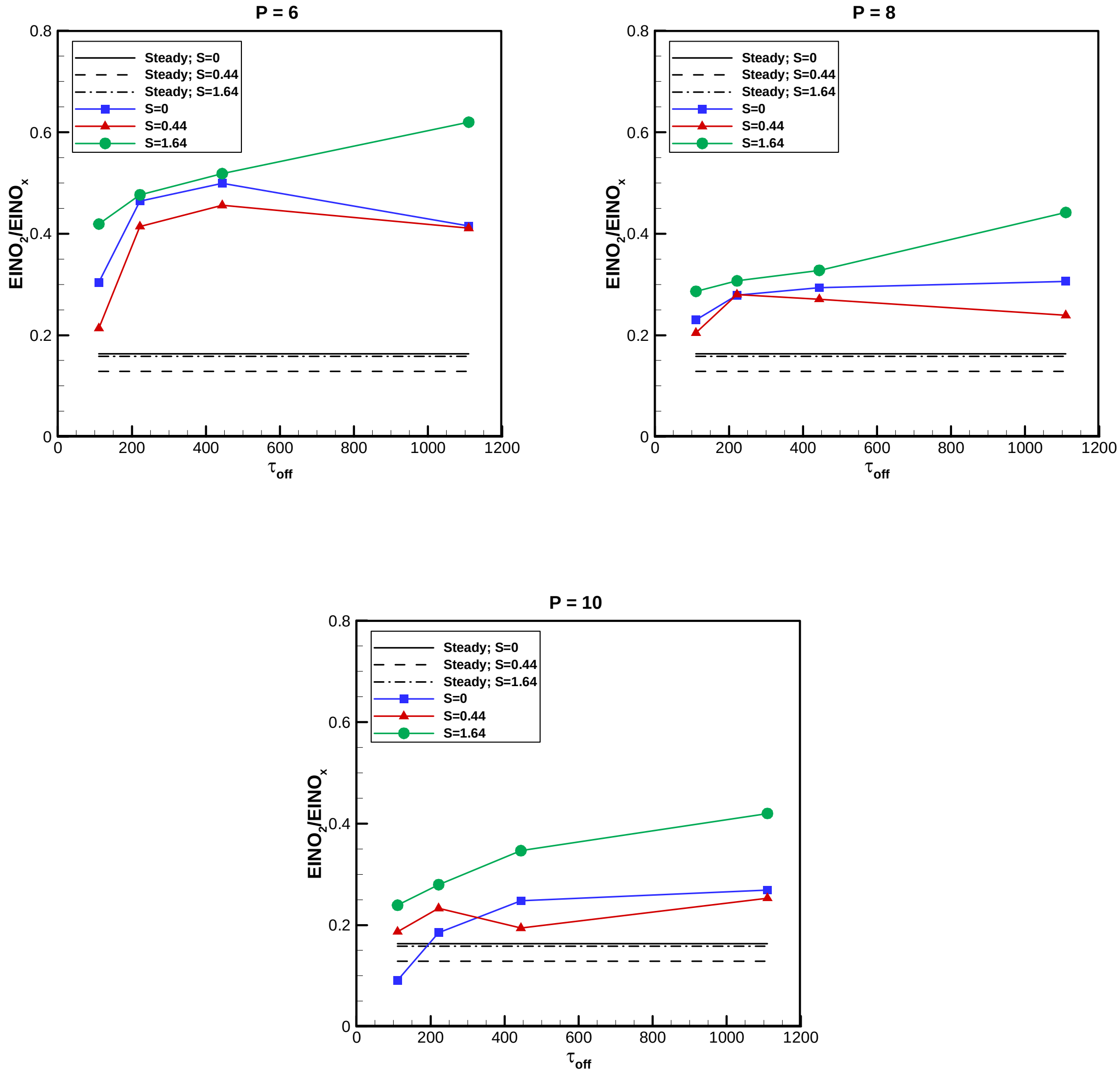

Figure 4.12 – Normalized emission indices of NO_2 for strongly-pulsed flames, both with and without swirl, on the combustor centerline at z/L = 1.8 for various injection conditions. The co-flow is 3.5 SCFM.

CHAPTER 5

OH PLIF IMAGING

Hydroxyl radical (OH) PLIF imaging was employed to study the reaction zones in swirled, strongly-pulsed diffusion jet flames. The PLIF imaging was performed over the entire region downstream of the quarl for steady flames, and in regions of LOC I and LOC II (see Fig. 2.9 in experimental setup) for strongly-pulsed flames, due to the fact that downstream of LOC II, most strongly-pulsed flames showed little remaining flame structure. Statistics from the PLIF imaging were employed to evaluate the relative concentration and the spatial variations of the OH distribution. The statistical analysis provides the time-averaged distribution of the OH zones for steady flames, and also gives information on the variations of the cycle-averaged OH zones for strongly-pulsed flames. All of the OH PLIF images shown here have been corrected with the variation in the laser sheet intensity profile, as discussed in Chapter 2.

5.1 OH PLIF of Steady Flames with/without Swirl

The intermediate product of the hydroxyl radical (OH) in hydrocarbon combustion is considered as a good marker for the reaction zone and is commonly used for this purpose, due to its peak concentration being typically near the location of the peak combustion temperature [53]. For this reason the detection of OH by the laser induced fluorescence has been extensively reported in many combustion studies and the spatial distribution of OH is widely regarded to provide a satisfactory indication of the location of the reaction zones [68, 89, 90].

Selected images of OH PLIF imaging for steady flames, both with and without swirl, are shown in Figs. 5.1 and 5.2 for co-flow strengths of 2.5 and 3.5 SCFM, respectively. The laser sheet propagated from left to right in all images shown. Some modest attenuation of the laser sheet as it propagates through the flame is evident, especially in the downstream regions of flames. The relatively weaker fluorescence signal in the centerline region of the flames, where little OH is expected, is believed to be due to interference arising from the soot precursors (polycyclic aromatic hydrocarbons or PAH) and soot particles in these highly-sooting ethylene/air flames [68, 89]. It is evident that the reaction zone structures, as marked by OH radicals, reflect the large-scale nature of the flow in the turbulent jet flames studied here, especially in the downstream regions of flames. For non-swirled flames, comparatively thin OH zones prevail in the upstream regions of flames near the exit of the quarl. The OH zones slightly broaden and become more contorted with downstream distance from the quarl exit. It should be remarked that, due to the slow three-body recombination reaction, OH can persist even beyond the visible tip of flames [90, 91]. The overall structure of the OH zones for non-swirled steady flames are similar to those reported by Lee *et al*. [90] with the identical fuel as the current study, but with a different Reynolds number, and are also in qualitative agreement with Seitzman *et al*.'s observations [91] using a different fuel (hydrogen).

The OH zones are generally seen to be situated further away from the flame centerline and to have slightly greater thickness as the swirl level is gradually increased, as seen in Figs. 5.1 and 5.2. In addition, the OH zones in swirled flames also appear somewhat more convoluted than those in non-swirled flames. The decrease in flame length due to swirl is also apparent, consistent with the visual flame-length results shown in Fig. 3.1 previously. The increased co-flow strength generally also results in a somewhat more convoluted OH-zone structure for swirled flames. The structure of the OH zones for swirled steady flames was also studied by Tummers *et al.* [92], who reported the convoluted OH-zone structure possibly being due to the azimuthal motion caused by swirl. In addition, Tummers *et al.* observed no significant OH fluorescence inside the recirculation zone and suggested that mainly unreacted fuel and some combustion products were recirculated, but that significant combustion did not occur inside the recirculation zone. The lack of OH signal near the flame centerline for the flames studied here with the strongest swirl level (S = 1.6), in which the recirculation zone is believed to occur, is consistent with Tummers *et al.*'s conclusion [92].

Statistics based on the OH PLIF images were made from an ensemble of 70 images for a given swirl level and flame downstream location to show the impact of swirl on the extent and distribution of the reaction zones. The information of statistics accounts for the spatial variations of OH distribution and is not meant to quantify the OH concentration. Due to the lack of OH signal in the downstream regions of some flames, in particular the strongly-pulsed flames, statistical comparisons were only performed at LOC I and LOC II. The distribution of the reaction zones was analyzed in terms of the reaction zone area, as determined from counting the number of pixels containing OH signals with a pixel value being above a specified threshold level. The threshold level was defined as half of the maximum value of the OH PLIF intensity, which was also equivalent to half of the pixel depth of an 8-bit grayscale image. Test cases with different thresholds were examined to ensure that most of the soot-related interference signals were eliminated, while sufficient OH signals were still available for the statistical analysis. The threshold used in the current study is consistent with that cited in the literature for either CH [68] or OH [90] flame zone-thickness measurements.

The effect of swirl on the computed mean area of the reaction zones (denoted $\tilde{A}_{OH}$) for steady flames is illustrated in Fig. 5.3. As was seen in Figs. 5.1 and 5.2, the OH zones broaden with downstream distance, which results in greater reaction zones areas at LOC II than at LOC I for flames with any given swirl level, as seen in Fig. 5.3. The increase in the OH-zone area with the downstream distance is consistent with the increasing thickness of both CH and OH zones in the streamwise direction reported previously in turbulent non-premixed flames [68, 90]. This may be explained by considering that as the flame elements move downstream, the overall gradient of the fuel/air mixture fraction decreases due to more complete mixing, leading to more and broader mixing layers where the mixture fraction is approaching to the stoichiometric ratio, resulting in the thick CH or OH zones in downstream of flames [68]. The area of the reaction zones in steady flames generally increases as the swirl level is increased, as seen in Fig. 5.3. This trend is possibly associated with the broader mixture fraction profile due to swirl, as suggested by other studies on swirled steady flames [28, 30].

The impact of co-flow swirl on the mixture fraction of a turbulent non-premixed flame was studied by Feikema and co-workers [28]. Feikema *et al*. reported that the mean mixture fraction, when swirl was added to the co-flow stream, was significantly reduced due to the intense mixing, as indicated by the large increase in the mean dissipation rate in their study. The well-mixed regions, where the mixture fraction approached the stoichiometric ratio, were subsequently broadened by the presence of the centrifugal force in the swirling flow, and in turn broadened the OH zones, which generally resided on the lean side of stoichiometric mixture. This is consistent with the observed increase in OH-zone area reported here. The increased area in the OH zones for swirled flames may also be in part due to the more convoluted OH structures in swirled flames than in non-swirled flames, as seen in Figs. 5.1 and 5.2.

The increased co-flow strength is found to have little impact on the OH-zone area for non-swirled flames, but generally results in a somewhat greater OH-zone area in swirled flames.

The increase in the OH-zone area with the increased co-flow strength may be related to the more convoluted OH-zone structure for flames with a high co-flow flow rate mentioned previously.

The mean pixel intensity of the OH zones for steady flames with different swirl levels, normalized for each specific region by that of non-swirled flames at LOC I with a co-flow of 2.5 SCFM, is shown in Fig. 5.4. It is seen that the OH zones at a given downstream location have a comparable mean pixel intensity for any given swirl level, with a value that decreases only slightly (2-5%) with downstream distance. The slightly decreased value of the mean pixel intensity for the OH zones at a further downstream location suggests that the OH zones may be somewhat more broadly distributed in space in moving downstream, possibly due to the growth of the large-scale structures of the flow, as seen in Figs. 5.1 and 5.2.

The root-mean-square (RMS) of the reaction-zone area, normalized by $\tilde{A}_{OH}$, for steady flames, both with and without swirl, are shown in Fig. 5.5. The RMS of variation in $\tilde{A}_{OH}$ indicates the degree to which the reaction zones are subjected to the local flow fluctuations [90, 93]. The value of the RMS is found to be relatively lower at LOC I, compared to at LOC II, for flames with any given swirl level and increases up to 75% at a further downstream location of LOC II. The relatively higher value of the RMS at LOC II compared to LOC I suggests an increased impact of turbulence on the flame structure in the further downstream regions as the large-scale structures of the flow gradually develop with downstream distance. This is consistent with the observations of more convoluted OH-zone structures at LOC II shown in Figs. 5.1 and 5.2. Specifically, thin OH structures are observed near the quarl exit, and broader and more convoluted OH structures appear in regions further downstream. The imposition of co-flow swirl is seen to increase the value of the RMS OH concentration fluctuations, suggesting a relatively stronger effect of flow-flame interaction in swirled flames, consistent with more convoluted OH structures in swirled flames seen in Figs. 5.1 and 5.2. The higher values of the RMS with strong swirl (S = 1.6) may also be associated with the recirculation zone, around which intense turbulence and large fluctuations in flame temperature generally occur [30]. The increased co-flow strength also results in an increase in the value of the RMS for swirled flames, suggesting a relatively stronger flow-flame interaction for swirled flames with a higher co-flow flow rate, consistent with the more contorted OH-zone structure for swirled flames with a higher co-flow flow rate shown in Fig. 5.2 compared to those with a lower co-flow flow rate seen in Fig. 5.1. The overall results of the OH-zone statistics for steady flames reported here, both with and without swirl, are consistent with the literature studies on non-swirled [90, 93] and swirled [30] turbulent non-premixed jet flames. The OH-zone statistics for strongly-pulsed flames are discussed in the next section.

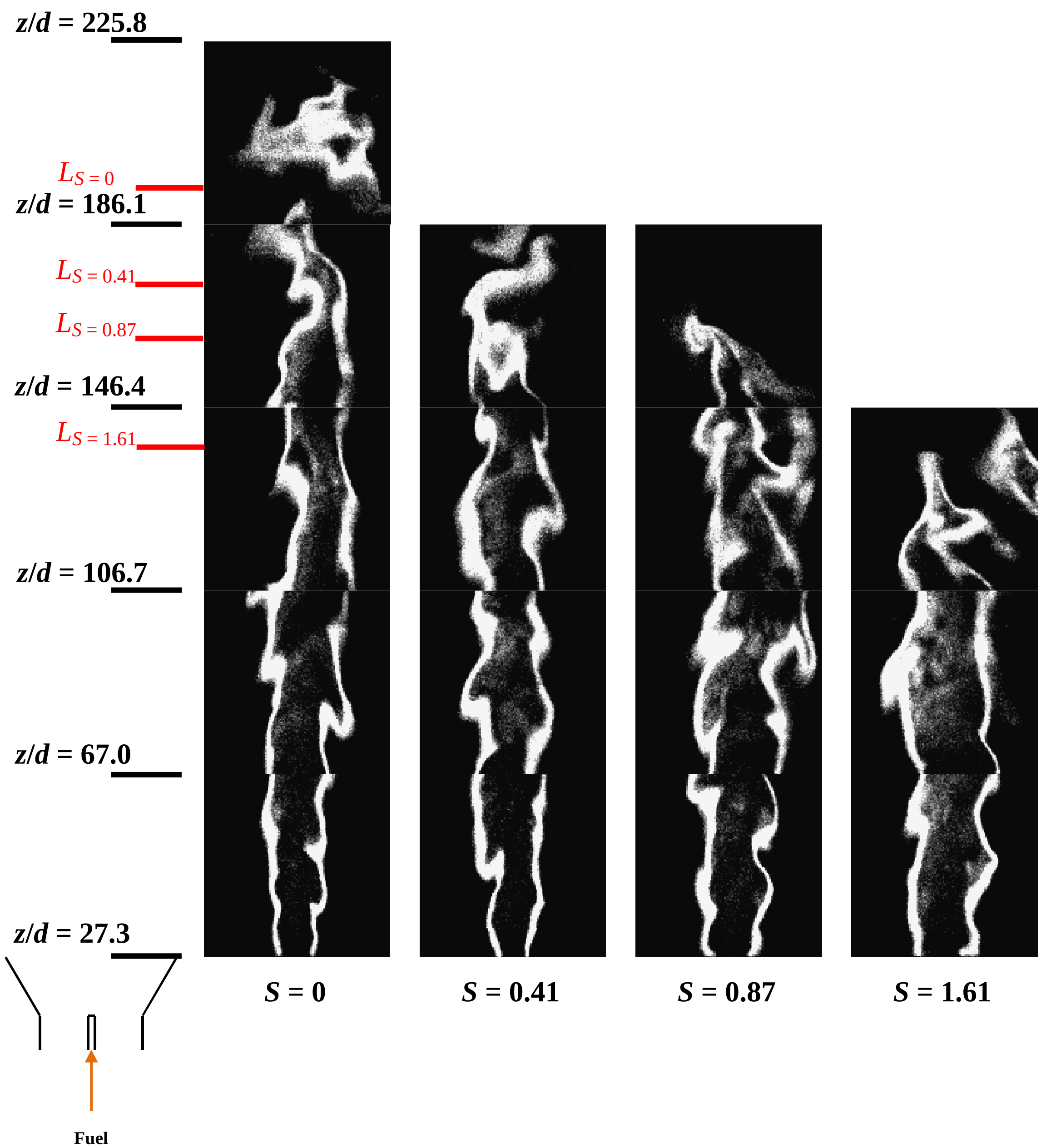

Figure 5.1 – Composite, instantaneous OH PLIF images of steady flames with various swirl levels. The co-flow is 2.5 SCFM. The red marker indicates the mean visual flame length of the flame for each swirl level. The individual image dimensions are 3.125” × 3.125”.

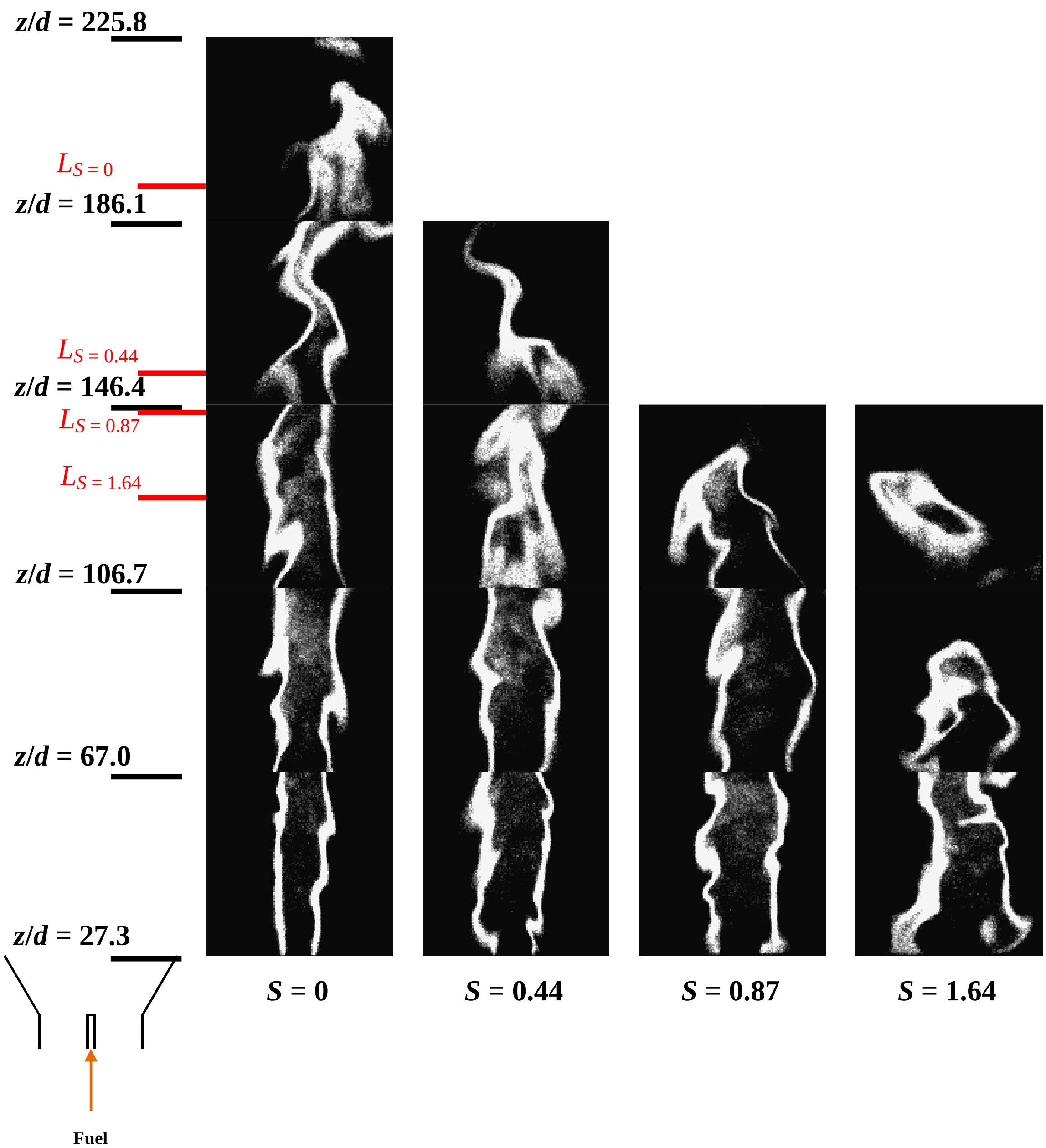

Figure 5.2 – Composite, instantaneous OH PLIF images of steady flames with various swirl levels. The co-flow is 3.5 SCFM. The red marker indicates the mean visible flame length of the flame for each swirl level. The individual image dimensions are 3.125” × 3.125”.

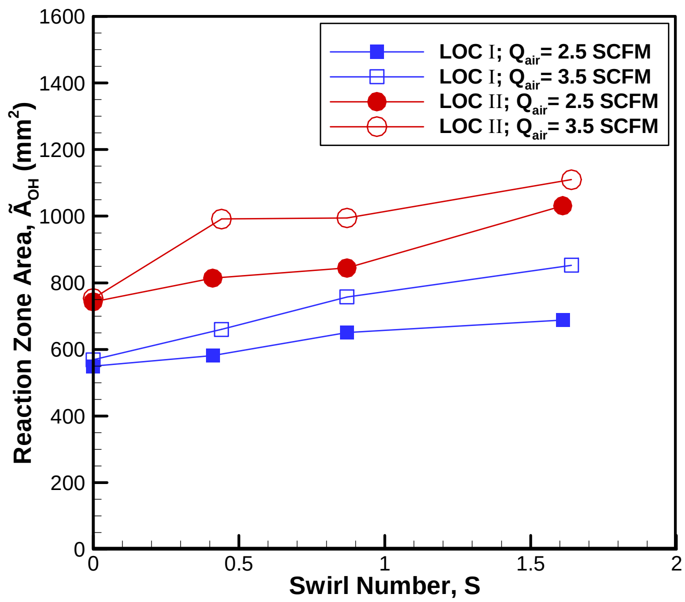

Figure 5.3 – Impact of swirl on the mean reaction zone area of steady flames with varied co-flow flow rates at downstream locations LOC I and LOCII.

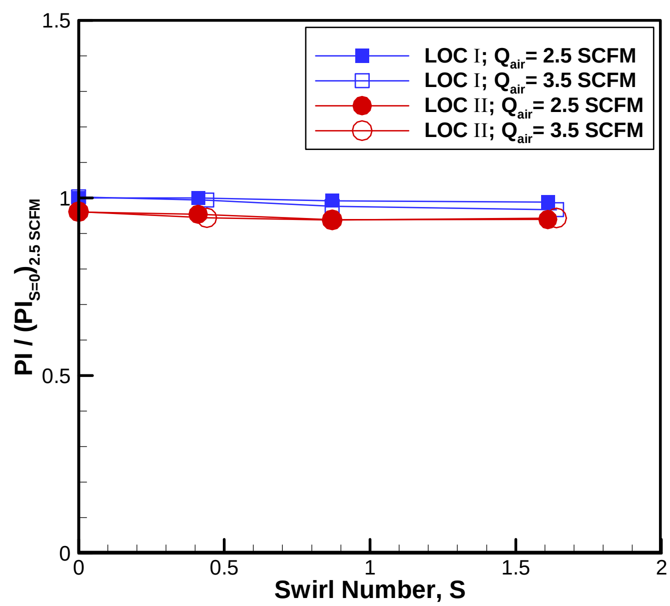

Figure 5.4 – Impact of swirl on the normalized pixel intensity of the reaction zone area of steady flames with varied co-flow flow rates at downstream locations LOC I and LOC II.

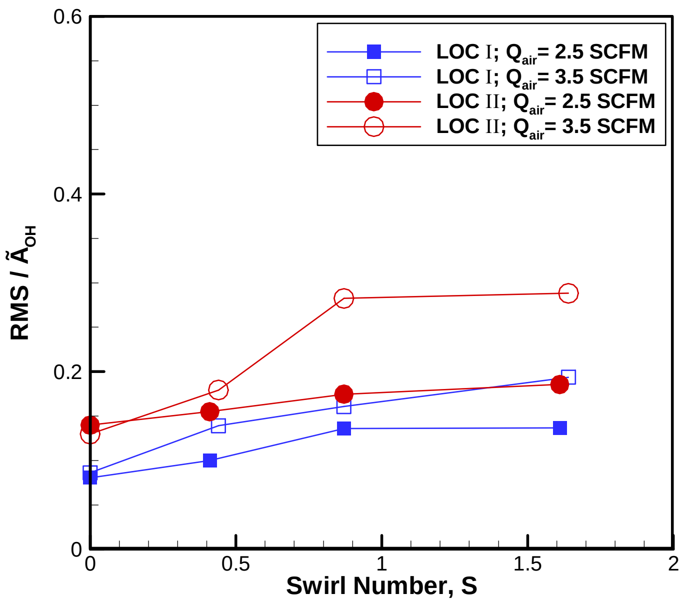

Figure 5.5 – Impact of swirl on the normalized root-mean-square (RMS) of the reaction zone area of steady flames with varied co-flow flow rates at downstream locations LOC I and LOC II.

5.2 OH PLIF of Strongly-Pulsed Flames with/without Swirl

5.2.1. OH-Zone Structure of Strongly-Pulsed Flames with/without Swirl

All of the OH PLIF images presented in this section along with those shown in Appendix D for strongly-pulsed flames, both with and without swirl, were taken at specific times relative to the start of the fuel injection interval. This was done by phase-locking the laser to the fuel jet injection cycle. Representative OH PLIF image sequences for non-swirled, strongly-pulsed flames are shown in Fig. 5.6 for various injection times and with a fixed jet-off time of t_{off} = 20 ms. Following a particular structure in time (see Fig. 5.6) reveals some similarity in the reaction zone structure for a fixed value of the elapsed time after the start of a particular injection interval. For example, the OH structures at times t_1 and t_2 are very similar for all injection times, and the OH structures at times t_5 and t_6 for P = 8 are also similar to those at t_5 and t_6 for P = 10. In addition, a compact reaction zone structure with a short tail is confirmed for flames with a short injection time of P = 6. As the injection time is increased, the reaction zone structure at an elapsed time of approximately $t \geq 40$ ms relative to the inception of fuel injection gradually becomes similar to that of a steady flame (for example, for $t = t_4$ and $t = t_5$ for P = 8; $t = t_3$, $t = t_4$, and $t = t_5$ for P = 10). Except for the apparent discontinuity at the instantaneous flame tip (discussed later), these OH PLIF-based observations of the reaction zone structure for non-swirled, strongly-pulsed flames are broadly consistent with the observation of the luminous flame structure for these types of flames. Specifically, for short injection times, flames appear to exhibit a compact, puff-like structure and elongated flames, similar in behavior to steady flames, occur for long injection times.

The effect of jet-off time on the reaction zone structure of non-swirled, strongly-pulsed flames can be seen in the image sequences presented in Fig. 5.7. Except for times near the start of the injection interval, i.e. $t \leq t_3$, flames with different jet-off times at a fixed injection time exhibit a similar reaction zone structure. As mentioned previously, the degree of interaction between flame puffs is essentially governed by the jet-off time. A closely-spaced reaction zone structure between two adjacent flame puffs is observed for strongly-pulsed flames with short jet-off times (see t_1 and t_7 in Fig. 5.7 (a)), consistent with the increased competition between flame puffs for the available oxidizer with decreased jet-off time. In addition, the reaction zone structure at $t = t_3$ and t_4 in Fig. 5.7 for flames with a long jet-off time of t_{off} = 100 ms seems to exhibit a somewhat more puff-like structure than for the cases with shorter jet-off times. The puff-like OH-zone structure is consistent with the previous observation that flames with an injection time of $P \leq 8$ can exhibit a puff-like structure for a sufficiently long jet-off time. The relatively more upstream location of the OH-zone leading edge for flames with a relatively longer jet-off time (most evident for $t = t_3$) is also consistent with the decreased celerity with increased jet-off time, due to a greater momentum exchange between the fuel jet and the co-flow, due to the lack of competition between flame puffs. In general, the strongly-pulsed flames without swirl shown in Figs. 5.6 and 5.7 appear to have a more convoluted reaction zone structure than steady flames (compare Figs. 5.1 and 5.2), suggesting a relatively stronger impact of flow on the flame structure for pulsed flames than for steady flames, possibly due to the increased coherence and intensity of large-scale motions in the near field caused by the strongly-pulsed fuel injection.

It is noted that there are, in many cases, apparent discontinuities or “holes” at the instantaneous flame tip (marked by red circles in Figs 5.6 and 5.7) in the early period of the fuel injection interval. The OH zones for the flames that exhibit these holes are generally highly-wrinkled and quite broad, somewhat similar to the reaction zone structure in a premixed flame [94]. Based on a further examination without the quarl present, the hole appears to most probably be due to the non-ignition of injected fuel, possibly due to the high strain rate near the exit of the fuel nozzle, leading to a high turbulent mixing rate competitive with the chemical reaction rate, resulting in the non-ignition of fuel.

The interactions between the flow turbulence and the reactant chemistry in a turbulent flame are typically characterized by the Damköhler number (*Da*), which represents the ratio of a characteristic flow time (τ_{flow}) to a characteristic chemical time (τ_{chem}), i.e., $Da = \tau_{flow}/\tau_{chem}$. To estimate the *Da* at the exit of the fuel nozzle, the characteristic flow time can be taken to be the inverse of the global strain rate (U_{jet}/d) and the characteristic chemical time is retreated from a laminar ethylene flame (δ_L/S_L, where δ_L is the laminar flame thickness and S_L is the laminar flame speed) [40, 82]. This gives a Damköhler number of approximately 0.69 at the instant of fuel injection for the conditions of the current work, suggesting that the reaction rate is slow in comparison with the mixing rate, resulting in the non-ignition of fuel. It is suggested that when the Damköhler number is less than unity, the combustion system approaches the limit of a homogeneous, reaction mixture [40, 95], which could in turn result in the broad OH-zone structure, as seen in Figs. 5.6 and 5.7.

The discontinuity in the reaction zone is observed for all non-swirled strongly-pulsed flames. The discontinuity disappears more rapidly (closer to the start of the fuel injection interval) for flames with a jet-off time of τ_{off} = 111, possibly due to the more closely-spaced flame puff structures, by which the flame puff in the previous injection cycle may provide a combustible environment with high temperature that facilitates the ignition of the following injected fuel puff.

The effects of swirl on the flame zone structure of strongly-pulsed flames are illustrated in the selected OH PLIF image sequences shown in Figs. 5.8 and 5.9 for flames with interacting (τ_{off} = 111) and isolated flame puff structures (τ_{off} = 1110), respectively. Similar to the observation in steady flames, the OH zones for swirled flames appear to be slightly thicker and are generally located further away from the flame centerline than those for non-swirled flames. In addition, the OH zones are somewhat more convoluted for the case of swirled flames with the same injection conditions, possibly due to an increased impact of flow on the flame structure as the swirl level is increased, as mentioned previously. It is evident that the separation between flame puffs for highly-interacting flames (τ_{off} = 111) is decreased as the swirl level is increased, as shown in Fig. 5.8, consistent with the observations on flame luminosity seen in Fig. 3.5. With sufficiently strong swirl, the separation between flame puffs ceases to be ascertainable. This decreased separation is consistent with the decreased flame puff celerity, higher rate of entrainment and increased jet/co-flow momentum exchange due to swirl discussed previously.

The co-flow strength is found to have some impact on the OH-zone structure for strongly-pulsed flames, both with and without swirl, as seen in Figs 5.8 and 5.9. For non-swirled, strongly-pulsed flames, the OH-zone structure is found to be slightly closer to the flame centerline with a high co-flow flow rate. This relatively narrower flame is possibly due to the slower spread rate of the fuel jet due to the decreased shear between the fuel jet and the co-flow air. For swirled, strongly-pulsed flames, the increased co-flow strength generally results in a more convoluted OH-zone structure, similar to those seen in steady flames, suggesting a relatively stronger flow-flame interaction for these flames. The discontinuity in the OH zones is generally seen to diminish when swirl is imposed on the co-flow stream, possibly due to the decreased strain rate caused by swirl [10] which is a consequence of the decreased flame puff celerity in swirled flames. The discontinuity of the OH zones in swirled flames can still occur, but with a significantly decreased frequency compared to non-swirled flames. The less-frequently seen discontinuity in the OH zones in swirled flames may suggest a broader flammability limit with swirl, consistent with Feikema *et al.*'s study [10], in which the blowout limits of a non-premixed flame can be significantly improved by adding swirl to the co-flow stream.

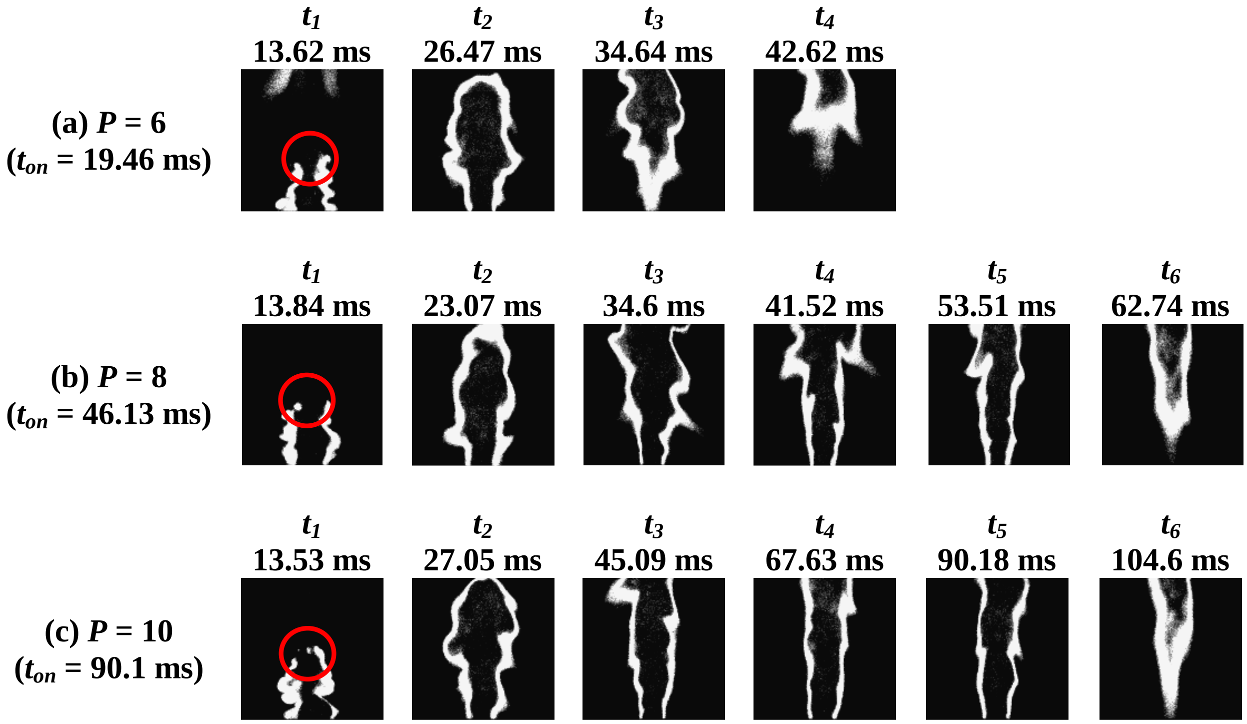

Figure 5.6 – Sequence of representative OH PLIF images through a typical fuel injection interval for non-swirled, strongly-pulsed flames with an injection time of (a) P = 6; (b) P = 8; and (c) P = 10. The jet-off time is t_{off} = 20 ms (τ_{off} = 222) in all cases. The times cited are the elapsed times after the start of the fuel injection interval. The co-flow is 2.5 SCFM. The discontinuity in the OH zones is marked with a red circle. The image size is 3.125” × 3.125”.

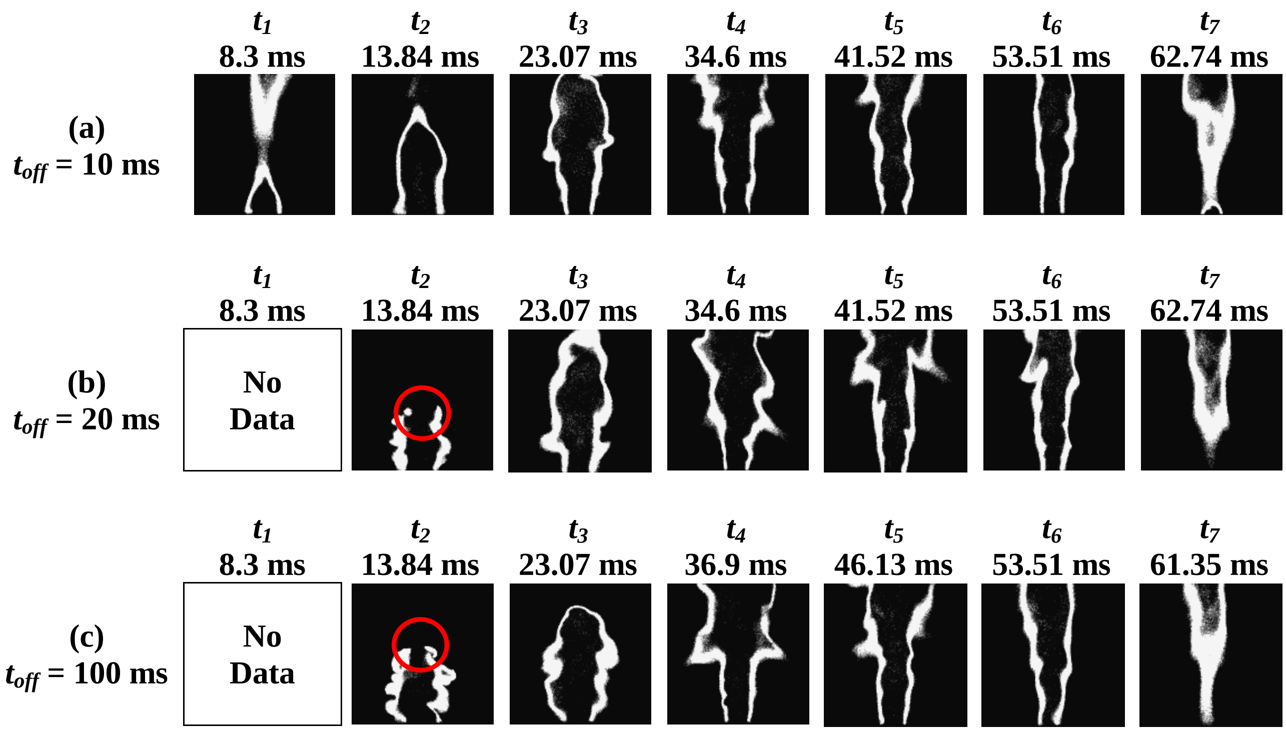

Figure 5.7 – Sequence of representative OH PLIF images through a typical fuel injection interval for non-swirled, strongly-pulsed flames with a jet-off time of (a) t_{off} = 10 ms (τ_{off} = 111); (b) t_{off} = 20 ms (τ_{off} = 222); and (c) t_{off} = 100 ms (τ_{off} = 1110). The injection time is t_{on} = 46.13 ms (P = 8) in all cases. The times cited are the elapsed times after the start of the fuel injection interval. The co-flow is 2.5 SCFM. The discontinuity in the OH zones is marked with a red circle. The image size is 3.125” × 3.125”.

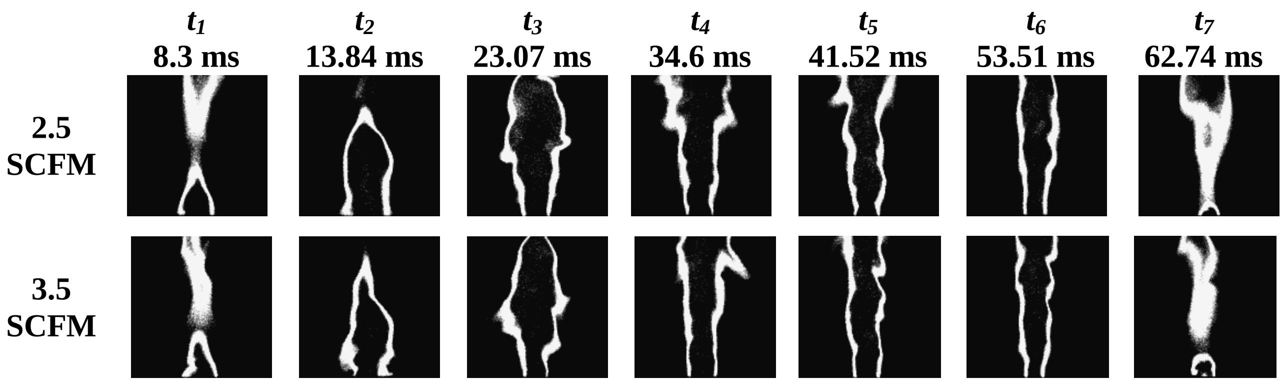

(a) *S* = 0

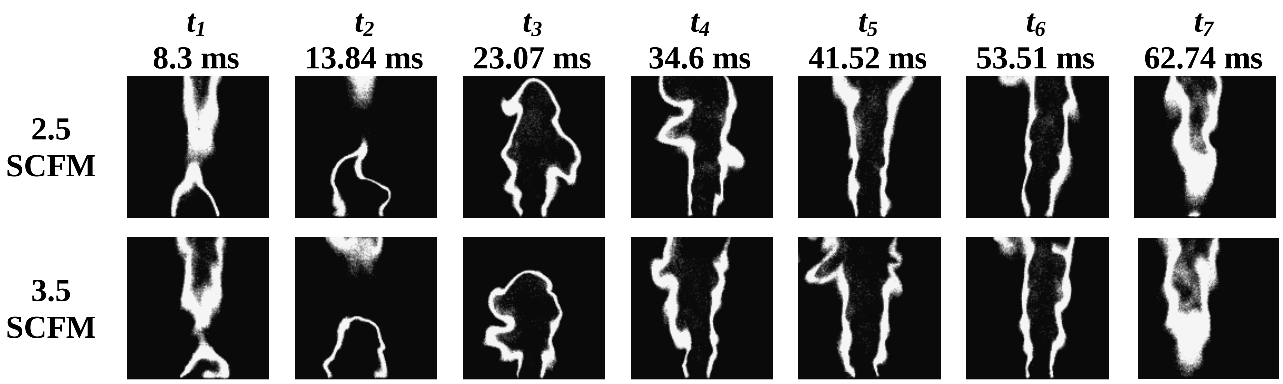

(b) *S* = 0.4

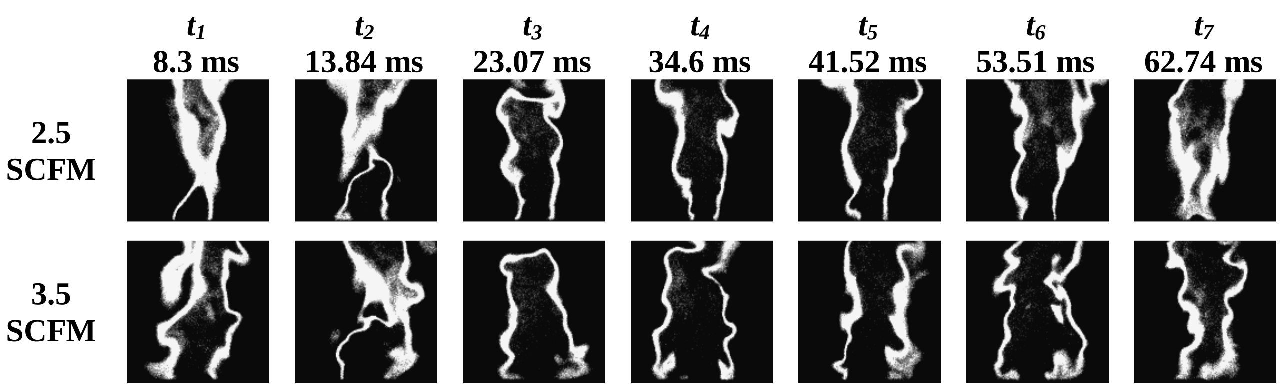

(c) *S* = 1.6

Figure 5.8 – Sequence of representative OH PLIF images through a typical fuel injection interval for strongly-pulsed flames with interacting flame structures and with a swirl level of (a) S = 0; (b) S = 0.4; and (c) S = 1.6. The times cited are the elapsed times after the start of the fuel injection interval. The injection conditions are P = 8 (t_{on} = 46.13 ms) and τ_{off} = 111 (t_{off} = 10 ms). The image size is 3.125” × 3.125”.

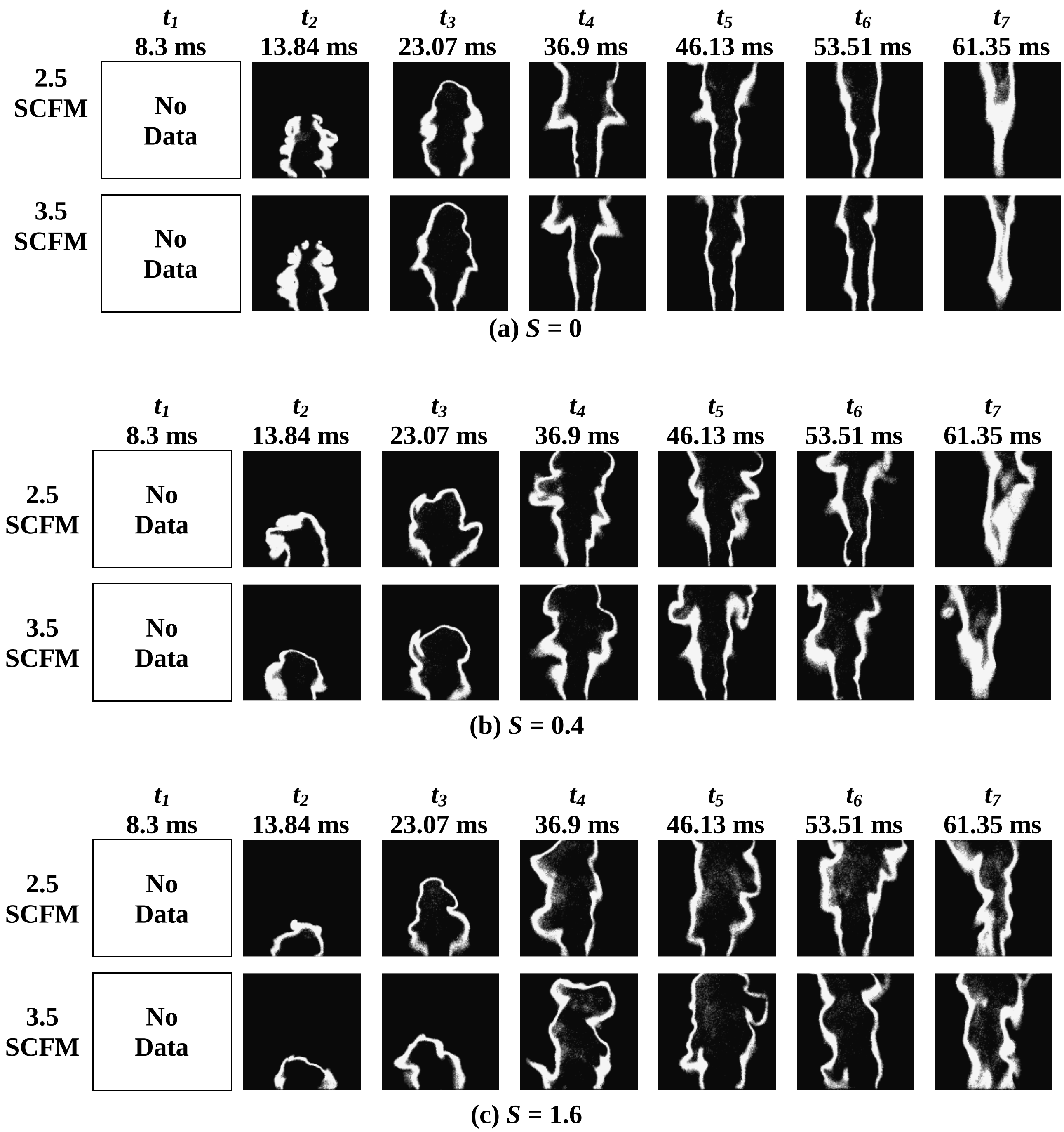

Figure 5.9 – Sequence of representative OH PLIF images through a typical fuel injection interval for strongly-pulsed flames with isolated flame puff structures and with a swirl level of (a) S = 0; (b) S = 0.4; and (c) S = 1.6. The times cited are the elapsed times after the start of the fuel injection interval. The injection conditions are P = 8 (t_{on} = 46.13 ms) and τ_{off} = 1110 (t_{off} = 100 ms). The image size is 3.125” × 3.125”.

5.2.2. Statistics of OH Zones for Strongly-Pulsed Flames with/without Swirl

Time-traces of the mean OH-zone area ($\tilde{A}_{OH}$) and the normalized RMS at LOC I for strongly-pulsed flames, both with and without swirl, are shown in Figs. 5.10-5.12 for P = 6, 8, and 10, respectively, for different values of the jet-off time. The peak values of $\tilde{A}_{OH}$ and the maximum peak values of the normalized RMS for each case are summarized in Tables 5.1 and 5.2, respectively. The dashed line in each plot represents the value for the steady flame with the corresponding swirl level. Due to the fuel pulsing, the OH-zone statistics for strongly-pulsed flames, regardless of the swirl level, are strong functions of time. The peak value of $\tilde{A}_{OH}$ for strongly-pulsed flames, both with and without swirl, generally occurs at the moment when the tail of the flame puff starts to appear at LOC I, as seen, for example, at $t = t_7$ in Figs. 5.8 and 5.9. The comparatively broad OH zone (i.e., high value of $\tilde{A}_{OH}$) seen near the flame centerline at the end of fuel injection in those images ($t = t_7$ in Figs. 5.8 and 5.9) is possibly due to the combined effect of the rapid flame puff tail burn-out [48] and the slow three-body OH radical recombination [30]. The separation between any two adjacent peaks of $\tilde{A}_{OH}$ is mainly governed by the fuel injection parameters (t_{on} (or P) and t_{off} (or τ_{off})), due to the fact that the separation between any two injected fuel puffs in strongly-pulsed flames, both with and without swirl, is controlled by the injection time and the jet-off time, even though the spaced-separation between two flame puffs can also be decreased by the presence of swirl, as discussed previously.

The peak value of $\tilde{A}_{OH}$ is generally not seen to be strongly impacted by the jet-off time, but is seen to increase with increased swirl level and appears to be a maximum for flames with a short injection time of P = 6, as seen in Table 5.1. The increased peak value of $\tilde{A}_{OH}$ for strongly-pulsed flames with swirl is consistent with the increased value of $\tilde{A}_{OH}$ for steady flames with swirl, possibly due to the broader distribution of the reacting mixture, as suggested by Masri *et al*.

[30]. As seen in Figs. 5.8 and 5.9, the more convoluted structure of the OH zones for swirled flames could also contribute to the increase in the computed value of $\tilde{A}_{OH}$. The high peak value of $\tilde{A}_{OH}$ for flames with P = 6 may be associated with the rapid tail burn-out for these flames possibly due to the relatively leaner overall reactant mixture for flames with shorter injection times resulting from the small injected fuel volume compared with the available air. Another possibility for the high values of $\tilde{A}_{OH}$ for flames with P = 6 may be the persistence of a premixed-like OH-zone structure within such a short injection interval, as suggested by Fig. 5.6. The premixed-like OH-zone structure is generally broad and convoluted, consistent with the high value of $\tilde{A}_{OH}$.

The overall values of $\tilde{A}_{OH}$ for strongly-pulsed flames, both with and without swirl, are generally higher than those for steady flames, both with and without swirl. The peak values are up to a factor of two higher than those of steady flames for both swirled and non-swirled cases, as seen in Table 5.1. The values of $\tilde{A}_{OH}$ however do not exceed those of steady flames in the early stages of fuel injection or during the interval between two fuel injections, where the minimum $\tilde{A}_{OH}$ is in Figs 5.10-5.12. At these times a single flame puff is starting to develop and passing through the image field (i.e. LOC I), for example at $t = t_2$ in Figs. 5.8 and 5.9. After that time, the value of $\tilde{A}_{OH}$ rises and, for some injection conditions, reaches a plateau, followed by the peak $\tilde{A}_{OH}$ at the end of fuel injection. The value in the plateau region, for non-swirled flames, is comparable to $\tilde{A}_{OH}$ of non-swirled steady flames, but becomes slightly higher than that of steady flames for swirled flames. The plateau region is most apparent for flames with a long injection time of P = 10, consistent with the fact that strongly-pulsed flames with long injection times ($P \geq 10$) have an elongated flame structure similar to that of a steady flame. As the jet-off time is increased, the values of $\tilde{A}_{OH}$ for strongly-pulsed flames, both with and without swirl, can decrease to essentially zero during the period of jet-off time, when no reaction is apparent at LOC I. As mentioned previously, however, the spatial separation between two adjacent flame puffs can be decreased as the swirl level is increased, as seen in Fig. 5.8. The decreased spatial separation between flame puffs at LOC I directly leads to an increase in the value of $\tilde{A}_{OH}$. The generally higher values of $\tilde{A}_{OH}$ for non-swirled, strongly-pulsed flames compared to those of steady flames without swirl are consistent with Kim *et al.*'s study of turbulent non-premixed jet flames with acoustic forcing [46]. Kim *et al*. attributed the increased OH-zone area to the increased flame-vortex interaction due to the acoustic excitation, which also resulted in some enhanced air entrainment. The overall increase in the values of $\tilde{A}_{OH}$ for strongly-pulsed flames with swirl, consistent with the steady flames results, may suggest an even more rapid rate of air entrainment due to the added swirl, consistent with Feikema *et al.*'s [28] and Masri *et al.*'s [30] studies.

The normalized RMS profiles of $\tilde{A}_{OH}$ are also seen to have high values during the injection interval, and some flames appear to exhibit a double-peak in the RMS profile. This is believed to be a general result – the lack of a distinct double-peak in the RMS profile for some flames is likely mostly an artifact of the limited repetition rate of the laser. The peak RMS values do not coincide with the peak $\tilde{A}_{OH}$; instead, they generally accompany low values of $\tilde{A}_{OH}$. In general, the first peak RMS occurs at the moment when the flame puff is developing and the flame front edge is passing through LOC I, such as $t = t_1$ in Fig. 5.6, $t = t_2$ in Fig. 5.7, and $t = t_2$ and $t = t_3$ in Fig. 5.9. The first high RMS value associated with the high fluctuation of the OH-zone distribution may be due to the transition of the OH-zone structure, from a highly wrinkled and thick (premixed-like) reaction zone structure, which varies strongly from time to time, to the smooth and thin (pure diffusion flame-like) reaction zone structure. The second peak value of the

RMS, where it is observed, occurs immediately after the peak $\tilde{A}_{OH}$ appears, at the moment when the tail of the flame puff starts to disappear at LOC I, for example at $t = t_4$ for $P = 6$ shown in Fig. 5.6. This second peak RMS value may be associated with the intrusion of the surrounding co-flow air across the combustor centerline.

The values of the peak RMS generally appear to be higher for swirled flames than those for non-swirled flames, as seen in Table 5.2, possibly due to the relatively stronger flow-flame interaction in swirled flames, consistent with the steady-flame results. In addition, the peak RMS values are generally lower for flames with a short normalized jet-off time of $\tau_{off} = 111$, possibly due to the more closely-spaced flame structures, leading to more rapid ignition between successive flame puffs, resulting in less of a transition in the OH-zone structure. However, the peak RMS values are not seen to be strongly impacted by the injection time, consistent with the independence of the OH-zone discontinuity on the injection time, as seen in Fig. 5.6.

Following the first peak in the RMS values, the value of the normalized RMS rapidly decreases to a lower value, where the RMS values of non-swirled, strongly-pulsed flames become comparable to those of non-swirled, steady flames. For strongly-pulsed flames with swirl, by contrast, the RMS values are generally higher than those for steady flames with the corresponding swirl level. The decreased spatial separation between flame puffs in swirled flames is also evident in the normalized RMS profile. With sufficiently strong swirl, the RMS profile for flames with strongly-interacting flame structures ($\tau_{off} = 111$) appears to be similar to that for steady flames, but with a somewhat higher value. The overall RMS results suggest a higher degree of the flow-flame interaction in swirled flames, possibly due to the increased turbulence level due to swirl [11, 14, 30], consistent with the steady-flame results.

The effect of the co-flow strength on the OH PLIF statistics for strongly-pulsed flames, both with and without swirl, can be seen by comparing Fig. 5.11, for a co-flow of 2.5 SCFM, with Fig. 5.13, for a co-flow of 3.5 SCFM. The profiles of $\tilde{A}_{OH}$ and RMS in those two figures are generally comparable, but the values of $\tilde{A}_{OH}$ and RMS are slightly different. For non-swirled flames, for example, with a co-flow of 3.5 SCFM, the values of $\tilde{A}_{OH}$ in the moment when the tail of the flame puff is first seen at LOC I (such as $t = t_7$ in Figs. 5.8 and 5.9), corresponding to the moment when the peak $\tilde{A}_{OH}$ occurs in Fig. 5.13, are slightly lower than those for flames with a co-flow of 2.5 SCFM, as seen in Fig. 5.11, possibly due to the narrower OH-zone structure of the flame puff tail for flames with a higher co-flow flow rate, as seen in Figs. 5.8 and 5.9. The more slender OH tail structure may be more subjected to the intrusion of the surrounding co-flow air, thus resulting in the relatively higher peak value of RMS for flames with the higher co-flow flow rate. The overall values of $\tilde{A}_{OH}$ and RMS are generally higher for swirled flames with a co-flow of 3.5 SCFM than those with a co-flow of 2.5 SCFM. The increased values of $\tilde{A}_{OH}$ and RMS with the increased co-flow strength are consistent with the more convoluted OH-zone structure and the relatively stronger flow-flame interaction for swirled flames with a higher co-flow flow rate, as discussed previously in Section 5.2.1. The decreased fluctuation amplitude of $\tilde{A}_{OH}$ and RMS (the difference between the peak and the lowest values) for some swirled flames with a co-flow of 3.5 SCFM is consistent with the more decrease in the spaced-separation between flame puffs with the increased co-flow strength, as seen in Fig. 5.8.

The effect of the quarl on the values of $\tilde{A}_{OH}$ and RMS for strongly-pulsed flames, both with and without swirl, with an injection time of $P = 8$ can be seen by comparing Fig. 5.11, with the quarl present, with Fig. 5.14, where the quarl is absent. The values for steady flames in Fig. 5.14 are with the quarl present. The addition of the quarl is not found to have a significant impact on the values of $\tilde{A}_{OH}$ and RMS for non-swirled flames, but does result in an increase in the cycle-averaged values of $\tilde{A}_{OH}$ for swirled flames, especially for flames with the strongest swirl (S= 1.61). The decreased fluctuation amplitude of $\tilde{A}_{OH}$ and RMS for flames with a swirl level of S = 1.61 with the addition of the quarl is consistent with the more closely-spaced separation between flame puffs for swirled flames when the quarl is present discussed previously.

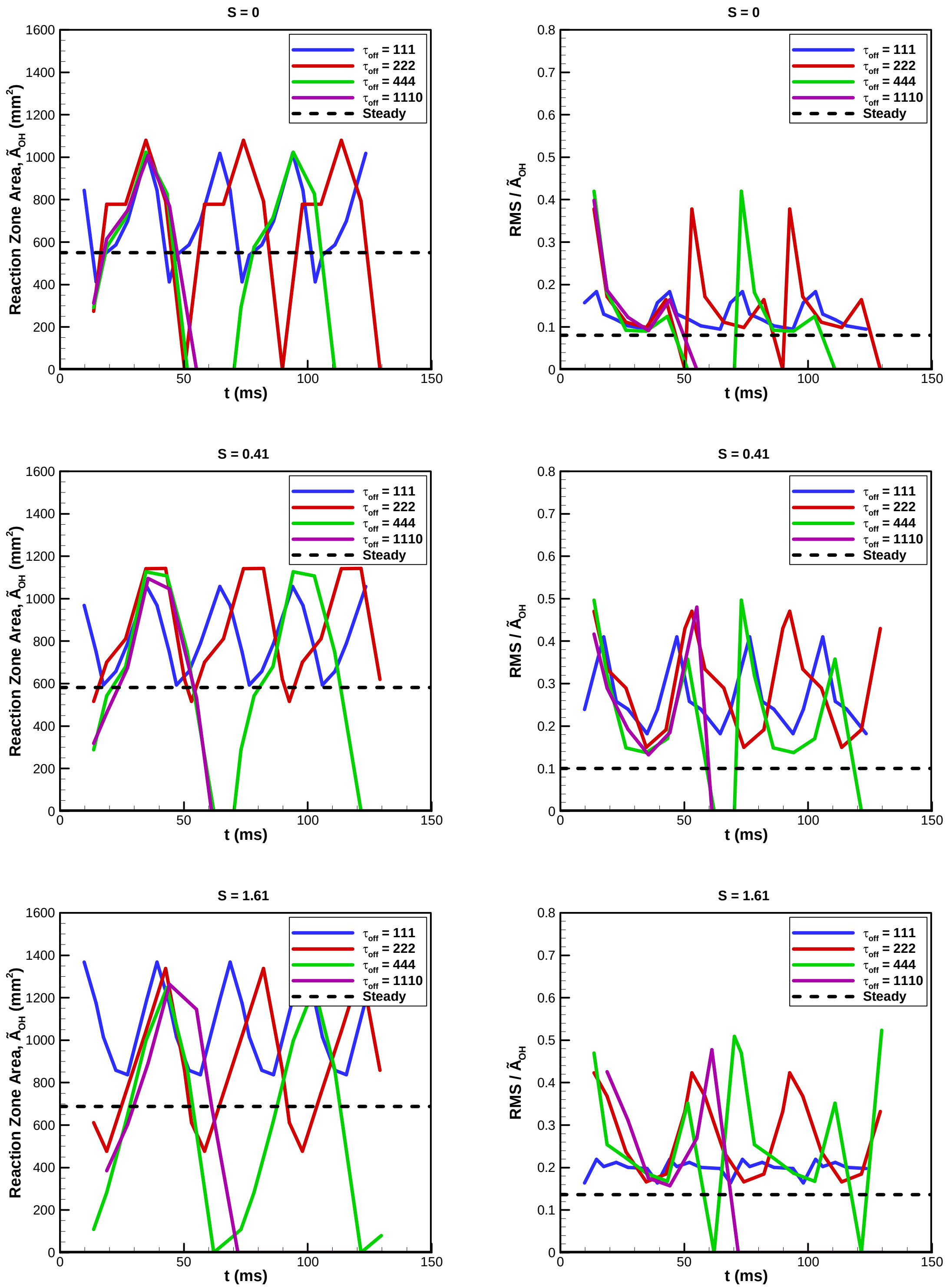

Figure 5.10 – The impact of swirl on the reaction zone area and the normalized RMS of the reaction zone area of strongly-pulsed flames with a dimensionless injection time of *P* = 6. The co-flow is 2.5 SCFM. Results are at LOC I with the quarl present.

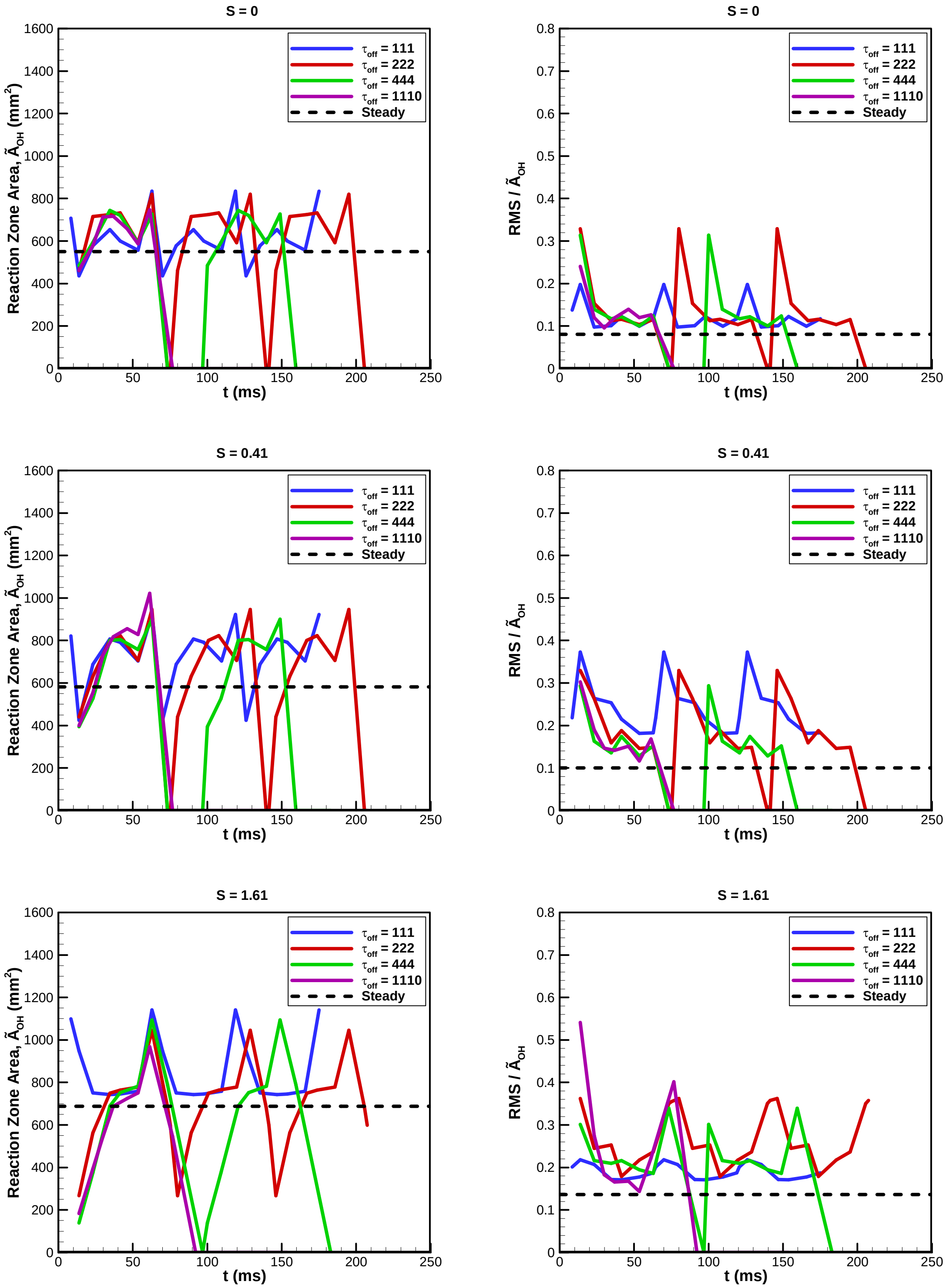

Figure 5.11 – The impact of swirl on the reaction zone area and the normalized RMS of the reaction zone area of strongly-pulsed flames with a dimensionless injection time of *P* = 8. The co-flow is 2.5 SCFM. Results are at LOC I with the quarl present.

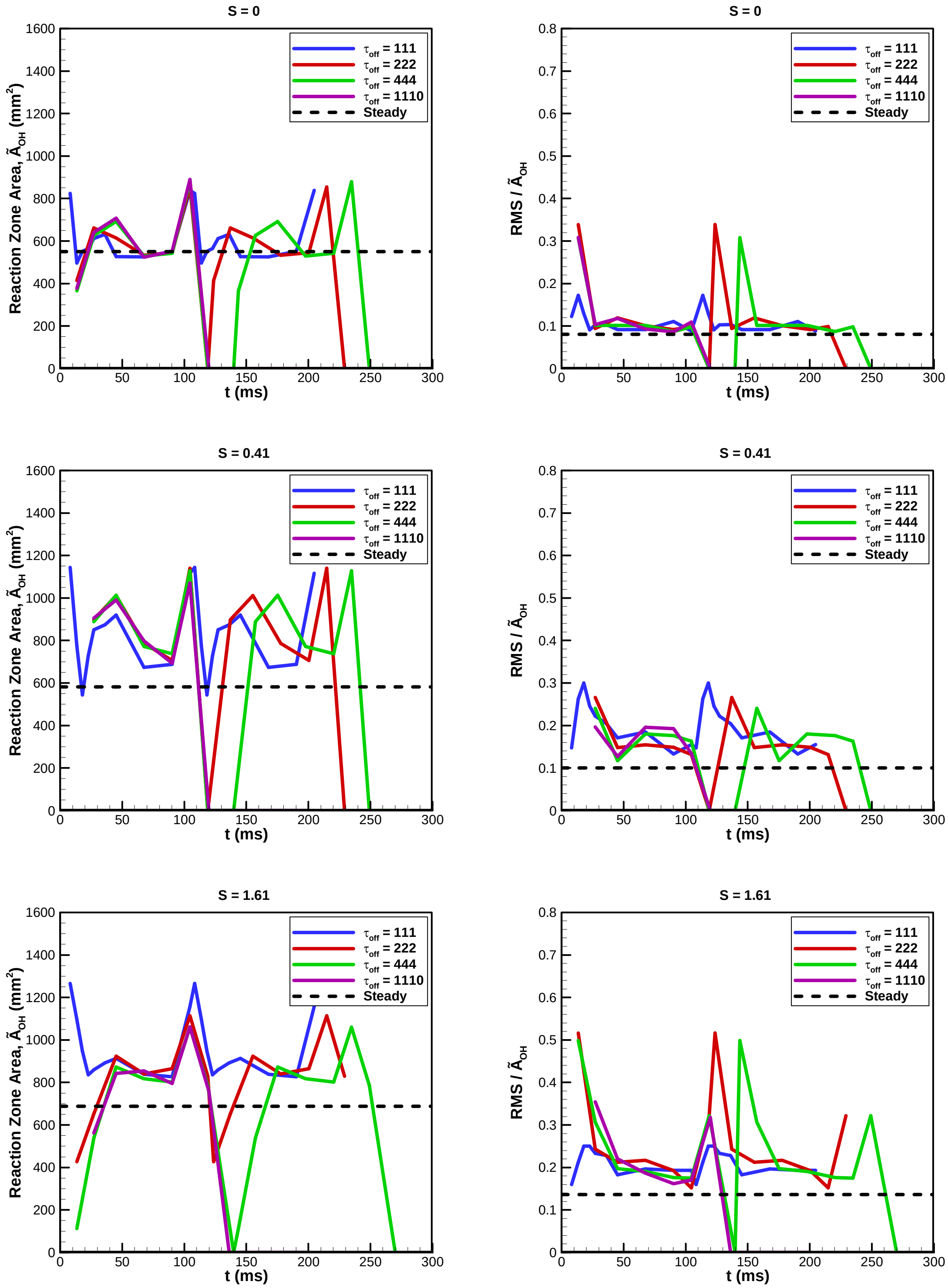

Figure 5.12 – The impact of swirl on the reaction zone area and the normalized RMS of the reaction zone area of strongly-pulsed flames with a dimensionless injection time of *P* = 10. The co-flow is 2.5 SCFM. Results are at LOC I with the quarl present.

Peak Values of $\tilde{A}_{OH}$ (Unit: mm^2)						
***S* = 0**	***Q_{air}* = 2.5 SCFM**		**τ_{off} = 111**	**τ_{off} = 222**	**τ_{off} = 444**	**τ_{off} = 1110**
		***P* = 6**	1017.62	1079.01	1023.56	1008.29
		***P* = 8**	834.15	820.62	743.72	746.68
		***P* = 10**	838.77	854.26	879.46	889.83
		Steady	549.81			
	***Q_{air}* = 3.5 SCFM**		**τ_{off} = 111**	**τ_{off} = 222**	**τ_{off} = 444**	**τ_{off} = 1110**
		***P* = 8**	691.3159	737.8174	671.5303	727.2793
		Steady	569.05			
***S* = 0.4**	***Q_{air}* = 2.5 SCFM**		**τ_{off} = 111**	**τ_{off} = 222**	**τ_{off} = 444**	**τ_{off} = 1110**
		***P* = 6**	1057.34	1143.00	1126.48	1095.28
		***P* = 8**	922.90	946.39	900.75	1021.69
		***P* = 10**	1143.22	1140.48	1127.96	1070.59
		Steady	581.67			
	***Q_{air}* = 3.5 SCFM**		**τ_{off} = 111**	**τ_{off} = 222**	**τ_{off} = 444**	**τ_{off} = 1110**
		***P* = 8**	869.3206	908.7867	869.3236	1014.871
		Steady	660.07			
***S* = 1.6**	***Q_{air}* = 2.5 SCFM**		**τ_{off} = 111**	**τ_{off} = 222**	**τ_{off} = 444**	**τ_{off} = 1110**
		***P* = 6**	1368.47	1338.05	1248.43	1263.418
		***P* = 8**	1140.65	1045.24	1093.98	967.6391
		***P* = 10**	1265.68	1113.69	1059.41	1060.82
		Steady	688.04			
	***Q_{air}* = 3.5 SCFM**		**τ_{off} = 111**	**τ_{off} = 222**	**τ_{off} = 444**	**τ_{off} = 1110**
		***P* = 8**	1098.266	1280.465	1276.836	1078.539
		Steady	853.13			

Table 5.1 – Summary of the peak values of $\tilde{A}_{OH}$ for each flame case.

Maximum Values of RMS/$\tilde{A}_{OH}$						
S = 0	Q_{air} = 2.5 SCFM		τ_{off} = 111	τ_{off} = 222	τ_{off} = 444	τ_{off} = 1110
		P = 6	0.18	0.38	0.42	0.40
		P = 8	0.20	0.33	0.31	0.24
		P = 10	0.17	0.34	0.31	0.31
		Steady	0.08			
	Q_{air} = 3.5 SCFM		τ_{off} = 111	τ_{off} = 222	τ_{off} = 444	τ_{off} = 1110
		P = 8	0.23	0.29	0.30	0.24
		Steady	0.09			
S = 0.4	Q_{air} = 2.5 SCFM		τ_{off} = 111	τ_{off} = 222	τ_{off} = 444	τ_{off} = 1110
		P = 6	0.41	0.47	0.50	0.48
		P = 8	0.37	0.33	0.29	0.30
		P = 10	0.30	0.27	0.24	0.20
		Steady	0.1			
	Q_{air} = 3.5 SCFM		τ_{off} = 111	τ_{off} = 222	τ_{off} = 444	τ_{off} = 1110
		P = 8	0.41	0.28	0.27	0.26
		Steady	0.14			
S = 1.6	Q_{air} = 2.5 SCFM		τ_{off} = 111	τ_{off} = 222	τ_{off} = 444	τ_{off} = 1110
		P = 6	0.22	0.42	0.47	0.48
		P = 8	0.22	0.36	0.34	0.54
		P = 10	0.25	0.52	0.50	0.35
		Steady	0.14			
	Q_{air} = 3.5 SCFM		τ_{off} = 111	τ_{off} = 222	τ_{off} = 444	τ_{off} = 1110
		P = 8	0.27	0.43	0.47	0.35
		Steady	0.19			

Table 5.2 – Summary of the maximum peak values of the normalized RMS for each flame case.

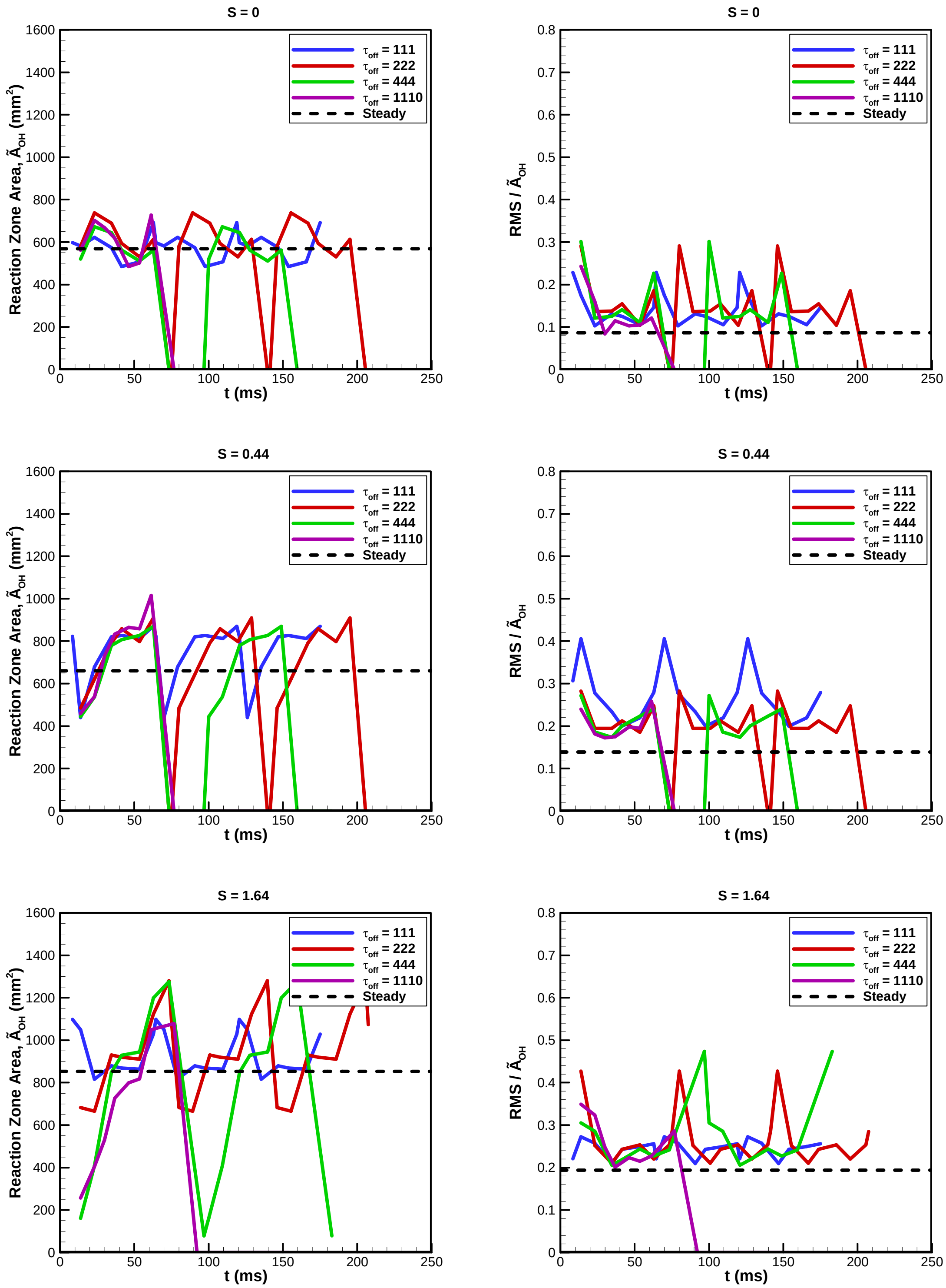

Figure 5.13 – The impact of swirl on the reaction zone area and the normalized RMS of the reaction zone area of strongly-pulsed flames with a dimensionless injection time of *P* = 8. The co-flow is 3.5 SCFM. Results are at LOC I with the quarl present.

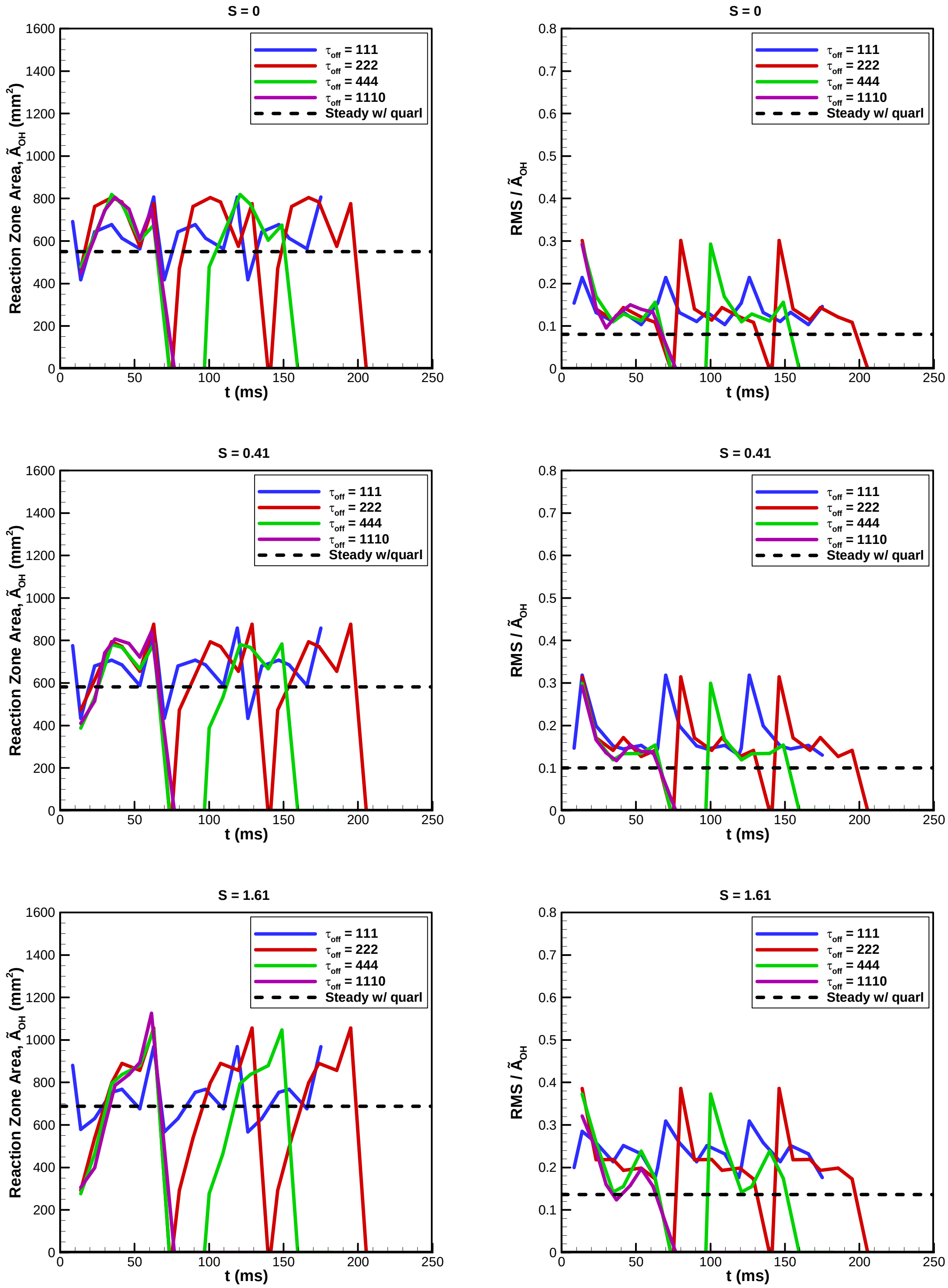

Figure 5.14 – The impact of swirl on the reaction zone area and the normalized RMS of the reaction zone area of strongly-pulsed flames with a dimensionless injection time of *P* = 8. The co-flow is 2.5 SCFM. Results are at LOC I without the quarl present.

CHAPTER 6

CONCLUSIONS

This work studied the structure, dynamics and emissions of turbulent, strongly-pulsed jet diffusion flames in the presence of swirl. Three major diagnostics techniques were employed in this study: High-speed video imaging, standard emissions analyzers, and OH planar laser-induced fluorescence (PLIF). The high-speed video imaging of the flame luminosity allowed for the determination of the flame length and the flame puff celerity as well as the detailed study of the flame puff interactions. The concentration levels of CO and NO in the flames were measured by using standard emissions analyzers combined with an aspirated sampling probe. Finally, OH-PLIF imaging was employed to study the structure of reaction zones within the flames. The principal conclusions resulting from this work are summarized below.

Large-Scale Flame Structure

- The strongly-pulsed flames with a co-flow swirl were found to be 4-34% shorter, in terms of visual flame length, than those without swirl for the same injection conditions. The imposition of swirl had a relatively stronger effect on the length of steady flames than that of strongly-pulsed flames. In addition, the length of strongly-pulsed flames was generally impacted more by swirl for longer injection times than for shorter injection times. The relatively weaker effect of swirl on the length of strongly-pulsed flames compared to that on steady flames appeared to result from a combination of the relatively shorter residence time and the lesser amount of heat release (due to the smaller injected fuel volume) of strongly-pulsed flames than that of steady flames.

- The flames with swirl generally exhibited a flame puff celerity as much as 39% lower than for flames without swirl. The decreased flame length and flame puff celerity, corresponding to a greater momentum exchange between the fuel and the co-flow air, are consistent with an increased rate of air entrainment into each flame puff structure due to swirl.
- The separation between flame puffs decreased with the imposition of swirl. The decreased flame puff separation is consistent with the decrease in flame puff celerity due to swirl. At the same time, a decreased separation is expected to result in a stronger competition between flame puffs for the entrainment of available oxidizer, limiting the increased rate of oxidizer entrainment due to swirl.
- The length of swirled, strongly-pulsed flames was more sensitive to the co-flow strength for cases with longer injection times than those with shorter injection times. The strength of the co-flow also had a greater impact on the length of swirled flames with interacting structures than those with isolated flame puffs. The higher co-flow strength resulted in a greater increase in the length of non-swirled, strongly-pulsed flames with shorter injection times. The flame length of non-swirled flames was less sensitive to the co-flow strength for cases with interacting structures than those with isolated flame puffs. The different sensitivities to co-flow strength reflect a combination of the degree of competition between flame puffs and the residence time of interaction between the fuel and the co-flow air.
- The addition of the quarl resulted in no significant impact on the flame length of non-swirled, strongly-pulsed flames. For strongly-pulsed flames with swirl, the maximum reduction in flame length was about 34% for flames with the quarl, compared to 23% for the cases without the quarl. The quarl favors the formation of a recirculation zone where rapid entrainment and intense mixing occur, and thus results in a greater decrease in flame length.

- Three scaling relations successfully correlated the observed changes in flame length with the injection time, the fuel/air volumetric flow rate ratio, and the jet-on fraction.

CO/NO Emissions

- The level of CO emissions for strongly-pulsed flames, both with and without swirl, decreased substantially as the jet-off time was decreased. The decreased CO levels were associated with the increased residence time associated with the increased flame length. The CO levels were as much as a factor of 2.5 lower for flames with swirl than for those without swirl. The decreased CO emissions are consistent with more rapid and complete mixing between the fuel and the air by imposing swirl in the co-flow stream.
- Swirl appeared to have a stronger impact on the CO emissions for strongly-pulsed flames with shorter injection times than for those with longer injection times. Any changes in the rate of air entrainment caused by changes in the recirculation zone due to swirl can be expected to have a greater impact on the CO emissions of the compact flames that occur for short injection times.
- The higher co-flow strength generally resulted in an increase in CO levels, particularly for flames with short injection times. For non-swirled flames, the increased CO emissions are consistent with a slower rate of mixing due to decreased shear between the fuel and the co-flow air with higher co-flow strength. The increase in CO levels, for flames with swirl, is consistent with more rapid dilution and mixing with the cold oxidizer brought by more swirling co-flow air. The co-flow strength had a negligible impact on the CO emissions for both swirled and non-swirled flames with sufficiently long injection times.

- The presence of the quarl was not found to have a significant impact on the CO emissions for non-swirled, strongly-pulsed flames. For strongly-pulsed flames with swirl, in the absence of the quarl, the CO levels generally increased as the swirl level was increased. The addition of the quarl presumably favors the formation of an enlarged recirculation zone, allowing enhanced mixing between the fuel and the air, resulting in a decrease in CO levels.
- The NO concentrations of strongly-pulsed flames, both with and without swirl, for most injection conditions, were below those of steady flames. The observed changes in the NO emissions levels are consistent with changes in the rate of air entrainment caused by changes in the degree of interaction between flame puffs. The NO emissions gradually approached to the steady-flame values as the jet-off time was decreased.
- The imposition of swirl, for short injection times, was in some cases found to result in an increase in the levels of NO, consistent with the decreased CO levels observed for the same injection conditions. The elevated NO emissions, in many cases still lower than those of steady flames, are believed to be due to a longer combustion residence time due to the flow recirculation within the swirl-induced recirculation zone.
- The NO levels of strongly-pulsed flames with swirl were generally seen to slightly decrease with increased co-flow strength, consistent with a relatively greater increase in the CO levels.
- The CO emissions correlated strongly with the global residence time when taking into account the impact of air dilution over an injection cycle on the flame length of strongly-pulsed flames, both with and without swirl. The NO emissions did not successfully correlate with the global residence time, suggesting that other NO production mechanisms or other factors that could affect the NO production in hydrocarbon flames needed to be taken into account when developing the NO emissions scaling for such flames.

- For some specific cases, a simultaneous decrease in both CO and NO levels was observed in strongly-pulsed flames with swirl. This may result from rapid oxidizer entrainment (but not rapid enough to quench CO oxidation) leading to some partial fuel/air premixing and low levels of both CO and NO emissions. The lengths of these flames were generally significantly shorter than those of steady flames. These results suggest the potential of the combination of the strongly-pulsed fuel injection and co-flow swirl for developing a compact, low emissions combustor.

Flame Zone Structure

- For steady flames without swirl, the OH zones appeared to be comparatively thin in the upstream regions of flames near the exit of the quarl, and gradually gained thickness and became more contorted with downstream distance from the quarl exit. As the swirl level was gradually increased, the OH zones were generally seen to be situated further away from the flame centerline with a slightly greater thickness. In addition, the OH zones in swirled flames appeared to be more convoluted than those in non-swirled flames.
- For strongly-pulsed flames, both with and without swirl, the OH zones appeared to be more convoluted than those for steady flames, suggesting the enhanced intensity of large-sale motions caused by the strongly-pulsed fuel injection.
- For strongly-pulsed flames, both with and without swirl, the reaction zones in many cases were observed to exhibit discontinuities at the instantaneous flame tip in the early period of fuel injection. The discontinuity in the reaction zone likely resulted from the non-ignition of injected fuel, due to a relatively slower reaction rate in comparison with the mixing rate. The discontinuity in the OH zone was generally seen to diminish with increased swirl level.

- Statistics generated from the OH PLIF signals showed that the reaction zone area was generally higher (up to a factor of two) for strongly-pulsed flames, both with and without swirl, compared to those for steady flames. The reaction zone area was generally seen to increase with increased swirl level, consistent with a broader and more convoluted OH-zone structure in swirled flames. The highest value of the reaction zone area generally occurred near the tail of the flame puff, where a broader OH zone prevailed, likely due to the combined effect of the rapid flame puff tail burn-out and the slow three-body OH radical recombination.
- The root-mean-square (RMS) of the reaction zone area indicated the degree to which the reaction zones were subjected to the local flow fluctuations. For strongly-pulsed flames, the RMS values were generally higher for the cases with swirl than for those without swirl, suggesting a relatively stronger impact of flow turbulence on the flame structure for swirled flames, consistent with the steady-flame result.
- In many cases, strongly-pulsed flames, both with and without swirl, appeared to exhibit a double-peak in the RMS profile. The first peak RMS generally occurred at the moment when the flame puff was developing and going through the transition from the premixed-like reaction zone structure to the pure diffusion flame-like reaction zone structure. The second peak appeared at the moment when the tail of the flame puff started to disappear, which led to the intrusion of the surrounding co-flow air across the combustor centerline and thus resulted in high RMS values.

CHAPTER 7

FUTURE WORK

This work has shed new insight into the impact of swirl on the flame structure and exhaust emissions of strongly-pulsed flames. Further investigations are suggested to achieve a better understanding of the combustion processes in these flames and to further demonstrate the potential practical benefits of this combustion strategy.

Experiments over a wider range of Reynolds number may yield additional information on the combustion performance that may prove useful in the practical development of swirl burners incorporating strongly-pulsed fuel injection.

CH-PLIF imaging, which shows a relatively narrower flame zone than OH-PLIF imaging, is a common tool to locate the location of the flame front. The CH radical is often considered superior to OH radical as a reaction zone marker because 1) CH is produced and destroyed in a faster mechanism than OH; and 2) CH resides at a location more nearly corresponding to the location of the peak heat release compared to that given by OH. Simultaneous imaging of CH/OH radicals would enable the study of the reaction zone structure of strongly-pulsed flames with swirl in greater detail, increasing the understanding of the detailed flame zone structure and the flame ignition/extinction behavior.

Central to any non-premixed combustion process the flowfield leading to the entrainment of the oxidizer into the flame. Flow information critical to achieving a better understanding of the fuel/air mixing in swirled, strongly-pulsed flames includes local turbulence information, such as the time-varying velocity field, the vorticity field and the strain rate. This information could be obtained by employing Particle Image Velocimetry (PIV). This technique has the ability to provide non-intrusive measurements of the flow field with high spatial resolution. In addition, PIV can give quantitative determination of the rate of air entrainment into the flame. Specifically, PIV simultaneously with PLIF would enable a comprehensive study of the interaction between the flow dynamics and the chemistry reaction.

Other experiments that could reveal temporally- and spatially-resolved information of composition and temperature fields of swirled, strongly-pulsed flames would definitely bring more and greater insights into the fundamental processes operative in these flames.

BIBLIOGRAPHY

[1] "The Annual Energy Review 2010." U. S. Energy Information Administration, Department of Energy, October, 2011. http://www.eia.gov/aer.

[2] B. T. Zinn. "Pulse Combustion: Recent Applications and Research Issues." 24th Symposium (International) on Combustion, The Combustion Institute, 1297-1305, 1992.

[3] J. A. Lovett and S. R. Turns. "Experiments on Axisymmetrically Pulsed Turbulent Jet Flames." AIAA Journal 28(1), 38-46, 1990.

[4] K. R. Mcmanus, U. Vandsburger, and C. T. Bowman. "Combustor Performance Enhancement Through Direct Shear Layer Excitation." Combustion and Flame, 82, 75-92, 1990.

[5] Y. M. Tang, G. Waldherr, J. I. Jagoda, and B. T. Zinn. "Heat Release Timing in a Nonpremixed Helmholtz Pulse Combustor." Combustion and Flame, 100, 251-561, 1995.

[6] J. O. Keller, T. T. Bramlette, P. K. Barr, and J. R. Alvarez. "NO_x and CO Emissions from a Pulse Combustor Operating in a Lean Premixed Mode." Combustion and Flame, 99, 460-466, 1994.

[7] J. C. Hermanson, R. Dugnani, and H. Johari. "Structure and Flame Length of Fully-Modulated, Pulsed Diffusion Flames." Combustion Science and Technology, 155, 203-255, 2000.

[8] J. C. Hermanson and M. Fregeau. "Flame Structure Dynamics and Buoyancy Effects in Pulsed Turbulent Diffusion Flames." AIAA Paper 2006-1451, 2006.

[9] A. K. Gupta, D. G. Lilley, and N. Syred. "Swirl Flows." Abacus Press, Tunbridge Wells, England, 1984.

[10] D. Feikema, R. –H. Chen, and J. F. Driscoll. "Blowout of Nonpremixed Flames: Maximum Coaxial Air Velocities Achievable, with and without Swirl." Combustion and Flame, 86, 347-358, 1991.

[11] R. –H. Chen and J. F. Driscoll. "The Role of the Recirculation Vortex in Improving Fuel-Air Mixing within Swirling Flames." 22nd Symposium (International) on Combustion, The Combustion Institute, 531-540, 1988.

[12] M. Sadakata and J. M. Beér. “Spatial Distribution of Nitric Oxide Formation Rates in a Swirling Turbulent Methane-Air Flame.” 15th Symposium (International) on Combustion, The Combustion Institute, 93-103, 1977.

[13] P. Schmittel, B. Günther, B. Lenze, W. Lueckel, and H. Bockhorn. “Turbulent Swirling Flames: Experimental Investigation of the Flow Field and Formation of Nitrogen Oxide.” 28th Symposium (International) on Combustion, The Combustion Institute, 303-309, 2000.

[14] J. M. Beér and N. A. Chigier. “Combustion Aerodynamics.” Krieger, Applied Science Publishers, London, 1972.

[15] R. –H. Chen. “Some Characteristics of NO_x Emission of Turbulent Nonpremixed Hydrogen-Air Flames Stabilized by Swirl-Generated Flow Recirculation.” Combustion Science and Technology, 110, 443-460, 1995.

[16] S. R. Turns and R. V. Bandaru. “Carbon Monoxide Emissions from Turbulent Nonpremixed Jet Flames.” Combustion and Flame, 94, 462-468, 1993.

[17] C. O. Paschereit, E. Gutmark, and W. Weisenstein. “Coherent Structures in Swirling Flows and their Role in Acoustic Combustion Control.” Physics of Fluids 11(9), 2667-2678, 1999.

[18] C. O. Paschereit, E. Gutmark, and W. Weisenstein. “Excitation of Thermoacoustic Instabilities by Interaction of Acoustics and Unstable Swirling Flow.” AIAA Journal 38(6), 1025-1034, 2000.

[19] C. J. Lawn, S. Evesque, and W. Polifkek. “A Model for the Thermoacoustic Response of a Premixed Swirl Burner, Part I: Acoustic Aspects.” Combustion Science and Technology, 176, 1331-1358, 2004.

[20] Y. Haralupas and A. Selbach. “Imposed Oscillations and Non-Premixed Flames.” Progress in Energy and Combustion Science, 28, 75-104, 2002.

[21] A. Coghe, G. Solero, and G. Scribano. “Recirculation Phenomena in a Natural Gas Swirl Combustor.” Experimental Thermal and Fluid Science, 28, 709-714, 2004.

[22] M. G. Mungal and J. M. O’Neil. “Visual Observations of a Turbulent Diffusion Flame.” Combustion and Flame, 78, 377-389, 1989.

[23] M. G. Mungal, P. S. Karasso, and A. Lozano.”The Visible Structure of Turbulent Jet Diffusion Flames: Large-Scale Organization and Flame Tip Oscillation.” Combustion Science and Technology, 76, 165-185, 1991.

[24] P. G. Parikh and R. J. Moffat. “Resonant Entrainment of a Confined Pulsed Jet.” Journal of Fluids Engineering (ASME Transactions) 104(4), 482-488, 1982.

[25] K. Lakshminarasimhan, M. D. Ryan, N. T. Clemens, and O. A. Ezekoye. “Mixing Characteristics in Strongly Forced Non-Premixed Methane Jet Flames.” Proceedings of the Combustion Institute, 31, 1617-1624, 2007.

[26] K. Lakshminarasimhan, N. T. Clemens, and O. A. Ezekoye. “Characteristics of Strongly-Forced Turbulent Jets and Non-Premixed Jet Flame.” Experiments in Fluids, 41, 523-542, 2006.

[27] E. Ghaem-Maghami and H. Johari. “Velocity Field of Isolated Turbulent Puffs.” AIAA Paper 2007-1318, 2007.

[28] D. A. Feikema, D. Everest, and J. F. Driscoll. “Images of Dissipation Layers to Quantify Mixing within a Turbulent Jet.” AIAA Journal 34(12), 2531-2538, 1996.

[29] R. W. Bilger. “Turbulent Flows with Nonpremixed Reactants.” Turbulent Reaction Flows, edited by P. A. Libby and F. A. Williams, Vol. 44, Topics in Applied Physics, Springer-Verlag, New York, 65-113, 1980.

[30] A. R. Masri, P. A. M. Kalt, and R. S. Barlow. “The Compositional Structure of Swirl-Stabilized Turbulent Nonpremixed Flames.” Combustion and Flame, 137, 1-37, 2004.

[31] Y. M. Al-Abdeli and A. R. Masri. “Stability Characteristics and Flowfields of Turbulent Non-Premixed Swirling Flames.” Combustion Theory and Modelling, 7, 731-766, 2003.

[32] J. Panda and D. K. McLaughlin. “Experiments on the Instabilities of a Swirling Jet.” Physics of Fluids 6(1), 263-276, 1994.

[33] V. Tangirala, R. –H. Chen, and J. F. Driscoll. “Effect of Heat Release and Swirl on the Recirculation within Swirl-Stabilized Flames.” Combustion Science and Technology, 51, 75-95, 1987.

[34] N. Syred and J. M. Beér. “Combustion in Swirling Flows: A Review.” Combustion and Flame, 23, 143-201, 1974.

[35] Y. –C. Chao, Y. –W. Huang, and D. –C. Wu. “Feasibility of Controlling NO_x Emissions from a Jet Flame by Acoustic Excitation.” Combustion Science and Technology, 158, 461-484, 2000.

[36] C. O. Paschereit and E. J. Gutmark. “Enhanced Stability and Reduced Emissions in an Elliptic Swirl-Stabilized Burner.” AIAA Journal 46(5), 1063-1071, 2008.

[37] T. S. Cheng, Y. –C. Chao, D. –C. Wu, T. Yuan, C. –C. Lu, C. –K. Cheng, and J. –M. Chang. “Effects of Fuel-Air Mixing on Flame Structures and NO_x Emissions in Swirling Methane Jet Flames.” 27th Symposium (International) on Combustion, The Combustion Institute, 1229-1237, 1998.

[38] G. J. R. Newbold, G. J. Nathan, D. S. Nobes, and S. R. Turns. “Measurement and Prediction of NO_x Emissions from Unconfined Propane Flames from Turbulent-Jet, Bluff-Body, Swirl, and Processing Jet Burners.” Proceedings of the Combustion Institute, 28, 481-487, 2000.

[39] R. Puri and R. J. Santoro. “The Role of Soot Particle Formation on the Production of Carbon Monoxide in Fires.” Fire Safety Science – Proceedings of the Third International Symposium, 595-604, 1991.

[40] S. R. Turns. “An Introduction to Combustion: Concepts and Applications.” McGraw-Hill, 2000.

[41] I. Glassman and R. A. Yetter. “Combustion.” Academic Press, 2008.

[42] S. R. Turns. “Understanding NO_x Formation in Nonpremixed Flames: Experiments and Modeling.” Progress in Energy and Combustion Science, 21, 361-385, 1995.

[43] C. T. Bowman. “Control of Combustion-Generated Nitrogen Oxide Emissions: Technology Driven by Regulation.” 24th Symposium (International) on Combustion, The Combustion Institute, 859-878, 1992.

[44] J. E. Broadwell and A. E. Lutz. “A Turbulent Jet Chemical Reaction Model: NOx Production in Jet Flames.” Combustion and Flame, 114, 319-335, 1998.

[45] J. O. Keller and I. Hongo. “Pulse Combustion: The Mechanisms of NOx Production.” Combustion and Flame, 80, 219-237, 1990.

[46] M. Kim, Y. Choi, J. Oh, and Y. Yoon. “Flame-Vortex Interaction and Mixing Behaviors of Turbulent Non-Premixed Jet Flames under Acoustic Forcing.” Combustion and Flame, 156, 2252-2263, 2009.

[47] S. R. Turns and F. H. Myhr. “Oxides of Nitrogen Emissions from Turbulent Jet Flames: Part I – Fuel Effects and Flame Radiation.” Combustion and Flame, 87, 319-335, 1991.

[48] M. Fregeau. “Turbulent Structure and Emissions of Strongly-Pulsed Jet Diffusion Flames.” Ph. D. Dissertation, University of Washington, 2007.

[49] J. C. Hermanson, E. Ghaem-Maghami, and H. Johari. "CO/Unbruned Hydrocarbon Emissions of Strongly-Pulsed, Turbulent Diffusion Flames." Combustion Science and Technology, 176, 1855-1866, 2004.

[50] M. Fregeau, P. Y. Tsai, and J. C. Hermanson. "CO/NO Emissions of Strongly-Pulsed Turbulent Nonpremixed Flames." AIAA Paper 2006-809, 2006.

[51] R. –H. Chen and J. F. Driscoll. "Nitric Oxide Levels of Jet Diffusion Flames: Effects of Coaxial Air and other Mixing Parameters." 23rd Symposium (International) on Combustion, The Combustion Institute, 281-288, 1990.

[52] J. Warnatz, U. Mass, and R. W. Dibble. "Combustion: Physical and Chemical Fundamentals, Modelling and Simulation, Experiments and Pollutant Formation." Springer, 1996.

[53] K. Kohse-Höinghaus. "Laser Techniques for the Quantitative Detection of Reactive Intermediates in Combustion Systems." Progress in Energy and Combustion Science, 20, 203-279, 1994.

[54] J. C. Hermanson, H. Johari, D. P. Stocker, and U. Hegde. "Buoyancy Effects in Strongly-Pulsed, Turbulent Diffusion Flames." Combustion and Flame, 139, 61-76, 2004.

[55] Y. M. Al-Abdeli and A. R. Masri. "Recirculation and Flowfield Regimes of Unconfined Non-reacting Swirling Flows." Experimental Thermal and Fluid Science, 27, 655-665, 2003.

[56] S. C. Crowe and F. H. Champagne. "Orderly Structure in Jet Turbulence." Journal of Fluid Mechanics, 48:547-591, 1971.

[57] P. J. Vermeulen, V. Ramesh, and W. K. Yu. "Measurement of Entrainment by Acoustically Pulsed Axisymmetric Air Jets." Journal of Engineering Gas Turbines and Power, 108:479-484, 1986.

[58] H. A. Becker and S. Yamazaki. "Entrainment, Momentum Flux and Temperature in Vertical Free Turbulent Diffusion Flames." Combustion and Flame, 33, 123-149, 1978.

[59] E. A. Kocp and F. K. Browand. "Instability and Turbulence in Stratified Fluid with Shear." Journal of Fluid Mechanics, 93:135-159, 1979.

[60] J. Panda and D. K. McLaughlin. "Experiments on the Instability of a Swirling Jet." Physics of Fluids, 6(1), 263-276, 1994.

[61] A. Nauert, P. Petersson, M. Linne, and A. Dreizler. "Experimental Analysis of Flashback in Lean Premixed Swirling Flames: Conditions Close to Flashback." Experiments in Fluids, 43:89-100, 2007.

[62] H. Liang and T. Maxworthy. "An Experimental Investigation of Swirling Jets." Journal of Fluid Mechanics, 525:115-159, 2005.

[63] I. K. Toh, D. Honnery, and J. Soria. "Axial Plus Tangential Entry Swirling Jet." Experiments in Fluids, 48:309-325, 2010.

[64] B. Haynes and H. Wagner. "Soot Formation." Progress in Energy and Combustion Science, 7, 229-273, 1981.

[65] C. A. Idicheria, I. G. Boxx, and N. T. Clemens. "Characteristics of Turbulent Nonpremixed Jet Flames under Normal- and Low-Gravity Conditions." Combustion and Flame, 138, 384-400, 2004.

[66] M. C. Drake, S. M. Correa, R. W. Pitz, W.Shyy, and C. P. Fenimore. "Superequilibrium and Thermal Nitric Oxide Formation in Turbulent Diffusion Flames." Combustion and Flame, 69, 347-365, 1987.

[67] W. Meier, I. Boxx, M. Stőhr, C. D. Carter. "Laser-Based Investigations in Gas Turbine Model Combustors." Experiments in Fluids, 49:865-882, 2010.

[68] J. M. Donbar, J. F. Driscoll, and C. D. Carter. "Reaction Zone Structure in Turbulent Nonpremixed Jet Flames – From CH-OH PLIF Images." Combustion and Flame, 122, 1-19, 2000.

[69] W. R. Hawthorne, D. D. Weddel, and H. C. Hottel. "Mixing and Combustion in Turbulent Gas Jets." 3rd Symposium (International) on Combustion, The Combustion Institute, 266-288, 1949.

[70] W. J. A. Dahm and A. G. Mayman. "Blowout Limits of Turbulent Jet Diffusion Flames for Arbitrary Source Conditions." AIAA Journal 28(7), 1157-1162, 1990.

[71] W. J. A. Dahm and P. E. Dimotakis. "Mixing at Large Schmidt Number in the Self-Similar Far Field of Turbulent Jets." Journal of Fluid Mechanics, 217:299-330, 1990.

[72] J. C. Hermanson, R. Sangras, J. E. Usowicz, and H. Johari. "Effects of Coflow on Turbulent Flame Puffs." AIAA Journal 40(7), 1355-1362, 2002.

[73] H. Johari. "Mixing in Thermals with and without Buoyancy Reversal." Journal of the Atmospheric Sciences, 49(16), 1412-1426, 1992.

[74] J. E. Broadwell, W. J. A. Dahm, and M. G. Mungal. "Blowout of Turbulent Diffusion Flames." 20th Symposium (International) on Combustion, The Combustion Institute, 303-310, 1984.

[75] M. F. Zabielski, L. G. Dodge, M. B. Colket III, and D. J. Seery. "The Optical and Probe Measurement of NO: A Comparative Study." 18th Symposium (International) on Combustion, The Combustion Institute, 1591-1598, 1981.

[76] Y. –H. Liao and J. C. Hermanson. "The Effect of Swirl on the Flame Structure of Strongly-Pulsed Turbulent Diffusion Flames." 7th US National Combustion Meeting, Georgia Institute of Technology/The Combustion Institute, March 2011.

[77] N. Peters and S. Donnerhack. "Structure and Similarity of Nitric Oxide Production in Turbulent Diffusion Flames." 18th Symposium (International) on Combustion, The Combustion Institute, 33-42, 1981.

[78] Ph. Meunier, M. Costa, and M. G. Carvalho. "On NO_x Emissions from Turbulent Propane Diffusion Flames." Combustion and Flame, 112, 221-230, 1998.

[79] M. Costa, C. Parente, and A. Santos. "Nitrogen Oxides Emissions from Buoyancy and Momentum Controlled Turbulent Methane Jet Diffusion Flames." Experimental Thermal and Fluid Science, 28, 729-734, 2004.

[80] M. G. Mitchell, O. I. Smith, and A. R. Karagozian. "Passive Fuel-Air Mixing and Emissions Control via Lobed Injectors." AIAA Journal 42(1), 61-69, 2004.

[81] T. S. Cheng, Y. –C. Chao, D. –C. Wu, H. –W. Hsu, and T. Yuan. "Effects of Partial Premixing on Pollutant Emissions in Swirling Methane Jet Flames." Combustion and Flame, 125, 865-878, 2001.

[82] J. F. Driscoll, R. –H. Chen, and Y. Yoon. "Nitric Oxide Levels of Turbulent Jet Diffusion Flames: Effects of Residence Time and Damköhler Number." Combustion and Flame, 88, 37-49, 1992.

[83] M. C. Drake and B. J. Blint. "Relative Importance of Nitric Oxide Formation Mechanisms in Laminar Opposed-flow Diffusion Flames." Combustion and Flames, 83, 185-203, 1991.

[84] J. Janicka and W. Kollmann. "A Two-Variables Formalism for the Treatment of Chemical Reactions in Turbulent H_2-Air Diffusion Flames." 17th Symposium (International) on Combustion, The Combustion Institute, 421-430, 1979.

[85] A. N. Hayhurst and I. M. Vince. "Nitric Oxide Formation from N_2 in Flames: The Importance of "Prompt" NO." Progress in Energy and Combustion Science, 6, 35-51, 1980.

[86] N. A. Rokke, J. E. Hustad, O. K. Sonju, and F. A. Williams. "Scaling of Nitric Oxide Emissions from Buoyancy-Dominated Hydrocarbon Turbulent-Jet Diffusion Flames." 24th Symposium (International) on Combustion, The Combustion Institute, 385-393, 1992.

[87] S. R. Turns, F. H. Myhr, R. V. Bandaru, and E. R. Maund. "Oxides of Nitrogen Emissions from Turbulent Jet Flames: Part II-Fuel Dilution and Partial Premixing Effects." Combustion and Flame, 93, 255-269, 1993.

[88] M. Hori. "Experimental Study of Nitrogen Dioxide Formation in Combustion Systems." 21st Symposium (International) on Combustion, The Combustion Institute, 1181-1188, 1986.

[89] T. R. Meyer, S. Roy, V. M. Belovich, E. Corporan, and J. R. Gord. "Simultaneous Planar Laser-Induced Incandescence, OH Planar Laser-Induced Fluorescence, and Droplet Mie Scattering in Swirl-Stabilized Spray Flames." Applied Optics, 44, 445-454.

[90] S. –Y. Lee, S. R. Turns, and R. J. Santoro. "Measurements of Soot, OH, and PAH Concentrations in Turbulent Ethylene/Air Jet Flames." Combustion and Flame, 156, 2264-2275, 2009.

[91] J. M. Seitzman, A. Üngüt, P. H. Paul, and R. K. Hanson. "Imaging and Characterization of OH Structures in a Turbulent Nonpremixed Flame." 23rd Symposium (International) on Combustion, The Combustion Institute, 637-644, 1990.

[92] M. J. Tummers, A. W. Hübner, E. H. van Veen, K. Hanjalić, and Th. H. van der Meer. "Hysteresis and Transition in Swirling Nonpremixed Flames." Combustion and Flame, 156, 447-459, 2009.

[93] N. T. Clemens, P. H. Paul, and M. G. Mungal. "The Structure of OH Fields in High Reynolds Number Turbulent Jet Diffusion Flames." Combustion Science and Technology, 129, 168-184, 1997.

[94] R. K. Cheng, B. Bedat, and L. W. Kostiuk. "Effects of Buoyancy on Lean Premixed V-Flames Part I: Laminar and Turbulent Flame Structures." Combustion and Flame, 116, 360-375, 1999.

[95] R. S. Barlow, R. W. Dibble, J. –Y. Chen, and R. P. Lucht. "Effect of Damköhler Number on Superequilibrium OH Concentration in Turbulent Nonpremixed Jet Flames." Combustion and Flame, 82, 235-251, 1990.

[96] A. C. Eckbreth. "Laser Diagnostics for Combustion Temperature and Species." Abacus Press, 1988.

[97] S. H. Stårner, R. W. Bilger, R. W. Dibble, R. S. Barlow, D. C. Fourguette, and M. B. Long. "Joint Planar CH and OH LIF Imaging in Piloted Turbulent Jet Diffusion Flames near Extinction." 24th Symposium (International) on Combustion, The Combustion Institute, 341-349, 1992.

[98] P. Kothnur, M. Tsurikov, N. Clemens, J. Donbar, and C. Carter. "Planar Imaging of CH/OH and Velocity in Turbulent Nonpremixed Jet Flames." AIAA Paper 2002-0167, 2002.

[99] M. A. Mikofski, T. C. Williams, C. R. Shaddix, A. C. Fernandez-Pello, and L. G. Blevins. "Structure of Laminar Sooting Inverse Diffusion Flames." Combustion and Flame, 149, 463-478, 2007.

[100] J. E. Broadwell and R. E. Breidenthal. "A Simple Model of Mixing and Chemical Reaction in a Turbulent Shear Layer." Journal of Fluid Mechanics, 125:397-410, 1982.

[101] M. Gharib, E. Rambod, and K. Shariff. "A Universal Time Scale for Vortex Ring Formation." Journal of Fluid Mechanics, 360:121-140, 1998.

[102] P. S. Krueger, J. O. Dabiri, and M. Gharib. "The Formation Number of Vortex Rings Formed in Uniform Background Co-Flow." Journal of Fluid Mechanics, 556:147-166, 2006.

APPENDIX A

LASER-INDUCED FLUORESCENCE

Laser diagnostics in combustion has gained extensive attention since the late 20^{th} century. Laser techniques are capable of performing measurements, such as combustion temperature and species concentrations, with simultaneous high spatial and temporal resolution, which physical probing methods are challenged to provide. In addition, the non-intrusive nature of laser techniques allow diagnostics in complicated combustion applications, such as swirled flames and recirculation zone structures, without disturbing the flame behaviors. Laser-Induced Fluorescence is one powerful and commonly-used technique for examining species concentrations in flames.

A.1 General Concept

Laser-Induced Fluorescence (LIF) is a spectroscopic technique that enables the detection of reactive intermediates in combustion at low levels (ppm level). LIF can be carried out either as a point or as planar measurement. The latter is referred to as Planar LIF (PLIF), which is commonly employed in combustion studies to either simply image the spatial distribution or quantitatively measure the concentration of a selected reactive species. Only a brief summary of PLIF is presented here; a more detailed and complete description of LIF theory is given by Eckberth [96].

LIF is often understood as an absorption process followed by light emission. This process can be summarized in Fig. A.1 using the schematic energy level of OH as an example. If the wavelength of the laser radiation matches an electronic energy transition of the OH radical, the

OH radical can become excited by absorption of laser radiation from the ground state, leading to an upper excited electronic state. Shortly after the excited energy level is populated, the OH radical returns to the ground state and releases energy through spontaneous emission in the form of fluorescence. In general, the wavelength of fluorescence is different from that of the incident excitation and occurs primarily, but not entirely, at longer wavelengths since the emission involves generally higher electronic states not originally involved in the absorption process. The difference in the wavelength of incident excitation and fluorescence emission benefits the detection of LIF signal since the interference from scattered laser light can be minimized with optical filters. Due to the fact that the fluorescence intensity is proportional to the number density of the species, the fluorescence intensity provides information on the concentration of the probed species [96].

A.2 Brief Review of OH PLIF Studies

The hydroxyl radical (OH) has been considered as a good marker for the reaction zone in hydrocarbon combustion, mainly due to its peak concentration being around the peak combustion temperature [53]. The abundant concentration of OH in most flames also facilitate the detection of the LIF signal [96]. Because of its well-known spectroscopy, a large number of combustion studies with PLIF have reported detection of the OH radical.

The OH radical, in the combustion reaction, is indicative of fuel-lean regions within the flame where combustion products reside [97]. Compared to OH, CH PLIF provides a relatively narrower rendering of the flame zone indicative of the fuel-rich side of the flame element [97]. CH is often considered superior to OH as a reaction zone marker because CH is produced and destroyed in a faster mechanism than OH [98]. However, the relatively lower concentration of

CH than that of OH makes it much more difficult to be detected than OH [68]. Detection of CH can be further complicated by overlapping fluorescence from polycyclic aromatic hydrocarbons (PAH) in highly-sooty fuel [68], such as ethylene used in this work. Therefore, it was proposed to primarily employ OH PLIF imaging to study the reaction zone structures of swirled, strongly-pulsed flames in the current study even though minor fluorescence interference is still inevitable.

Seitzman *et al*. [91] employed the PLIF imaging to study the spatial structures of OH distribution in non-premixed hydrogen flames with a Reynolds number ranging from Re = 2,300 to 50,000. At low Reynolds numbers, they observed the OH zones to be continuous and laminar-like. As the Reynolds number increased, the OH structure became more convoluted and was characterized by thin filaments of high OH concentration in the upstream regions of flames connecting larger, more diffuse structures in the relatively downstream regions of flames. In any case, the OH zones structure appeared to be governed by the large vertical structures in the flame. The OH zones with low concentrations was still observed beyond the tip of flames, possibly due to the slow three-body recombination reaction.

Clemens *et al*. [93] studied the OH zones structure in turbulent H_2/Ar jet diffusion flames at moderate to high Reynolds number ($Re = 3 \times 10^4$ to 1.5×10^5). For the lowest Re case, in agreement with Seitzman *et al*.'s study [91], the OH zones appeared as thin filaments connected by diffuse regions. For the highest Re case, the OH zones were relatively broader over the entire length of the flame and appeared to be more influenced by small-scale turbulence, but beyond the flame tip a large-scale helical instability was present as revealed by OH PLIF imaging. Statistics from the OH PLIF signals showed that over the entire extent of the flame, the RMS values of OH signals were largest for the lowest Re case, owing to large fluctuations in the thin OH zones. With increasing Reynolds number, the radial RMS profiles for the lower half of the flame exhibited double peaks. Clemens *et al*. suggested that the double-peak RMS profiles, particularly prevalent at the highest *Re*, were results of the distributed OH zones combined with small-scale mixing on the rich and lean sides of the reaction zone.

A.3 OH PLIF Challenges in Hydrocarbon Combustion

As mentioned previously, implementation of OH PLIF in hydrocarbon fueled combustion is very challenging due to the fluorescence interference arising from the fuel chemistry. An example of OH PLIF with interference in a laminar ethylene diffusion flame is shown in Fig. A.2. The fluorescence interference is clearly evident and it remains with the incident laser turned away from the OH absorption line (283 nm). The fluorescence interference is also observed in laminar methane-fueled flames, but with the relatively weaker signal than that in ethylene fueled flames. The interference grows quickly with downstream distance in the flame and seems to prevail over the most extent of the flame in turbulent flames.

Detailed interference on the LIF process is described in the reference book of Eckbreth [96]. For hydrocarbon fueled combustion, the fragments of hydrocarbon species and soot particulates possess very broad absorption spectra throughout the ultraviolet and violet spectral regions. Because of the abundance of these species, serious fluorescence interferences can result. Soot particulates further complicate problems since they can fluoresce, Raman scatter, and incandesce by interacting with the incident laser radiation.

No attempt was made here to distinguish from what species the interference, as shown in Fig. A.2, originates. However, attempts to minimize the fluorescence interference were made by first reducing the gate width of camera down to 20 ns due to the relatively long lifetime of PAH and soot particles fluorescences compared to that of OH fluorescence [96, 99]. Next, the laser fluence per pulse was lowered to be approximately 0.02 J/cm^2 by further increasing the overall height of the incident laser sheet. Regardless of fluorescence, scattering, or incandescence, the irradiance of these interferences is strongly dependent on the laser fluence [96]. However, the lower the laser fluence is, the weaker and the less the OH fluorescence is detected [96]. The current laser fluence of 0.02 J/cm^2 was found to be optimum for the purpose of this work; it allows sufficient OH fluorescence to be detected while the fluorescent interference is attenuated to an acceptable level without serious deterioration of OH fluorescence signals.

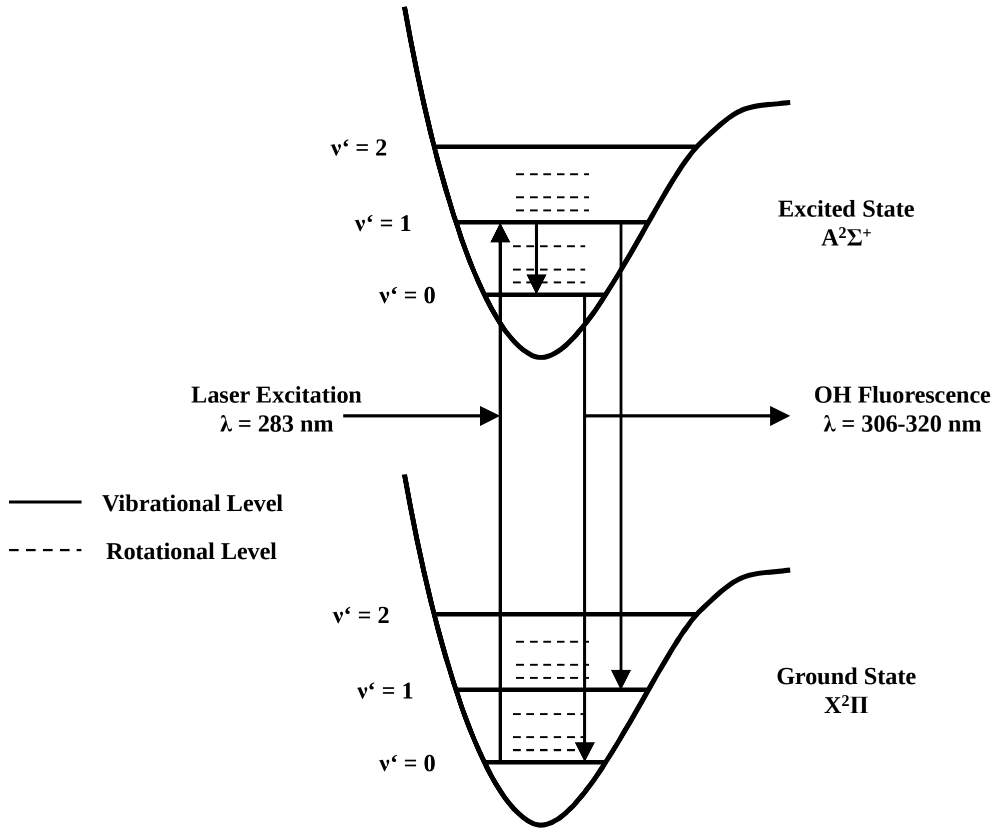

Figure A.1 – Schematic energy level diagram of the energy transitions involved in laser excitation and fluorescence of the OH radical.

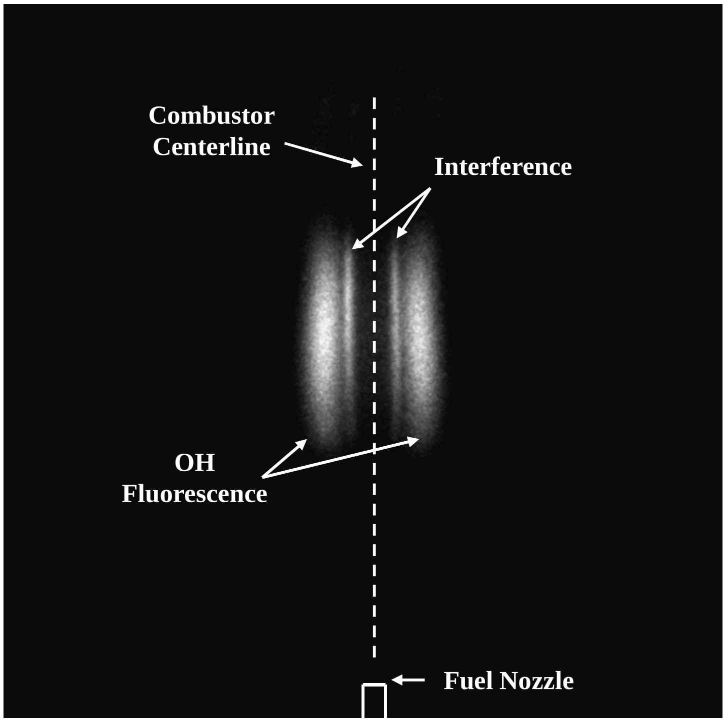

Figure A.2 – Example of fluorescence interference with OH PLIF in a laminar ethylene-fueled diffusion flame.

APPENDIX B

VISUAL FLAME IMAGE SEQUENCES – Q_{air} = 2.5 SCFM

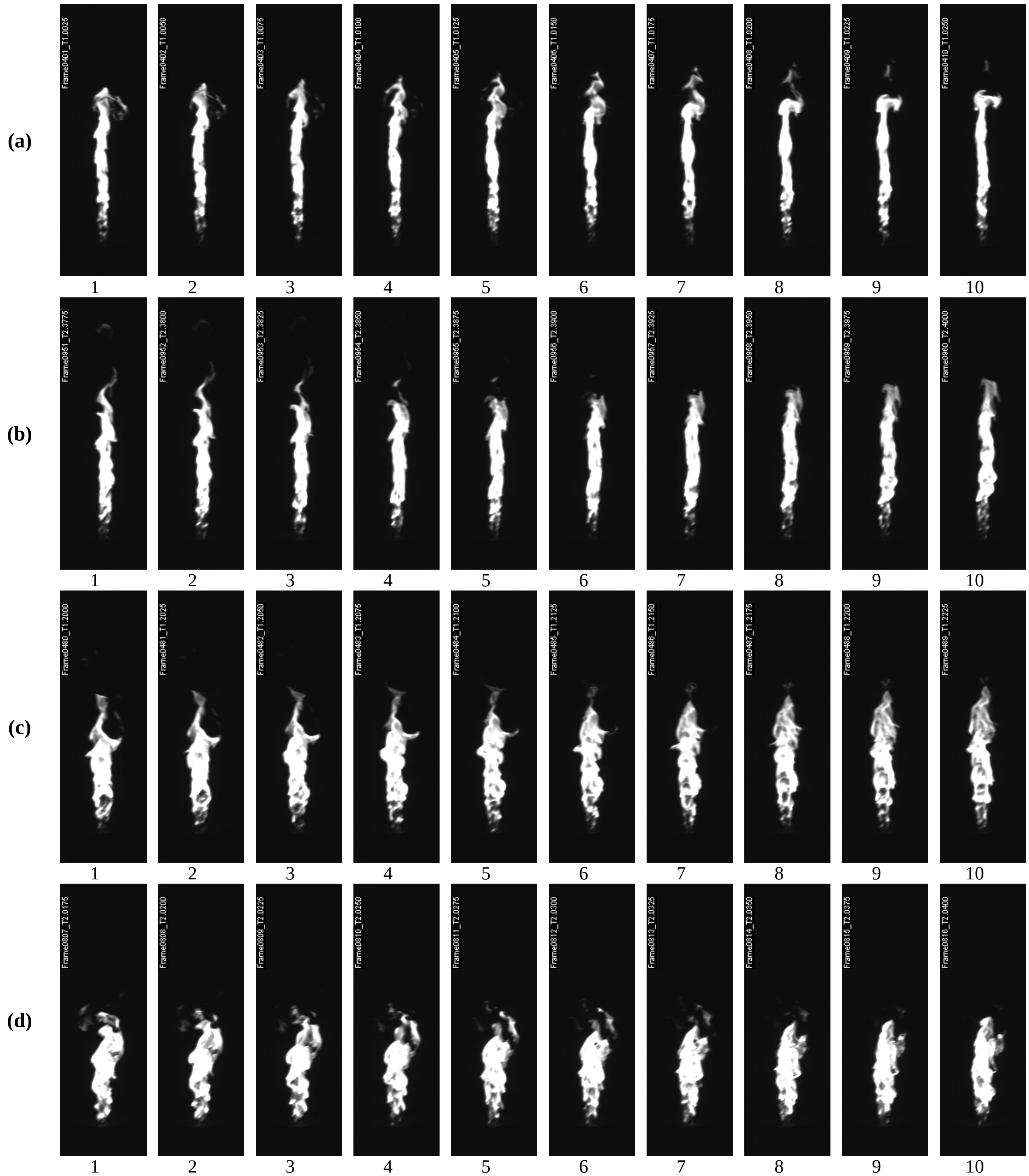

Figure B.1 – Visual sequences of steady flames with a co-flow of 2.5 SCFM. (a) *S* = 0. (b) *S* = 0.41. (c) *S* = 0.87. (d) *S* = 1.61. Framing interval Δ*t* = 2.5 ms; image height 57.9 cm.

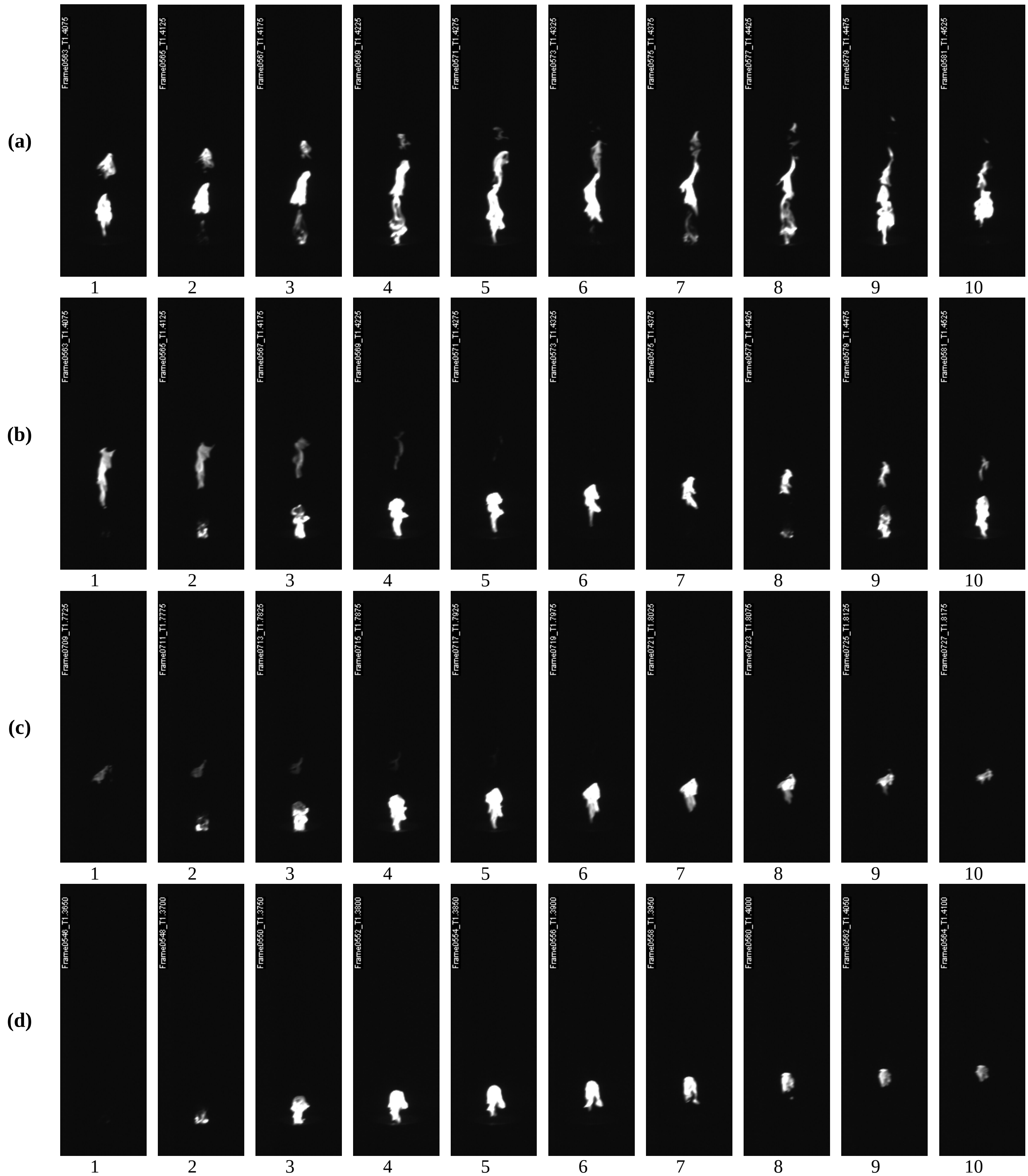

Figure B.2 – Visual sequences of P = 5 flames with the swirl level of S = 0 and a co-flow of 2.5 SCFM. (a) τ_{off} = 111. (b) τ_{off} = 222. (c) τ_{off} = 444. (d) τ_{off} = 1110. Framing interval Δt = 5 ms; image height 57.9 cm.

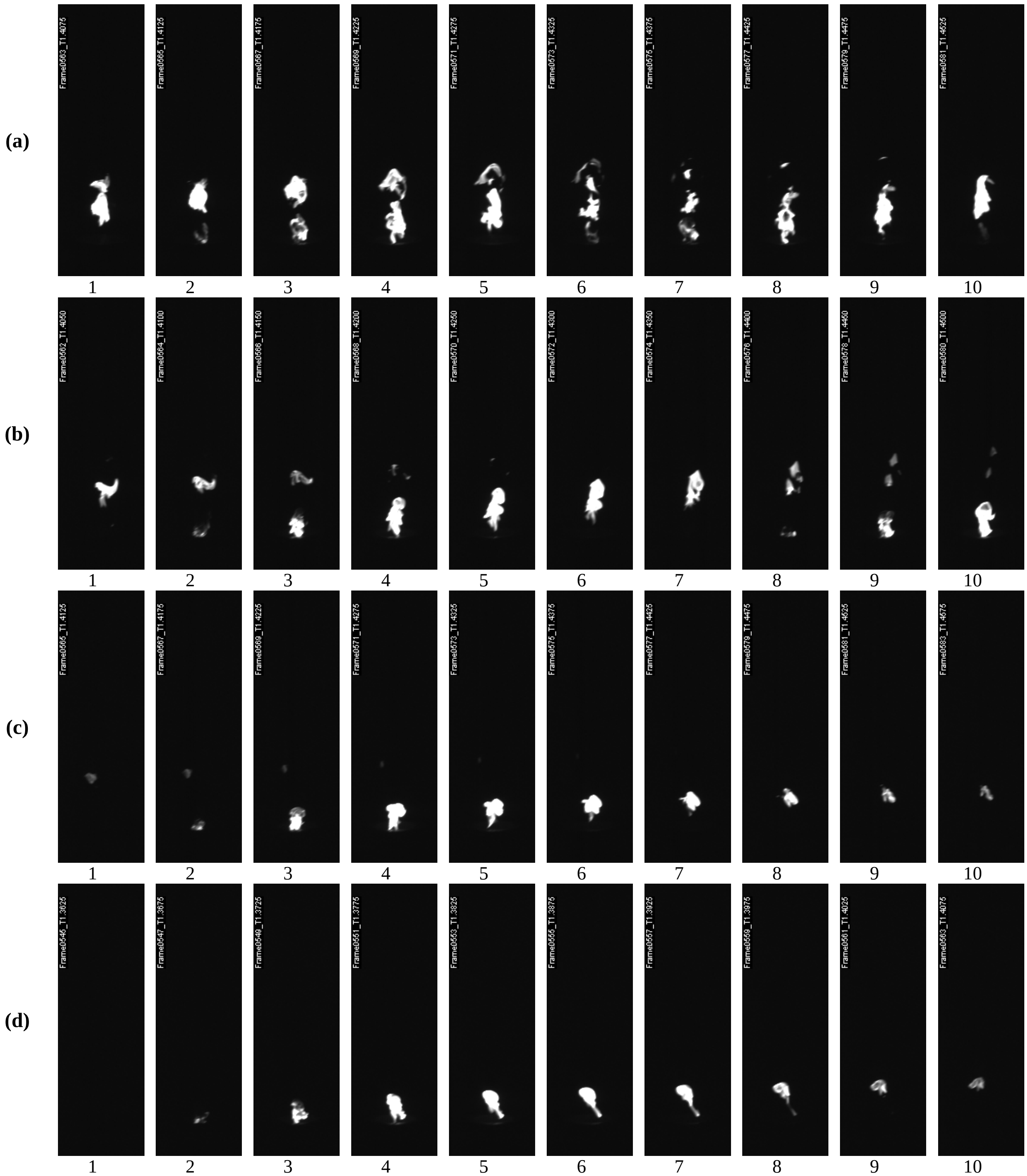

Figure B.3 – Visual sequences of P = 5 flames with the swirl level of S = 0.41 and a co-flow of 2.5 SCFM. (a) τ_{off} = 111. (b) τ_{off} = 222. (c) τ_{off} = 444. (d) τ_{off} = 1110. Framing interval Δt = 5 ms; image height 57.9 cm.

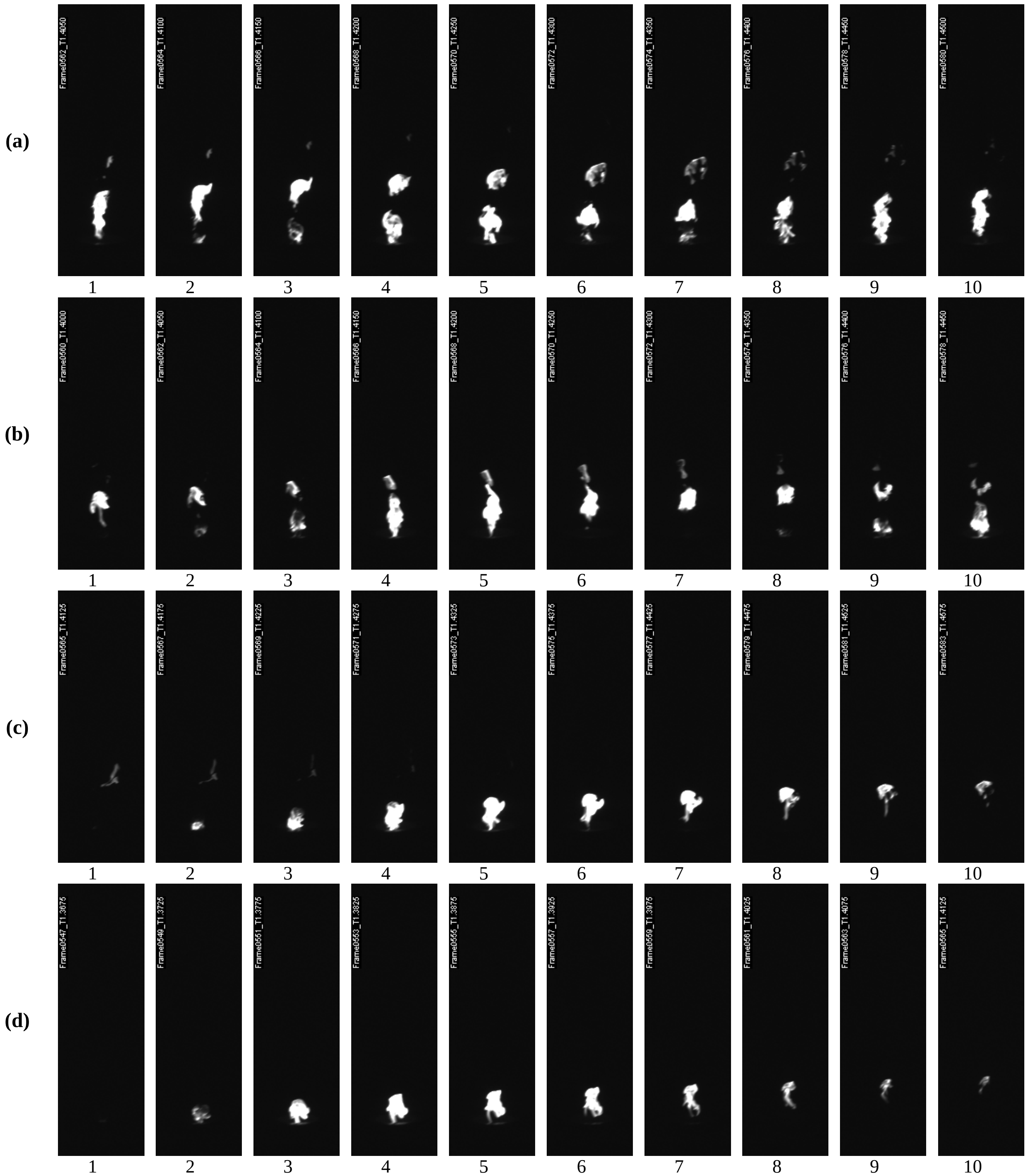

Figure B.4 – Visual sequences of P = 5 flames with the swirl level of S = 1.61 and a co-flow of 2.5 SCFM. (a) τ_{off} = 111. (b) τ_{off} = 222. (c) τ_{off} = 444. (d) τ_{off} = 1110. Framing interval Δt = 5 ms; image height 57.9 cm.

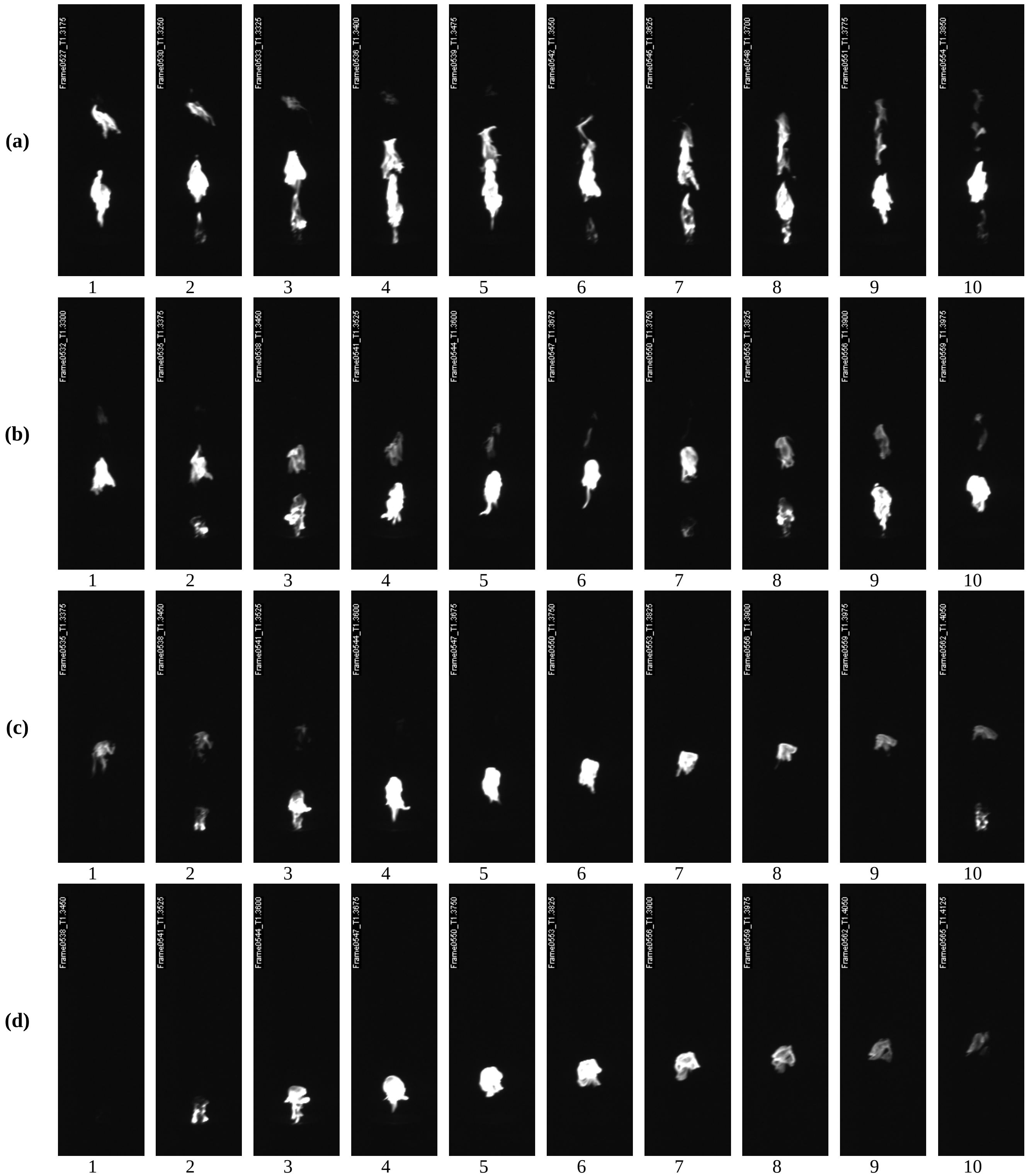

Figure B.5 – Visual sequences of P = 6 flames with the swirl level of S = 0 and a co-flow of 2.5 SCFM. (a) τ_{off} = 111. (b) τ_{off} = 222. (c) τ_{off} = 444. (d) τ_{off} = 1110. Framing interval Δt = 7.5 ms; image height 57.9 cm.

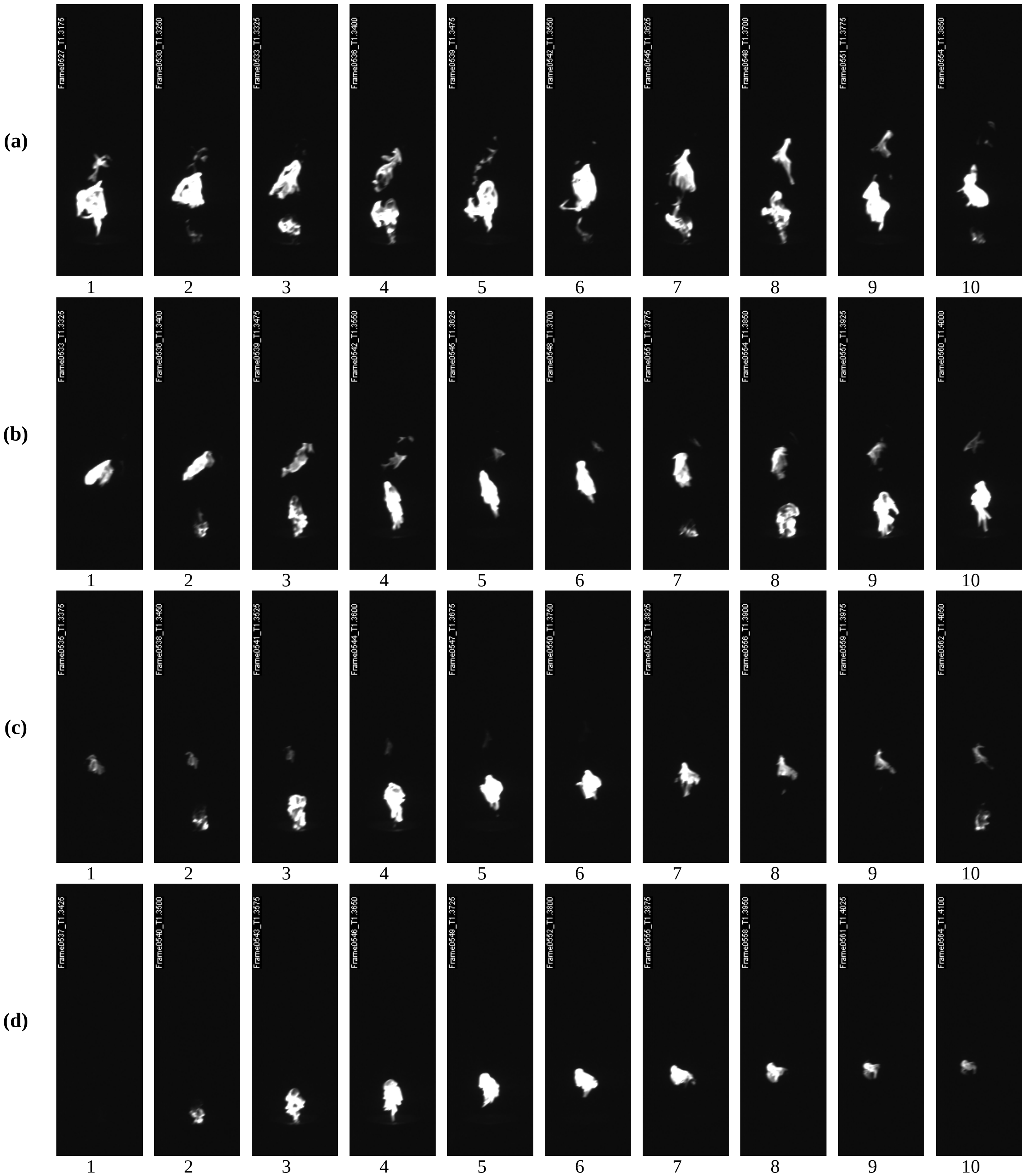

Figure B.6 – Visual sequences of P = 6 flames with the swirl level of S = 0.41 and a co-flow of 2.5 SCFM. (a) τ_{off} = 111. (b) τ_{off} = 222. (c) τ_{off} = 444. (d) τ_{off} = 1110. Framing interval Δt = 7.5 ms; image height 57.9 cm.

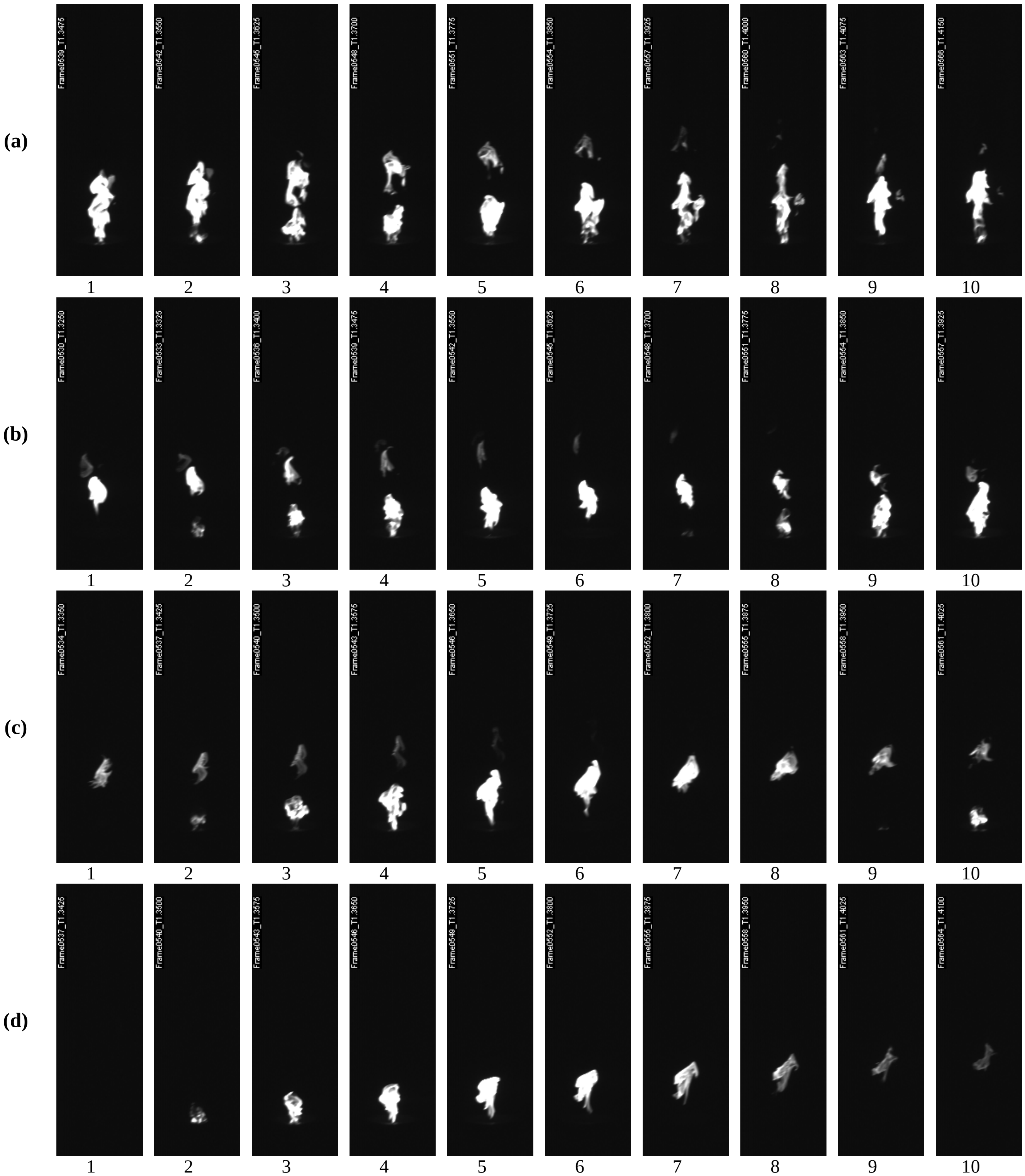

Figure B.7 – Visual sequences of *P* = 6 flames with the swirl level of *S* = 1.61 and a co-flow of 2.5 SCFM. (a) τ_{off} = 111. (b) τ_{off} = 222. (c) τ_{off} = 444. (d) τ_{off} = 1110. Framing interval Δt = 7.5 ms; image height 57.9 cm.

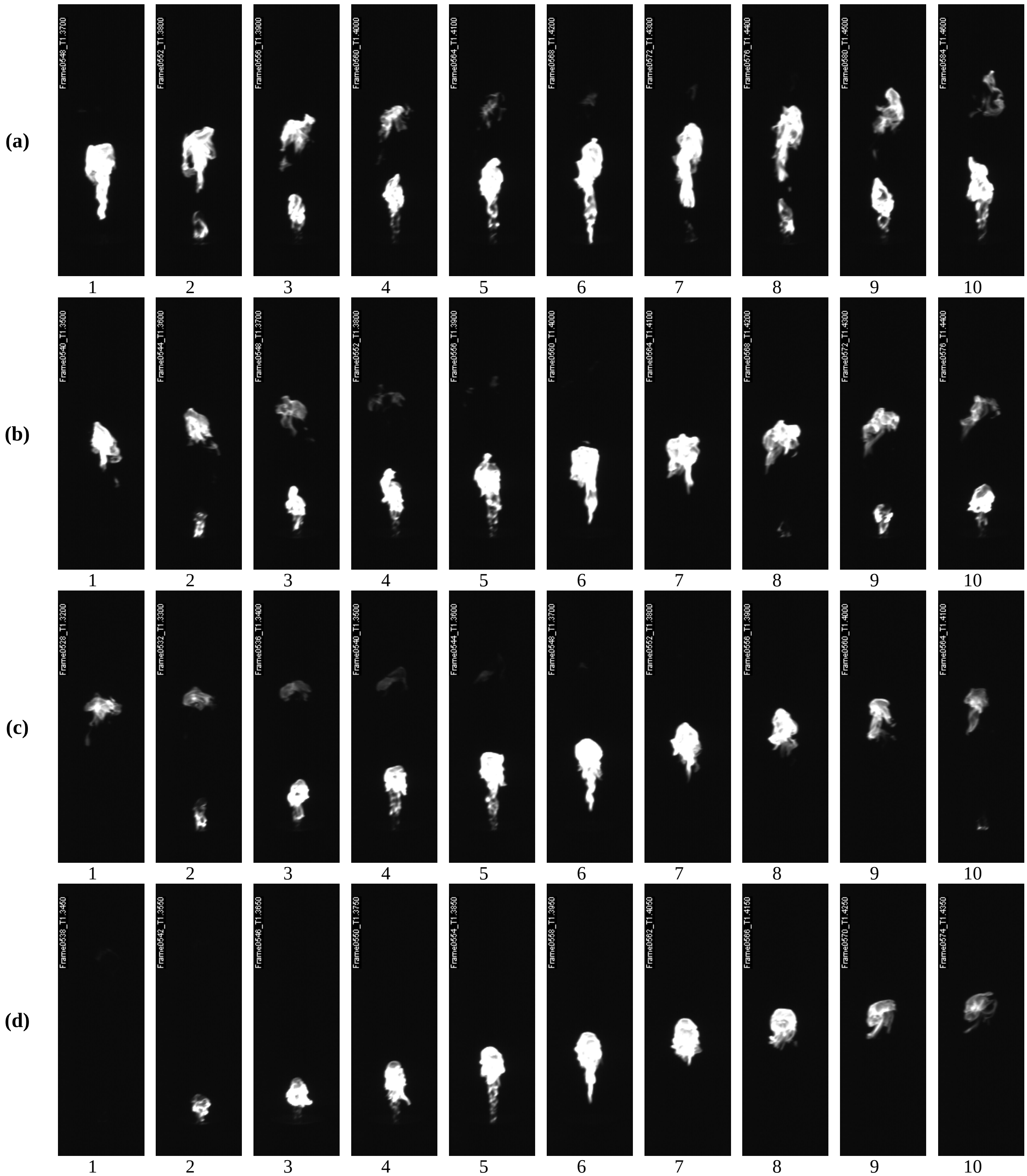

Figure B.8 – Visual sequences of P = 8 flames with the swirl level of S = 0 and a co-flow of 2.5 SCFM. (a) τ_{off} = 111. (b) τ_{off} = 222. (c) τ_{off} = 444. (d) τ_{off} = 1110. Framing interval Δt = 10 ms; image height 57.9 cm.

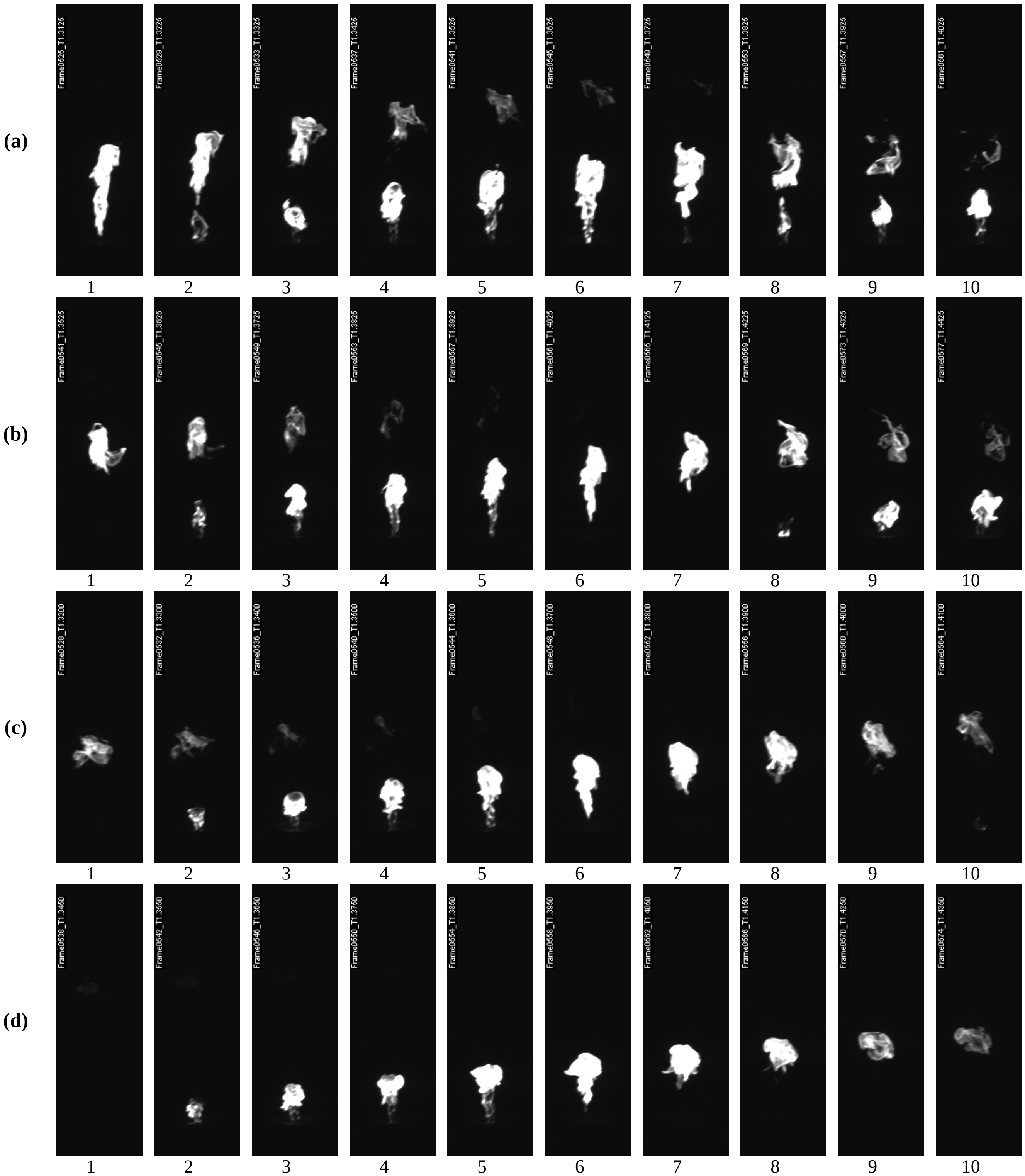

Figure B.9 – Visual sequences of P = 8 flames with the swirl level of S = 0.41 and a co-flow of 2.5 SCFM. (a) τ_{off} = 111. (b) τ_{off} = 222. (c) τ_{off} = 444. (d) τ_{off} = 1110. Framing interval Δt = 10 ms; image height 57.9 cm.

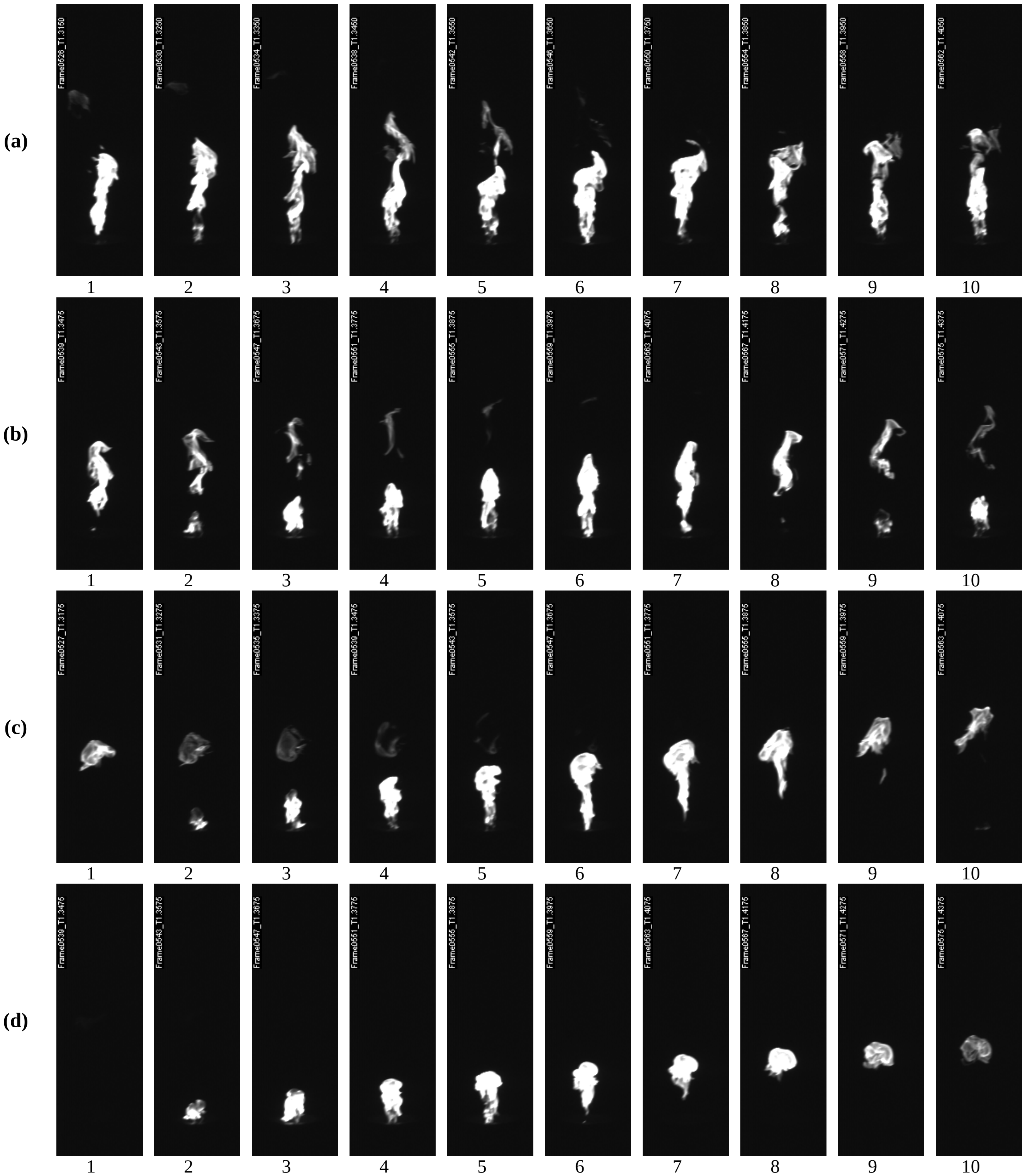

Figure B.10 – Visual sequences of P = 8 flames with the swirl level of S = 1.61 and a co-flow of 2.5 SCFM. (a) τ_{off} = 111. (b) τ_{off} = 222. (c) τ_{off} = 444. (d) τ_{off} = 1110. Framing interval Δt = 10 ms; image height 57.9 cm.

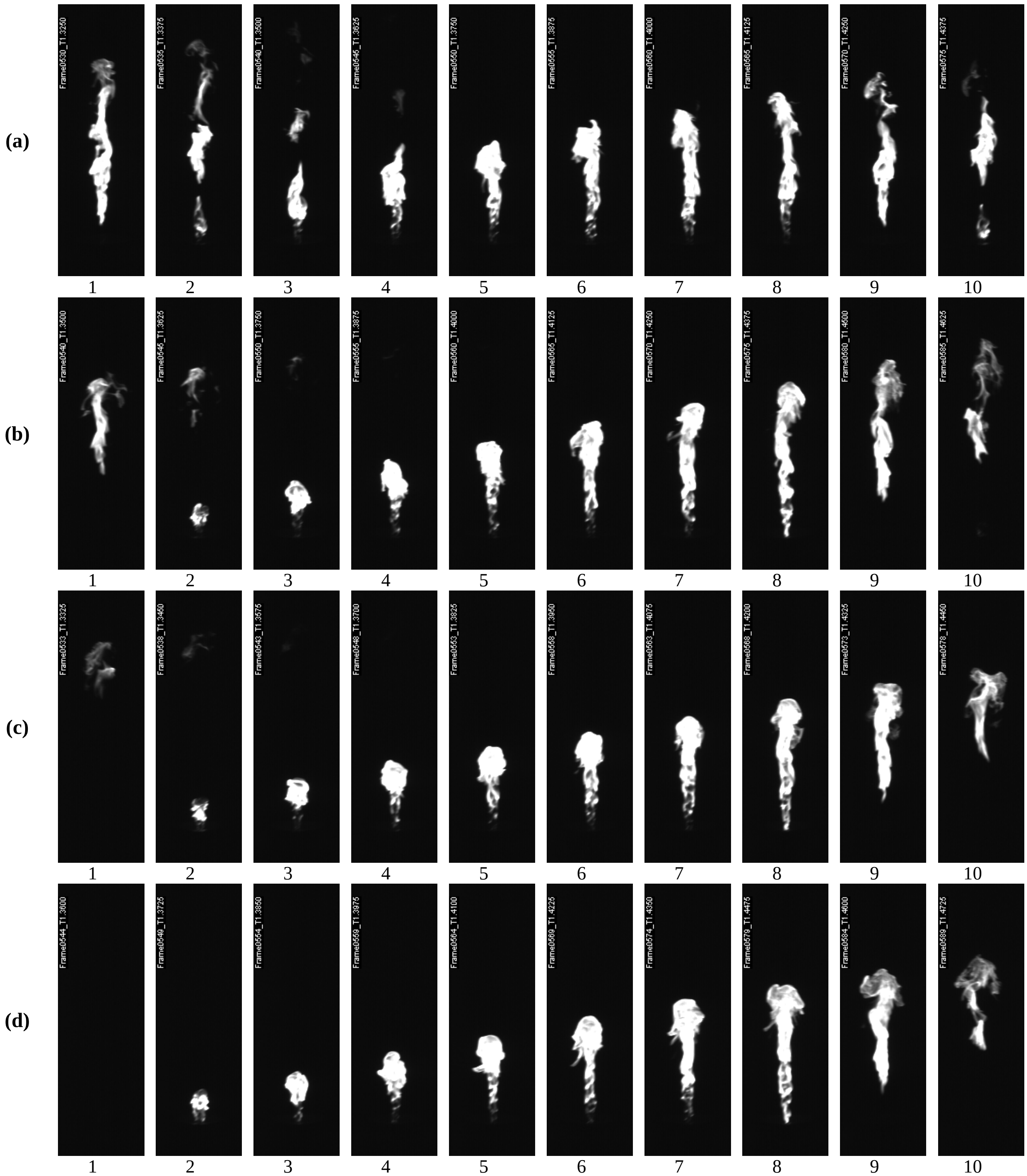

Figure B.11 – Visual sequences of P = 10 flames with the swirl level of S = 0 and a co-flow of 2.5 SCFM. (a) τ_{off} = 111. (b) τ_{off} = 222. (c) τ_{off} = 444. (d) τ_{off} = 1110. Framing interval Δt = 12.5 ms; image height 57.9 cm.

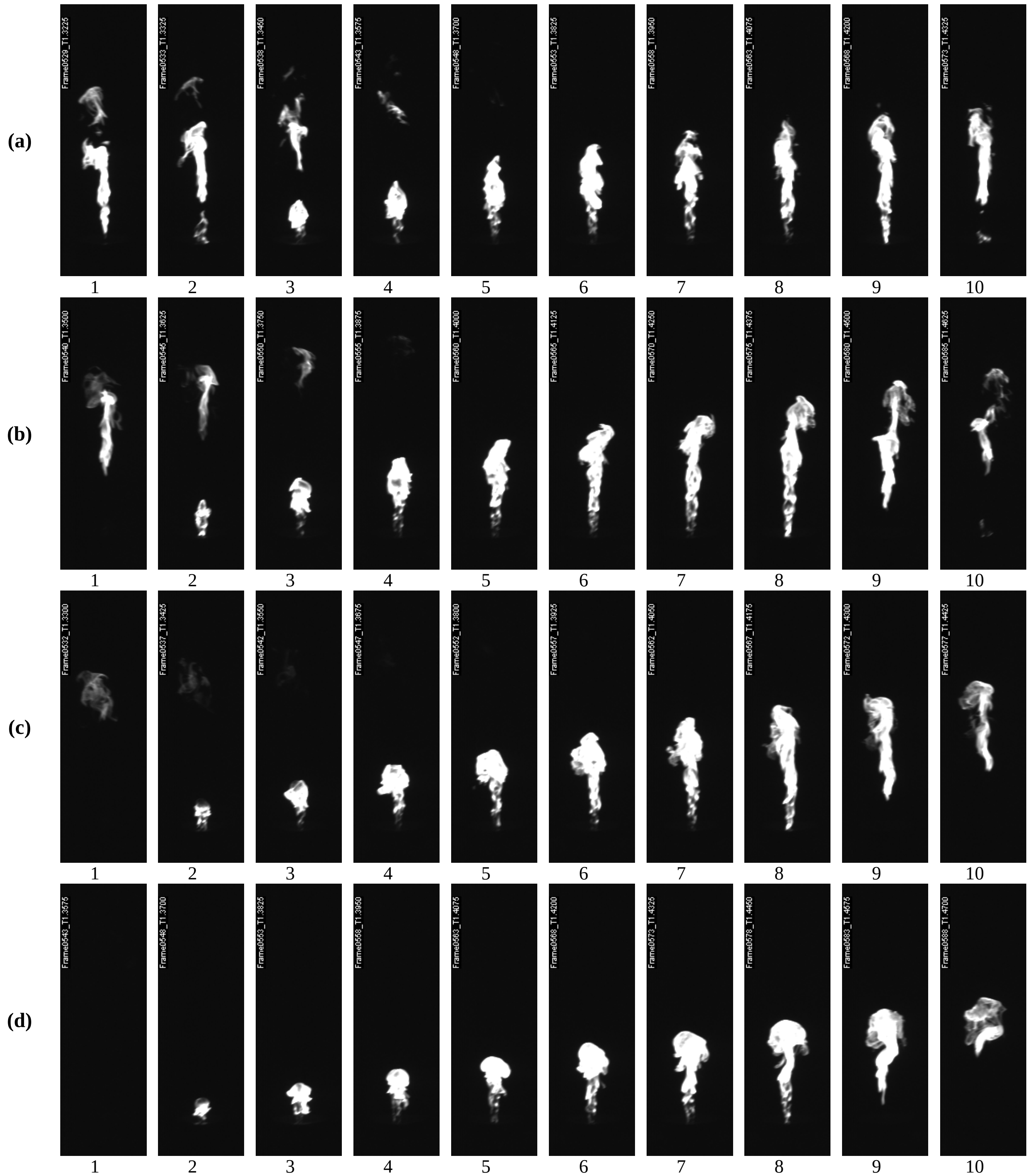

Figure B.12 – Visual sequences of P = 10 flames with the swirl level of S = 0.41 and a co-flow of 2.5 SCFM. (a) τ_{off} = 111. (b) τ_{off} = 222. (c) τ_{off} = 444. (d) τ_{off} = 1110. Framing interval Δt = 12.5 ms; image height 57.9 cm.

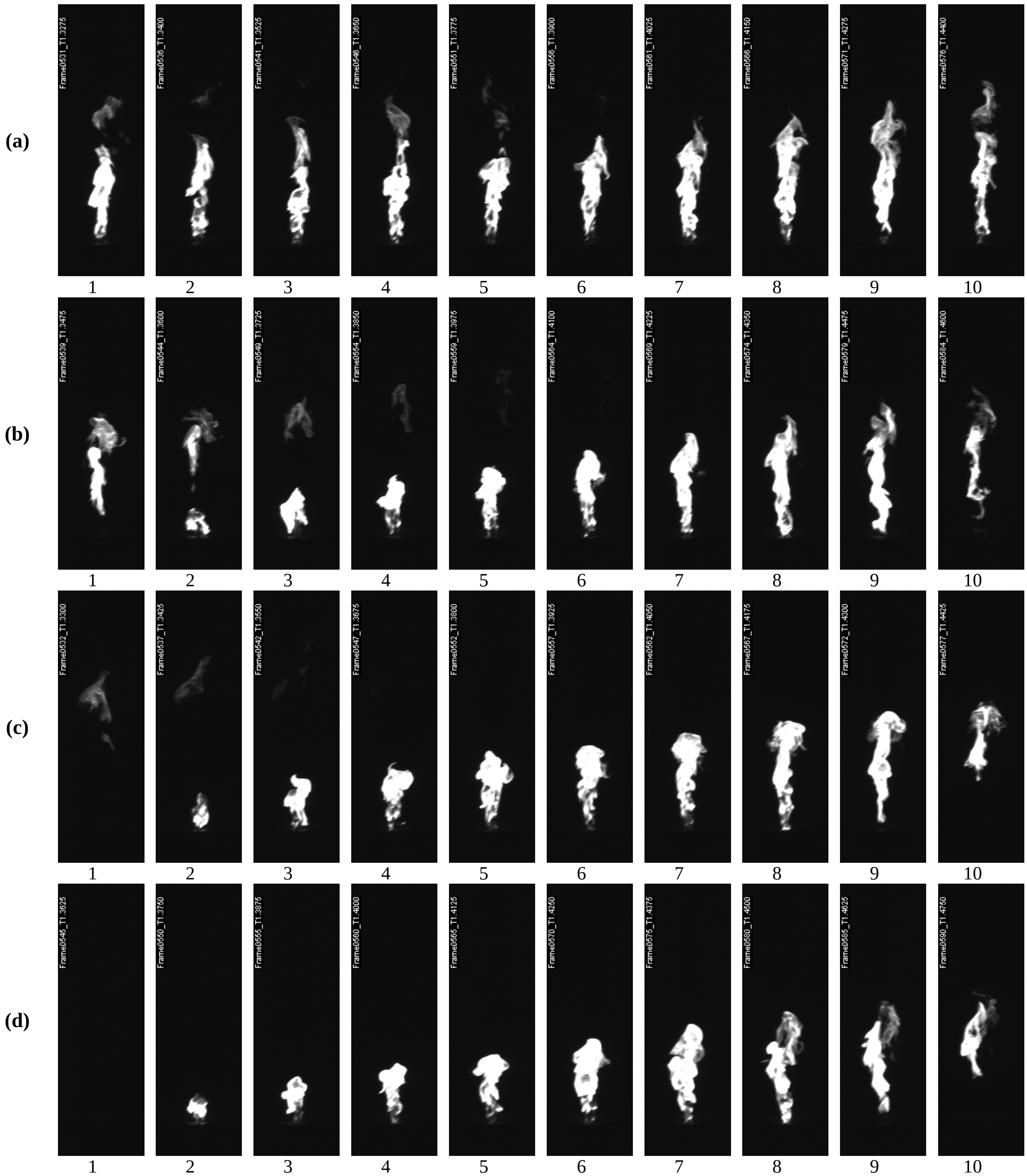

Figure B.13 – Visual sequences of P = 10 flames with the swirl level of S = 1.61 and a co-flow of 2.5 SCFM. (a) τ_{off} = 111. (b) τ_{off} = 222. (c) τ_{off} = 444. (d) τ_{off} = 1110. Framing interval Δt = 12.5 ms; image height 57.9 cm.

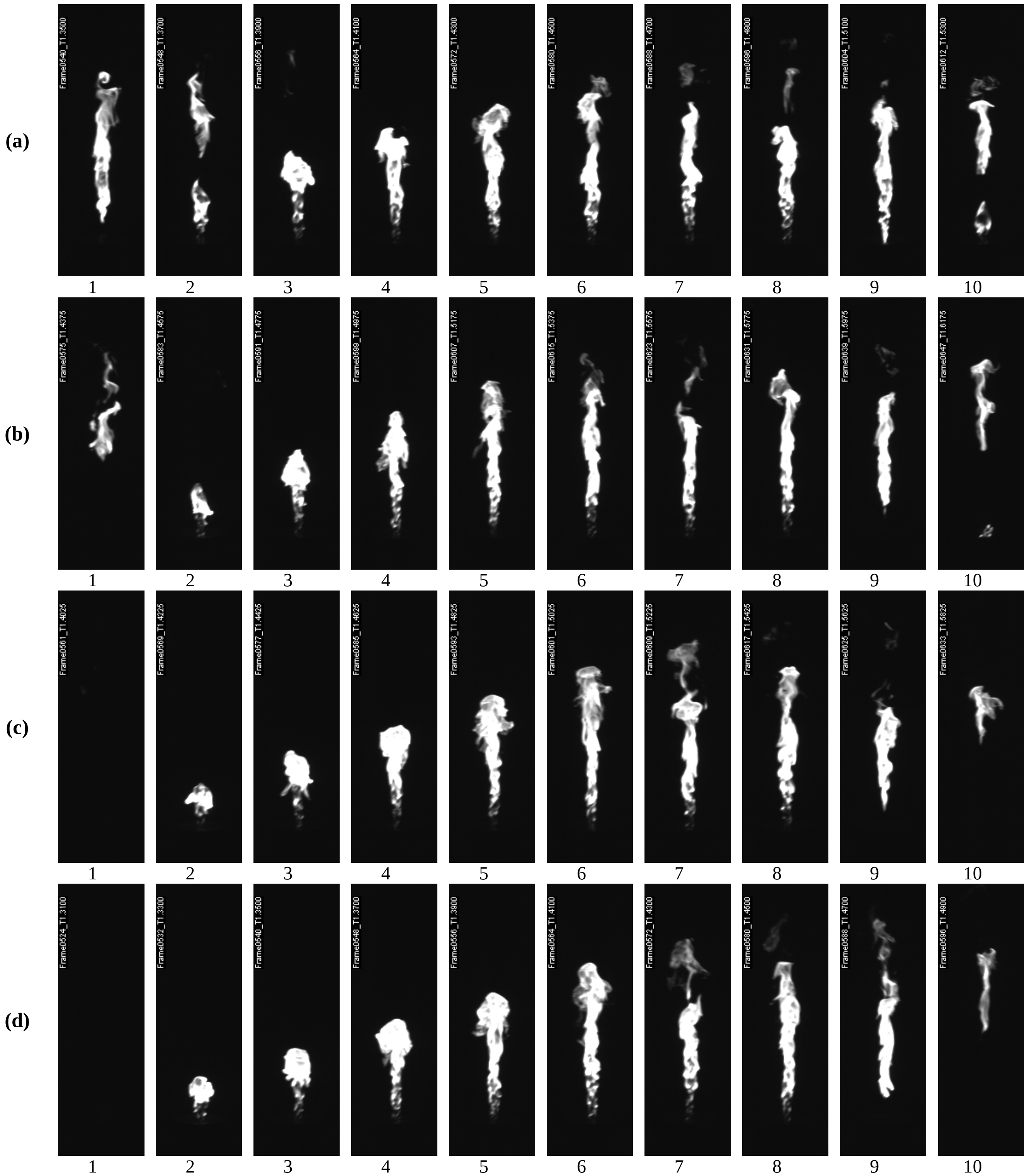

Figure B.14 – Visual sequences of P = 12 flames with the swirl level of S = 0 and a co-flow of 2.5 SCFM. (a) τ_{off} = 111. (b) τ_{off} = 222. (c) τ_{off} = 444. (d) τ_{off} = 1110. Framing interval Δt = 20 ms; image height 57.9 cm.

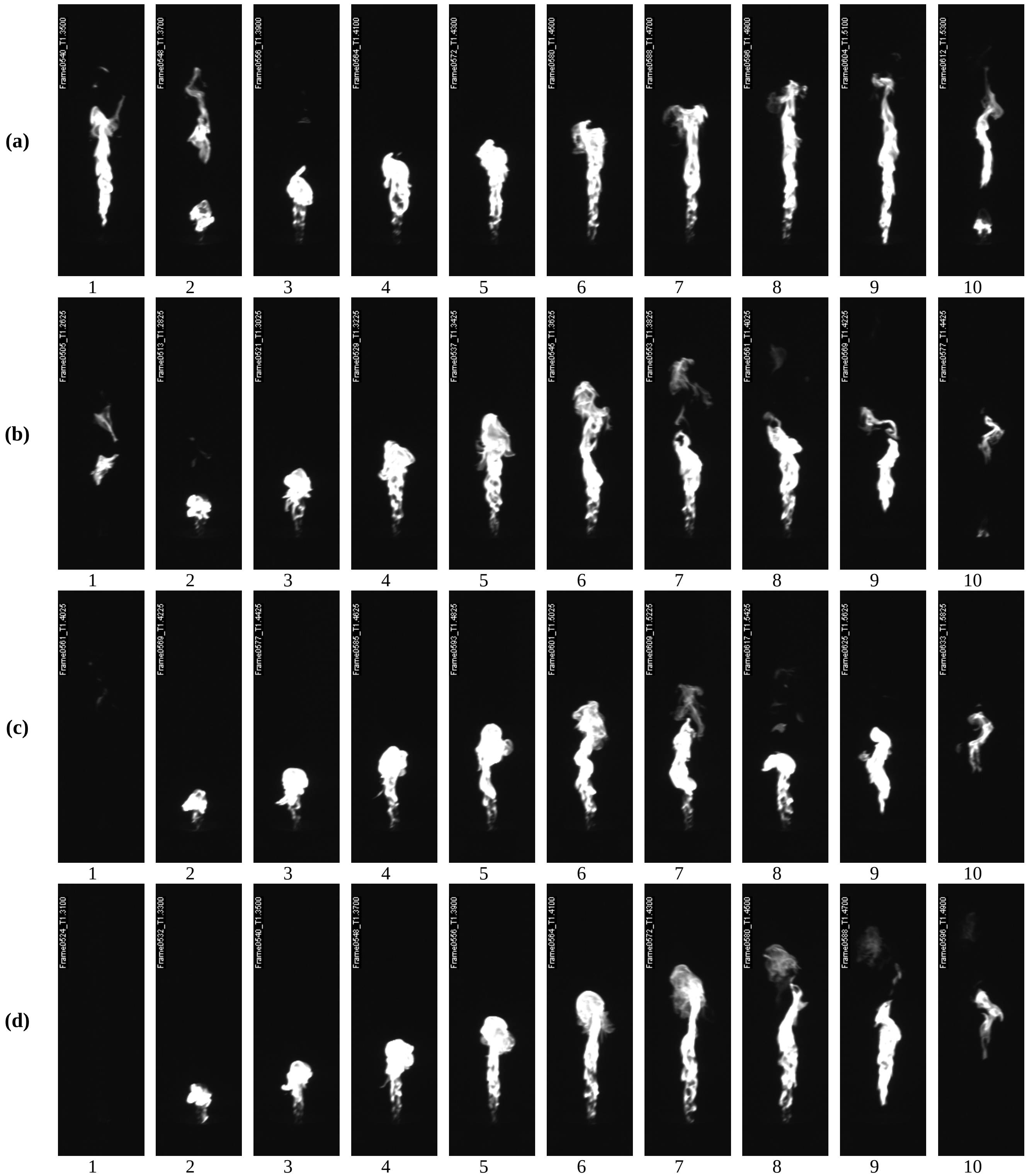

Figure B.15 – Visual sequences of P = 12 flames with the swirl level of S = 0.41 and a co-flow of 2.5 SCFM. (a) τ_{off} = 111. (b) τ_{off} = 222. (c) τ_{off} = 444. (d) τ_{off} = 1110. Framing interval Δt = 20 ms; image height 57.9 cm.

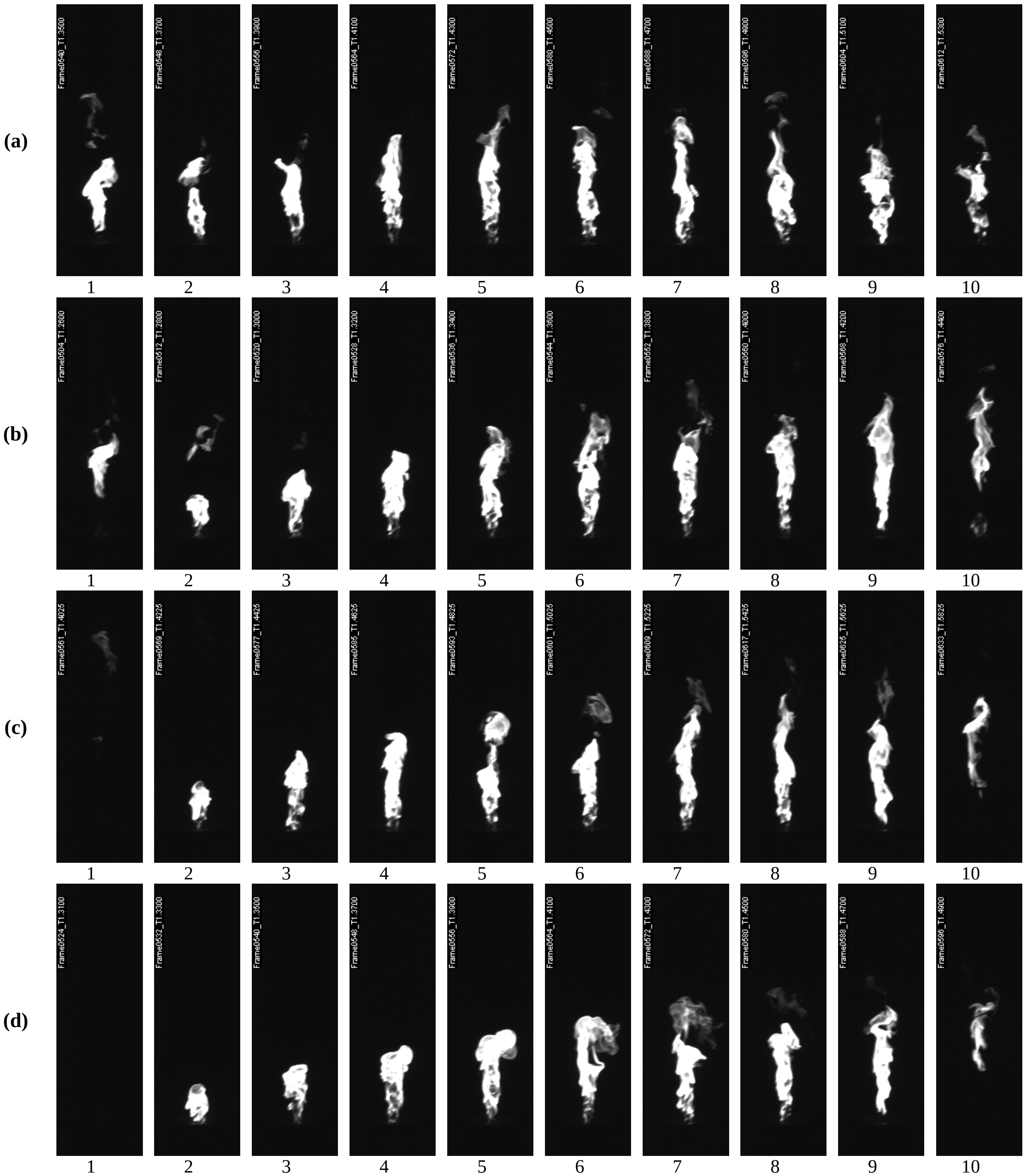

Figure B.16 – Visual sequences of P = 12 flames with the swirl level of S = 1.61 and a co-flow of 2.5 SCFM. (a) τ_{off} = 111. (b) τ_{off} = 222. (c) τ_{off} = 444. (d) τ_{off} = 1110. Framing interval Δt = 20 ms; image height 57.9 cm.

APPENDIX C

VISUAL FLAME IMAGE SEQUENCES – Q_{air} = 3.5 SCFM

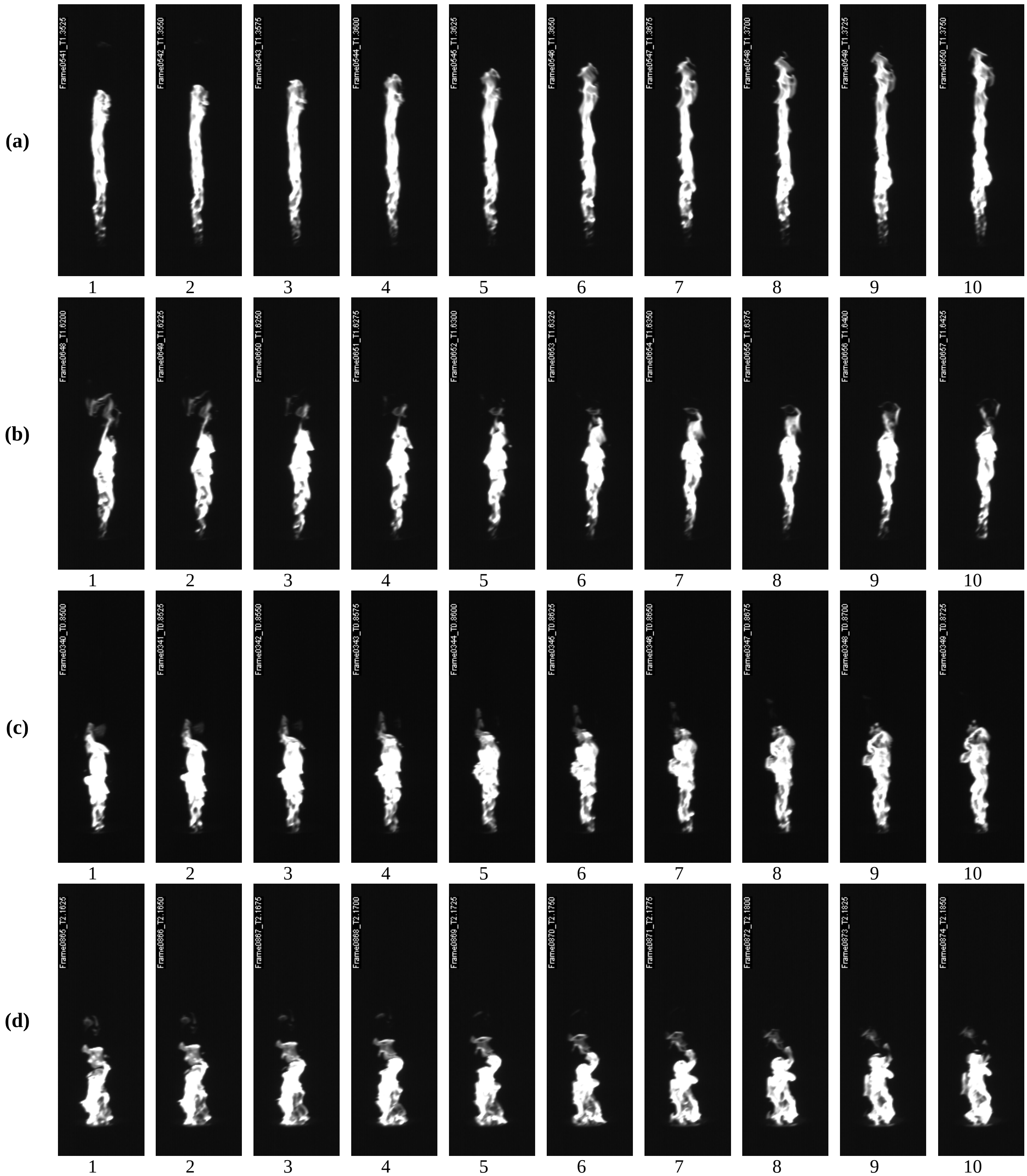

Figure C.1 – Visual sequences of steady flames with a co-flow of 3.5 SCFM. (a) S = 0. (b) S = 0.44. (c) S = 0.87. (d) S = 1.64. Framing interval Δt = 2.5 ms; image height 57.9 cm.

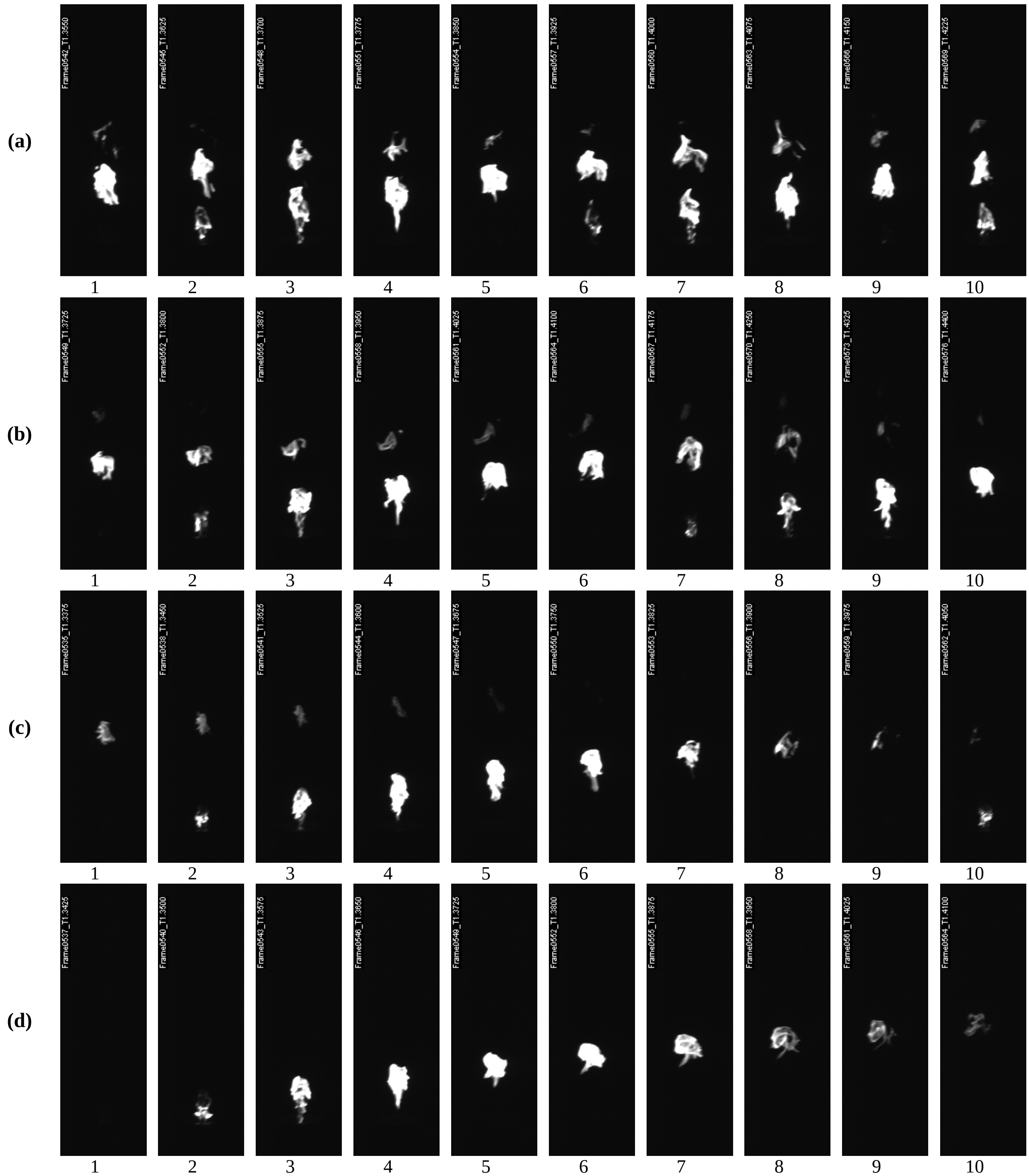

Figure C.2 – Visual sequences of P = 6 flames with the swirl level of S = 0 and a co-flow of 3.5 SCFM. (a) τ_{off} = 111. (b) τ_{off} = 222. (c) τ_{off} = 444. (d) τ_{off} = 1110. Framing interval Δt = 7.5 ms; image height 57.9 cm.

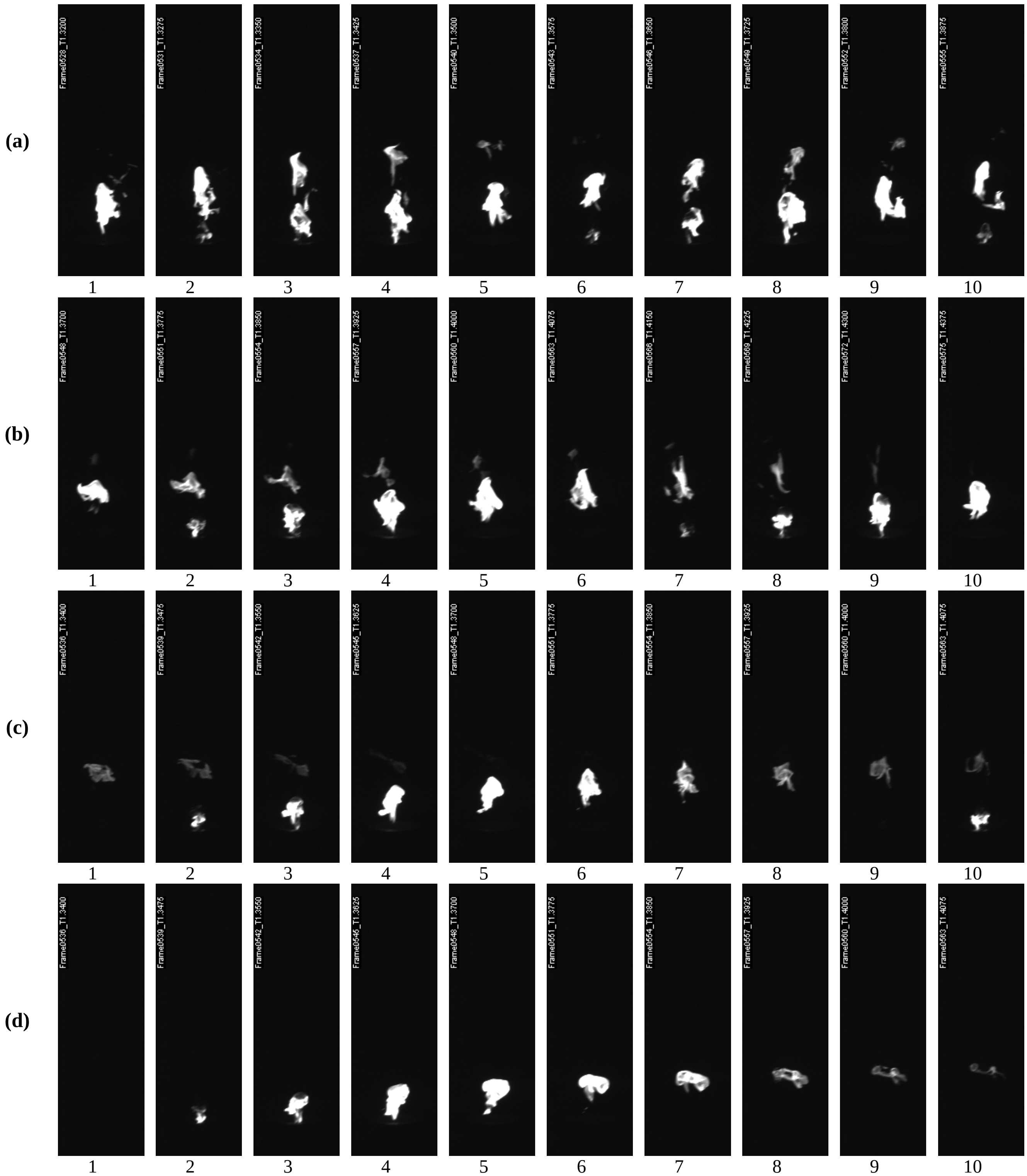

Figure C.3 – Visual sequences of P = 6 flames with the swirl level of S = 0.44 and a co-flow of 3.5 SCFM. (a) τ_{off} = 111. (b) τ_{off} = 222. (c) τ_{off} = 444. (d) τ_{off} = 1110. Framing interval Δt = 7.5 ms; image height 57.9 cm.

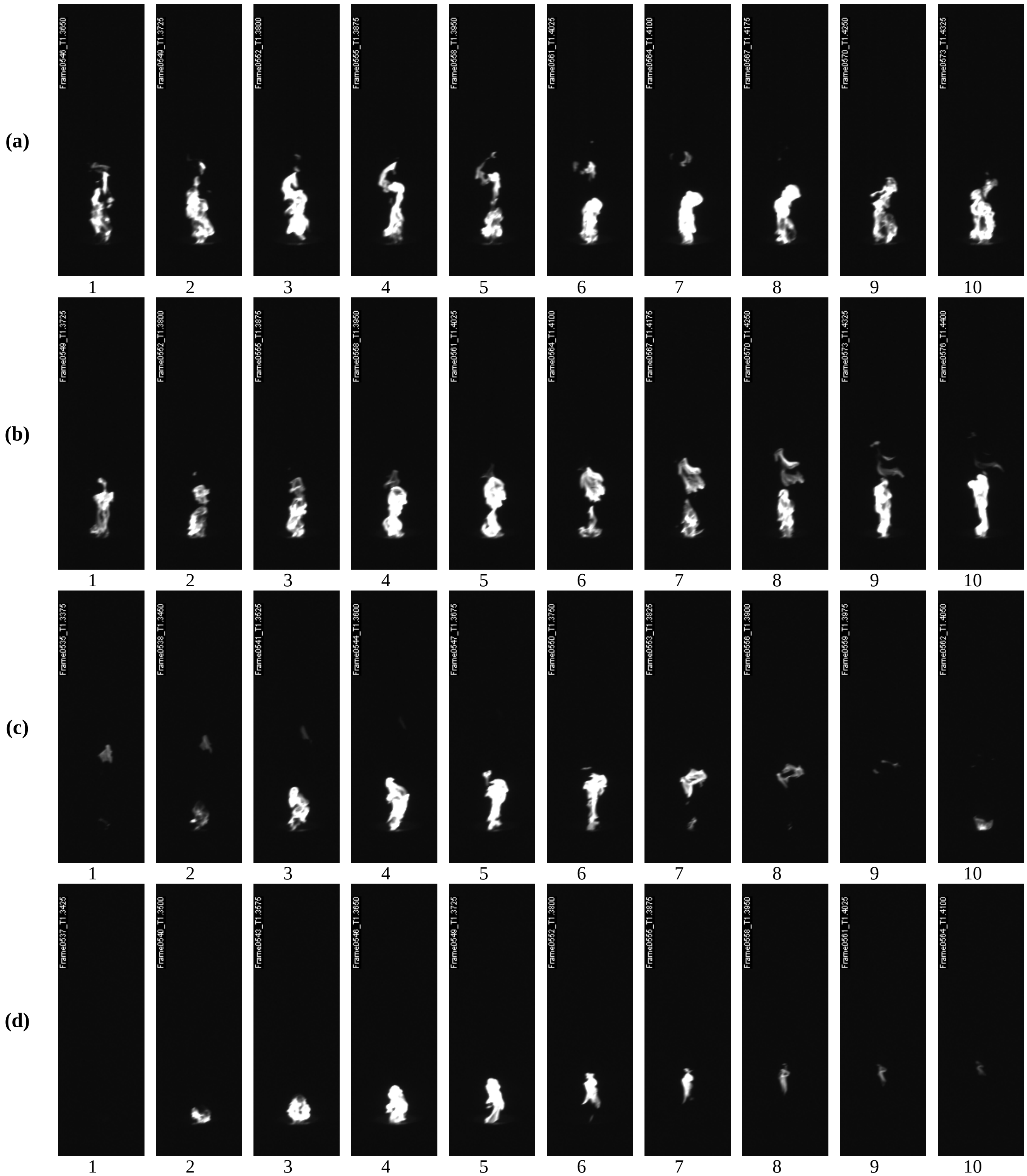

Figure C.4 – Visual sequences of P = 6 flames with the swirl level of S = 1.64 and a co-flow of 3.5 SCFM. (a) τ_{off} = 111. (b) τ_{off} = 222. (c) τ_{off} = 444. (d) τ_{off} = 1110. Framing interval Δt = 7.5 ms; image height 57.9 cm.

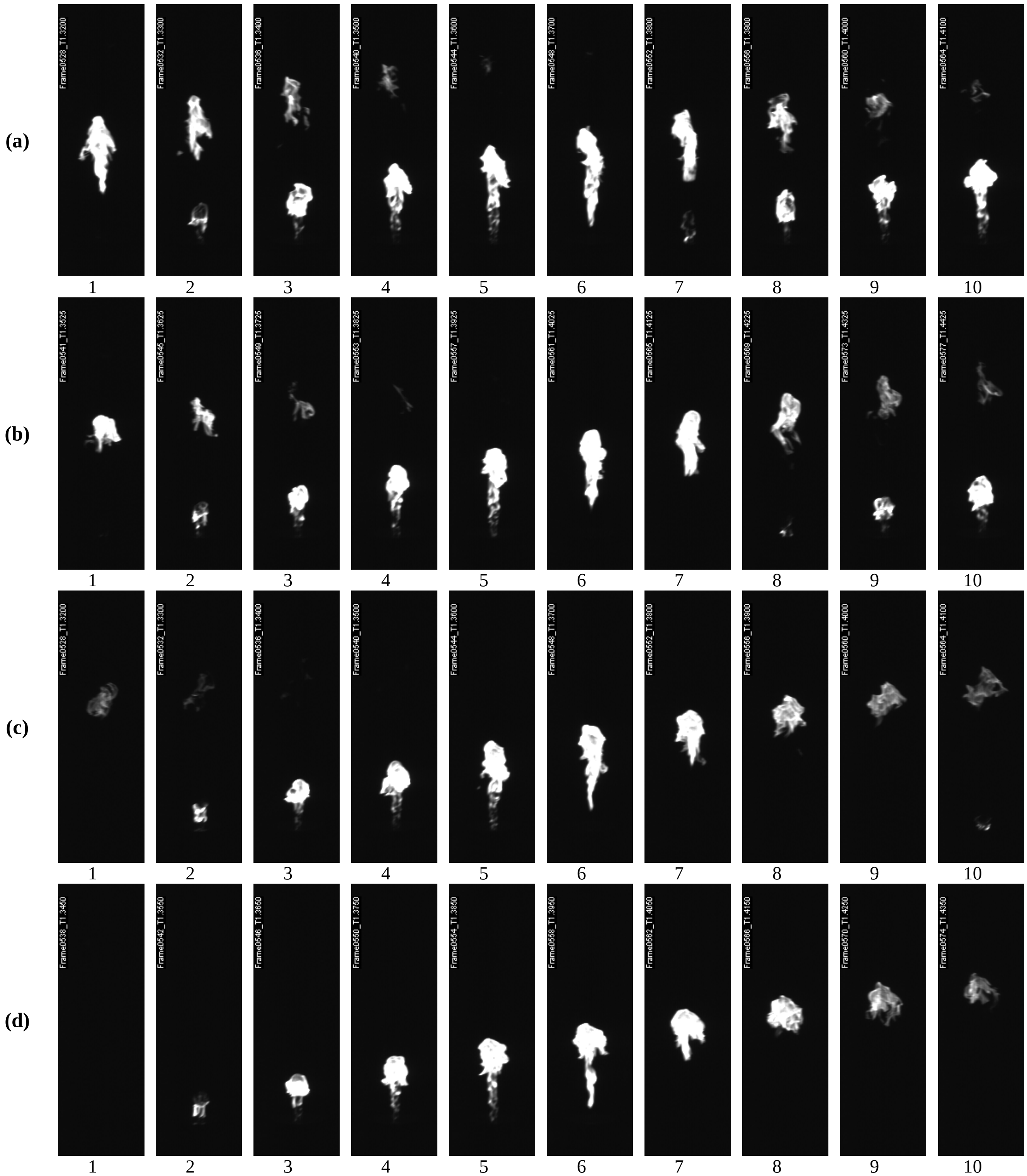

Figure C.5 – Visual sequences of P = 8 flames with the swirl level of S = 0 and a co-flow of 3.5 SCFM. (a) τ_{off} = 111. (b) τ_{off} = 222. (c) τ_{off} = 444. (d) τ_{off} = 1110. Framing interval Δt = 10 ms; image height 57.9 cm.

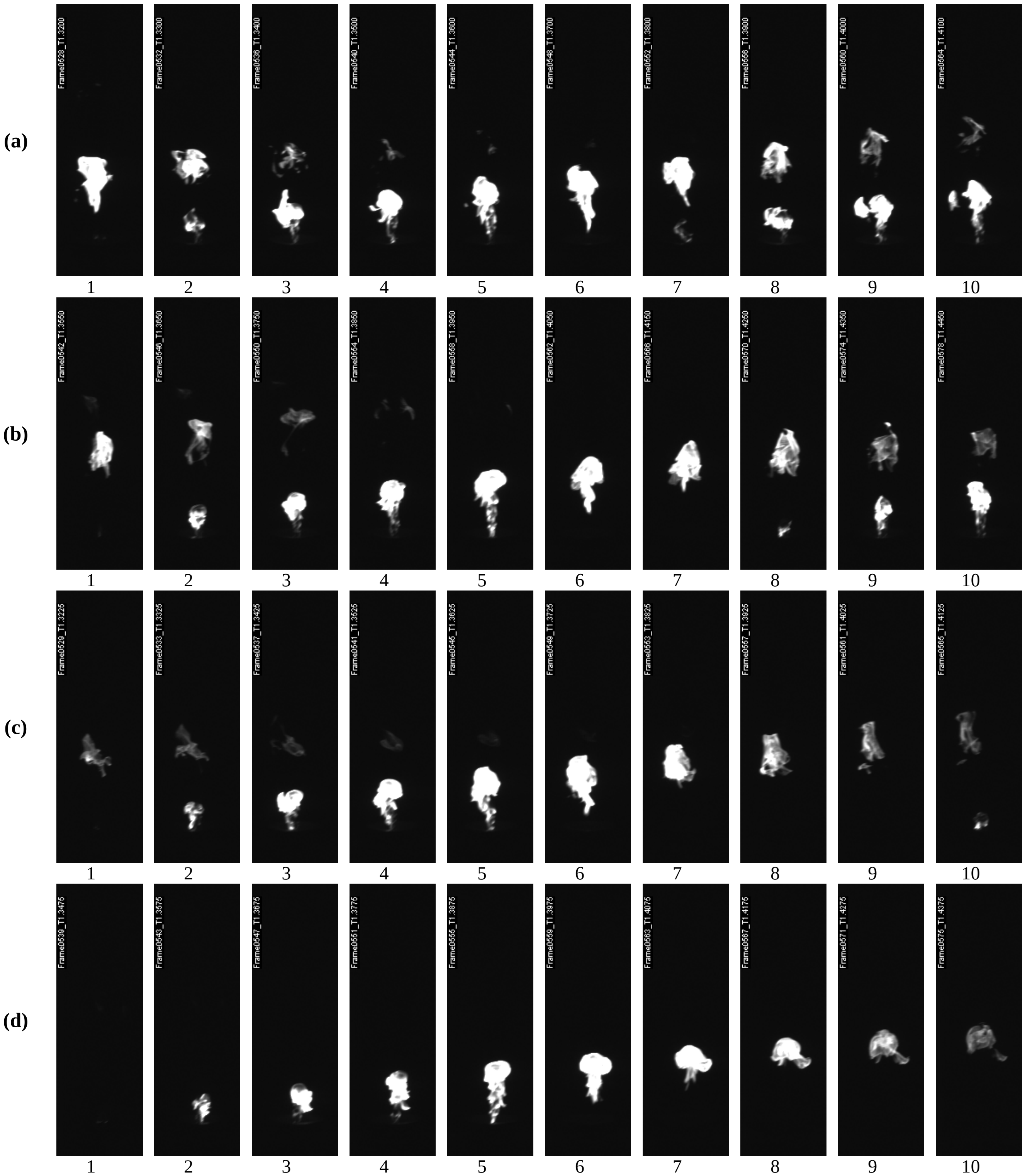

Figure C.6 – Visual sequences of P = 8 flames with the swirl level of S = 0.44 and a co-flow of 3.5 SCFM. (a) τ_{off} = 111. (b) τ_{off} = 222. (c) τ_{off} = 444. (d) τ_{off} = 1110. Framing interval Δt = 10 ms; image height 57.9 cm.

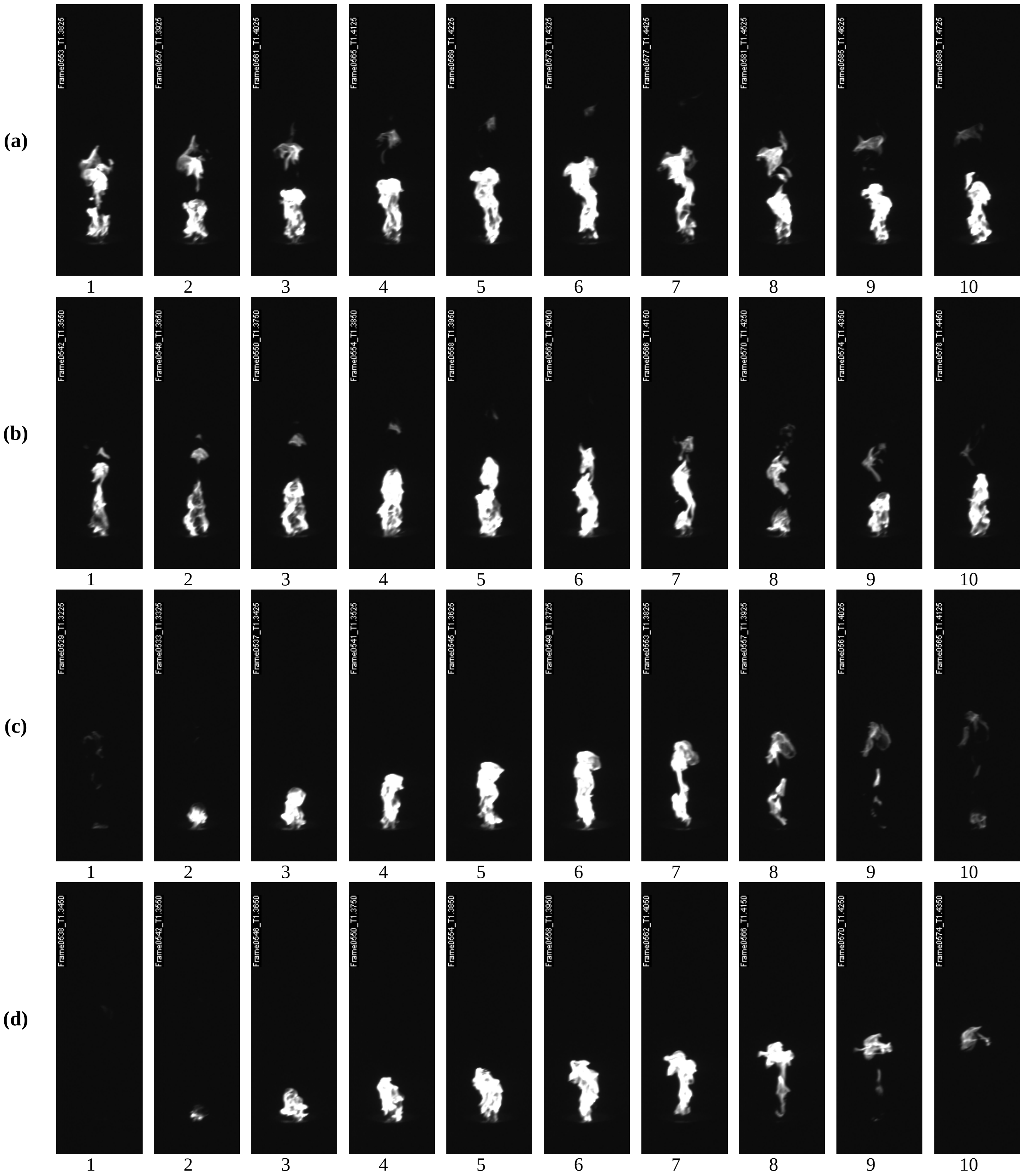

Figure C.7 – Visual sequences of P = 8 flames with the swirl level of S = 1.64 and a co-flow of 3.5 SCFM. (a) τ_{off} = 111. (b) τ_{off} = 222. (c) τ_{off} = 444. (d) τ_{off} = 1110. Framing interval Δt = 10 ms; image height 57.9 cm.

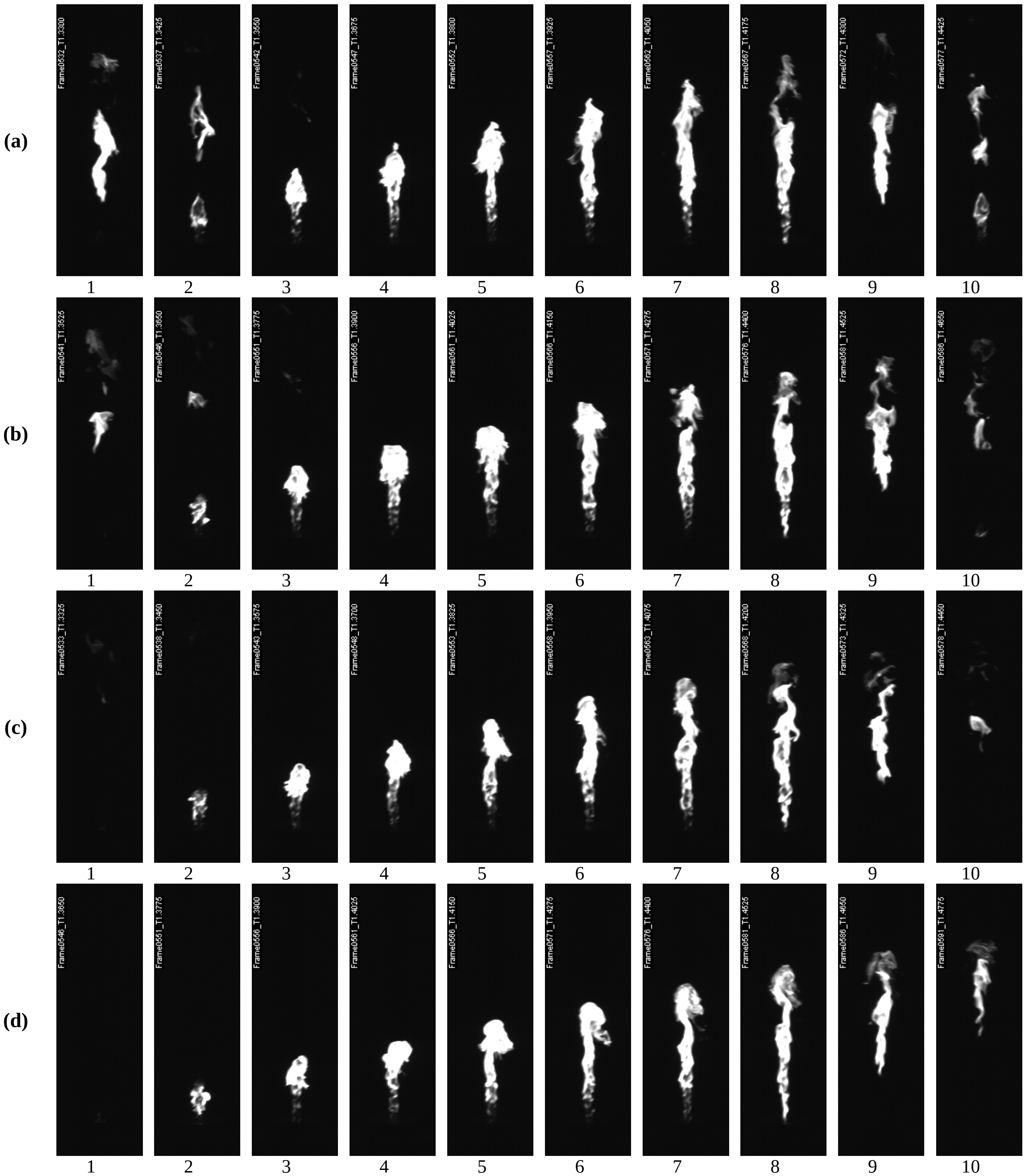

Figure C.8 – Visual sequences of P = 10 flames with the swirl level of S = 0 and a co-flow of 3.5 SCFM. (a) τ_{off} = 111. (b) τ_{off} = 222. (c) τ_{off} = 444. (d) τ_{off} = 1110. Framing interval Δt = 12.5 ms; image height 57.9 cm.

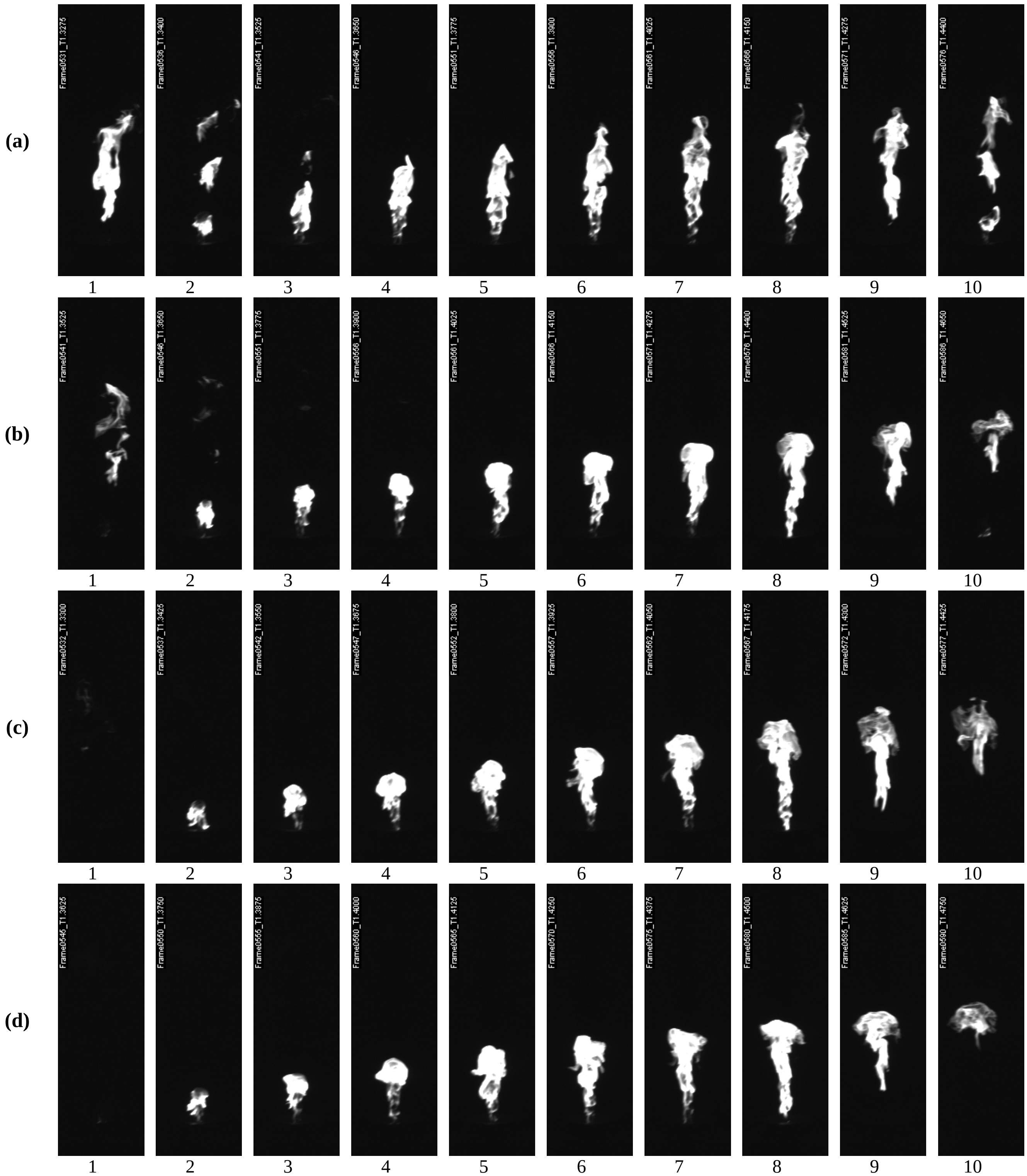

Figure C.9 – Visual sequences of P = 10 flames with the swirl level of S = 0.44 and a co-flow of 3.5 SCFM. (a) τ_{off} = 111. (b) τ_{off} = 222. (c) τ_{off} = 444. (d) τ_{off} = 1110. Framing interval Δt = 12.5 ms; image height 57.9 cm.

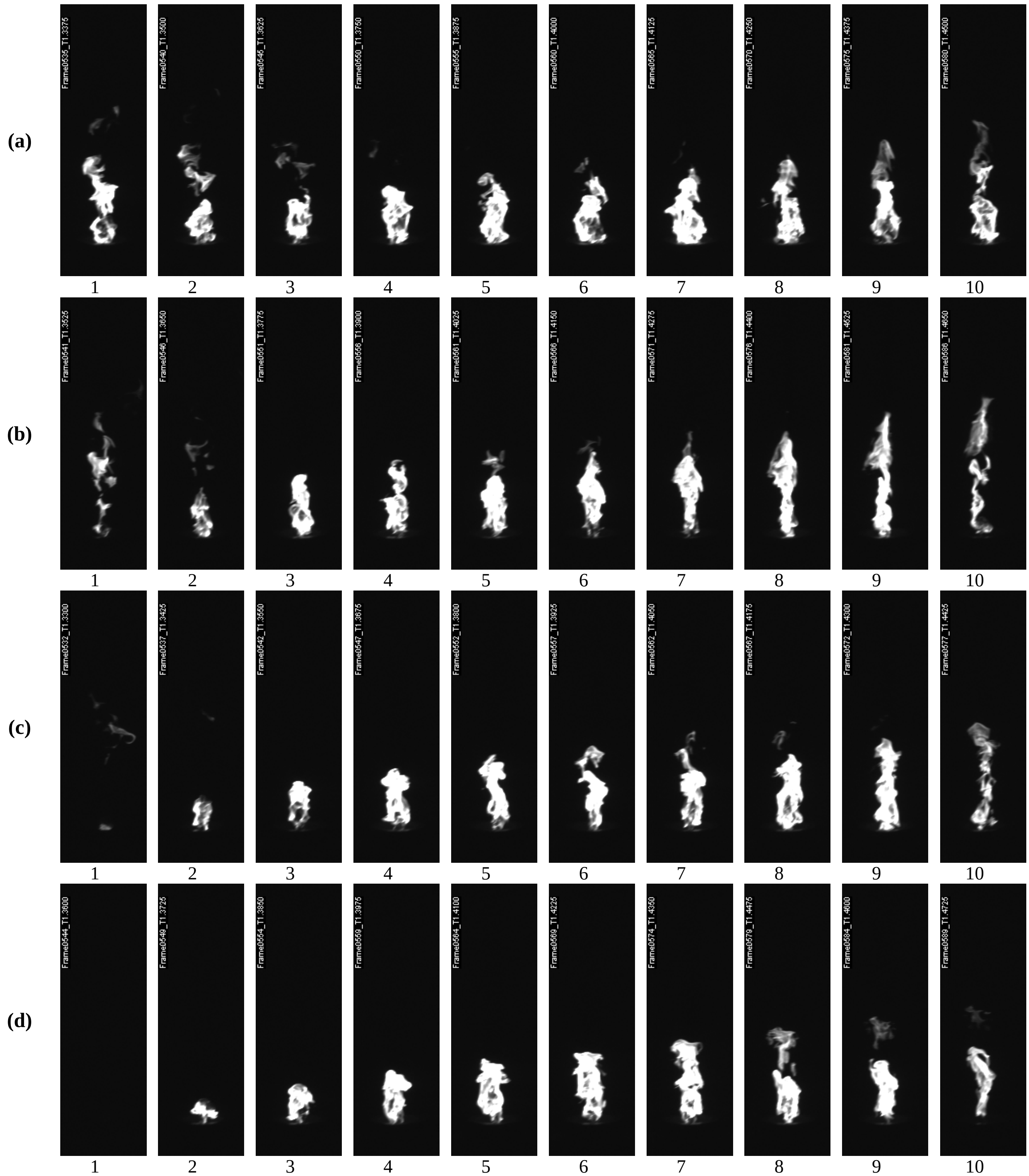

Figure C.10 – Visual sequences of P = 10 flames with the swirl level of S = 1.64 and a co-flow of 3.5 SCFM. (a) τ_{off} = 111. (b) τ_{off} = 222. (c) τ_{off} = 444. (d) τ_{off} = 1110. Framing interval Δt = 12.5 ms; image height 57.9 cm.

APPENDIX D

OH-PLIF IMAGE SEQUENCES

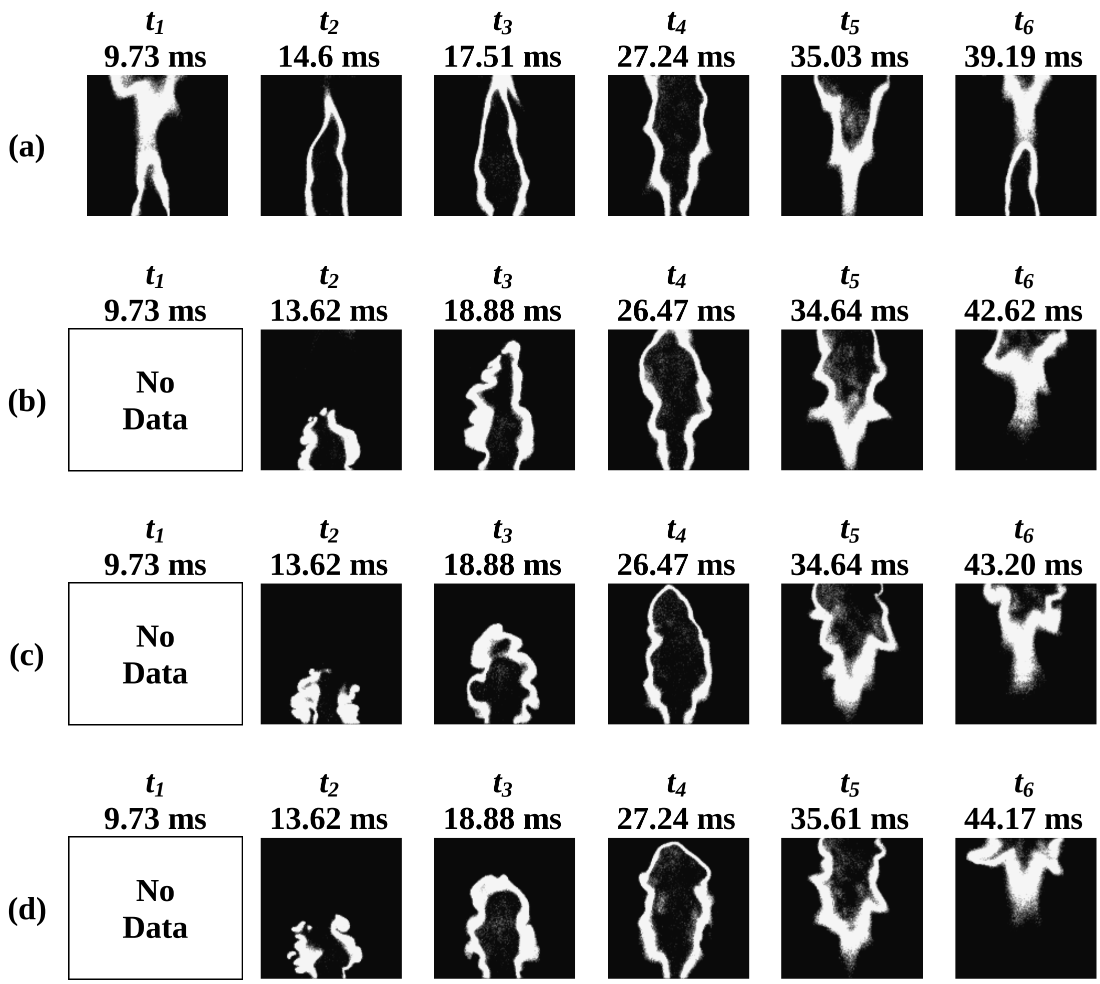

Figure D.1 – OH-PLIF sequences of P = 6 (t_{on} = 19.46 ms) flames with the swirl level of S = 0 and a co-flow of 2.5 SCFM. (a) t_{off} = 10 ms. (b) t_{off} = 20 ms. (c) t_{off} = 40 ms. (d) t_{off} = 100 ms. The times cited are the elapsed times after the start of the fuel injection interval. The image size is 3.125” × 3.125”.

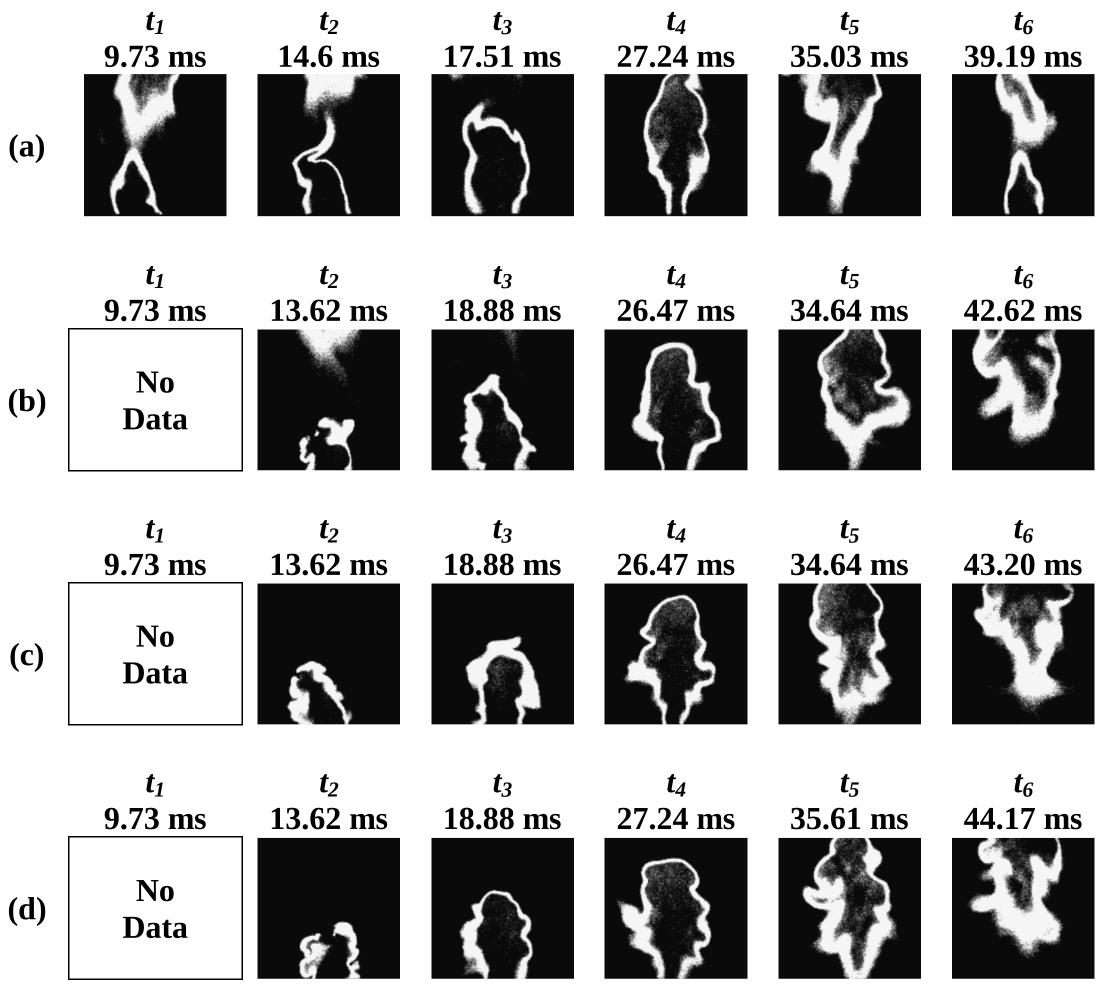

Figure D.2 – OH-PLIF sequences of P = 6 (t_{on} = 19.46 ms) flames with the swirl level of S = 0.41 and a co-flow of 2.5 SCFM. (a) t_{off} = 10 ms. (b) t_{off} = 20 ms. (c) t_{off} = 40 ms. (d) t_{off} = 100 ms. The times cited are the elapsed times after the start of the fuel injection interval. The image size is 3.125” × 3.125”.

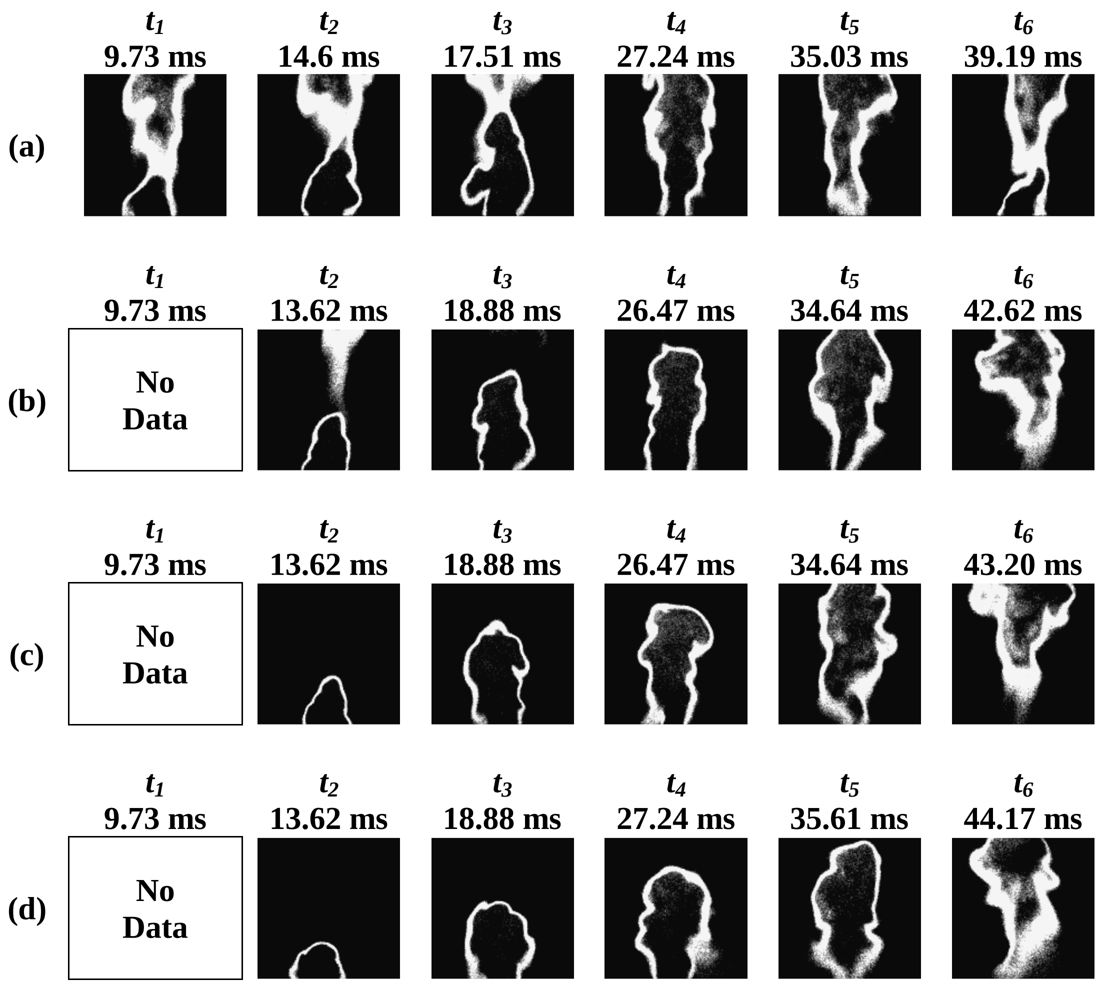

Figure D.3 – OH-PLIF sequences of P = 6 (t_{on} = 19.46 ms) flames with the swirl level of S = 1.61 and a co-flow of 2.5 SCFM. (a) t_{off} = 10 ms. (b) t_{off} = 20 ms. (c) t_{off} = 40 ms. (d) t_{off} = 100 ms. The times cited are the elapsed times after the start of the fuel injection interval. The image size is 3.125” × 3.125”.

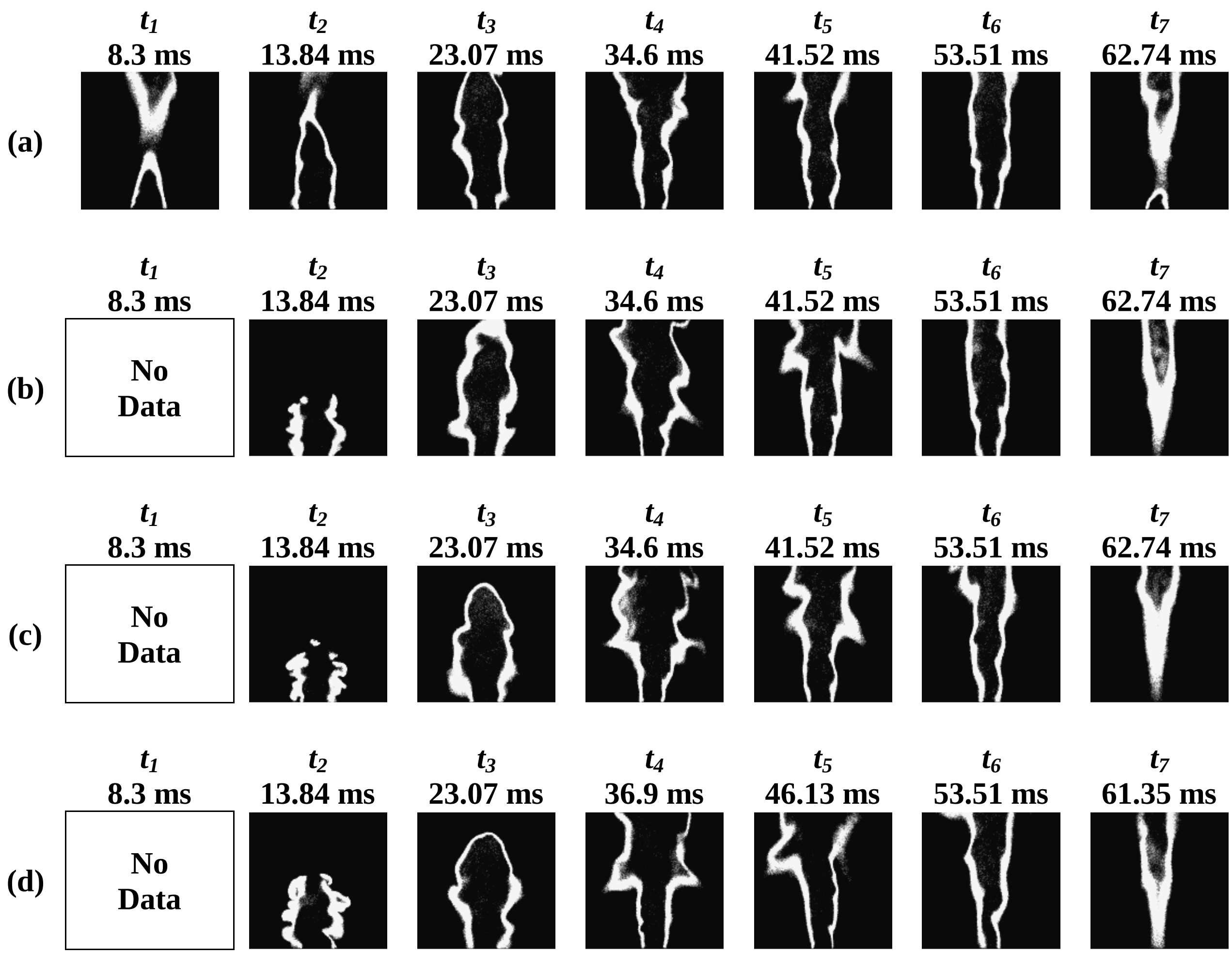

Figure D.4 – OH-PLIF sequences of P = 8 (t_{on} = 46.13 ms) flames with the swirl level of S = 0 and a co-flow of 2.5 SCFM. (a) t_{off} = 10 ms. (b) t_{off} = 20 ms. (c) t_{off} = 40 ms. (d) t_{off} = 100 ms. The times cited are the elapsed times after the start of the fuel injection interval. The image size is 3.125” × 3.125”.

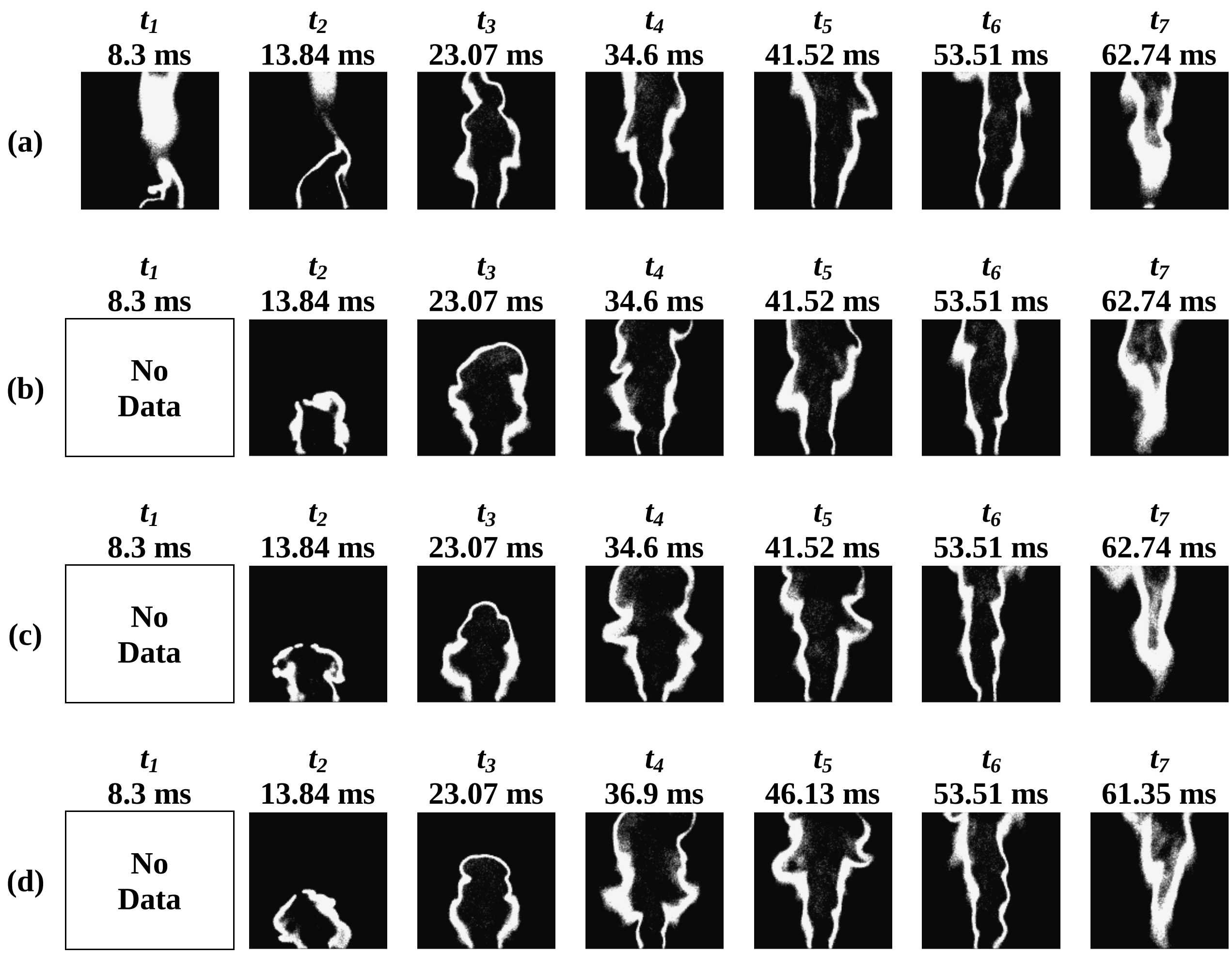

Figure D.5 – OH-PLIF sequences of P = 8 (t_{on} = 46.13 ms) flames with the swirl level of S = 0.41 and a co-flow of 2.5 SCFM. (a) t_{off} = 10 ms. (b) t_{off} = 20 ms. (c) t_{off} = 40 ms. (d) t_{off} = 100 ms. The times cited are the elapsed times after the start of the fuel injection interval. The image size is 3.125" × 3.125".

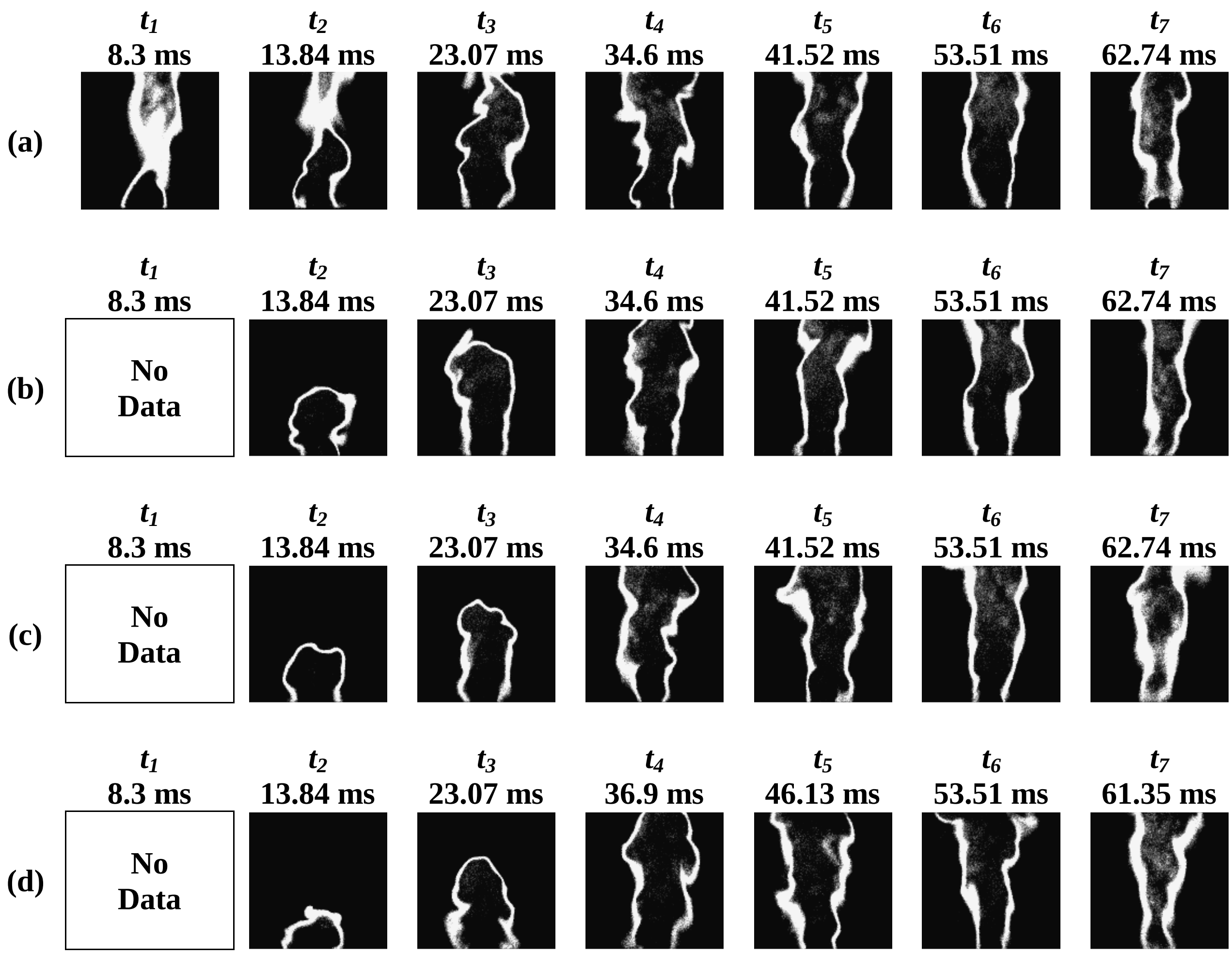

Figure D.6 – OH-PLIF sequences of P = 8 (t_{on} = 46.13 ms) flames with the swirl level of S = 1.61 and a co-flow of 2.5 SCFM. (a) t_{off} = 10 ms. (b) t_{off} = 20 ms. (c) t_{off} = 40 ms. (d) t_{off} = 100 ms. The times cited are the elapsed times after the start of the fuel injection interval. The image size is 3.125” × 3.125”.

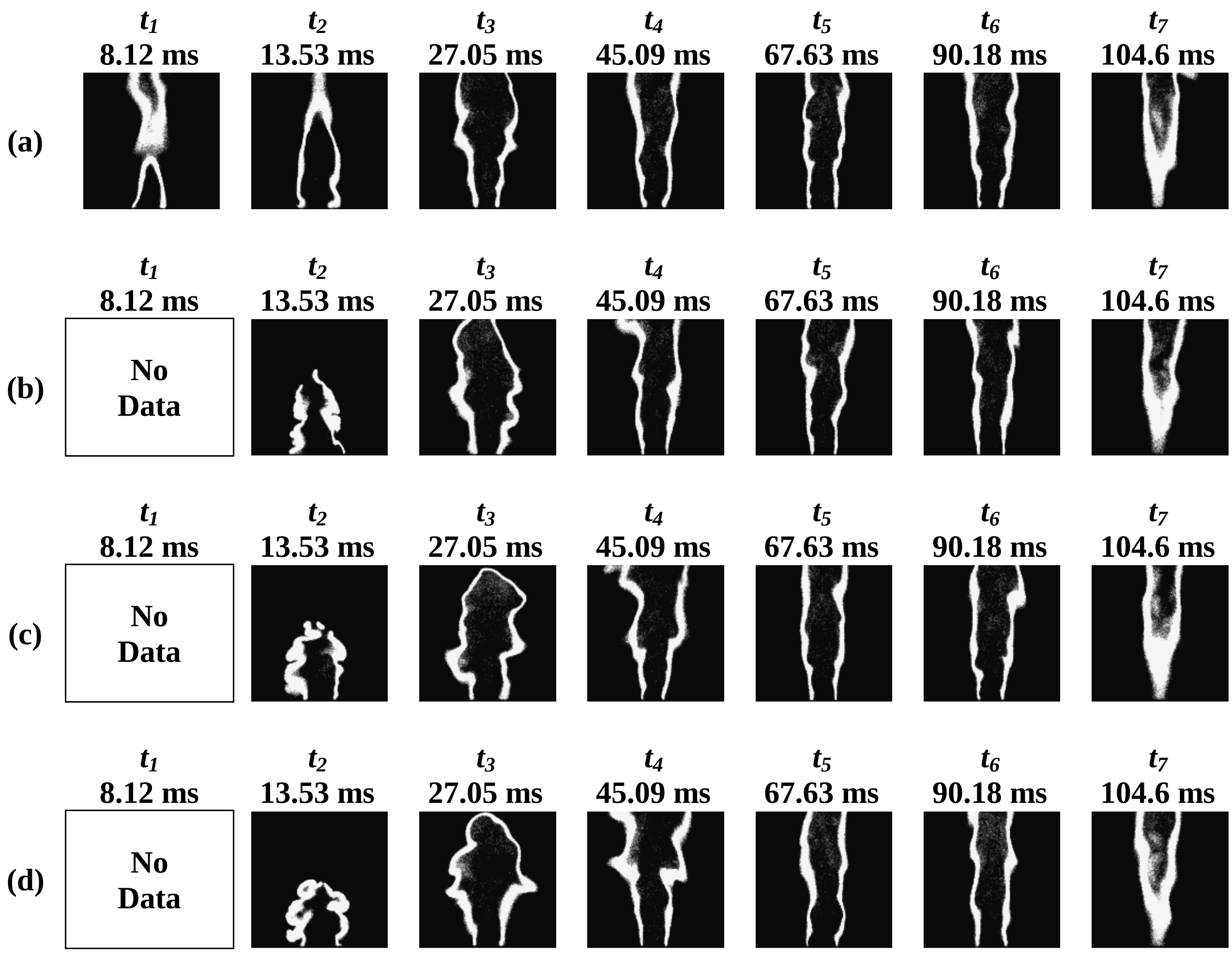

Figure D.7 – OH-PLIF sequences of P = 10 (t_{on} = 90.1 ms) flames with the swirl level of S = 0 and a co-flow of 2.5 SCFM. (a) t_{off} = 10 ms. (b) t_{off} = 20 ms. (c) t_{off} = 40 ms. (d) t_{off} = 100 ms. The times cited are the elapsed times after the start of the fuel injection interval. The image size is 3.125” × 3.125”.

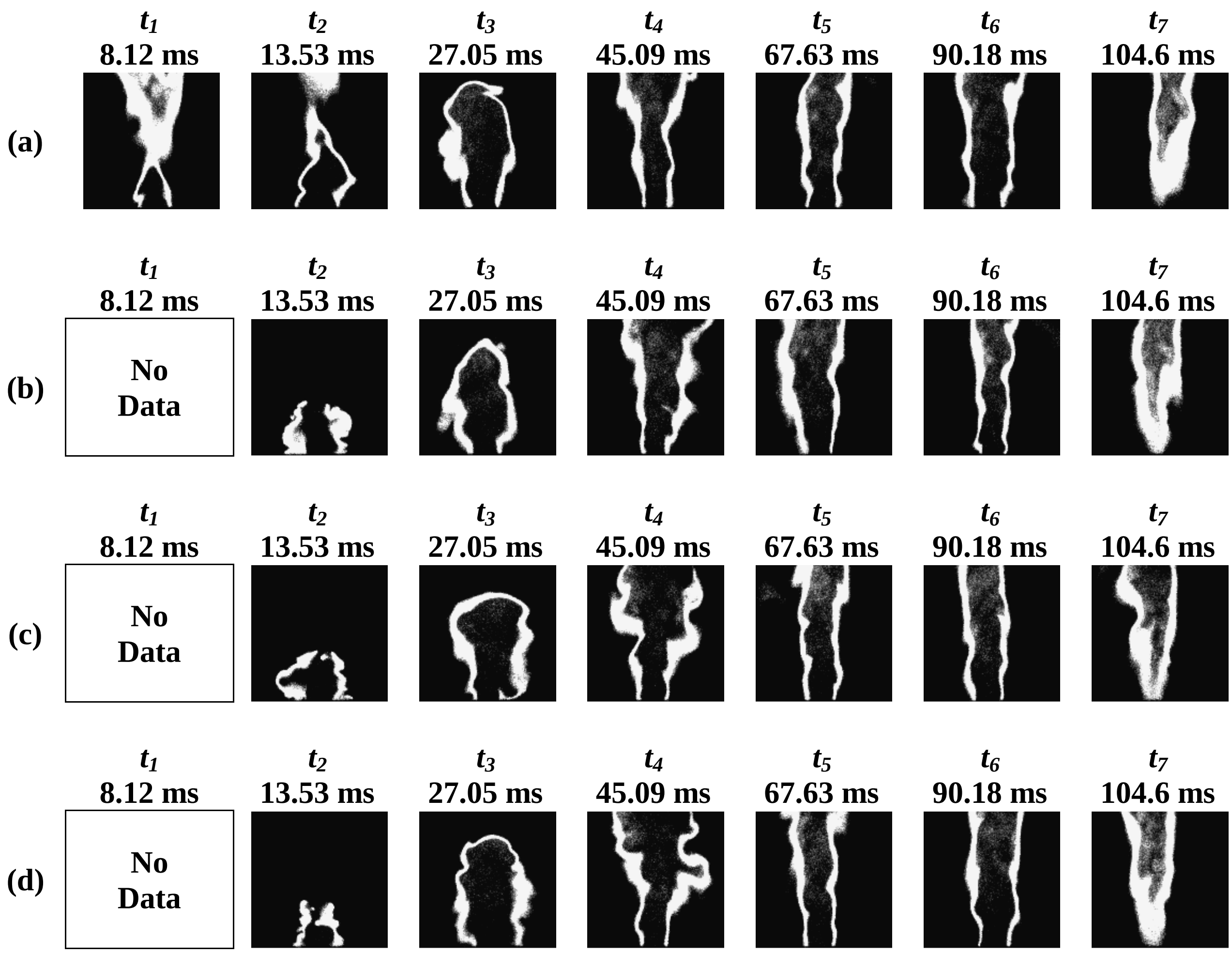

Figure D.8 – OH-PLIF sequences of P = 10 (t_{on} = 90.1 ms) flames with the swirl level of S = 0.41 and a co-flow of 2.5 SCFM. (a) t_{off} = 10 ms. (b) t_{off} = 20 ms. (c) t_{off} = 40 ms. (d) t_{off} = 100 ms. The times cited are the elapsed times after the start of the fuel injection interval. The image size is 3.125” × 3.125”.

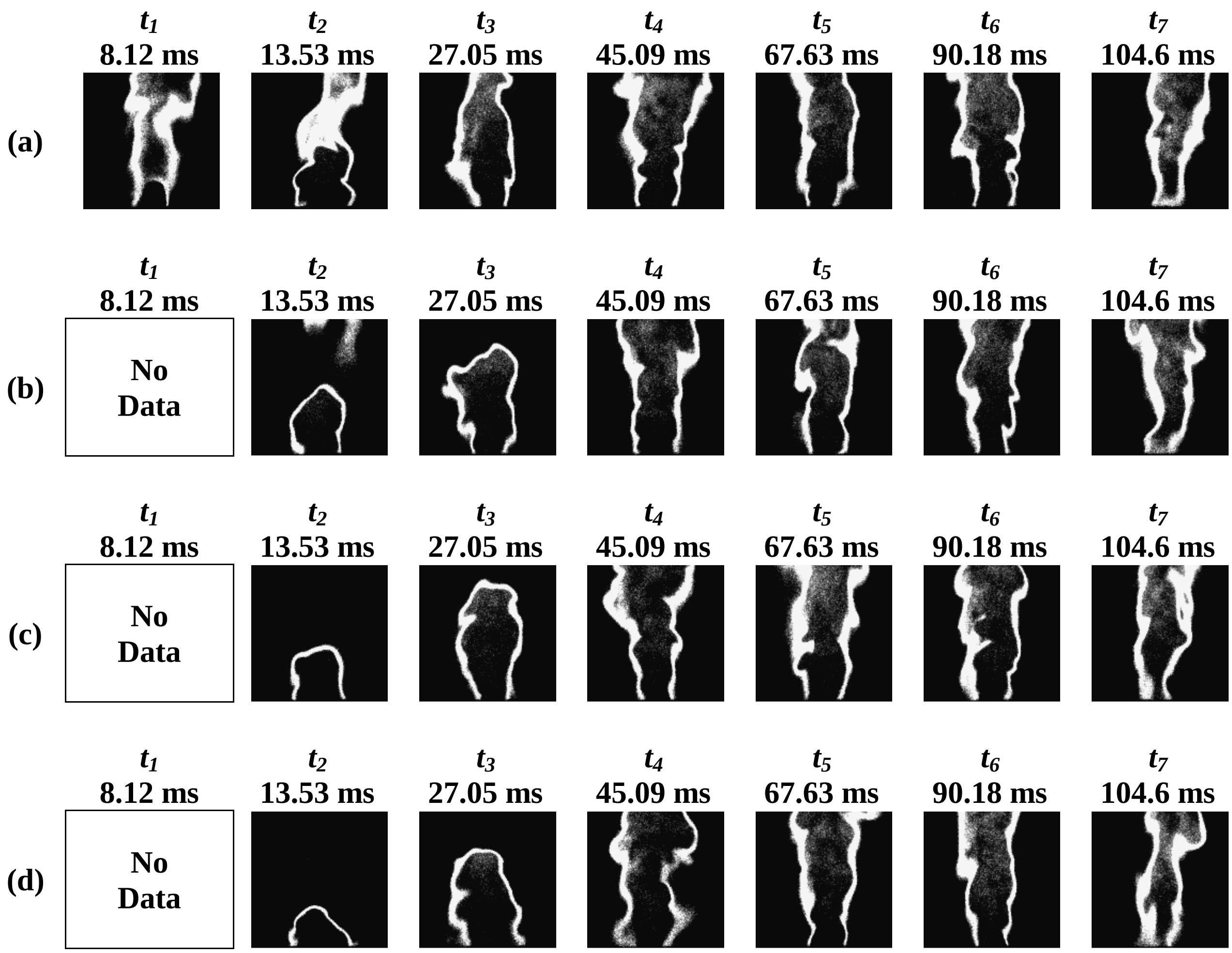

Figure D.9 – OH-PLIF sequences of P = 10 (t_{on} = 90.1 ms) flames with the swirl level of S = 1.61 and a co-flow of 2.5 SCFM. (a) t_{off} = 10 ms. (b) t_{off} = 20 ms. (c) t_{off} = 40 ms. (d) t_{off} = 100 ms. The times cited are the elapsed times after the start of the fuel injection interval. The image size is 3.125" × 3.125".

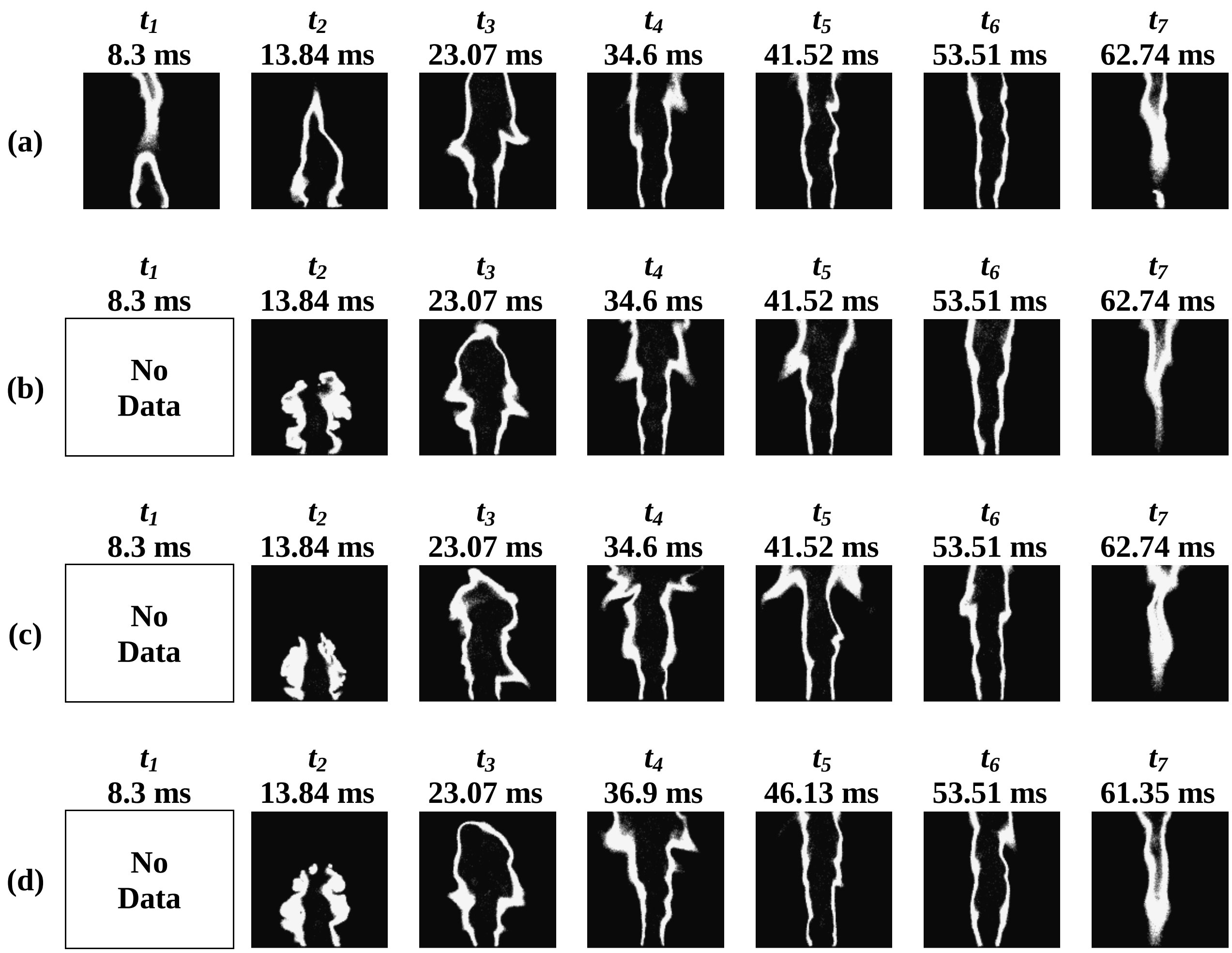

Figure D.10 – OH-PLIF sequences of P = 8 (t_{on} = 46.13 ms) flames with the swirl level of S = 0 and a co-flow of 3.5 SCFM. (a) t_{off} = 10 ms. (b) t_{off} = 20 ms. (c) t_{off} = 40 ms. (d) t_{off} = 100 ms. The times cited are the elapsed times after the start of the fuel injection interval. The image size is 3.125” × 3.125”.

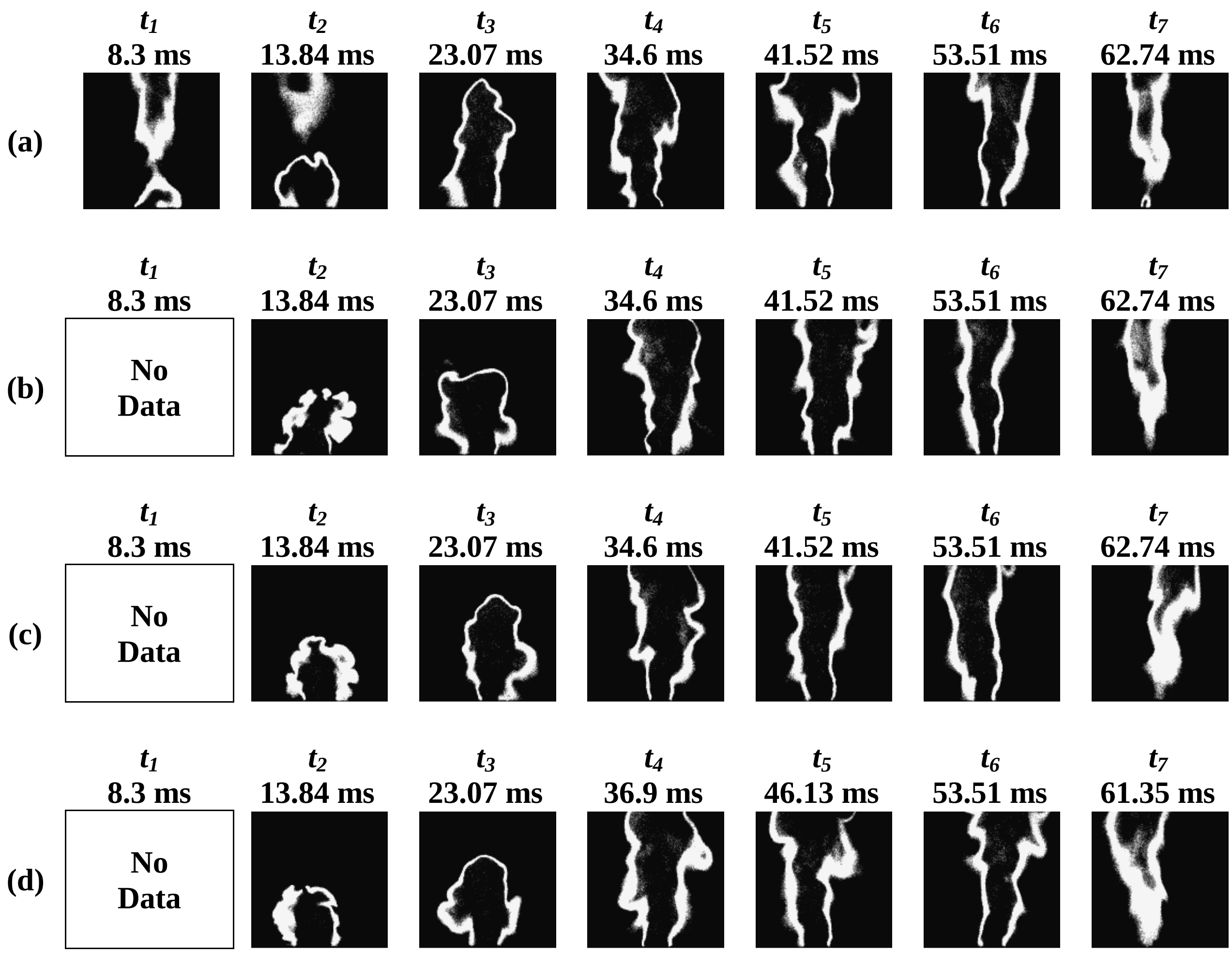

Figure D.11 – OH-PLIF sequences of P = 8 (t_{on} = 46.13 ms) flames with the swirl level of S = 0.44 and a co-flow of 3.5 SCFM. (a) t_{off} = 10 ms. (b) t_{off} = 20 ms. (c) t_{off} = 40 ms. (d) t_{off} = 100 ms. The times cited are the elapsed times after the start of the fuel injection interval. The image size is 3.125” × 3.125”.

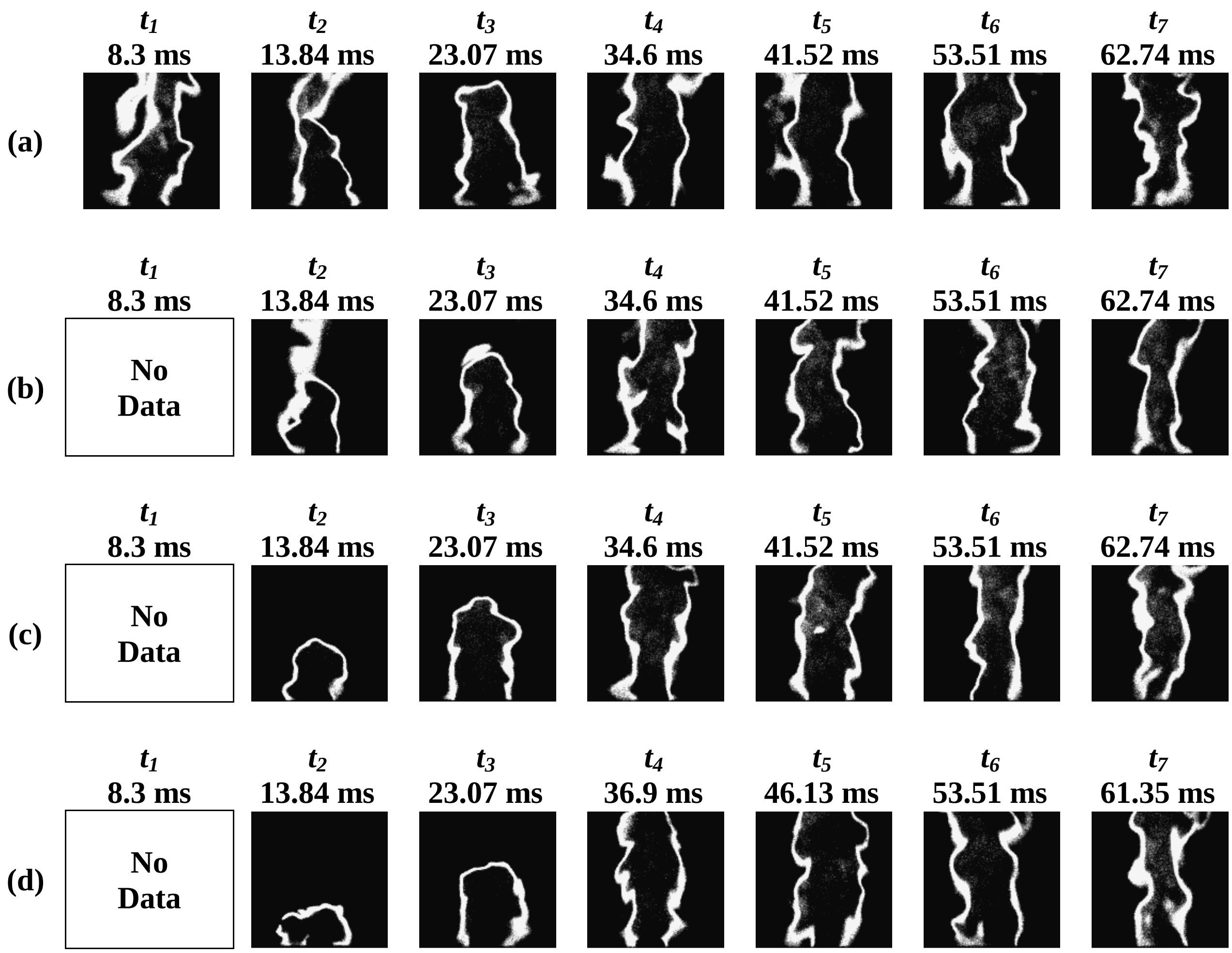

Figure D.12 – OH-PLIF sequences of P = 8 (t_{on} = 46.13 ms) flames with the swirl level of S = 1.64 and a co-flow of 3.5 SCFM. (a) t_{off} = 10 ms. (b) t_{off} = 20 ms. (c) t_{off} = 40 ms. (d) t_{off} = 100 ms. The times cited are the elapsed times after the start of the fuel injection interval. The image size is 3.125” × 3.125”.

VITA

Ying-Hao Liao was born in Taiwan, R. O. C. He received both of his Bachelor of Science and Master of Science in Mechanical Engineering from the National Chiao Tung University in Taiwan in 2001 and 2003, respectively. After graduating from the National Chiao Tung University, he worked for Industrial Technology Research Institute in Taiwan. In 2012 he earned a Doctor of Philosophy in Aeronautics and Astronautics at the University of Washington.

- ## Conference Presentations and Papers:

Y. –H. Liao and J. C. Hermanson. "The Effect of Swirl on the Structure of Strongly-Pulsed Turbulent Diffusion Flames." Paper T33, *7th US National Combustion Meeting, Atlanta*, GA, March 2011.

Y. –H. Liao and J. C. Hermanson. "The CO/NO_x Emissions of Strongly-Pulsed Turbulent Jet Diffusion Flames with Swirl." Paper T34, *7th US National Combustion Meeting*, Atlanta, GA, March 2011.

Y. –H. Liao and J. C. Hermanson. "Effect of Swirl on Strongly-Pulsed Turbulent Diffusion Flames." *American Physical Society Division of Fluid Dynamics 62nd Annual Meeting*, Minneapolis, MN, November, 2009.

M. Fregeau, **Y. –H. Liao**, J. C. Hermanson, D. P. Stocker, and U. G. Hegde. "Effects of Injection Conditions on Strongly-Pulsed Turbulent Jet Flame Structure." AIAA Paper 2008-1016, *46th Aerospace Sciences Meeting*, Reno, NV, January 2008.

- ## Invited Seminar:

"Structure, Dynamics, and Emissions of Swirled, Strongly-Pulsed Turbulent Diffusion Jet Flames." *University of Texas at Austin*, October 2011.